ΕΘΝΙΚΟ ΜΕΤΣΟΒΙΟ ΠΟΛΥΤΕΧΝΕΙΟ
ΣΧΟΛΗ ΗΛΕΚΤΡΟΛΟΓΩΝ ΜΗΧΑΝΙΚΩΝ ΚΑΙ ΜΗΧΑΝΙΚΩΝ ΥΠΟΛΟΓΙΣΤΩΝ
ΤΟΜΕΑΣ ΣΥΣΤΗΜΑΤΩΝ ΜΕΤΑΔΟΣΗΣ ΠΛΗΡΟΦΟΡΙΑΣ ΚΑΙ ΤΕΧΝΟΛΟΓΙΑΣ ΥΛΙΚΩΝ

Μοντελοποίηση Καναλιού και Αξιολόγηση Επίδοσης Ασύρματων Επίγειων και Δορυφορικών Συστημάτων Επικοινωνιών Νέας Γενιάς Υψηλών Ταχυτήτων

Διδακτορική Διατριβή

Χαρίλαος Η. Κουρόγιωργας

Αθήνα, Μάιος 2015

ΕΘΝΙΚΟ ΜΕΤΣΟΒΙΟ ΠΟΛΥΤΕΧΝΕΙΟ
ΣΧΟΛΗ ΗΛΕΚΤΡΟΛΟΓΩΝ ΜΗΧΑΝΙΚΩΝ ΚΑΙ ΜΗΧΑΝΙΚΩΝ ΥΠΟΛΟΓΙΣΤΩΝ
ΤΟΜΕΑΣ ΣΥΣΤΗΜΑΤΩΝ ΜΕΤΑΔΟΣΗΣ ΠΛΗΡΟΦΟΡΙΑΣ ΚΑΙ ΤΕΧΝΟΛΟΓΙΑΣ ΥΛΙΚΩΝ

Μοντελοποίηση Καναλιού και Αξιολόγηση Επίδοσης Ασύρματων Επίγειων και Δορυφορικών Συστημάτων Επικοινωνιών Νέας Γενιάς Υψηλών Ταχυτήτων

Διδακτορική Διατριβή

Χαρίλαος Κουρόγιωργας

Τριμελής Συμβουλευτική Επιτροπή:
Αθανάσιος Δ. Παναγόπουλος
Spiros Ventouras
Ιωάννης Δ. Κανελλόπουλος

Η Επιτροπή Εξέτασης

……………………
Α. Δ. Παναγόπουλος
Επίκ. Καθηγητής, ΕΜΠ

……………………
S. Ventouras
Senior Researcher, RAL Space, UK

……………………
Ι. Δ. Κανελλόπουλος
Καθηγητής, ΕΜΠ

……………………
A. Vilhar
Researcher, JSI, Slovenia

……………………
Γ. Φικιώρης
Αναπλ. Καθηγητής, ΕΜΠ

……………………
Γ. Τσούλος
Αναπλ. Καθηγητής,
Πανεπ. Πελοποννήσου

……………………
Γ. Ευθύμογλου
Αναπλ. Καθηγητής, Πανεπιστήμιο Πειραιώς

Αθήνα, Μάιος 2015

....

Χαρίλαος Η. Κουρόγιωργας

Διδάκτωρ Ηλεκτρολόγος Μηχανικός και Μηχανικός Υπολογιστών Ε.Μ.Π.

Contents

CONTENTS 6

1. ΜΟΝΤΕΛΟΠΟΙΗΣΗ ΚΑΝΑΛΙΟΥ ΚΑΙ ΑΞΙΟΛΟΓΗΣΗ ΤΗΣ ΕΠΙΔΟΣΗΣ ΑΣΥΡΜΑΤΩΝ ΕΠΙΓΕΙΩΝ ΚΑΙ ΔΟΡΥΦΟΡΙΚΩΝ ΣΥΣΤΗΜΑΤΩΝ ΜΕΤΑΔΟΣΗΣ ΝΕΑΣ ΓΕΝΙΑΣ 25

1.1 Εισαγωγή 25

1.2 Μοντελοποίηση των στατιστικών χαρακτηριστικών πρώτης τάξης της απόσβεσης λόγω βροχής 27

1.2.1 Μέθοδος πρόβλεψης πιθανότητας αποκοπής για επίγειες και δορυφορικές ζεύξεις υπό βροχή με συχνότητα λειτουργίας άνω των 10 GHz 29
1.2.2 Μέθοδος υπολογισμού της πιθανότητας αποκοπής δορυφορικού συστήματος διπλού διαφορισμού θέσης 33
1.2.3 Μέθοδος υπολογισμού πιθανότητας αποκοπής σε επίγεια ασύρματα συστήματα με χρήση του διαφορισμού δρόμου για συχνότητες λειτουργίας άνω των 10 GHz 34
1.2.4 Μοντελοποίηση της πιθανότητας αποκοπής σε δορυφορικά συστήματα διπλού διαφορισμού με χρήση των συναρτήσεων Archimedean Copulas 37
1.2.5 Μοντελοποίηση της έντασης βροχόπτωσης 38
1.2.6 Μοντελοποίηση της απόσβεση λόγω βροχής 39
1.2.7 Μοντελοποίηση της απόδοσης δορυφορικών συστημάτων χρονικού διαφορισμού με τη Λογαριθμοκανονική κατανομή 40
1.2.8 Μοντελοποίηση της απόδοσης δορυφορικών συστημάτων χρονικού διαφορισμού με συναρτήσεις Copulas 42

1.3 Μοντελοποίηση δυναμικών χαρακτηριστικών της απόσβεσης λόγω βροχής και των σπινθηρισμών 44

1.3.1 Μοντελοποίηση της δυναμικής παραμέτρου της απόσβεσης λόγω βροχής 45
1.3.2 Στοχαστική μοντελοποίηση της απόσβεσης λόγω βροχής για ζεύξεις Γης με δορυφόρους MEO/LEO σε συχνότητες άνω των 10GHz 46
1.3.3 Μοντέλο παραγωγής χρονοσειρών απόσβεσης λόγω βροχής κάνοντας χρήση των συναρτήσεων copulas 48
1.3.4 Παραγωγή χρονοσειρών πεδίων βροχής 51
1.3.5 Μοντέλο παραγωγής χρονοσειρών του σπινθηρισμού λόγω των τροποσφαιρικών στροβίλων 53

1.4 Αξιολόγηση της Επίδοσης Γνωστικών Δορυφορικών Συστημάτων Επικοινωνιών και Συστημάτων Παρατήρησής Γης σε Συχνότητες άνω των 10 GHz 56

1.4.1 Στατιστική κατανομή παρεμβολών για δορυφορικά γνωστικά συστήματα που λειτουργούν σε συχνότητες άνω των 10 GHz 57
1.4.2 Στατιστικός χαρακτηρισμός των παρεμβολών από επικείμενους δορυφόρους για επίγειους σταθμούς σε κινητές πλατφόρμες που λειτουργούν σε συχνότητες άνω των 10 GHz 59
1.4.3 Γνωστικό σύστημα συνύπαρξης άνω ζεύξης δορυφορικού συστήματος και επίγειας ασύρματης ζεύξης στην Ka ζώνη συχνοτήτων 61
1.4.4 Απόδοση κάτω ζεύξης υψηλής μετάδοσης δεδομένων για συστήματα παρατήρησης Γης 63

1.5 Συμπεράσματα 65

2 INTRODUCTION……………………………………………………………………………………67

2.1 Propagation Impairments and Propagation Modeling 69
2.1.1 Review of Tropospheric effects and first order statistics modeling................................ 70
2.1.2 Fade Dynamics.. 80
2.1.3 Frequency Scaling... 83
2.1.4 Diversity Systems.. 85
2.1.5 Spatial Correlation of Total Attenuation 87
2.1.6 Space-Time Channel Models 88

2.2 Fade Mitigation Techniques 89

2.3 Future Wireless Terrestrial and Satellite Communication Systems 93

3 REVIEW ON TROPOSPHERIC ATTENUATION TIME SERIES SYNTHESIZERS 97

3.1 Rain Attenuation Synthesizers...98
3.1.1 Filter-based Models.. 98
3.1.2 Models based on SDEs.. 102
3.1.3 Synthetic Storm Technique 106
3.1.4 Models Based on Data... 106
3.1.5 Models based on conditional probabilities 107
3.1.6 Markov Chain Models 109

3.2 Clouds Attenuation Time Series..111

3.3 Time Series of Attenuation due to Atmospheric Gases 115

3.4 Scintillation Time Series..116

3.5 Total Tropospheric Attenuation Time Series Generation..118

4 LONG TERM OUTAGE PREDICTION MODELING OF WIRELESS SYSTEMS OPERATING ABOVE 10 GHZ 121

4.1 Modeling of Rain Rate and Terrestrial Link and Slant Path Rain Attenuation with the Inverse Gaussian Distribution...123
4.1.1 Modeling of Rain Rate 123
4.1.2 Modeling of Slant Path and Terrestrial Link Rain Attenuation...................................... 126

4.2 Outage Prediction Models for LOS Terrestrial and Satellite Links operating above 10GHz 130
4.2.1 Rain Rate Statistics 130
4.2.2 Outage Prediction Methodology.. 132
4.2.3 Numerical results... 135

4.3 On the Earth-Space Site Diversity Modeling: A Novel Physical-Mathematical Outage Prediction Model...143
4.3.1 Outage Prediction Model 143
4.3.2 Numerical Results and Comparison Tests 147

4.4 Outage Performance of Broadband Fixed Wireless Access Diversity Networks 150
4.4.1 System Model 150
4.4.2 Outage Performance Prediction Final Formulas 152
4.4.3 Numerical Results and Discussion 154

4.5 Outage Prediction Modeling Using Archimedean Copula Functions 156
4.5.1 Rain Rate Modeling 157
4.5.2 Rain Attenuation Modeling Using Copulas 159

4.6 Performance of Time Diversity Satellite Systems 162
4.6.1 Model based on Lognormal Distribution 162
4.6.2 Model Based on Copulas 168

Appendix A: Single Variable IG Distribution 171

Appendix B: Bivariate IG Distribution 172

Appendix C: Copulas Theory 174

5 RAIN ATTENUATION AND SCINTILLATION DYNAMICS MODELING 176

5.1 Modeling of dynamic parameter of rain attenuation 177

5.2 Stochastic Dynamic MEO/LEO Channel Model Operating Above 10GHz 181
5.2.1 The Dynamic Model 181
5.2.2 Fade Slope of LEO Channel Prediction Model 184
5.2.3 Numerical Results and Discussion 186

5.3 Time Series Synthesis of Rain Attenuation Using Copula Functions 190
5.3.1 Joint Statistics of Rain Attenuation on Temporal Domain Using Gaussian Copula 191
5.3.2 Proposed Time Series Synthesizer 194
5.3.3 Numerical Results 195

5.4 Space-Time Rain Rate Field Generator for Multi-Antenna Satellite Communication Applications 196
5.4.1 Rain Rate Field Generator 196
5.4.2 Computation of Rain Attenuation 199
5.4.3 Numerical Results 200

5.5 A Tropospheric Scintillation Time Series Synthesizer Based on Stochastic Differential Equations 202
5.5.1 First Order Statistics of Scintillation 202
5.5.2 Scintillation Time Series Synthesizer 203
5.5.3 Numerical Results and Discussion 204

Appendix A. Fractional Brownian Motion 207

6 PERFORMANCE ASSESSMENT OF COGNITIVE AND EARTH OBSERVATION SATELLITE COMMUNICATION SYSTEMS OPERATING ABOVE 10 GHZ 210

6.1 Interference Statistical Distribution for Cognitive Satellite Communication Systems Operating above 10GHz 211

- 6.1.1 System Model ... 211
- 6.1.2 Satellite Channel Model ... 213
- 6.1.3 Interference Statistical Distribution ... 214
- 6.1.4 Numerical Results and Discussion ... 216

6.2 Statistical Characterization of Adjacent Satellite Interference for Earth Stations on Mobile Platforms Operating at Ku and Ka Band ... 219

- 6.2.1 Channel Model ... 219
- 6.2.2 Statistical Interference Analysis ... 220
- 6.2.3 Numerical Results ... 223

6.3 Cognitive Satellite Uplink and Terrestrial Fixed-Service Coexistence in Ka-band ... 226

- 6.3.1 Statistical Interference Analysis ... 226
- 6.3.2 Numerical Results and Discussion ... 228

6.4 Earth Observation High Date Rate Downlink Performance ... 232

7 CONCLUSIONS AND FUTURE WORK ... 245

7.1 General Conclusions ... 245

- 7.1.1 Long Term Outage Prediction Modeling of Wireless Systems Operating above 10 GHz 245
- 7.1.2 Rain Attenuations and Scintillation Dynamics Modeling ... 246
- 7.1.3 Cognitive and Earth Observation Satellite Communication Systems ... 248

7.2 Future Work ... 249

- 7.2.1 Long Term Outage Prediction Modeling of Wireless Systems Operating above 10 GHz 249
- 7.2.2 Rain Attenuations and Scintillation Dynamics Modeling ... 250
- 7.2.3 Cognitive and Earth Observation Satellite Communication Systems ... 251

REFERENCES ... 253

Εικόνα 1-1 Πιθανότητα υπέρβασης της ένταση βροχόπτωσης για την Αθήνα, Ελλάδα, από την ITU-R. P. 837-5 (κόκκινη γραμμή) και χρησιμοποιείται για την προσαρμογή της IG κατανομής...........30
Εικόνα 1-2 Πιθανότητα υπέρβασης της ένταση βροχόπτωσης για την Yamaguchi, Ιαπωνία, από την DBSG3 (κόκκινη γραμμή) και χρησιμοποιείται για την προσαρμογή της IG κατανομής................30
Εικόνα 1-3 Η Γεωμετρία της ζεύξης Γης-δορυφόρου 31
Εικόνα 1-4 RMS τιμή του σφάλματος του προτεινόμενου μοντέλου και της ITU-R. P. 530-14......32
Εικόνα 1-5 RMS τιμή του σφάλματος του προτεινόμενου μοντέλου και της ITU-R. P. 618...........33
Εικόνα 1-6 RMS τιμή σφάλματος του προτεινόμενου μοντέλου και της σύστασης ITU-R. P. 618 .34
Εικόνα 1-7 Γεωμετρία συστήματος διαφορισμού δρόμου..35
Εικόνα 1-8. Πιθανότητα αποκοπής για τις τεχνικές MRC και SC για 60^o και 90^o γωνίες διαχωρισμού των ζεύξεων στην Αθήνα, Ελλάδα..36
Εικόνα 1-9 Πιθανότητα αποκοπής για τις τεχνικές MRC και SC για 80^o και 120^o γωνίες διαχωρισμού των ζεύξεων στην Σεούλ, Νότια Κορέα...37
Εικόνα 1-10 Από κοινού και για κάθε σημείο πιθανότητα υπέρβασης μαζί με τις προσαρμοσμένες συναρτήσεις Copulas για το έτος 2003. 38
Εικόνα 1-11 Από κοινού και για κάθε σημείο πιθανότητα υπέρβασης μαζί με τις προσαρμοσμένες συναρτήσεις Copulas για τα έτη 2003-2009...39
Εικόνα 1-12 Πιθανότητα υπέρβασης της απόσβεσης για κάθε ζεύξη και από κοινού πιθανότητα από μετρήσεις και συναρτήσεις copulas για δύο επίγειου σταθμούς. 40
Εικόνα 1-13 Πιθανότητα υπέρβασης με και χωρίς διαφορισμό στο πεδίο του χρόνου από δεδομένα και το προτεινόμενο μοντέλο στους 19 GHz...41
Εικόνα 1-14 Πιθανότητα υπέρβασης με και χωρίς διαφορισμό στο πεδίο του χρόνου από δεδομένα και το προτεινόμενο μοντέλο στους 40 GHz...42
Εικόνα 1-15 Πιθανότητα υπέρβασης της απόσβεσης για την περιοχή Spino d'Adda στα 19 GHz ..43
Εικόνα 1-16 Πιθανότητα υπέρβασης της απόσβεσης για την περιοχή Spino d'Adda στα40 GHz ...43
Εικόνα 1-17 Πιθανότητα υπέρβασης της απόσβεσης για την περιοχή Kuala Lumpur στα 12 GHz .44
Εικόνα 1-18 Δυναμική παράμετρος σε συνάρτηση της γωνίας ανύψωσης για την Αθήνα, Ελλάδα.46
Εικόνα 1-19 Παράδειγμα χρονοσειρών απόσβεσης σε ζεύξη μεταξύ Αθήνας και IRIDIUM LEO δορυφόρου στα 20GHz 47
Εικόνα 1-20 Πιθανότητα υπέρβασης της απόσβεσης για ζεύξει μεταξύ Αθήνας, Παρισιού και του δορυφόρου IRIDIUM στα 20 GHz και 40 GHz. 48
Εικόνα 1-21 Παράδειγμα χρονοσειρών απόσβεσης για την περιοχή της Λιουμπλιάνας.................50
Εικόνα 1-22 Αθροιστική κατανομή της απόσβεσης για συστήματα χωρίς καθυστέρηση και με καθυστέρηση ενός λεπτού..50
Εικόνα 1-23 Η συσχέτιση κατά τον Kendall από χρονοσειρές και από θεωρητική έκφραση...........51
Εικόνα 1-24 Πεδία βροχής τις χρονικές στιγμές t_0, t_0 +60 sec και t_0 + 5min 52
Εικόνα 1-25 Πιθανότητα υπέρβασης για μία ζεύξη με τον επίγειο σταθμό τοποθετημένο στη Βιέννη, Αυστρία από την προτεινόμενη μεθοδολογία και τη σύσταση ITU-R. P. 618 53
Εικόνα 1-26 Πιθανότητα υπέρβασης της απόσβεσης και από κοινού πιθανότητα υπέρβασης της απόσβεσης για ένα σύστημα διαφορισμού θέσης..53
Εικόνα 1-27 Παράδειγμα παραγωγής χρονσειρών σπινθηρισμού...55
Εικόνα 1-28 Πιθανότητα υπέρβασης σπινθηρισμού από δεδομένα και χρονοσειρές.......................55
Εικόνα 1-29 Κατανομή φάσματος ισχύος με βάση τη θεωρία και τις παραγόμενες χρονοσειρές 56
Εικόνα 1-30 Γεωμετρία διπλού δορυφορικού συστήματος...57
Εικόνα 1-31 Πιθανότητα αποκοπής λόγω παρεμβολών για τον πρωτεύοντα χρήστη 59
Εικόνα 1-32 Γεωμετρία συστήματος για τη μελέτη του λόγου CNIR..60
Εικόνα 1-33 Πιθανότητα αποκοπής για έναν και δύο παρεμβάλοντες δορυφόρους 61
Εικόνα 1-34 Πιθανότητα αποκοπής της άνω ζεύξης για κινητούς δέκτες στην Ka ζώνη συχνοτήτων 61
Εικόνα 1-35 Πιθανότητα αποκοπής για μία γωνία διαχωρισμού μεταξύ των ζεύξεων ίση με 30^o....63
Εικόνα 1-36 Πιθανότητα αποκοπής για 1, 2 και 3 παρεμβάλοντες χρήστες..................................63

Εικόνα 1-37 Χωρητικότητα αποκοπής για τη Matera, Ιταλίας για συχνότητα 26.5 GHz.................64
Εικόνα 1-38 Χωρητικότητα αποκοπής για τη Matera σε συχνότητα λειτουργίας 40 GHz...............65

Figure 2.1 Specific attenuation coefficient vs. frequency 72
Figure 2.2. Cloud attenuation for a temperate climate 72
Figure 2.3. Exceedance probability of rain rate calculated with ITU-R. P. 837 73
Figure 2.4. CCDF of rain attenuation 74
Figure 2.5. CCDF of rain attenuation 75
Figure 2.6. CCDF of scintillation depth 77
Figure 2.7. CCDF of total attenuation 80
Figure 2.8. CCDF of hitting times 83
Figure 2.9. Dual-site diversity system 92
Figure 2.10. Rain Attenuation time series correlated in space for two sites and the attenuation for the dual site diversity system (selection combining) 92
Figure 2.11. Orbital diversity system with two satellites 93
Figure 3.1. Block Diagram of the M-B model 99
Figure 3.2. A snapshot of rain attenuation time series 99
Figure 3.3. Block Diagram of the Enhanced Maseng-Bakken model 100
Figure 3.4. A snapshot of rain attenuation time series with EMB 101
Figure 3.5. Block Diagram of rain attenuation time series synthesizer for Gamma distributed rain attenuation 103
Figure 3.6. Vertical structure of rain rate in the two-layer model 106
Figure 3.7. (a)CCDF of ILWC for Athens from Time series and theoretical, (b) Snapshot of ILWC time series, (c) Snapshot of clouds attenuation 114
Figure 3.8. Block diagram of generating IWVC time series 115
Figure 3.9. Block diagram of scintillation time series synthesizer 117
Figure 3.10. Block diagram for generating total tropospheric attenuation time series a) ITU-R. P. 1853 and b) Resteghini method derived from (ITU-R. P. 1853, 2012) and (Resteghini, 2014), respectively 119
Figure 4.1. CCDF of Rain Rate for Prague, Czech republic 124
Figure 4.2. CCDF of Rain Rate for Athens, Greece 124
Figure 4.3. CCDF of Rain Rate for Tokyo, Japan 125
Figure 4.4. CCDF of Rain Rate for Rio de Janeiro, Brazil 125
Figure 4.5. CCDF of Rain Rate for Austin, U.S. 126
Figure 4.6. CCDF of Rain Rate for Yamguchi, Japan 126
Figure 4.7. CCDF of rain attenuation for Clarksburg, U.S. 127
Figure 4.8. CCDF of rain attenuation for Spino d'Adda, Italy. 128
Figure 4.9. CCDF of rain attenuation for UniTech Lae, Papua New Guinea 128
Figure 4.10. CCDF of rain attenuation for a LOS terrestrial link at Mendlesham, GB. 129
Figure 4.11. CCDF of rain attenuation for a LOS terrestrial link at Darmstadt, Germany 129
Figure 4.12. CCDF of rain attenuation for a LOS terrestrial link located at Tokyo, Japan 130
Figure 4.13. CCDF of rain rate for the region of Athens, Greece, derived from ITU-R. P. 837-6 (red dashed line) used for the fitting of IG distribution (blue solid line). 131
Figure 4.14 CCDF of rain rate for the region of Yamaguchi, Japan, derived from DBSG3 (red circles) used for the fitting of IG distribution (blue solid line). 131
Figure 4.15. Earth-space link geometry 132
Figure 4.16 Mean error of IG model (red circles) and ITU-R. P. 530-14 (black crosses) 136
Figure 4.17 Standard deviation of the error of IG model (red circles) and ITU.R P. 530-14 (black crosses) 137
Figure 4.18 RMS error of IG model (red circles) and ITU-R. P. 530-14 (black crosses) 137
Figure 4.19 Mean value of the error for the IG model and the ITU-R. P. 618 model 138
Figure 4.20 Standard deviation of the error for the IG model and the ITU-R. P. 618 model 139
Figure 4.21 RMS value of the error for the IG model and the ITU-R. P. 618 model 139

Figure 4.22 CCDF of rain attenuation derived from the application of SST (solid line) on measured rain rate times series in NTUA, site 1 (Ku band), from the IG model (dashed line) and ITU-R. P. 618-10 (dash-dotted line). 141
Figure 4.23 CCDF of rain attenuation derived from the application of SST (solid line) on measured rain rate times series in NTUA, site 2 (Ka band), from the IG model (dashed line) and ITU-R. P. 618-10 (dash-dotted line). 142
Figure 4.24 CCDF of rain attenuation for Bangkok, Thailand with f=20GHz and $\theta=30^o$ curve from ITU-R. P. 618 (o) and the IG fitted curve (solid line) with parameters μ_A=0.2656 dB and $\lambda_A=8.4\cdot 10^{-3}$ dB 144
Figure 4.25 CCDF of rain attenuation for La Conception, Canada for f=13GHz and $\theta=18^o$ with curve from DBSG3 database (o) and the IG distribution (solid line) with parameters μ_A=0.0209 dB and $\lambda_A=2.99\cdot 10^{-4}$ dB 145
Figure 4.26. Experimental data (+) and simulated (solid line) joint CCDF of rain attenuation for two Earth stations with a distance 22.7 km, f=13GHz and $\theta=18^o$ located at La Conception and Vernet, in Canada 147
Figure 4.27 Experimental (+) and simulated (solid line) joint CCDF of rain attenuation for two Earth stations with a distance 10.9 km, operating frequency 11.4GHz and elevation angle 33^o located at Graz and Michelbachberg, in Austria 147
Figure 4.28 Mean value of the error (%) for every time percentage for the proposed model (o) and ITU-R. P. 618 (+) 149
Figure 4.29 Standard deviation of the error (%) for every time percentage for the proposed model (o) and ITU-R. P. 618 (+) 150
Figure 4.30 RMS value of the error (%) for every time percentage for the proposed model (o) and ITU-R. P. 618 (+) 150
Figure 4.31 Geometry of a site diversity system 151
Figure 4.32 Outage probability for MRC and SC diversity systems with 60^o and 90^o separation angle and the corresponding single link, in Athens, Greece. 155
Figure 4.33 Outage probability for MRC and SC diversity systems with 80^o and 120^o separation angle and the corresponding single link in Seoul, South Korea. 156
Figure 4.34. Joint and single statistics of rain rate from experiments at UK and the fitted Copula expressions for a single year 2003 158
Figure 4.35 Joint and single statistics of rain rate from experiments at UK and the fitted Copula expressions for 7 years (2003-2009) 158
Figure 4.36. Joint and single statistics of rain rate from experiment at Athens and the fitted Copula expressions for 1 year (2010-2011) 159
Figure 4.37 Joint and single statistics of rain attenuation from experimental data for two Earth stations at St. Jovite and Arundel of Canada 160
Figure 4.38 Joint and single statistics of rain attenuation from experimental data for two Earth stations at Palmetto of US. 160
Figure 4.39 Joint and single statistics of rain attenuation from experimental data for two Earth stations at Atlanta of US 161
Figure 4.40 Joint and single statistics of rain attenuation from synthesized data using SST for Gera Lario of Italy 161
Figure 4.41 CCDF of rain attenuation for a single link with and without time diversity derived from the proposed model and from simulations 164
Figure 4.42 CCDF of rain attenuation for a link without time delay and for various delays. 165
Figure 4.43. Gain achieved with the adoption of time diversity for 0.01% and 1% time percentages 166
Figure 4.44. CCDF of rain attenuation with and without TD derived from data and the proposed model for Spino d'Adda at 19 GHz 166

Figure 4.45. CCDF of rain attenuation with and without TD derived from data and the proposed model for Spino d'Adda at 40 GHz 167
Figure 4.46. Time diversity gains for Paris, France for various elevation angles 168
Figure 4.47. Time diversity gains for Tampa, Florida for various elevation angles 168
Figure 4.48 Time diversity prediction performance in Spino d'Adda at 19GHz 170
Figure 4.49Time diversity prediction performance in Spino d'Adda at 40GHz 170
Figure 4.50 Time diversity prediction performance in Kuala Lumpur, at 12GHz 171
Figure 5.1 Rain attenuation dynamic parameter vs elevation angle for Athens, Greece for different values of *g* parameter and frequency of the link 179
Figure 5.2 Rain attenuation autocorrelation functions for various time delays and elevation angles. 180
Figure 5.3 Rain attenuation autocorrelation functions for various frequencies and elevation angles 181
Figure 5.4 Rain attenuation autocorrelation functions for various values of *G* parameter and elevation angles 181
Figure 5.5 Flow diagram for the generation of time series of rain attenuation for LEO links. 184
Figure 5.6 Snapshot of time series of rain attenuation during one orbit of the IRIDIUM, in Athens, at 20GHz 187
Figure 5.7 CCDF of rain attenuation for LEO links between IRIDIUM satellite and ground stations Athens, Paris, for *f*=20GHz (blue lines and green lines, respectively) and *f*=40GHz (red lines and black lines, respectively) derived from theoretical calculations (solid lines) and from time series (dashed lines) 187
Figure 5.8. Rain attenuation time series snapshot for a pass of the MEO satellite of O3b constellation with the Earth station located at Athens, Greece 188
Figure 5.9. CCDF of rain attenuation for an Earth-MEO link with the Earth station located at Athens, Greece 189
Figure 5.10. CCDF of rain attenuation for an Earth-MEO link with the Earth station located at Kuala Lumpur, Malaysia 189
Figure 5.11. CCDF of fade slope (dB/s) for links between IRIDIUM satellite and ground stations in Athens and Paris for rain attenuation threshold 5 dB and two different frequencies 20 GHz and 40 GHz. For Athens Δt= 5 sec and for Paris Δt= 1 min 190
Figure 5.12 CCDF of rain attenuation for a ground station at Ljubljana from experiments and from copula fitting for 15 and 60 min time delays 192
Figure 5.13 Copula parameter as a function of time delay 192
Figure 5.14. Copula parameter from (5.28) and from the experiments 193
Figure 5.15 Copula parameter from (4) and from the experiments. 193
Figure 5.16 Time series of rain attenuation for a ground station in Ljubljana using the proposed synthesizer 195
Figure 5.17 CCDF of rain attenuation for zero time delay from time series synthesizer and the theoretical values and the joint CCDF of rain attenuation for 1 min time delay 196
Figure 5.18 Kendall's τ correlation from time series and theoretical expression 196
Figure 5.19. Rain rate fields at time t_0 (a), t_0+60 sec (b) and t_0+5 min 198
Figure 5.20 CCDF of rain rate and joint CCDF of rain rate 199
Figure 5.21. CCDF of rain attenuation for Vienna, Europe derived from simulations (red line) and ITU-R. P. 618 (blue line) 200
Figure 5.22 CCDF of Rain Attenuation at Wallops Island 200
Figure 5.23 CCDF of Rain Attenuation at Wakkanai, Japan 201
Figure 5.24 Single site and joint for site diversity systems CCDFs of rain attenuation 201
Figure 5.25 Single site and joint for orbital diversity systems CCDFs of rain attenuation 202
Figure 5.26 Simulated scintillation time series snapshots using the parameters for experiment no.1 205

Figure 5.27 Simulated scintillation time series snapshots using the parameters for experiment no.2 206
Figure 5.28 Simulated and theoretical CCDF of the absolute value of scintillation....206
Figure 5.29 PSD derived from the time series generator for experiment no. 1....207
Figure 5.30 PSD derived from the time series generator for experiment no. 2....207
Figure 5.31 Time series of fractional Brownian motion with Hurst index 0.25....208
Figure 5.32 Time series of fractional Brownian motion with Hurst index 0.5....209
Figure 5.33 Time series of fractional Brownian motion with Hurst index 0.75....209
Figure 6.1 Geometry of a dual Cognitive SatCom system....212
Figure 6.2 Spatially correlated time series of rain attenuation for two convergent links....214
Figure 6.3. Spatially correlated time series of rain attenuation for the four links....216
Figure 6.4 Correlated *SIR* time series for both users....216
Figure 6.5 Outage probability due to interference for the incumbent user....217
Figure 6.6. Outage probability due to interference for the cognitive user....218
Figure 6.7 CDF of *SIR* given that rain attenuation does not exceed the marginal values corresponding to five different time percentages for the incumbent user....218
Figure 6.8. CDF of *SIR* given that rain attenuation does not exceed a marginal value for four different separation angles for the incumbent user. 219
Figure 6.9 Configuration of the interference Scenarios. 221
Figure 6.10 CDF of downlink CNIR at Ka Band....224
Figure 6.11 CDF of downlink CNIR for multiple inteferring satellites at Ku band....224
Figure 6.12 CDF of uplink CNIR for ESOMPS at Ka Band....225
Figure 6.13 CDF of uplink CNIR at uplink for multiple interfering ESOMPS at Ku Band. 226
Figure 6.14 *SNIR* statistics for a separation angle of 30^o and one FSS interfering link: Theoretical vs. Simulation results....230
Figure 6.15 *SNIR* statistics for a separation angle of 30^o and for different cities: Impact of climatic conditions....230
Figure 6.16 *SIR* statistics considering one FSS interfering link: Theoretical vs. simulation results and impact of separation angle. 231
Figure 6.17. *SNIR* statistics considering the co-existence of 1, 2 and 3 FSS interfering links....232
Figure 6.18. SIR statistics for 1 and 2 FSS interfering links. 232
Figure 6.19: Outage capacity given that the link is available for Matera at Ka band: a) All time percentages b) Larger than 10^{-4} 239
Figure 6.20: Outage capacity given that the link is available for Svalbard at Ka band: a) All time percentages b) Larger than 10^{-4} 240
Figure 6.21: Outage capacity given that the link is available for Weilheim at Ka band: a) All time percentages b) Larger than 10^{-4} 241
Figure 6.22 Outage capacity, given that the link is available, for Matera at Q band....242
Figure 6.23 Outage Capacity, given that the link is available, for Svalbard at Q band: a) All time percentages, b) Larger than 10^{-4} 243
Figure 6.24: Outage capacity, given that the link is available, for Weilheim at Q band....244

Περίληψη

Η παρούσα Διατριβή επικεντρώνεται στη μελέτη ασύρματων επίγειων και δορυφορικών συστημάτων επικοινωνιών νέας γενιάς τα οποία προσφέρουν υψηλές ταχύτητες μετάδοσης. Πιο συγκεκριμένα, τα αποτελέσματα τα οποία παρουσιάζονται επικεντρώνονται κυρίως στη μοντελοποίηση καναλιού, η οποία και απαιτείται πρώτον για την αξιόπιστη σχεδίαση των συστημάτων νέας γενιάς και δεύτερον για την αξιολόγηση της επίδοσης των. Η παρούσα Διατριβή επικεντρώνεται σε ραδιο-συστήματα τα οποία λειτουργούν σε συχνότητες πάνω από 10 GHz, δηλαδή στην Ka ζώνη συχνοτήτων, εφ' όσον το ελεύθερο εύρος ζώνης προς χρήση για μελλοντικά συστήματα είναι μεγαλύτερο από αυτό στις ζώνες συχνοτήτων L- και S-.και C. Σε τέτοιες υψηλές συχνότητες, τα φαινόμενα που λαμβάνουν χώρα στην ατμόσφαιρα επηρεάζουν το διαδιδόμενο σήμα, προκαλώντας τόσο την απόσβεση αυτού όσο και σπινθηρισμούς στο πλάτος αυτού με αποτέλεσμα τη μείωση της απόδοσης των συστημάτων. Στην Ka(20/30GHz) ζώνη συχνοτήτων, η βροχόπτωση αποτελεί τον κυριότερο παράγοντα εξασθένισης και για το λόγο αυτό η Διατριβή επικεντρώνεται κυρίως στη μοντελοποίηση της απόσβεσης λόγω βροχόπτωσης. Η απόσβεση η οποία εισάγεται στο σύστημα λόγω των ατμοσφαιρικών φαινομένων αντιμετωπίζεται είτε χρησιμοποιώντας ένα σταθερό περιθώριο κέρδους στη σχεδίαση του συστήματος είτε χρησιμοποιώντας τεχνικές άμβλυνσης διαλείψεων (ΤΑΔ). Παρ' όλα αυτά, από τη στιγμή που η ατμοσφαιρική απόσβεση εισάγει αρκετά dB απόσβεσης για μικρό χρονικό διάστημα, η χρήση ενός σταθερού περιθωρίου στον ισολογισμό ισχύος αποτελεί μία τεχνική ιδιαίτερα ακριβή και για το λόγο αυτό οι ΤΑΔ είναι υποχρεωτικές για τη σχεδίαση αποδοτικών συστημάτων. Οι ΤΑΔ αποτελούνται από τεχνικές διαφορισμού και προσαρμοστικές τεχνικές. Επομένως, η χρήση αυτών εξαρτάται από τα στατιστικά χαρακτηριστικά πρώτης τάξης του καναλιού καθώς και από τα δυναμικά χαρακτηριστικά του. Και τα δύο στατιστικά χαρακτηριστικά της απόσβεσης λόγω βροχής εξετάζονται λεπτομερώς στην παρούσα Διατριβή.

Αρχικά στο πρώτο κεφάλαιο στην παρούσα Διατριβή παρουσιάζονται τα φαινόμενα διάδοσης τα οποία επηρεάζουν τα σήματα σε υψηλές συχνότητες και δίνονται τα κυριότερα μοντέλα διάδοσης από τη βιβλιογραφία. Στο τέλος του πρώτου κεφαλαίου, περιγράφονται οι ΤΑΔ και οι τεχνολογίες που πρόκειται να χρησιμοποιηθούν στα ραδιο-συστήματα νέας γενιάς. Δεδομένης της χρησιμότητας και της κρισιμότητας της αξιόπιστης περιγραφής των δυναμικών χαρακτηριστικών του καναλιού για τη σχεδίαση ενός συστήματος που κάνει χρήση προσαρμοστικών ΤΑΔ, το δεύτερο κεφάλαιο είναι κυρίως αφιερωμένο στην περιγραφή των μοντέλων για την παραγωγή χρνοσειρών τροποσφαιρικής απόσβεσης που έχουν αναπτυχθεί τα τελευταία χρόνια.

Στο τρίτο κεφάλαιο της Διατριβής, παρουσιάζονται μοντέλα, που προέκυψαν από την έρευνα στα πλαίσια της διδακτορικής μελέτης, τα οποία αναπαράγουν τα χαρακτηριστικά πρώτης τάξης της απόσβεσης βροχής. Πιο συγκεκριμένα, η κατανομή Inverse Gaussian (IG) προτείνεται για τη μοντελοποίηση των αθροιστικών κατανομών της

έντασης βροχόπτωσης και της απόσβεσης βροχής και αναπτύχθηκε ένα μοντέλο πρόβλεψης της πιθανότητας υπέρβασης της απόσβεσης λόγω βροχής, δεδομένου ότι η κατανομή της έντασης βροχόπτωσης είναι γνωστή. Επιπλέον, προτείνονται δύο μοντέλα βασισμένα στη διδιάστατη κατανομή IG για την πρόβλεψη της από κοινού πιθανότητας υπέρβασης της απόσβεσης λόγω βροχής σε δύο χωρικά συσχετισμένες ζεύξεις για δορυφορικά και επίγεια συστήματα. Για τις τεχνικές διαφορισμού, οι συναρτήσεις copulas εξετάζονται και αξιολογούνται για τη μοντελοποίηση και αναπαραγωγή των από κοινού χαρακτηριστικών πρώτης τάξης της έντασης βροχόπτωσης και της απόσβεσης λόγω βροχής για τις τεχνικές του διαφορισμού στο πεδίο του χώρου και του χρόνου. Τέλος, χρησιμοποιώντας τις υποθέσεις του μοντέλου Maseng-Bakken, παρουσιάζεται μία θεωρητική έκφραση για τη μοντελοποίηση της από κοινού αθροιστικής κατανομής της απόσβεσης λόγω βροχής σε δορυφορικά συστήματα που κάνουν χρήση της τεχνικής διαφορισμού στο χρόνο.

Στο τέταρτο κεφάλαιο παρουσιάζονται μοντέλα των δυναμικών χαρακτηριστικών της απόσβεσης λόγω βροχής και των σπινθηρισμών λόγω τροποσφαιρικών στροβιλισμών. Αρχικά, εξήχθη έκφραση υπολογισμού της δυναμικής παραμέτρου της απόσβεσης σαν συνάρτηση των γεωμετρικών και ηλεκτρικών χαρακτηριστικών της ζεύξης καθώς και τν στατιστικών χαρακτηριστικών της έντασης βροχόπτωσης. Εν συνεχεία, γίνεται μία επέκταση του μοντέλου Maseng-Bakken για την παραγωγή χρονοσειρών της απόσβεσης βροχής για ζεύξεις μεταξύ επίγειου σταθμού και δορυφόρων μεσαίας ή χαμηλής τροχιάς. Η ιδιαιτερότητα που παρουσιάζουν οι ζεύξεις αυτές σε σύγκριση με τις ζεύξεις με γεωστατικούς δορυφόρους είναι ότι η γωνία ανύψωσης αυτών είναι χρονικά μεταβαλλόμενη και ως εκ τούτου οι παράμετροι του μοντέλου Maseng-Bakken, επίσης χρονικά μεταβαλλόμενες. Πάνω στο ίδιο πρόβλημα παρουσιάζεται αναλυτική έκφραση υπολογισμού της μεταβολής της απόσβεσης για αυτές τις ζεύξεις. Επίσης, για ζεύξεις με γεωστατικούς δορυφόρους, παρουσιάζεται μία μεθοδολογία για την παραγωγή χρονοσειρών απόσβεσης λόγω βροχής βασιζόμενη στις συναρτήσεις copulas και μία μέθοδο βασιζόμενη σε Στοχαστικές Διαφορικές Εξισώσεις (ΣΔΕ) για την παραγωγή χρονοσειρών δισδιάστατων πεδίων βροχής, από τα οποία μπορεί να υπολογιστούν χρονοσειρές απόσβεσης για μία ή πολλαπλές ζεύξεις. Το τελευταίο μοντέλο του κεφαλαίου αφορά στην παραγωγή χρονσειρών του σπινθηρισμού του πλάτους και βασίζεται στη θεωρία των ΣΔΕ με fractional κίνηση Brown.

Στο πέμπτο κεφάλαιο, αξιολογούνται σενάρια συνύπαρξης διαφορετικών δορυφορικών υπηρεσιών υπό βροχή μελετώντας την επίδραση των παρεμβολών. Επιπλέον, αναπτύχθηκαν αναλυτικές εκφράσεις για μοντέλα καναλιού για τον υπολογισμό της πιθανότητας αποκοπής σε συστήματα με επίγειους σταθμούς σε κινητές πλατφόρμες για τη μελέτη της επίδρασης παρεμβολών τόσο στην άνω όσο και στην κάτω ζεύξη για έναν ή πολλαπλούς παρεμβάλλοντες χρήστες. Επίσης, μελετάται το σενάριο συνύπαρξης μία ασύρματης επίγειας ζεύξης και μίας δορυφορικής ζεύξης. Τέλος, μελετάται η απόδοση της κάτω ζεύξης ενός δορυφορικού συστήματος παρατήρησης Γης το οποίο λειτουργεί στην Ka και Q ζώνη συχνοτήτων και κάνει χρήση της τεχνικής προσαρμοσμένης

κωδικοποίησης και διαμόρφωσης. Ακολουθούν συμπεράσματα και προτάσεις για μελλοντική έρευνα.

Λέξεις κλειδιά: δορυφορικά συστήματα, μοντελοποίηση καναλιού, απόσβεση λόγω βροχής, στοχαστικές διαφορικές εξισώσεις, copulas, τεχνικές άμβλυνσης διαλείψεων, , παρεμβολές, υψηλές συχνότητες.

Abstract

The scope of this Thesis is the study of high data rate next generation wireless terrestrial and satellite communication systems. In particular, the research results presented in this Thesis are mainly concentrated on the channel modeling issue which are required for the reliable and accurate design of these systems and then to the evaluation of their performance for many applications. In this Thesis, the attention is directed to the radio systems which operate at frequencies above 10 GHz, i.e. Ka-band, since there is a small number of systems and services provided at these bands and so the available bandwidth is higher than this of L- and S- bands, leading to the achievement of higher data rates to the users. In frequencies above 10 GHz, the atmosphere affects the propagated signal causing its attenuation and scintillation and so the degradation of link's performance. At the Ka-band, rainfall is the dominant fading mechanism and so this Thesis is mostly concentrated on the modeling of rain attenuation. The attenuation which is inserted into the system due to tropospheric attenuation can be either compensated with static fade margins or using fade mitigation techniques (FMTs). However, since the tropospheric attenuation exceeds several dBs for a small time percentage, the static margin is cost inefficient and so the FMTs are mandatory for the efficient design of the system. The FMTs consist of diversity schemes and adaptive techniques. Such techniques depend on the first order statistics of the channel and its dynamics. Both statistical characteristics of rain attenuation are rigorously examined in the present Thesis.

Firstly, the propagation phenomena which affect the signal at high frequencies are briefly presented and explained and a state of the art on the propagation models is given. At the end of the first Chapter, the FMTs and a number of technologies which are considered for the next generation radio systems are briefly described. Due to the importance of time series synthesizers of tropospheric attenuation, the second Chapter is devoted to the description and presentation of a high number of synthesizers which have been developed at the past years.

In the third Chapter the models developed at the framework of this Thesis for capturing the first order statistics of rain attenuation are presented. More particularly, the Inverse Gaussian (IG) distribution is proposed for the modeling of rain rate and rain attenuation cumulative distribution functions and a prediction model of the exceedance probability of rain attenuation, given that the cumulative distribution of rain rate is known, is presented. Two models based on the bivariate IG distribution are also proposed for modeling the joint exceedance probability of rain attenuation induced in spatially separated links at satellite communications (site diversity) and wireless terrestrial systems (route diversity). Considering the diversity schemes, copula functions are examined for their capability to model and capture the joint statistics of rain attenuation for spatial diversity and time diversity schemes. Finally, using the theoretical assumptions of the well-known

Maseng-Bakken (M-B) model, a theoretical expression for the calculation of the unbalance cumulative distribution function of rain attenuation in time diversity schemes is presented.

The fourth Chapter of the Thesis is devoted to the presentation of the models of dynamics and synthesizers of rain attenuation and scintillation time series developed at the framework of this Thesis. Firstly, a theoretical expression for the calculation of the dynamic parameter of rain attenuation (and so its autocorrelation function can be derived) as a function of the dynamic parameter of rain rate, the geometrical and electrical characteristics of the link is derived. Also, the M-B model is extended for time dependent parameters of rain attenuation in order to generate rain attenuation time series for links between a ground station and a Medium Earth Orbit (MEO) or a Low Earth Orbit (LEO) satellite. A second synthesizer based on copula functions for rain attenuation induced on Earth-GEO links is proposed. The advantage of such synthesizer is that it depends on the Kendall's tau correlation on temporal domain which is mainly used for capturing the dependence of random variables and it is independent on the choice of the choice of the distribution of rain attenuation, since even empirical cumulative distributions can be used. A space-time rain rate synthesizer is also proposed using multi-dimensional stochastic differential equations (SDEs) for generating two-dimensional rain rate fields correlated on temporal domain. Such synthesizer can be used for the evaluation of multi-antenna satellite and wireless terrestrial systems. Finally, a scintillation time series synthesizer based on SDEs driven by fractional Brownian motion is presented. The synthesizer reproduces the desired power spectrum and the first order statistics of scintillation due to tropospheric turbulence.

In the fifth Chapter of the Thesis, the performance of coexisting and cognitive satellite and wireless terrestrial communication systems is examined. Using interference analysis, dual cognitive systems under rain are studied through the calculation of Signal-to-Interference (SIR) ratio with theoretical expressions and simulations. Moreover, since mobile terminals are gaining a lot of attention and interest for operating at Ka-band, the scenario of coexistence and spectrum share with fixed satellite services is studied through the Signal-to-Noise-plus Interference ratio (SNIR) and theoretical expressions are given for this metric for single interferer case and for a multi-dimensional SDE is proposed for the case of multiple interferers. Also, the fixed services and fixed satellite services are examined for cognitive use through the analysis of SNIR. Finally, the performance of an Earth Observation system using the technique of adaptive coding and modulation is studied.

In the last Chapter of this Thesis, some general and interesting conclusions are drawn and presented and finally ideas for future work based on the models and the research results of this Thesis are given.

Keywords: satellite systems, mmWaves, channel modeling, rain attenuation, stochastic differential equations, copulas, FMT, ESOMPs, cognitive satellite, interference.

Ευχαριστίες

Με την παρούσα παράγραφο, θα ήθελα να εκφράσω τις ευχαριστίες μου σε όλα εκείνα τα άτομα τα οποία συνέβαλαν είτε με συμβουλευτικό ρόλο, είτε μέσω συνεργασιών ή μέσω ηθικής υποστήριξης στο να ολοκληρωθεί η παρούσα διατριβή.

Πρώτα, θα ήθελα να ευχαριστήσω τον επιβλέποντα της παρούσας Διατριβής, τον κύριο καθηγητή Αθανάσιο Δ. Παναγόπουλο και αρχικά για την αποδοχή μου ως υποψήφιο διδάκτορα της σχολής και της εμπιστοσύνης που μου έδειξε. Ο κύριος Παναγόπουλος με την εξαίρετη γνώση του πάνω στο αντικείμενο της διατριβής και τη διαρκή του ενασχόληση με το συγκεκριμένο πεδίο βοήθησε στην εκπλήρωση της διατριβής μέσω των εύστοχων παρατηρήσεων, συμβουλών και παρακινήσεών του. Θα ήθελα επιπλέον να τον ευχαριστήσω για την ευκαιρία που μου έδωσε να εργαστώ πάνω σε ιδιαίτερα ενδιαφέροντα ερευνητικά προγράμματα επιτρέποντας μου με αυτό τον τρόπο να εμπλουτίσω τις γνώσεις μου πάνω στο αντικείμενο της Διατριβής αλλά και να έχω την απαραίτητη οικονομική υποστήριξη για την εκπόνηση της Διατριβής αυτής. Τέλος, η ηθική του γύρω από την εργασία, ο σεβασμός του απέναντι στην ακαδημαϊκή έρευνα και η εμπειρία του στην επίβλεψη συνέβαλαν στη δημιουργία ενός κατάλληλου περιβάλλοντος για την εκπόνηση της έρευνας στα πλαίσια της Διατριβής.

Επιπλέον, θα ήθελα να ευχαριστήσω τον κύριο καθηγητή Ιωάννη Δ. Κανελλόπουλο, αρχικά, για την αποδοχή να είναι μέρος της συμβουλευτικής επιτροπής και επιπλέον για τις συμβουλές και συζητήσεις γύρω από το αντικείμενο της Διατριβής. Τα μαθήματα του κυρίου Κανελλόπουλου αποτέλεσαν έμπνευση για εμένα και αιτία για να κάνω τη διατριβή μου πάνω στο παρόν ερευνητικό αντικείμενο. Θα ήθελα να ευχαριστήσω και το τρίτο μέλος της συμβουλευτικής επιτροπής, τον κύριο Σπύρο Βεντούρα, για την αποδοχή να είναι μέλος της συμβουλευτικής επιτροπής και της εμπιστοσύνης που μου έδειξε στη συνεργασία μας. Τέλος, θα ήθελα να εκφράσω και τις ευχαριστίες μου και στα υπόλοιπα 4 μέλη της εξεταστικής επιτροπή, τους καθηγητές Γεώργιο Φικιώρη, Γεώργιο Ευθύμογλου και Γιώργο Τσούλο και τον Δρ. Andrej Vilhar για τη σύμφωνη γνώμη τους στην αναγόρευσή μου ως Διδάκτωρ της σχολής.

Θα ήθελα επίσης να ευχαριστήσω και τους συνεργάτες κατά τη διάρκεια των μεταπτυχιακών σπουδών μου, τους κύριους καθηγητές Σπύρο Λιβιεράτο και Γεώργιο Χατζαράκη, τον Δρ. Σωτήριο Κανελλόπουλο, Δρ. Βασίλειο Σακαρέλλο, Δρ. Δημήτριο Σκραπαρλή, Δρ. Παντελή Αράπογλου, Δρ. Γεώργιο Καραγιάννη, Δρ. Κωνσταντίνο Λιώλη, Δρ. Σταυρούλα Βασσάκη, Δρ. Μάριο Πουλάκη, Δρ. Γεώργιο Πιτσιλαδή, Δρ. Νεκτάριο Μωραΐτη και τον Σταύρο Σαγκριώτη. Με τη συνεργασία μας σε επαγγελματικό επίπεδο και την υποστήριξη σε ηθικό και προσωπικό επίπεδο κατάφερα να φέρω εις πέρας την έρευνά μου. Η ηθική των ατόμων και των συνεργατών είναι αυτή που σε μία έντονη προσπάθεια κάνουν ευχάριστο το δρόμο προς την επίτευξη του σκοπού στο χώρο της εργασίας. Θα ήθελα να ευχαριστήσω επίσης και τους υποψήφιους διδάκτορες Νικόλαο Λύρα, Αποστόλη Παπαφραγκάκη και Αργύρη Ρουμελιώτη για τη συνεργασία μας. Τους εύχομαι ολόψυχα καλή επιτυχία στην εκπόνηση της διατριβής τους.

Θα ήθελα, όμως να εκφράσω την ευγνωμοσύνη μου στα άτομα εκτός εργασίας, με τα οποία μοιραστήκαμε προσωπικές στιγμές, προσωπικές σκέψεις και ανησυχίες και κατεύνασαν την αγωνία για το μέλλον και φυσικά έκαναν ευχάριστη την καθημερινότητά μου. Τις ευχαριστίες μου, λοιπόν, στους Άγγελο, Παναγιώτη, Άγγελο, Παναγιώτη, Πάττυ, Κώστα, Καρολίνα, Κλαίρη, Βάλια, τον Ιωάννη Γιαννούλη, το Δρ. Ιωάννη Λαζάρου, τον Δημήτριο Καλαβρουζιώτη, τον Βασίλειο Κατωπόδη, τον Παναγιώτη Γκρούμα, Δημήτρη Τράκα, Ιάσονα Κουβελιώτη-Λυσίκατο και τον Δρ. Γεώργιο Ορφανό.

Τέλος, να ευχαριστήσω ιδιαίτερα την οικογένειά μου, τη μητέρα μου, Ελένη Κορομβόκη, τον πατέρα μου, Ηλία Κουρόγιωργα και τον αδερφό μου, Γεώργιο Κουρόγιωργα. Η υποστήριξή τους στα πρώτα μου βήματα ως υποψήφιος Διδάκτορας τόσο οικονομικά όσο και ψυχικά μου έδωσαν τις βάσεις για να συνεχίσω και να επιτύχω το στόχο μου. Το πλέον σίγουρο είναι ότι η οικογένεια μου με οδήγησε σε αυτήν την επιτυχία. Οι θυσίες τους για τη μόρφωσή μου απέδωσαν την παρούσα μελέτη και την ικανοποίησή μου για αυτή.

1. Μοντελοποίηση Καναλιού και Αξιολόγηση της Επίδοσης Ασύρματων Επίγειων και Δορυφορικών Συστημάτων Μετάδοσης Νέας Γενιάς

1.1 Εισαγωγή

Η αύξηση της ζήτησης του όγκου δεδομένων και οι νέες εφαρμογές των επικοινωνιών τόσο στην καθημερινή μας ζωή όσο και στη βελτίωση της ποιότητας της ζωής μας, οδήγησαν στην αύξηση της ζήτησης υψηλών ταχυτήτων μετάδοσης δεδομένων. Το 2010, δημοσιοποιήθηκε η Ευρωπαϊκή ψηφιακής Ατζέντα, κατά την οποία έχουν τεθεί δύο στόχοι σε πανευρωπαϊκό επίπεδο. Ο πρώτος είναι η κάλυψη του 100% του πληθυσμού με ευρυζωνικές επικοινωνίες με ταχύτητες των 30Mbps και άνω, οπουδήποτε και ο δεύτερος, τουλάχιστον το 50% των νοικοκυριών να μπορούν να εξυπηρετούνται με ταχύτητες πάνω από 100% [DigAgenda10]. Για την επίτευξη των στόχων αυτών χρειάζεται η συνέργεια των ενσύρματων και ασύρματων δικτύων. Τα ενσύρματα μέσα μετάδοσης μπορεί να είναι είτε η οπτική ίνα είτε καλώδια χαλκού. Παρ' όλα αυτά, η εγκατάσταση αυτών μπορεί να είναι ιδιαίτερα ακριβή και αργή σε περίπτωση που δεν υπάρχει στην περιοχή ήδη κάποιο δίκτυο υποδομής. Για τον παραπάνω λόγο καθώς και για την μετάδοση δεδομένων οπουδήποτε πρέπει να γίνεται χρήση και των επίγειων ασυρμάτων επικοινωνιών και των δορυφορικών επικοινωνιών. Επιπλέον, σε όλες τις χώρες υπάρχουν περιοχές στις οποίες είτε υπάρχει ένα δίκτυο επικοινωνιών το οποίο προσφέρει χαμηλές ταχύτητες είτε δεν υπάρχει καθόλου δίκτυο. Τέτοιες περιοχές μπορεί να είναι είτε αγροτικές περιοχές είτε ορεινές ή και νησιά. Στην Ελλάδα υπάρχουν και οι τρεις τύποι των περιοχών αυτών. Σε τέτοιες περιοχές, οι δορυφορικές επικοινωνίες μπορούν να εξυπηρετήσουν πιο εύκολα τους χρήστες.

Το ενδογενές μεγαλύτερο πλεονέκτημα των δορυφορικών επικοινωνιών είναι η εκτεταμένη περιοχή κάλυψης που μπορούν να προσφέρουν. Οι τύποι των δορυφόρων που χρησιμοποιούνται μπορούν να κατηγοριοποιηθούν με βάση την τροχιά τους και είναι οι: α) γεωστατικοί δορυφόροι, οι οποίοι φαίνονται σαν σταθερά σημεία στον ορίζοντα από ένα σταθερό χρήστη στο έδαφος, β) οι δορυφόροι υψηλής τροχιάς, οι οποίοι μπορούν να χρησιμοποιηθούν σε ελλειπτική τροχιά για κάλυψη των πόλων, γ) οι δορυφόροι μεσαίας τροχιάς, οι οποίοι έχουν κερδίσει το ενδιαφέρον της κοινότητας των δορυφορικών επικοινωνιών ύστερα από το επιτυχημένο σύστημα της O3b [O3b] και δ) οι δορυφόροι χαμηλής τροχιάς οι οποίοι χρησιμοποιούνται είτε στα συστήματα παρατήρησης Γης [Toptisidis12] είτε για υπηρεσίες φωνής λόγω της χαμηλής καθυστέρησης μετάδοσης σε σχέση με τις άλλες τροχιές. Αν και το μεγαλύτερο πλεονέκτημα των δορυφόρων είναι η υψηλή περιοχή κάλυψης, το μειονέκτημά τους είναι η υψηλή καθυστέρηση για τη μετάδοση των δεδομένων λόγω της υψηλής απόστασης που έχουν από τους επίγειου χρήστες. Για το λόγο αυτό στο σύστημα O3b χρησιμοποιούνται αστερισμοί δορυφόρων για τη μείωση της καθυστέρηση αυτής.

Επιπλέον για τις ασύρματες επικοινωνίες και για την προσφορά υπηρεσιών υψηλών ταχυτήτων οπουδήποτε, χρειάζεται και η συνεργασία μεταξύ επίγειων ασύρματων και δορυφορικών δικτύων. Το πλέον επιτυχημένο παράδειγμα ασύρματων επίγειων επικοινωνιών είναι τα συστήματα κινητών επικοινωνιών, τα οποία πλέον με την ανάπτυξη των συστημάτων $4^{ης}$ γενιάς προσφέρουν υψηλές ταχύτητες μετάδοσης δεδομένων. Ασύρματες επικοινωνίες υψηλών ταχυτήτων χρησιμοποιούνται στη μετάδοση δεδομένων για δίκτυα κορμού, τα οποία όμως είναι ζεύξεις σημείου προς σημείο. Επομένως, σε σύγκριση με τα δορυφορικά δίκτυα, τα επίγεια δίκτυα έχουν μικρότερη περιοχή ραδιοκάλυψης.

Στα μελλοντικά συστήματα νέας γενιάς, προκειμένου να προσφέρονται υψηλές ταχύτητες μετάδοσης δεδομένων θα πρέπει να επιλεγεί και το κατάλληλο φάσμα στο οποίο θα γίνεται η μετάδοση των σημάτων. Δεδομένου ότι η χωρητικότητα ενός συστήματος είναι ανάλογη του φάσματος που χρησιμοποιείται για τη μετάδοση του σήματος, χρειάζεται να γίνει χρήση όσο μεγαλύτερου εύρους ζώνης. Ο μεγάλος αριθμός συστημάτων τόσο επίγειων όσο και δορυφορικών που λειτουργούν στις ζώνες συχνοτήτων L- και S-, έχουν προκαλέσει μία φασματική συμφόρηση, η οποία και οδηγεί τα μελλοντικά συστήματα να λειτουργούν σε συχνότητες άνω των 10 GHz. Όλο και περισσότερα δορυφορικά συστήματα λειτουργούν στη ζώνη συχνοτήτων Ka (O3b, KA-SAT) ενώ και στα μελλοντικά επίγεια δίκτυα $5^{ης}$ γενιάς που αρχίζουν να μελετώνται, μελετάται η χρήση χιλιοστομετρικών συχνοτήτων [Rappaport13]. Πέραν από την Ka ζώνη συχνοτήτων μελετάται και η χρήση της ζώνης Q για την επικοινωνία δορυφόρων με επίγειες δορυφορικές πύλες σε δίκτυα με αυξημένη ρυθμοαπόδοση όπως το σύστημα Terabit/sec [Thompson11]. Σε τέτοια δορυφορικά συστήματα μελετάται και η χρήση οπτικών συχνοτήτων για την επικοινωνία των επίγειων πυλών με τους δορυφόρους προκειμένου να αποστέλλονται τα δεδομένα μέσω δορυφόρου σε τελικούς χρήστες. Η χρήση οπτικών συχνοτήτων έχει το πλεονέκτημα πολύ μεγάλου εύρους ζώνης και επομένως πολύ υψηλών ταχυτήτων μετάδοσης.

Η παρούσα Διατριβή επικεντρώνεται στις ασύρματες ζεύξεις είτε επίγειες είτε Γης-δορυφόρου οι οποίες λειτουργούν στην Ka ή Q ζώνη συχνοτήτων. Σε αυτές τις συχνότητες, τα ατμοσφαιρικά φαινόμενα που λαμβάνουν χώρα επηρεάζουν την ισχύ και το πλάτος του σήματος το οποίο διαδίδεται. Πιο συγκεκριμένα, οι κατακρημνίσεις (βροχή, χαλάζι, χιόνι), τα νέφη και τα ατμοσφαιρικά αέρια (οξυγόνο, υδρατμοί) προκαλούν την απόσβεση της ισχύος του λαμβανόμενου σήματος, ενώ οι στροβιλισμοί στην τροπόσφαιρα που δημιουργούνται προκαλούν σπινθηρισμούς στο πλάτος του σήματος [ITU-R.P.618], [ITU-R.P.530], [Panagopoulos04a]. Από τα παραπάνω φαινόμενα και στις ζώνες συχνοτήτων που μελετώνται, η βροχόπτωση αποτελεί τον κυριότερο παράγοντα εξασθένισης και για το λόγο αυτό στην παρούσα Διατριβή μελετώνται κυρίως οι απώλειες λόγω βροχής.

Η επίδραση της ατμόσφαιρας μπορεί να προκαλέσει εξασθένιση πολλών δεκάδων dB στην ισχύ του σήματος για ένα μικρό χρονικό διάστημα. Επομένως, η χρήση ενός σταθερού περιθωρίου διαλείψεων για την αντιμετώπιση της απόσβεσης είναι μία τεχνική μη οικονομικά συμφέρουσα, εφ' όσον θα γινόταν χρήση των πόρων αυτών για πολύ μικρό χρονικό διάστημα, ενώ το υπόλοιπο θα παρέμεναν ανεκμετάλλευτοι. Επιπλέον, οι σταθμοί θα ήταν αρκετά οικονομικά ασύμφοροι. Για τους παραπάνω λόγους, έχουν αναπτυχθεί τεχνικές άμβλυνσης διαλείψεων (ΤΑΔ) [Panagopoulos04a]. Οι τεχνικές αυτές αποτελούν κυρίως δυναμικές τεχνικές, όπως η προσαρμοσμένη κωδικοποίηση και διαμόρφωση και ο έλεγχος ισχύος. Στην πρώτη, η τάξη της διαμόρφωσης και η κωδικοποίηση αλλάζουν με βάση τη λαμβανόμενη ισχύς ενώ στη δεύτερη περίπτωση προσαρμόζεται η εκπεμπόμενη ισχύς. Στις ΤΑΔ επιπλέον ανήκουν και οι τεχνικές διαφορισμού. Συγκεκριμένα, υπάρχουν οι εξής τεχνικές, ο διαφορισμός θέσης, τροχιάς, χρόνου και συχνότητας. Στο διαφορισμό θέσης, εγκαθίστανται δύο ή περισσότεροι επίγειοι σταθμοί οι οποίοι λαμβάνουν το ίδιο σήμα από το δορυφόρο. Ο διαφορισμός θέσης είναι ο πλέον αποτελεσματικός τρόπος για να αυξηθεί η διαθεσιμότητα του συστήματος αλλά είναι οικονομικά μη αποτελεσματικός διότι απαιτεί την εγκατάσταση άνω του ενός επίγειου σταθμού. Στο διαφορισμό τροχιάς, ένα επίγειος σταθμός λαμβάνει το ίδιο σήμα από δύο δορυφόρους. Οι δύο παραπάνω τεχνικές διαφορισμού, αποτελούν τεχνικές διαφορισμού στο πεδίο του χώρου και εκμεταλλεύονται τη μείωση της συσχέτισης των ατμοσφαιρικών φαινομένων με την απόσταση. Στο διαφορισμό χρόνου, εισάγεται μία περίοδο αναμονής. Σε περίπτωση που η απόσβεση είναι υψηλή (ή αντίστοιχα ο σηματοθορυβικός λόγος χαμηλός) τότε δεν αποστέλλεται κανένα σήμα για χρόνο ίσο με την περίοδο αναμονής. Ύστερα από το χρόνο αυτό, ο δορυφόρος στέλνει το ίδιο σήμα. Στην περίπτωση αυτή, βελτιώνεται η απόδοση του συστήματος λόγω της μείωσης της συσχέτισης του καναλιού διάδοσης με το χρόνο. Μία ακόμα τεχνική διαφορισμού είναι στο πεδίο της συχνότητας. Κατά την τεχνική αυτή σε περίπτωση αύξησης της απόσβεσης χρησιμοποιείται εναλλακτική μικρότερη ζώνη συχνοτήτων.

Για την αξιολόγηση και σχεδιασμό ενός συστήματος απαιτείται η μοντελοποίηση των στατιστικών χαρακτηριστικών πρώτης και δεύτερης τάξης του καναλιού διάδοσης. Τα στατιστικά χαρακτηριστικά πρώτης τάξης βοηθούν στον υπολογισμό της διαθεσιμότητας του συστήματος για τα διαφορετικά χαρακτηριστικά του συστήματος. Τα στατιστικά χαρακτηριστικά δεύτερης τάξης του καναλιού χρειάζονται σε συνδυασμό με τα στατιστικά χαρακτηριστικά πρώτης τάξη για την παραγωγή χρονοσειρών των απωλειών του καναλιού διάδοσης. Οι χρονοσειρές χρειάζονται για την αξιολόγηση της απόδοσης των προσαρμοστικών και δυναμικών ΤΑΔ στα δορυφορικά δίκτυα νέας γενιάς.

1.2 Μοντελοποίηση των στατιστικών χαρακτηριστικών πρώτης τάξης της απόσβεσης λόγω βροχής

Στην παρούσα υποενότητα θα παρουσιαστούν τα παρακάτω μοντέλα πρόβλεψης (αντίστοιχές δημοσιεύσεις σε διεθνή περιοδικά και σε συνέδρια με κριτές) σε δορυφορικά και επίγεια δίκτυα των στατιστικών χαρακτηριστικών πρώτης τάξης της απόσβεσης βροχής και της από κοινού πιθανότητας υπέρβασης για ζεύξεις χωρικά ή χρονικά συσχετισμένες:

[J1] C. Kourogiorgas, A. D. Panagopoulos, J. D. Kanellopoulos, "*An Engineering Method for the Prediction of Outage Probability of LOS Terrestrial Links Operating above 10 GHz*", IEEE Antennas and Wireless Propagation Letters, vol. 12, pp. 516-519, 2013.

[J2] C. Kourogiorgas, A. D Panagopoulos, "*A Physical-Mathematical Model for Predicting Slant Path Rain Attenuation Statistics*", IET Microwave, Antennas and Propagation, vol. 7, no. 12, pp. 970-975, 2013.

[J3] C. Kourogiorgas, A. D. Panagopoulos, J. D. Kanellopoulos, "*On the Earth-space Site Diversity Modeling: A novel physical mathematical model*", IEEE Transactions on Antennas and Propagation, vol. 60, no. 9, pp. 4391-4397, November 2012

[J4] C. I. Kourogiorgas, A. D. Panagopoulos, "*Outage Performance of Dual Branch Diversity Techniques in Broadband Fixed Wireless Access Networks*", IET Communications, vol. 8, no. 9, pp. 1648-1653, June 2014.

[J5] C. Kourogiorgas, A. D. Panagopoulos, et al, , "*On the Outage Probability Prediction of Time Diversity Scheme in Broadband Satellite Communication Systems*", Progress In Electromagnetics Research C, vol. 44, pp. 175-184, 2013

[C1] C. Kourogiorgas, A. D. Panagopoulos, G. K. Karagiannidis, J. D. Kanellopoulos, "On the modeling of rain rate and of slant path and terrestrial links rain attenuation with Inverse Gaussian distribution", MCM6 COST Action IC0802, 28-30 September 2011, Prague, Czech Republic.

[C2] C. Kourogiorgas, A. D. Panagopoulos, G. K. Karagiannidis, J. D. Kanellopoulos, "*On the Inverse Gaussian Modeling of Rain Rate and Slant Path and Terrestrial Links Rain Attenuations*", EuCAP 2012, 26–30 March, Prague, Czech Republic.

[C3] C. Kourogiorgas, A. D. Panagopoulos, J. D. Kanellopoulos, "Site Diversity Performance Using Two-Dimensional Inverse Gaussian Distribution", ESA Workshop on Radiowave Propagation 2011, 30 November–2 December, Noordwijk, Netherlands.

[C4] C. Kourogiorgas, A. D. Panagopoulos, "*On the Route Diversity Improvement Modeling for Broadband Radio Access Networks*", EuCAP 2013, 8-12 April 2013, Gothenburg, Sweden.

[C5] C. Kourogiorgas, S. N. Livieratos, A. D. Panagopoulos, G. E. Chatzarakis, "*Modeling of Joint Rainfall Rate and Rain Attenuation Statistics Using Archimedean Copula Functions*", EuCAP 2014, 6-11 April 2014, The Hague, The Netherlands.

[C6] C. Kourogiorgas, A. D. Panagopoulos, et al., "*Modeling of Joint Rain Attenuation for Time Diversity Satellite Communication Systems*", 2013 Joint Conference: 19th Ka and Broadband Communications, Navigation and Earth Observation Conference and 31st AIAA ICSSC, 14-17 October 2013, Florence, Italy.

[C7] C. Kourogiorgas, A. D. Panagopoulos, S. N. Livieratos, G. E. Chatzarakis, "*Time Diversity Prediction Modeling Using Copula Functions for Satellite Communication Systems Operating Above 10 GHz*", 2014 XXXIth URSI General Assembly and Scientific Symposium, 16-23 August 2014, Beijing, China

1.2.1 Μέθοδος πρόβλεψης πιθανότητας αποκοπής για επίγειες και δορυφορικές ζεύξεις υπό βροχή με συχνότητα λειτουργίας άνω των 10 GHz

Η παρούσα μέθοδος κάνει χρήση της υπόθεσης ότι τόσο η ένταση βροχόπτωσης (R) όσο και η απόσβεση λόγω βροχής (A) ακολουθούν την κατανομή της Inverse Gaussian (IG). Επομένως, η πιθανότητα υπέρβασης της έντασης βροχόπτωσης δίνεται από [Sehsardi93]:

$$P\left[R \geq R_{th}\right] = 1 - Q\left(\sqrt{\frac{\lambda_R}{R_{th}}}\left(1 - \frac{R_{th}}{\mu_R}\right)\right) - e^{2\frac{\lambda_R}{\mu_R}} Q\left(\sqrt{\frac{\lambda_R}{R_{th}}}\left(1 + \frac{R_{th}}{\mu_R}\right)\right), \tag{1.1}$$

όπου λ_R και μ_R οι στατιστικές παράμετροι της IG για την ένταση βροχόπτωσης. Αν και η υπόθεση ότι η πιθανότητα να βρέχει σε ένα σημείο είναι ίση με 1 δεν στέκει φυσικά, χρησιμοποιείται στη μαθηματική μοντελοποίηση της απόσβεσης διότι στη σχεδίαση ενδιαφέρουν οι πιθανότητες υπέρβασης μικρότερες του 0.1%. Στην Εικόνα 1-1 απεικονίζεται η πιθανότητα υπέρβασης της έντασης βροχόπτωσης για την περιοχή της Αθήνας όπως αυτή υπολογίζεται από την ITU-R. P. 837 [ITU-R.P.837] καθώς και η προσαρμογή της IG. Στην Εικόνα 1-2, δίνεται η πιθανότητα υπέρβασης για την περιοχή Yamaguchi της Ιαπωνίας, από τη βάση δεδομένων της ITU [DBSG3] και η προσαρμογή της IG. Από τις εικόνες φαίνεται ότι η κατανομή IG μπορεί να μοντελοποιήσει τα στατιστικά χαρακτηριστικά πρώτης τάξης της έντασης βροχόπτωσης.

Η πιθανότητα υπέρβασης για την ένταση βροχόπτωσης δίνεται από:

$$P\left[A \geq A_{th}\right] = 1 - Q\left(\sqrt{\frac{\lambda_A}{A_{th}}}\left(1 - \frac{A_{th}}{\mu_A}\right)\right) - e^{2\frac{\lambda_A}{\mu_A}} Q\left(\sqrt{\frac{\lambda_A}{A_{th}}}\left(1 + \frac{A_{th}}{\mu_A}\right)\right), \tag{1.2}$$

όπου μ_A και λ_A οι στατιστικές παράμετροι της IG για την απόσβεση λόγω βροχής.

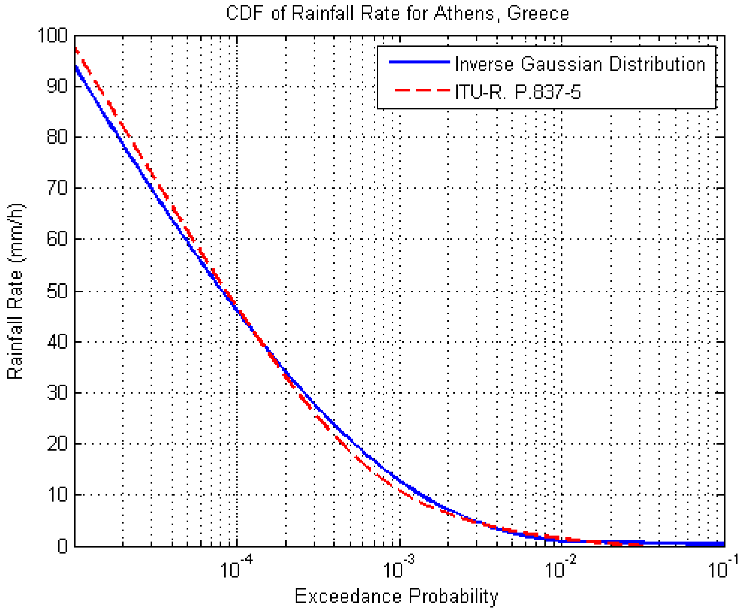

Εικόνα 1-1 Πιθανότητα υπέρβασης της ένταση βροχόπτωσης για την Αθήνα, Ελλάδα, από την ITU-R. P. 837-5 (κόκκινη γραμμή) και χρησιμοποιείται για την προσαρμογή της IG κατανομής

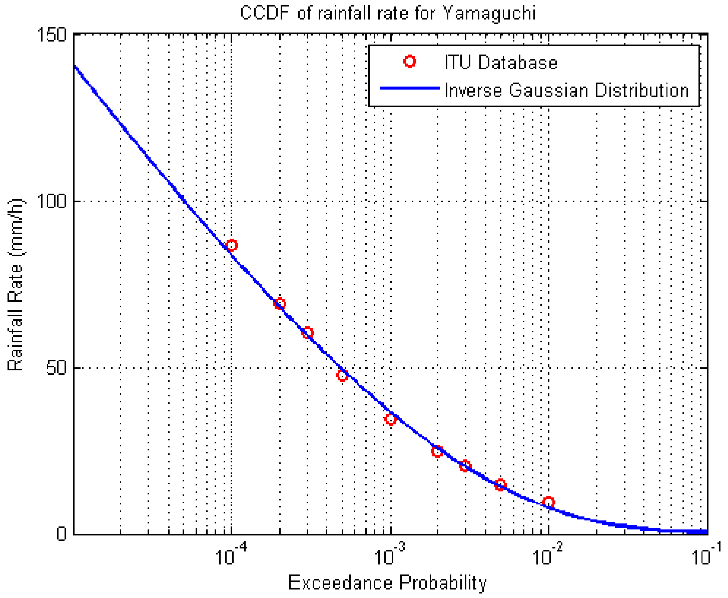

Εικόνα 1-2 Πιθανότητα υπέρβασης της ένταση βροχόπτωσης για την Yamaguchi, Ιαπωνία, από την DBSG3 (κόκκινη γραμμή) και χρησιμοποιείται για την προσαρμογή της IG κατανομής

Η δεύτερη υπόθεση της μεθόδου είναι ότι η ένταση βροχόπτωσης είναι ομοιόμορφη στο κάθετο [Crane80] και επομένως βάσει της γεωμετρία της ζεύξης όπως φαίνεται στην Εικόνα 1-3 ισχύει για την απόσβεση η οποία εισάγεται στην προβολή του κεκλιμένου ραδιοδρόμου στη Γη (A) ότι:

$$A = A_s \cos\theta \qquad (1.3)$$

όπου θ η γωνία ανύψωσης της ζεύξης και A_S η απόσβεση που εισάγεται στον κεκλιμένο ραδιοδρόμο και επομένως:

$$P[A_s \geq x_s] = P[A \geq x_D] \tag{1.4}$$

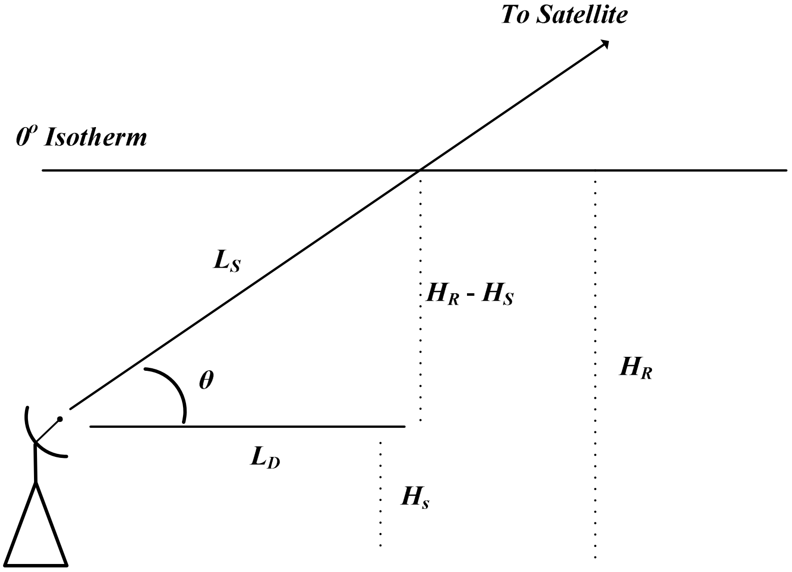

Εικόνα 1-3 Η Γεωμετρία της ζεύξης Γης-δορυφόρου

Επιπλέον, η σχέση που συνδέει τη ένταση βροχόπτωσης με την απόσβεση λόγω βροχής δίνεται από [Olsen78]:

$$A(t) = \int_0^{L_D} \Gamma(x,t)dx = \int_0^{L_D} a \cdot R(x,t)^b dx \tag{1.5}$$

, όπου *Γ(x,t)* η ειδική απόσβεση λόγω βροχής και ισούται με $aR(x,t)^b$ [29]. Θεωρείται ότι οι παράμετροι μ και λ είναι σταθεροί στο χρόνο και ότι η χωρική συσχέτιση της ειδικής απόσβεσης είναι [Lin75]:

$$\rho = \frac{G}{\sqrt{G^2 + \left(d = |x - x'|\right)^2}} \tag{1.6}$$

, όπου d η απόσταση των σημείων και Gσταθερά η οποία εξαρτάται από τα τοπικά χαρακτηριστικά του μέσου της βροχόπτωσης. Χρησιμοποιώντας τις παραπάνω υποθέσεις οι παράμετροι της κατανομής IG για την απόσβεση λόγω βροχής δίνονται από:

$$\mu_A = am_{R,b}L_D \tag{1.7}$$

$$\lambda_A = \frac{\left(am_{R,b}L_D\right)^3}{a^2\left(m_{R,2b} - m_{R,b}^2\right)H_1} \tag{1.8}$$

, όπου $H_1 = 2L_D G \sinh^{-1}\left(\frac{L_D}{G}\right) + 2G^2\left[1 - \sqrt{\left(\frac{L_D}{G}\right)^2 + 1}\right]$,

$$m_{R,b} = 2\sqrt{\frac{\lambda_R}{2\pi}e^{\lambda_R/\mu_R}}\left(\mu_R^2\right)^{\frac{b-1/2}{2}} K_{b-1/2}\left(\frac{\lambda_R}{\mu_R}\right) \text{ και } m_{R,2b} = 2\sqrt{\frac{\lambda_R}{2\pi}e^{\lambda_R/\mu_R}}\left(\mu_R^2\right)^{\frac{2b-1/2}{2}} K_{2b-1/2}\left(\frac{\lambda_R}{\mu_R}\right).$$

Η παραπάνω μεθοδολογία συγκρίθηκε τόσο για επίγειες όσο και για δορυφορικές ζεύξεις με τις μεθόδους της ITU-R. P. 530 και 618, αντίστοιχα, χρησιμοποιώντας δεδομένα από τη βάση της ITU, DBSG3. Για τη σύγκριση των μοντέλων χρησιμοποιήθηκε η μετρική από την ITU-R. P. 311 [ITU-R.P.311]. Για τις επίγειες ζεύξεις δίνονται στον Πίνακας 1, οι στατιστικές παράμετροι του σφάλματος ενώ στην Εικόνα 1-4, η τιμή RMS ανά ποσοστό πιθανότητας υπέρβασης.

Πίνακας 1. Μέση τιμή τυπική απόκλιση και RMS τιμή του σφάλματος

	ε_{mean} (%)	ε_{std} (%)	ε_{rms} (%)
IG model	-7.69	21	22.36
ITU-R. P.530-14	-9.53	20.64	22.7

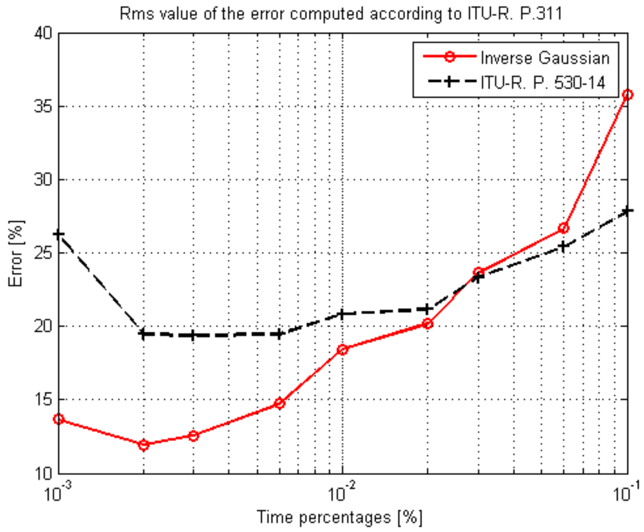

Εικόνα 1-4 RMS τιμή του σφάλματος του προτεινόμενου μοντέλου και της ITU-R. P. 530-14

Αντίστοιχα, για τις ζεύξεις Γης-δορυφόρου, στην δίνεται η RMS τιμή του σφάλματος ανά ποσοστό πιθανότητας υπέρβασης και στον τα στατιστικά χαρακτηριστικά του σφάλματος.

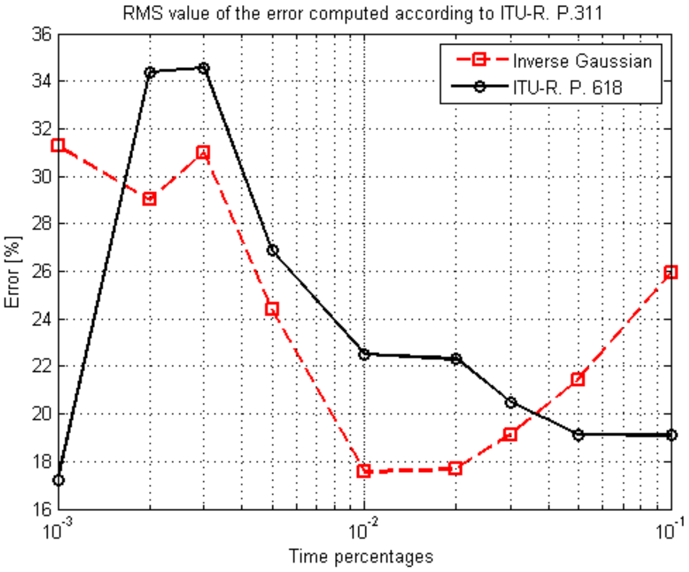

Εικόνα 1-5 RMS τιμή του σφάλματος του προτεινόμενου μοντέλου και της ITU-R. P. 618

Πίνακας 2. Μέση τιμή, τυπική απόκλιση και RMS τιμή του σφάλματος

	ε_{mean} (%)	ε_{std} (%)	ε_{rms} (%)
IG model	-1.55	21.53	21.59
ITU-R. P.618	-7.68	20.42	21.81

1.2.2 Μέθοδος υπολογισμού της πιθανότητας αποκοπής δορυφορικού συστήματος διπλού διαφορισμού θέσης

Στο παρόν μοντέλο κάνουμε τις εξής υποθέσεις:

α) Η κατανομή της απόσβεσης λόγω βροχής σε μία δορυφορική ζεύξη ακολουθεί την κατανομή IG

β) Η από κοινού κατανομή της απόσβεσης λόγω βροχής σε δύο δορυφορικές ζεύξεις ακολουθεί τη διδιάστατη κατανομή IG [Seshardi93]

Επομένως, η πιθανότητα αποκοπής δίνεται από:

$$P_{out} = P\left[A_1 \geq A_{th1}, A_2 \geq A_{th2}\right] \tag{1.9}$$

με $P\left[A_1 \geq A_{th1}, A_2 \geq A_{th2}\right]$την από κοινού πιθανότητα υπέρβασης της διδιάστατης κατνομή IG. Ο συντελεστής χωρικής συσχέτισης δίνεται από:

$$\rho_a = 0.94e^{-d/30} + 0.06e^{-(d/500)^2} \tag{1.10}$$

όπου d η απόσταση των δύο επίγειων σταθμών. Ο αλγόριθμος για τον υπολογισμό της πιθανότητας αποκοπής είναι ο εξής:

1) Υπολογισμός των παραμέτρων της μονοδιάστατης IG μέσω μοντέλων πρόβλεψης απόσβεσης
2) Υπολογισμός του συντελεστή συσχέτισης

3) Υπολογισμός της από κοινού πιθανότητας υπέρβασης της απόσβεσης για μία διδιάστατη κατανομή IG.

Χρησιμοποιώντας δεδομένα της ITU για πιθανότητα υπέρβασης της απόσβεσης λόγω βροχής που εισάγεται σε ένα σύστημα διπλού διαφορισμού θέσης, η προτεινόμενη μεθοδολογία συγκρίθηκε με τον μοντέλο της ITU-R. P. 618. Στην , δίνεται η RMS τιμή του σφάλματος ανά ποσοστό πιθανότητας υπέρβασης.

Πίνακας 3 Μέση τιμή, τυπική απόκλιση και RMS τιμή του σφάλματος

	Proposed Model	ITU-R. P. 618
ε_{mean} (%)	-0.75	-16.31
ε_{std} (%)	29.19	30.25
ε_{rms} (%)	29.2	34.37

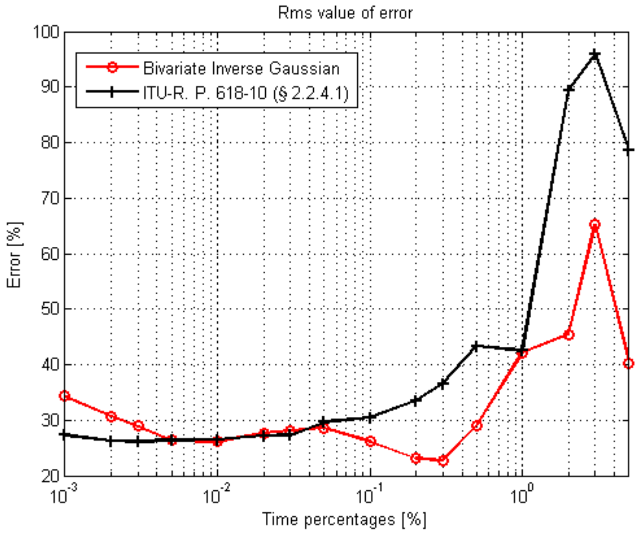

Εικόνα 1-6 RMS τιμή σφάλματος του προτεινόμενου μοντέλου και της σύστασης ITU-R. P. 618

1.2.3 Μέθοδος υπολογισμού πιθανότητας αποκοπής σε επίγεια ασύρματα συστήματα με χρήση του διαφορισμού δρόμου για συχνότητες λειτουργίας άνω των 10 GHz

Στην παρούσα Διατριβή προτάθηκε μοντέλο για τον υπολογισμό της πιθανότητας αποκοπής ασύρματων συστημάτων τα οποία κάνουν χρήση της τεχνικής διαφορισμού δρόμου. Η γεωμετρία του συστήματος δίνεται στην Εικόνα 1-7. Στην τεχνική αυτή, ο δέκτης είναι εξοπλισμένος με δύο υπερ-κατευθυντικές κεραίες και επικοινωνεί με δύο σταθμούς βάσης. Οι δύο σταθμοί αποστέλλουν το ίδιο σήμα και επομένως ο δέκτης μπορεί να κάνει χρήση τεχνικών συνδυασμού των σημάτων. Στο παρόν μοντέλο δίνονται μοντέλα υπολογισμού για τις τεχνικές επιλεκτικής επιλογής (Selection Combining - SC) και αθροιστικού συνδυασμού (Maximal Ratio Combining –MRC) [Skraparlis].

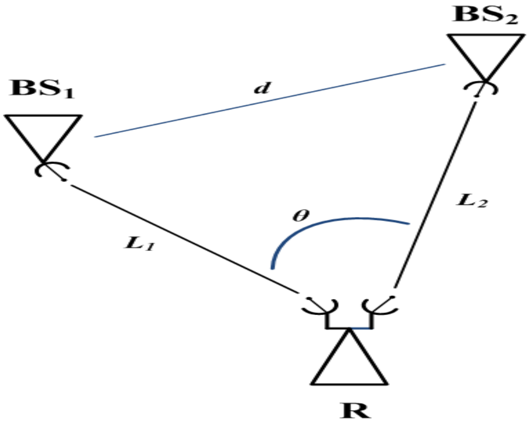

Εικόνα 1-7 Γεωμετρία συστήματος διαφορισμού δρόμου

Για τις παραπάνω τεχνικές, ο λαμβανόμενος σηματοθορυβικός λόγος, σε Watts, δίνεται από:

$$SNR_r = \begin{cases} \max\left(SNR_1, SNR_2\right), \text{ SC} \\ SNR_1 + SNR_2, \text{ MRC} \end{cases} \tag{1.11}$$

με SNR_1 ο σηματοθορυβικός λόγος του σήματος που στάλθηκε από τον BS1 και SNR_2 ο σηματοθορυβικός λόγος του σήματος που στάλθηκε από τον BS2.

Αποκοπή της λειτουργίας του συστήματος λαμβάνει χώρα όταν ο σηματοθορυβικός λόγος είναι χαμηλότερος από ένα κατώφλι. Επομένως, η πιθανότητα αποκοπής δίνεται από:

$$P_{out} = P\left[SNR_r \leq SNR_{th}\right] \tag{1.12}$$

Για την περίπτωση του SC, η πιθανότητα αποκοπής δίνεται από:

$$P_{out,SC} = P\left[\max\left(SNR_1, SNR_2\right) \leq SNR_{th}\right] = P\left[SNR_1 \leq SNR_{th}, SNR_2 \leq SNR_{th}\right] \tag{1.13}$$

Ενώ για την τεχνική MRC δίνεται από:

$$P_{out,MRC} = P\left[SNR_1 + SNR_2 \leq SNR_{th}\right] = P\left[SNR_1 \leq SNR_{th}, SNR_2 \leq SNR_{th} - SNR_1\right] \tag{1.14}$$

Οι παραπάνω κατανομές μεταφράζονται σε από κοινού πιθανότητες υπέρβασης της απόσβεσης λόγω βροχής. Για την απόσβεση λόγω βροχής υποθέτουμε ότι για μία ζεύξη ακολουθεί την κατανομή IG ενώ για χωρικά διαχωρισμένες ζεύξεις τη διδιάστατη IG με χωρικό συντελεστή συσχέτισης [ITU-R.P.1410]:

$$\rho_d = \frac{D_r}{\sqrt{D_r^2 + d^2}}\left(d = \sqrt{L_1^2 + L_2^2 - 2L_1L_2\cos(\theta)}\right) \tag{1.15}$$

με d η απόσταση μεταξύ των δύο σταθμών βάσης και D_r σταθερά η οποία δίνεται σε σχέση με τις γεωγραφικές συντεταγμένες των σταθμών:

$$D_r = 0.644\ln\left(\left|Latitude\right|\right) - 1.02, \quad 5^0 \leq \left|Latitude\right| \leq 90^0 \tag{1.16}$$

Στην Εικόνα 1-8, δίνεται η πιθανότητα αποκοπής του SC και MRC συστήματος για ένα σύστημα το οποίο βρίσκεται στην Αθήνα. Η συχνότητα λειτουργίας είναι 25 GHz και τα μήκη των μονοπατιών 4 km. Η πιθανότητα υπολογίστηκε για γωνίες διαχωρισμού 60° και 90°.

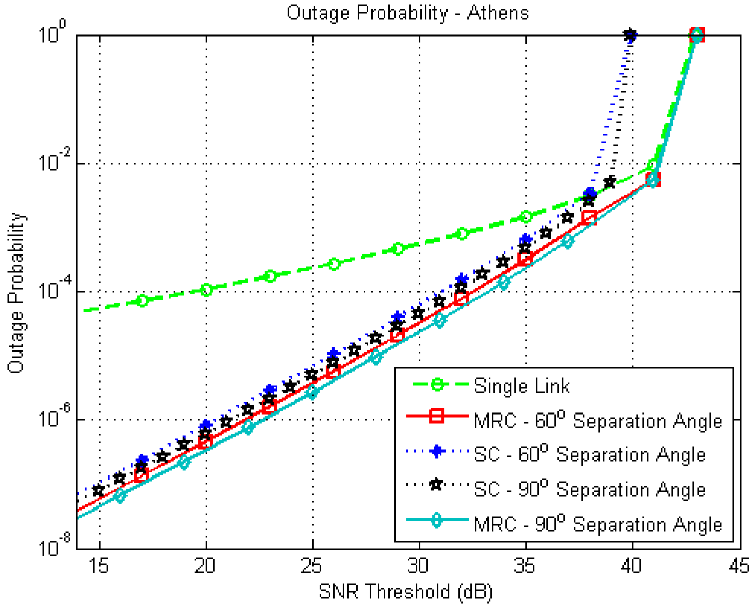

Εικόνα 1-8. Πιθανότητα αποκοπής για τις τεχνικές MRC και SC για 60° και 90° γωνίες διαχωρισμού των ζεύξεων στην Αθήνα, Ελλάδα

Στην Εικόνα 1-9, δίνονται οι ίδιες καμπύλες με την περίπτωση της Αθήνας αλλά για τη Σεούλ, με συχνότητα λειτουργίας τα 27 GHz και μήκη ραδιοδρόμων 3 km. Οι γωνίες διαχωρισμού είναι 80° και 120o.

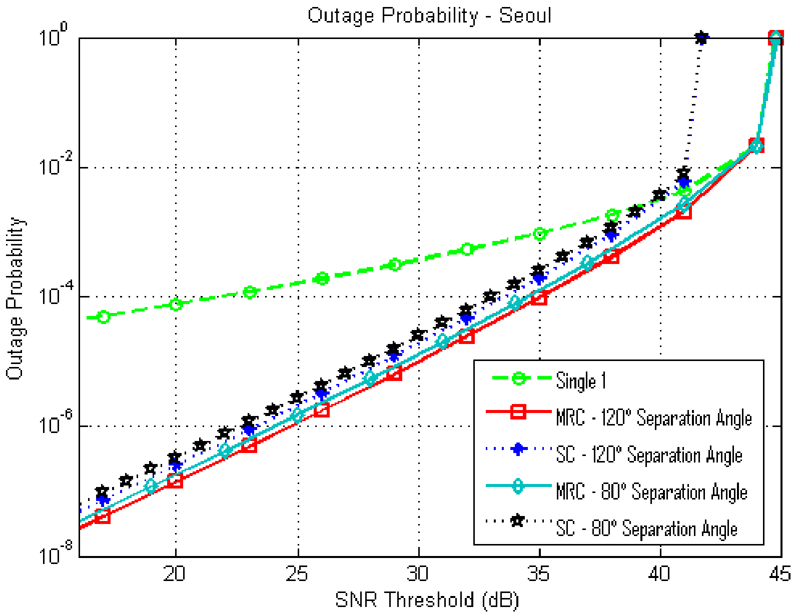

Εικόνα 1-9 Πιθανότητα αποκοπής για τις τεχνικές MRC και SC για 80^o και 120^o γωνίες διαχωρισμού των ζεύξεων στην Σεούλ, Νότια Κορέα

1.2.4 Μοντελοποίηση της πιθανότητας αποκοπής σε δορυφορικά συστήματα διπλού διαφορισμού με χρήση των συναρτήσεων Archimedean Copulas

Οι συναρτήσεις Copulas, χρησιμοποιούνται για τον υπολογισμό των από κοινού πιθανοτήτων δύο ή περισσοτέρων τυχαίων μεταβλητών. Στην παρούσα ενότητα, χρησιμοποιούμε τις συναρτήσεις copulas για τον υπολογισμό των από κοινού πιθανοτήτων της έντασης βροχόπτωσης και απόσβεσης λόγω βροχής. Χρησιμοποιούνται οι παρακάτω συναρτήσεις [Nelsen06]:

$$C(u,v)=\left(u^{-\theta}+v^{-\theta}-1\right)^{-1/\theta},\theta\in\left(0,+\infty\right)\ (5) \tag{1.17}$$

$$C(u,v)=\exp\left\{1-\left[(1-\ln u)^{\theta}+(1-\ln v)^{\theta}-1\right]^{\frac{1}{\theta}}\right\}\ (6) \\ ,\theta\in(0,+\infty) \tag{1.18}$$

$$C(u,v)=\frac{\theta}{\ln\left(e^{\frac{\theta}{u}}+e^{\frac{\theta}{v}}-e^{\theta}\right)},\theta\in\left(0,+\infty\right)\ (7) \tag{1.19}$$

$$C(u,v)=\left[\ln\left(e^{u^{-\theta}}+e^{v^{-\theta}}-e\right)\right]^{-1/\theta},\theta\in\left(0,+\infty\right)\ (8) \tag{1.20}$$

1.2.5 Μοντελοποίηση της έντασης βροχόπτωσης

Δεδομένου ότι γνωρίζουμε την πιθανότητα υπέρβασης της ένταση βροχόπτωσης για δύο σημεία και δίνεται από:

$$P\left[R_1 \geq R_{th}\right] = 1 - u \tag{1.21}$$

$$P\left[R_2 \geq R_{th}\right] = 1 - v \tag{1.22}$$

όπου u και v είναι τυχαίες μεταβλητές ομοιόμορφα κατανεμημένες στο διάστημα [0,1], η από κοινού πιθανότητα υπέρβασης δίνεται από:

$$P[R_1 \geq R_{th}, R_2 \geq R_{th}] = 1 - u - v + C(u,v) \tag{1.23}$$

Για την αξιολόγηση της μοντελοποίησης της από κοινού πιθανότητας έντασης βροχόπτωσης, χρησιμοποιήθηκαν δεδομένα από το British Atmospheric Data Center (BADC) [BADC]. Πιο συγκεκριμένα, αναλυθήκαν δεδομένα για 7 έτη τα οποία και μετρήθηκαν στις περιοχές Sparsholt και Cholbolton στο Ηνωμένο Βασίλειο, ταυτόχρονα. Στην Εικόνα 1-10, δίνεται η πιθανότητα υπέρβασης της έντασης βροχόπτωσης για τα δύο σημεία καθώς και την από κοινού πιθανότητα για το έτος 2003, ενώ στην Εικόνα 1-11 για τα έτη 2003-2009. Επιπλέον, δίνονται και οι προσαρμοσμένες συναρτήσεις Copulas και παρατηρούμε ότι μπορούν να μοντελοποιήσουν με ακρίβεια τα από κοινού στατιστικά χαρακτηριστικά.

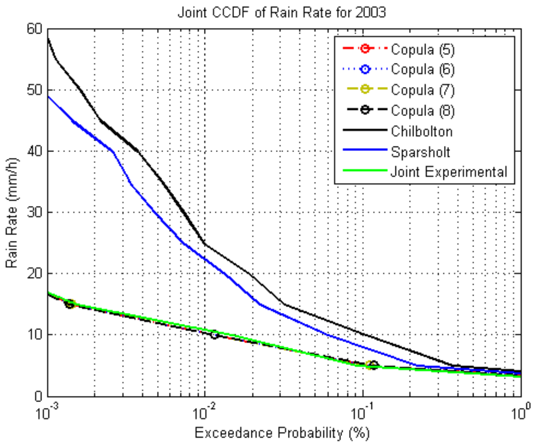

Εικόνα 1-10 Από κοινού και για κάθε σημείο πιθανότητα υπέρβασης μαζί με τις προσαρμοσμένες συναρτήσεις Copulas για το έτος 2003.

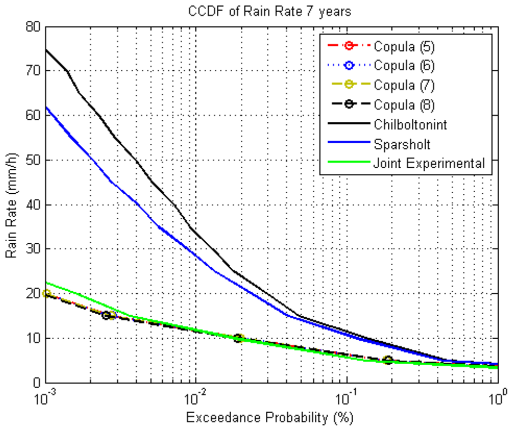

Εικόνα 1-11 Από κοινού και για κάθε σημείο πιθανότητα υπέρβασης μαζί με τις προσαρμοσμένες συναρτήσεις Copulas για τα έτη 2003-2009.

1.2.6 Μοντελοποίηση της απόσβεση λόγω βροχής

Παρόμοια με την ένταση βροχόπτωσης, εάν η πιθανότητα υπέρβασης της απόσβεσης είναι γνωστή, τότε οι τυχαίες μεταβλητές u και v μπορούν να υπολογισθούν για τις διάφορες τιμές της απόσβεσης (A_{th}):

$$P\left[A_1 \geq A_{th}\right] = 1 - u \tag{1.24}$$

$$P\left[A_2 \geq A_{th}\right] = 1 - v \tag{1.25}$$

Επομένως, μπορεί να υπολογιστεί και η από κοινού πιθανότητα υπέρβασης για δύο χωρικά διαχωρισμένες ζεύξεις:

$$P[A_1 \geq A_{th}, A_2 \geq A_{th}] = 1 - u - v + C(u,v) \tag{1.26}$$

Χρησιμοποιώντας δεδομένα από τη βάση της ITU [DBSG3], αξιολογήθηκε η μοντελοποίηση με χρήση συναρτήσεων Copulas. Στην Εικόνα 1-12, δίνεται η από κοινού πιθανότητα της απόσβεσης για δύο ζεύξεις με απόσταση 18 km. Οι σύο επίγειοι σταθμοί είναι τοποθετημένοι στις περιοχές St. Jovite και Arundel, Καναδάς και λειτουργούν σε συχνότητα 13 GHz. Παρατηρείται ότι οι συναρτήσεις copulas μοντελοποιούν με ακρίβεια την από κοινού πιθανότητα υπέρβασης της απόσβεσης.

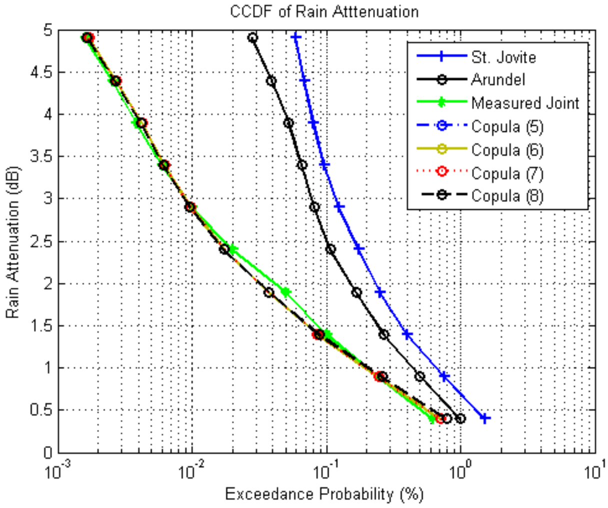

Εικόνα 1-12 Πιθανότητα υπέρβασης της απόσβεσης για κάθε ζεύξη και από κοινού πιθανότητα από μετρήσεις και συναρτήσεις copulas για δύο επίγειου σταθμούς.

1.2.7 Μοντελοποίηση της απόδοσης δορυφορικών συστημάτων χρονικού διαφορισμού με τη Λογαριθμοκανονική κατανομή

Στο παρόν μοντέλο γίνεται χρήση του μοντέλου Maseng-Bakken [Maseng81]. Με βάση το μοντέλο αυτό η απόσβεση λόγω βροχής ακολουθεί τη λογαριθμοκανονική κατανομή και επομένως η συνάρτηση πυκνότητας πιθανότητας δίνεται απο:

$$p_A\left(A\right)=\frac{1}{\sqrt{2\pi}S_A A}\exp\left\{-\frac{\left(\ln A-\ln A_m\right)^2}{2S_A^2}\right\} \tag{1.27}$$

όπου S_A η τυπική απόκλιση της ln(A) και A_m η μεσαία τιμή της λογαριθμοκανονικής κατανομής.

Επιπλέον, η απόσβεση λόγω βροχής (A_t) μοντελοποιείται σαν μία στοχαστική διαδικασία η οποία περιγράφεται με την παρακάτω Στοχαστική Διαφορική Εξίσωση (ΣΔΕ):

$$dA_t = A_t\beta_A\left[S_A^2-\ln\left(A_t/A_m\right)\right]dt+\sqrt{2\beta_A}A_tS_AdW_t \tag{1.28}$$

όπου β_A (sec^{-1}) παράμετρος από την οποία εξαρτώνται τα δυναμικά χαρακτηριστικά της απόσβεσης λόγω βροχής και W_t η κίνηση Brown [Karatzas05].

Από την παραπάνω ΣΔΕ υπολογίζεται η μεταβατική συνάρτηση πυκνότητας πιθανότητας, η οποία δίνει την πιθανότητα να έχω απόσβεση A τη χρονικής στιγμή t δεδομένου της τιμής που έχω τη στιγμή t_0:

$$p\left\{A(t),t\,|\,A(t_0),t_0\right\}=\frac{1}{\sqrt{2\pi}\,S_{a0}\left(\Delta t\right)A\left(t\right)}\exp\left\{-\frac{\left[\ln A\left(t\right)-\ln A_{m0}\left(\Delta t\right)\right]^2}{2S_{a0}^2\left(\Delta t\right)}\right\} \tag{1.29}$$

με

$$A_{m0}\left(\Delta t\right) = A_m^{\left[1-\exp(-\beta_A \Delta t)\right]} A\left(t_0\right)^{\exp(-\beta_A \Delta t)} \tag{1.30}$$

και

$$S_{a0}\left(\Delta t\right) = S_a \sqrt{1-\exp\left(-2\,\beta_A\,\Delta t\right)} \tag{1.31}$$

Επομένως η πιθανότητα αποκοπής για ένα σύστημα που κάνει χρήση της τεχνικής διαφορισμού χρόνου υπολογίζεται από:

$$P_{TD} = \Pr\left\{ A(t) \geq a_{thr},\ A(t_0) \geq a_{thr} \right\} = \int_{a_{thr}}^{\infty} \int_{a_{thr}}^{\infty} p\left\{ A(t),\, t \mid A(t_0),\, t_0 \right\}\, p\left\{A(t_0), t_0\right\} dA(t)\, d\left(A(t_0)\right) \tag{1.32}$$

Στην Εικόνα 1-13 και Εικόνα 1-14 δίνονται από κοινού πιθανότητες υπέρβασης της απόσβεσης για την περιοχή Spino d'Adda σε συχνότητες 19 GHz και 40 GHz για διάφορες τιμές χρονικής καθυστέρησης από [Fabbro09]. Για τον υπολογισμό της θεωρητικής τιμής των από κοινού πιθανοτήτων η δυναμική παράμετρος τέθηκε ίση με 10^{-4} $\sec^{-1}$ και για τα δύο πειράματα [Arapoglou08]. Από τις γραφικές φαίνεται ότι η μέθοδος θεωρείται ακριβής για τη μοντελοποίηση της από κοινού πιθανότητας.

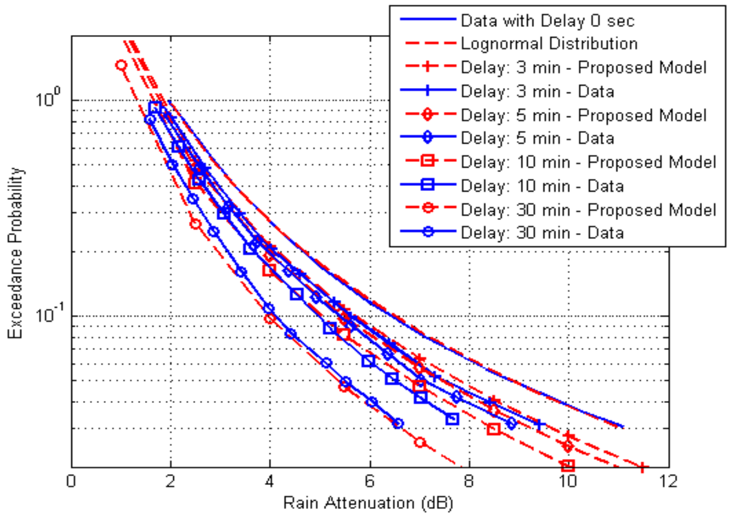

Εικόνα 1-13 Πιθανότητα υπέρβασης με και χωρίς διαφορισμό στο πεδίο του χρόνου από δεδομένα και το προτεινόμενο μοντέλο στους 19 GHz

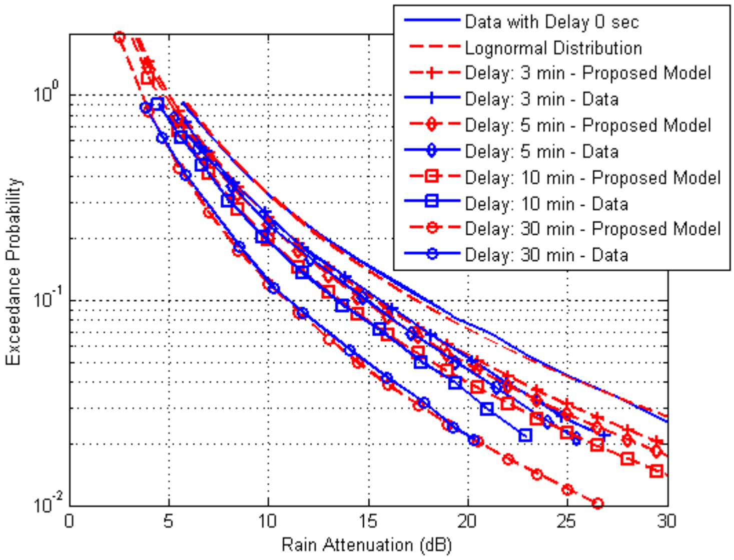

Εικόνα 1-14 Πιθανότητα υπέρβασης με και χωρίς διαφορισμό στο πεδίο του χρόνου από δεδομένα και το προτεινόμενο μοντέλο στους 40 GHz

1.2.8 Μοντελοποίηση της απόδοσης δορυφορικών συστημάτων χρονικού διαφορισμού με συναρτήσεις Copulas

Στην παρούσα ενότητα γίνεται χρήση των συναρτήσεων copulas για τη μοντελοποίηση της από κοινού πιθανότητας υπέρβασης της απόσβεσης λόγω βροχής για συστήματα που κάνουν χρήση του διαφορισμού στο πεδίο του χρόνου. Γνωρίζοντας την πιθανότητα υπέρβασης της απόσβεσης, υπολογίζεται η από κοινού πιθανότητα με χρήση των συναρτήσεων copulas ως:

$$P\left(A(t)\geq A_{th}, A(t+\Delta t)\geq A_{th}\right)=1-u-v+C(u,v) \tag{1.33}$$

Εξετάζονται οι παρακάτω συναρτήσεις Copulas:

$$C(u,v)=\left(u^{-\theta}+v^{-\theta}-1\right)^{-1/\theta}, \theta\in\left(0,+\infty\right) \tag{1.34}$$

$$C(u,v)=\exp\left[-\left(\left(-\ln u\right)^{\theta}+\left(-\ln v\right)^{\theta}\right)^{1/\theta}\right], \theta\in[1,+\infty) \tag{1.35}$$

Για την αξιολόγηση της μοντελοποίηση αρχικά χρησιμοποιήθηκαν δεδομένα από [Fabbro09] για το Spino d’Adda στις συχνότητες 19 GHz και 40 GHz για χρονικές καθυστερήσεις 1 min και 60 min. Τα αποτελέσματα δίνονται στην Εικόνα 1-15 και Εικόνα 1-16. Στην Εικόνα 1-17, δίνονται αποτελέσματα για την περιοχή Kuala Lumpur με συχνότητα λειτουργίας στα 12 GHz [Ismail00].

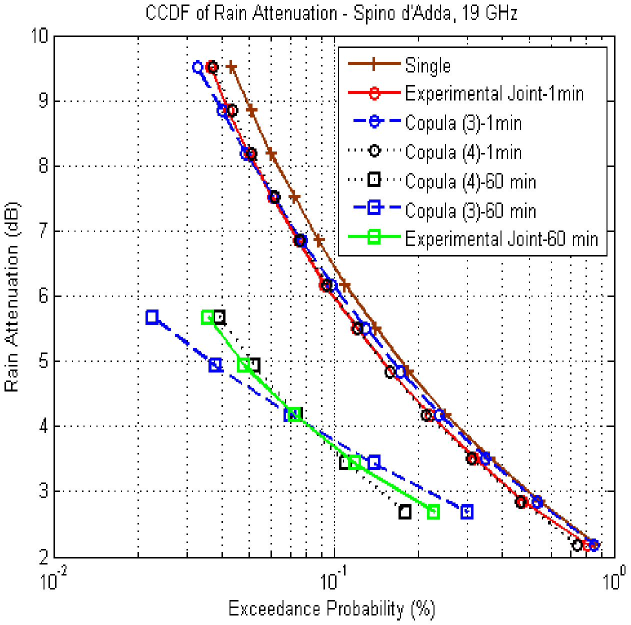

Εικόνα 1-15 Πιθανότητα υπέρβασης της απόσβεσης για την περιοχή Spino d'Adda στα 19 GHz

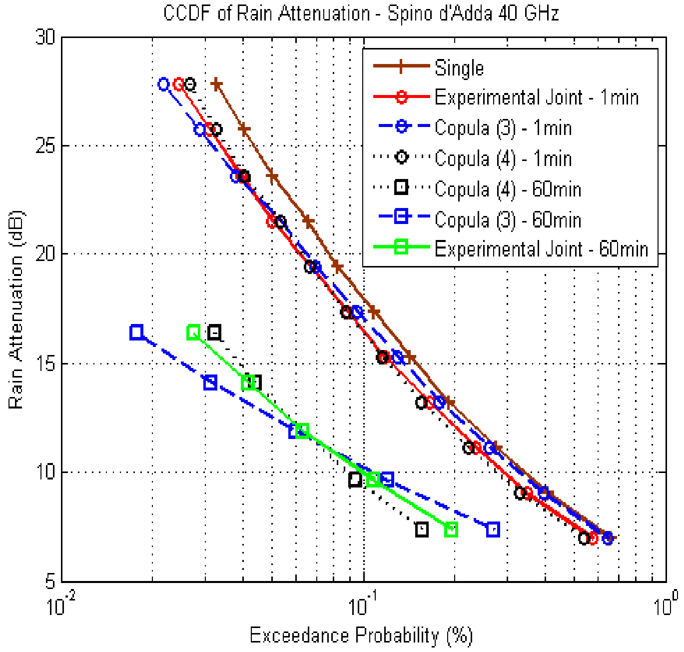

Εικόνα 1-16 Πιθανότητα υπέρβασης της απόσβεσης για την περιοχή Spino d'Adda στα40 GHz

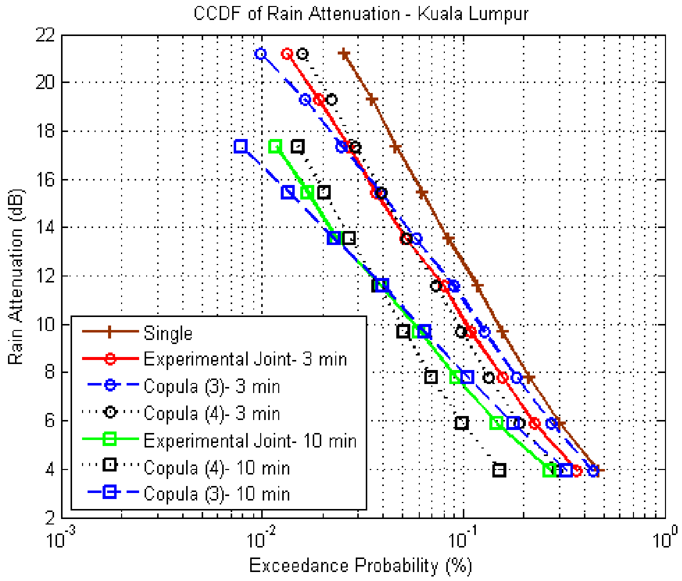

Εικόνα 1-17 Πιθανότητα υπέρβασης της απόσβεσης για την περιοχή Kuala Lumpur στα 12 GHz

1.3 Μοντελοποίηση δυναμικών χαρακτηριστικών της απόσβεσης λόγω βροχής και των σπινθηρισμών

Στην παρούσα ενότητα, παρουσιάζονται τα αποτελέσματα που προέκυψαν από τις παρακάτω δημοσιεύσεις (σε διεθνή περιοδικά και σε συνέδρια με κριτές) και αφορούν την μοντελοποίηση των δυναμικών χαρακτηριστικών και της παραγωγής χρονοσειρών του καναλιού.

[J1] C. I. Kourogiorgas, A. D. Panagopoulos, “A Rain Attenuation Stochastic Dynamic Model for LEO Satellite Systems Operating at Frequencies above 10 GHz”, IEEE Transactions on Vehicular Technology, vol. 64, issue 2, Feb. 2015.

[C1] C. Kourogiorgas, A. D. Panagopoulos, J. D. Kanellopoulos, “Synthesizing Rain Attenuation Time Series for an Earth-LEO Satellite Link”, MCM7 COST Action IC0802, 16-18 April 2012, Portsmouth, Great Britain.

[C2] C. Kourogiorgas, A. D. Panagopoulos, J. D. Kanellopoulos, P.-D. M. Arapoglou, “Rain Attenuation Time Series Synthesizer for LEO Satellite Systems Operating at Ka Band”, ASMS/SPSC 2012, 5-7 September 2012, Baiona, Spain.

[C3] C. Kourogiorgas, A. D. Panagopoulos, P.-D. M. Arapoglou, “Rain Attenuation Time Series Generator for Medium Earth Orbit Links Operating at Ka Band and above”, EuCAP 2014, 6-11 April 2014, The Hague, The Netherlands.

[C4] C. Kourogiorgas, G. A. Karagiannis, A. D. Panagopoulos, "Space-Time Rain Rate Field Generator for Multi-Antenna Satellite Communication Applications", EuCAP 2013, 8-12 April 2013, Gothenburg, Sweden.

[C5] C. Kourogiorgas, A. D. Panagopoulos, "A Tropospheric Scintillation Time Series Synthesizer based on Stochastic Differential Equations", 2013 Joint Conference: 19th Ka and Broadband Communications, Navigation and Earth Observation Conference and 31st AIAA ICSSC, 14-17 October 2013, Florence, Italy.

[C6] C. Kourgiorgas, A. Kelmendi, A. D. Panagopoulos, S. N. Livieratos, A. Vilhar, G. E. Chatzarakis, "Rain Attenuation Time Series Synthesizer based on Copula Functions", EuCAP 2015, Lisboa, April 2015.

1.3.1 Μοντελοποίηση της δυναμικής παραμέτρου της απόσβεσης λόγω βροχής

Η δυναμική παράμετρος όπως αυτή ορίζεται στο μοντέλο Maseng-Bakken [Maseng81], καθορίζει το πόσο γρήγορα μεταβάλλεται η απόσβεση λόγω βροχής. Επομένως εξαρτάται από τα γεωμετρικά και ηλεκτρικά χαρακτηριστικά της ζεύξης. Για τον υπολογισμό της δυναμικής παραμέτρου για την απόσβεση χρησιμοποιήθηκε η υπόθεση ότι τόσο η σημειακή ένταση βροχόπτωσης [Panagopoulos03], [Manning90] όσο και η απόσβεση λόγω βροχής ακολουθούν τη ΣΔΕ που προτείνεται στο [Maseng81]. Η έκφραση που προέκυψε δίνεται από:

$$\beta_A\left(\theta,\left|\Delta t_A\right|\right)=-\frac{1}{2\,|\,\Delta t_A\,|}\ln\left\{1-\frac{1}{S_A^2}\ln\left\{1+\frac{H_1(\theta)}{L(\theta)^2}\left[\exp\left(b^2S_R^2(1-\exp(-2\beta_R\,|\,\Delta t_R\,|))\right)-1\right]\right\}\right\} \tag{1.36}$$

με

$$H_1\left(\theta_t\right)=2L\left(\theta_t\right)g\sinh^{-1}\left(\frac{L\left(\theta_t\right)}{g}\right)+2g^2\left[1-\sqrt{\left(\frac{L\left(\theta_t\right)}{g}\right)^2+1}\right] \tag{1.37}$$

όπου το g σταθερά η οποία εξαρτάται από την περιοχή και την ένταση βροχόπτωσης.

Από την παραπάνω εξίσωση παρατηρούμε ότι η δυναμική παράμετρος εξαρτάται από τα στατιστικά χαρακτηριστικά της έντασης βροχόπτωσης, τα στατιστικά χαρακτηριστικά της απόσβεσης και από τη γωνία ανύψωσης. Στην Εικόνα 1-18, δίνεται η δυναμική παράμετρος της απόσβεσης σε συνάρτηση με τη γωνία ανύψωσης και για διαφορετικές τιμές της σταθεράς g και διαφορετικές τιμές της συχνότητας λειτουργίας για την περιοχή των Αθηνών. Παρατηρείται ότι όσο αυξάνεται η γωνία ανύψωσης αυξάνεται και η δυναμική παράμετρος

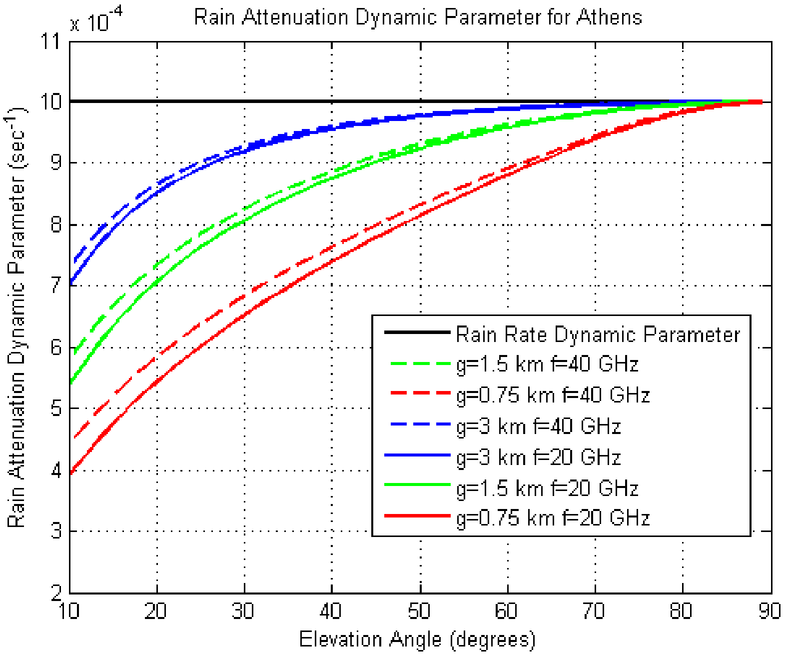

Εικόνα 1-18 Δυναμική παράμετρος σε συνάρτηση της γωνίας ανύψωσης για την Αθήνα, Ελλάδα

1.3.2 Στοχαστική μοντελοποίηση της απόσβεσης λόγω βροχής για ζεύξεις Γης με δορυφόρους MEO/LEO σε συχνότητες άνω των 10GHz

Μία ουσιαστική διαφορά για τη μοντελοποίηση της απόσβεσης σε ζεύξεις με MEO/LEO δορυφόρους σε σχέση με μία ζεςύξη Γης-GEO δορυφόρου είναι ότι η γωνία ανύψωσης της ζεύξης στην πρώτη περίπτωσής αλλάζει με το χρόνο καθώς οι δορυφόροι κινούνται πάνω από τον επίγειο σταθμό. Επομένως αλλάζουν με το χρόνο τόσο τα δυναμικά χαρακτηριστικά του καναλιού όσο και τα στατιστικά χαρακτηριστικά πρώτης τάξης [Panagopoulos03], [Panagopoulos04a]. Παρ' όλα αυτά στο προτεινόμενο μοντέλο γίνεται χρήση των υποθέσεων του μοντέλου [Maseng81], για δεδομένη γωνία ανύψωσης. Επομένως όταν η γωνία ανύψωσης είναι σταθερή η απόσβεση λόγω βροχής θεωρείται ότι ακολουθεί τη λογαριθμοκανονική κατανομή και η τυχαία μεταβλητή $X_t = \dfrac{\ln\left(A_t / A_m(\theta)\right)}{S_A(\theta)}$ περιγράφεται από:

$$dX_t = -\beta_A\left(\theta\right) X_t dt + \sqrt{2\beta_A\left(\theta\right)} dWt \tag{1.38}$$

όπου β_A η δυναμική παράμετρος. Η λύση της παραπάνω ΣΔΕ είναι:

$$X_t^{LEO} = e^{-\int_0^t \beta_A(\theta_s, |\Delta t_A|) ds} \left(X_0^{LEO} + \int_0^t \sqrt{2\beta_A\left(\theta_s, |\Delta t_A|\right)} \exp\left(\int_0^s \beta_A\left(\theta_{s'}, |\Delta t_A|\right) ds' \right) dW_s \right) \tag{1.39}$$

όπου X_0^{LEO} η αρχική τιμή της τυχαίας μεταβλητής. Η απόσβεση λόγω βροχής δίνεται μέσω του παρακάτω μετασχηματισμου:

$$A_t^{LEO} = A_m\left(\theta_t\right)\exp\left[X_t^{LEO} S_A(\theta_t)\right] \tag{1.40}$$

Χρησιμοποιώντας το παραπάνω μοντέλο, μπορούν να παραχθούν χρονοσειρές απόσβεσης βροχής για MEO/LEO δορυφόρους. Στην Εικόνα 1-19, δίνεται ένα παράδειγμα χρονοσειρών απόσβεσης βροχής για μία ζεύξη μεταξύ ενός επίγειου σταθμού στην Αθήνα και του δορυφόρου IRIDIUM για συχνότητα λειτουργίας 20 GHz. Στην Εικόνα 1-20, δίνεται η πιθανότητα υπέρβασης της απόσβεσης για ζεύξεις μεταξύ Αθήνας, Παρισιού και του IRIDIUM δορυφόρου για συχνότητες λειτουργίας στα 20 GHz και 40 GHz υπολογισμένη τόσο από τις χρονοσειρές όσο και από θεωρητικές εκφράσεις.

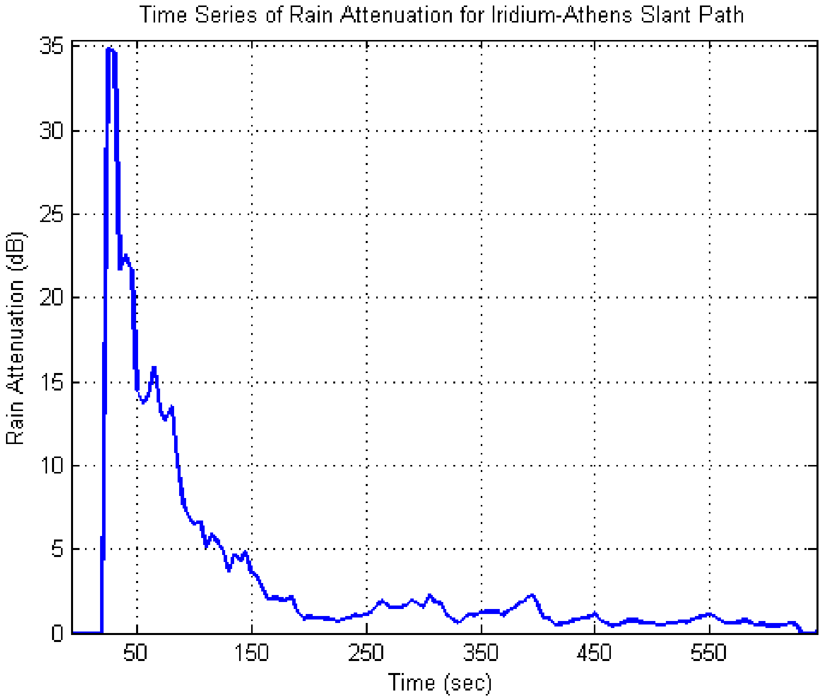

Εικόνα 1-19 Παράδειγμα χρονοσειρών απόσβεσης σε ζεύξη μεταξύ Αθήνας και IRIDIUM LEO δορυφόρου στα 20GHz

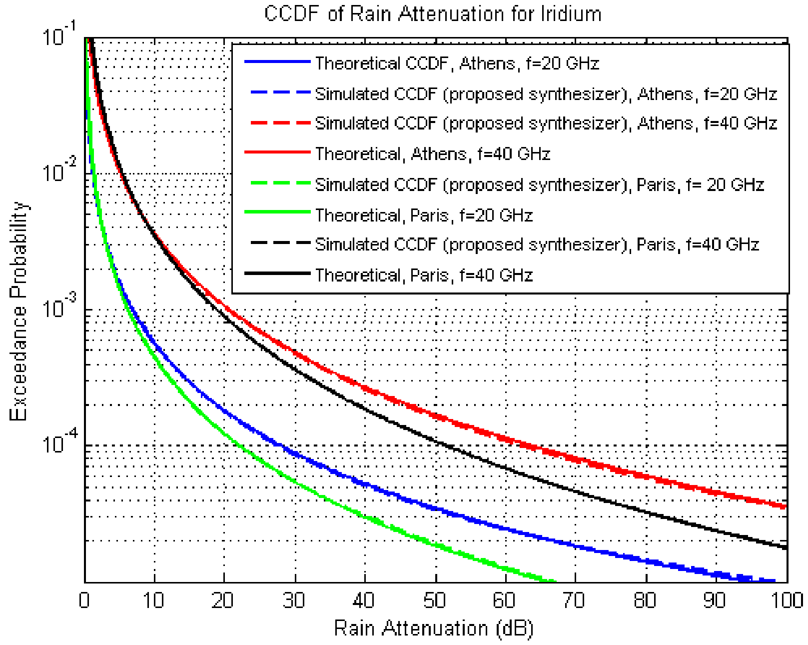

Εικόνα 1-20 Πιθανότητα υπέρβασης της απόσβεσης για ζεύξει μεταξύ Αθήνας, Παρισιού και του δορυφόρου IRIDIUM στα 20 GHz και 40 GHz.

1.3.3 Μοντέλο παραγωγής χρονοσειρών απόσβεσης λόγω βροχής κάνοντας χρήση των συναρτήσεων copulas

Σε προηγούμενη ενότητα χρησιμοποιήθηκαν οι συναρτήσεις copulas για τη μοντελοποίηση των από κοινού στατιστικών χαρακτηριστικών για την απόσβεση λόγω βροχής σε συστήματα που κάνουν χρήση της τεχνικής διαφορισμού θέσης και χρόνου. Στην παρούσα ενότητα θα παρουσιαστεί ένα μοντέλο για την παραγωγή χρονοσειρών της απόσβεση με χρήση των συναρτήσεων copulas.

Για το σκοπό αυτό χρησιμοποιείται η Gaussian copula πολλών μεταβλητών η οπία δίνεται από [Nelsen06]:

$$C(\mathbf{u}) = \Phi_R^n\left(\Phi^{-1}\left(u_1\right),\ldots,\Phi^{-1}\left(u_n\right)\right) \tag{1.41}$$

όπου Φ_R^n είναι η αθροιστική κατανομή μιας πολυμεταβλητής κανονικής κατανομής με τυχαίες μεταβλητές μηδενικής μέσης τιμής και πίνακα συσχέτισης **R**. Η συνάρτηση Φ^{-1} είναι η ανάστροφη αθροιστική κατανομή μηδενικής μέσης τιμής και τυπικής απόκλισης ίσης με 1.

Η Gaussian copula ελέγχθηκε για τη μοντελοποίηση των από κοινού χαρακτηριστικών πρώτης τάξης για απόσβεση συσχετισμένη στο χρόνο χρησιμοποιώντας δεδομένα από [Fabbro09], [Ismail00], [Kuhar14]. Στον Πίνακας 4, δίνονται τα στατιστικά χαρακτηριστικά του σχετικού σφάλματος για τα τέσσερα πειράματα.

TABLE I.

Πίνακας 4. Στατιστικά χαρακτηριστικά του σχετικού σφάλματος για την Gaussian Copula

Experiment	Mean error	Std	RMS
Spino 19GHz	-0,5%	4,88%	4,9%
Spino 40 GHz	-0,91%	6,3%	6,3%
Ljubljana	-1%	9,9%	9,9%
KLM	-2,9%	13,4%	13,7%

Από τα παραπάνω πειράματα και την προσαρμογή της Gaussian copula, εξήχθησαν δύο εκφράσεις για την παράμετρο της συγκεκριμένης συνάρτησης copula για ευρωπαϊκές περιοχές:

$$\rho\left(\Delta t\right) = 0.31e^{-\left(\frac{\Delta t}{52}\right)} + 0.69e^{-\left(\frac{\Delta t}{1390}\right)^{2}} \tag{1.42}$$

και για τροπικές περιοχές:

$$\rho\left(\Delta t\right) = e^{-\left(\frac{\Delta t}{60.1}\right)} \tag{1.43}$$

Από τον ορισμό της Gaussian copula, μπορεί να υπολογιστεί η συσχέτιση ορισμένη κατά τον Kendall (τ) ως [Nelsen06]:

$$\tau = \frac{2}{\pi}\sin^{-1}\left(\rho\right) \tag{1.44}$$

Με βάση τη μοντελοποίηση της παραμέτρου της Gaussian copula και τον ορισμό αυτής, μπορούν να παραχθούν χρονοσειρές απόσβεσης λόγω βροχής με βάση τον παρακάτω αλγόριθμο:

- Δημιουργία πολλαπλών τυχαίων μεταβλητών που ακολουθούν την κατανομή Gauss με μηδενική μέση τιμή και πίνακα συσχέτισης **R**
- Υπολογισμός της αθροιστικής κατανομής για το κάθε δείγμα
- Υπολογισμός της ανάστροφης αθροιστικής κατανομής για το κάθε δείγμα που προέκυψε από το προηγούμενο βήμα. Η αθροιστική κατανομή που χρησιμοποιείται σε αυτό το βήμα μπορεί να είναι οποιασδήποτε μορφής.

Στην , δίνεται ένα παράδειγμα χρονοσειρών της απόσβεσης για ένα σταθμό βάσης στη Λιουμπλιάνα, Σλοβενία, με συχνότητα λειτουργίας 20.2 GHz και γωνία ανύψωσης 36.3^{o}.

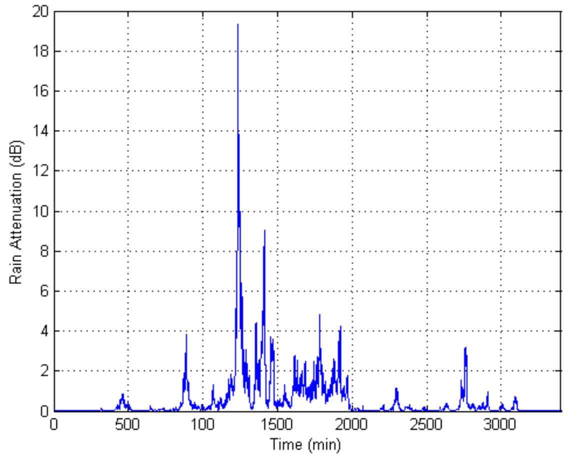

Εικόνα 1-21 Παράδειγμα χρονοσειρών απόσβεσης για την περιοχή της Λιουμπλιάνας

Το προτεινόμενο μοντέλο εξετάζεται ως προς τα στατιστικά χαρακτηριστικά πρώτης και δεύτερης τάξης των χρονοσειρών. Στην Εικόνα 1-22 δίνεται για την περιοχή της Λιουμπλιάνας η πιθανότητα υπέρβασης της απόσβεσης όπως αυτή υπολογίζεται από τις χρονοσειρές, τα δεδομένα και θεωρητική έκφραση της κατανομής Weibull για συστήματα με καθυστέρηση 1 λεπτού και χωρίς καθυστέρηση. Παρατηρείται ότι η μέθοδος αναπαράγει τα στατιστικά χαρακτηριστικά πρώτης τάξης. Στην Εικόνα 1-23, δίνεται η συσχέτιση κατά Kendall όπως αυτή υπολογίζεται από τη θεωρητικής εξίσωση που δόθηκε προηγουμένως όσο και από τις χρονοσειρές.

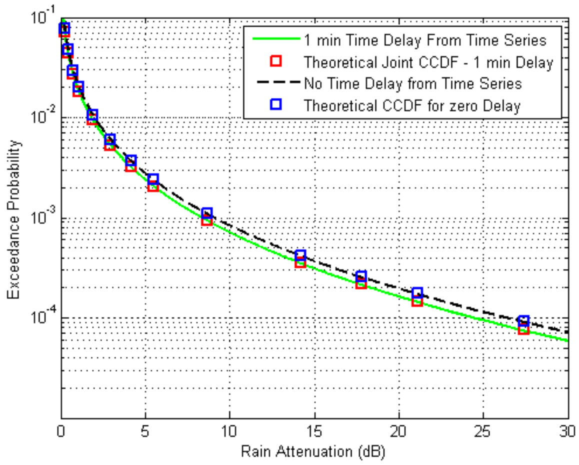

Εικόνα 1-22 Αθροιστική κατανομή της απόσβεσης για συστήματα χωρίς καθυστέρηση και με καθυστέρηση ενός λεπτού.

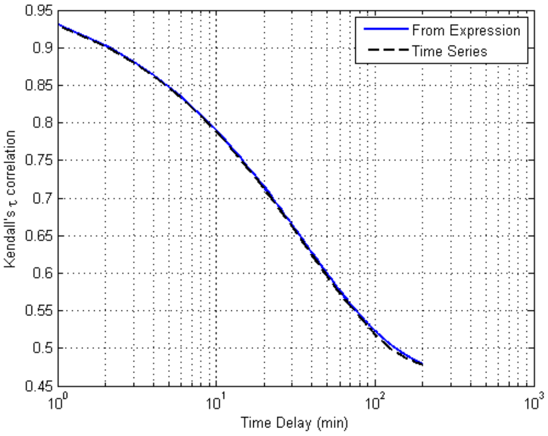

Εικόνα 1-23 Η συσχέτιση κατά τον Kendall από χρονοσειρές και από θεωρητική έκφραση

1.3.4 *Παραγωγή χρονοσειρών πεδίων βροχής*

Στο [Manning90], δείχνεται ότι η ΣΔΕ που προτείνεται στο [Maseng81] περιγράφει και τη σημειακή ένταση βροχόπτωσης. Κάνοντας χρήση των πολυδιάστατων ΣΔΕ και της χωρικής συσχέτισης για την ένταση βροχόπτωσης όπως προτείνεται στο [Paraboni], μπορούν να δημιουργηθούν χρονοσειρές πεδίων βροχής.

Η μορφή της πολυδιάστατης ΣΔΕ δίνεται από:

$$d\mathbf{R}_t = \mathbf{F}\left(\mathbf{R}_t\right)dt + \mathbf{Z}\left(\mathbf{R}_t\right)d\mathbf{W}_t \qquad (1.45)$$

, όπου ακολουθώντας τη μεθοδολογία [Karagiannis12], μπορούν να υπολογιστούν οι παράμετροι της ΣΔΕ.

Στην Εικόνα 1-24, δίνονται τρία πεδία βροχής σε τρεις διαφορετικές στιγμές t_0, t_0+1 min, t_0+5 min, για την περιοχή της Αθήνας.

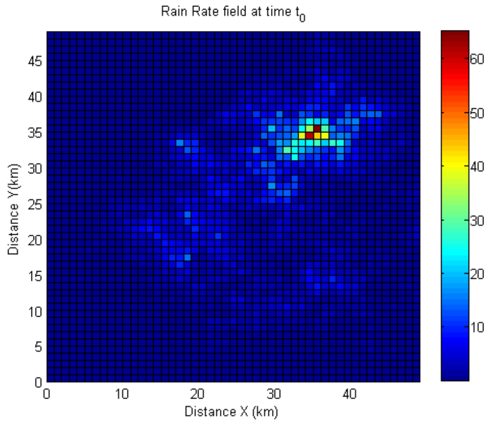

(a)

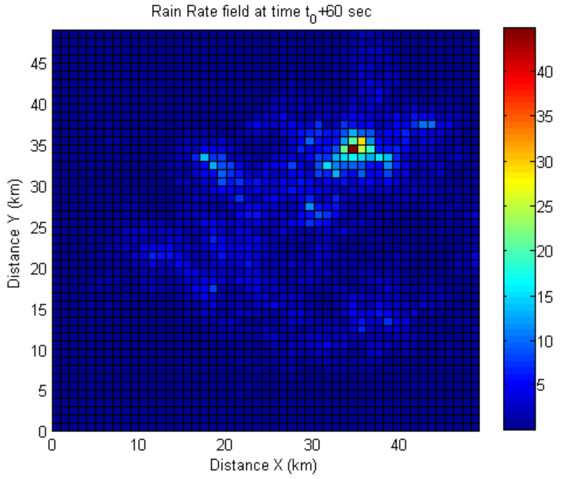

(b)

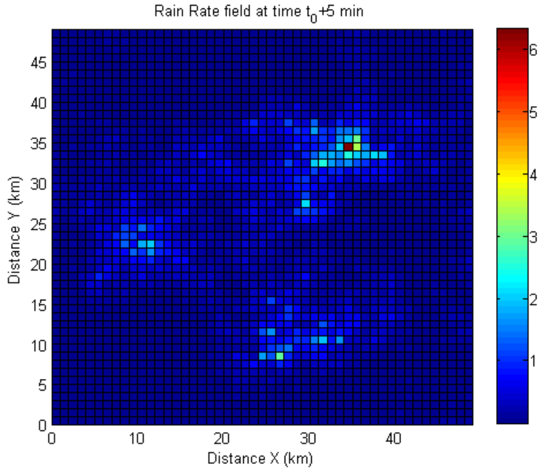

(c)

Εικόνα 1-24 Πεδία βροχής τις χρονικές στιγμές t_0, t_0 +60 sec και t_0 + 5min

Από τα πεδία βροχής μπορεί να υπολογιστεί η ειδική απόσβεση μέσω της έκφρασης

$$A_0(x,y) = aR(x,y)^b \tag{1.46}$$

, όπου τα *a* και *b* υπολογίζονται από τη σύσταση ITU-R. P. 838 [ITU-R. P.838] και χρονοσειρές απόσβεσης για μία ζεύξη να υπολογιστούν μέσω αριθμητικής επίλυσης της:

$$A = \int_0^L A_0\left(z = \sqrt{x^2 + y^2}\right) dz \tag{1.47}$$

Στην Εικόνα 1-25, δίνεται η πιθανότητα υπέρβασης της απόσβεσης για μία ζεύξη Γης-δορυφόρου με τον επίγειο σταθμό τοποθετημένο στη Βιέννη, Αυστρία, συχνότητα λειτουργίας 25 GHz και γωνία ανύψωσης 30^o.

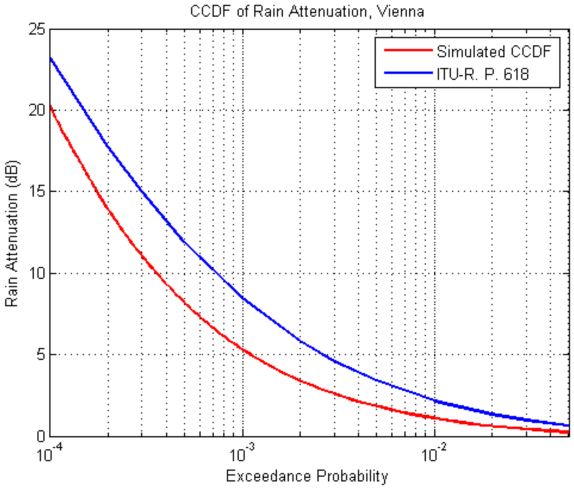

Εικόνα 1-25 Πιθανότητα υπέρβασης για μία ζεύξη με τον επίγειο σταθμό τοποθετημένο στη Βιέννη, Αυστρία από την προτεινόμενη μεθοδολογία και τη σύσταση ITU-R. P. 618

Στην Εικόνα 1-26, δίνεται η από κοινού πιθανότητα υπέρβασης της απόσβεσης για ένα δορυφορικό σύστημα διπλού διαφορισμού θέσης με τους επίγειου σταθμού τοποθετημένους στην Αθήνα σε απόσταση 9 km. Η συχνότητα λειτουργίας είναι 30 GHz και η γωνία ανύψωσης 25^{o}.

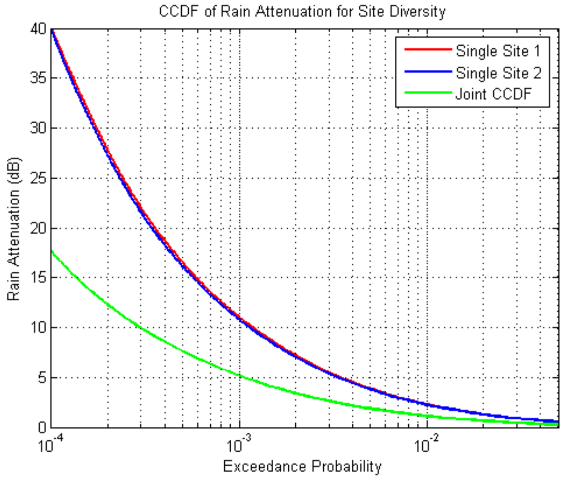

Εικόνα 1-26 Πιθανότητα υπέρβασης της απόσβεσης και από κοινού πιθανότητα υπέρβασης της απόσβεσης για ένα σύστημα διαφορισμού θέσης

1.3.5 Μοντέλο παραγωγής χρονοσειρών του σπινθηρισμού λόγω των τροποσφαιρικών στροβίλων

Το προτεινόμενο μοντέλο βασίζεται στη fractional κίνηση Brown (fBm) [Mishura08]. Το προτεινόμενο μοντέλο αναπαράγει τόσο τα στατιστικά χαρακτηριστικά πρώτης τάξης όσο και το φάσμα ισχύος. Βάσει των μοντέλων [Mousley82] και [Vasseur99], δείχνεται ότι βραχυπρόθεσμα η λογαριθμική τιμή του κανονικοποιημένου πλάτους (χ) ακολουθεί Gauss κατανομή μηδενικής μέσης τιμής με δεδομένη διακύμανση σ_{χ}^{2}:

$$p_{st}\left(\chi/\sigma_{\chi}^{2}\right)=\frac{1}{\sqrt{2\pi\sigma_{\chi}^{2}}}\exp\left(-\frac{\chi^{2}}{2\sigma_{\chi}^{2}}\right) \tag{1.48}$$

Η μακροπρόθεσμη κατανομή του χ είναι:

$$p_{lt}=\int_{0}^{+\infty}p_{st}\left(\chi/\sigma_{\chi}^{2}\right)p\left(\sigma_{\chi}^{2}\right)d\sigma_{\chi}^{2} \tag{1.49}$$

όπου $p\left(\sigma_{\chi}^{2}\right)$ η συνάρτηση πυκνότητας πιθανότητας της διακύμανσης η οποία ακολουθεί τη λογαριθμοκανονική κατανομή::

$$p\left(\sigma_{\chi}^{2}\right)=\frac{1}{\sqrt{2\pi}\sigma_{\chi}^{2}s}\exp\left(-\frac{\left[\ln\left(\sigma_{\chi}^{2}/m\right)\right]^{2}}{2s^{2}}\right) \tag{1.50}$$

Για την παραγωγή χρονοσειρών αρχικά παράγονται χρονοσειρές της τυχαίας μεταβλητής $\chi_{t,1}$ η οποία έχει μηδενική μέση τιμή και διακύμανση 1 [Shao95]:

$$d\chi_{t,1}=-\lambda\chi_{t,1}dt+\sigma dB_{H} \tag{1.51}$$

με B_H fBm με δείκτη Hurst H και λύση [Shao95], [Cheridito03]:

$$\chi_{t,1}=e^{-\lambda t}\sigma\int_{0}^{t}e^{\lambda u}dB_{u}^{H} \tag{1.52}$$

Η παράμετρος σ δίνονται από:

$$\sigma=\frac{1}{\sqrt{\frac{\Gamma(2H+1)\sin(\pi H)}{2\pi}\int_{-\infty}^{+\infty}\frac{|y|^{1-2H}}{\lambda^{2}+y^{2}}dy}} \tag{1.53}$$

, ο δείκτης Hurst από την τιμή που επιθυμούμε στη εκθετική μείωση του φάσματος ισχύος:

$$F_{\chi_{t,1}}(f)\sim f^{-(2H+1)} \tag{1.54}$$

και η τιμή της παραμέτρου λ από τη συχνότητα στο γόνατο του φάσματος ισχύος: $\omega_{c}=\lambda^{\frac{1}{\mathrm{H}+1/2}}$

Τέλος, για την παραγωγή χρονοσειρών, πολλαπλασιάζονται οι χρονοσειρές του $\chi_{t,1}$ με την τυπική απόκλιση των σπινθηρισμών σ_{χ}:

$$\chi_{t}=\sigma_{\chi}\chi_{t,1} \tag{1.55}$$

Στην , δίνεται ένα παράδειγμα χρονοσειρών του σπινθηρισμού για την περιοχή Louvain-la-neuve, Βέλγιο, ενώ στην δίνεται η πιθανότητα υπέρβασης κατ' απόλυτη τιμή του σπινθηρισμού από τις χρονοσειρές και τα δεδομένα [Vasseur99] και στην το φάσμα ισχύος από τη θεωρία και τις χρονοσειρές.

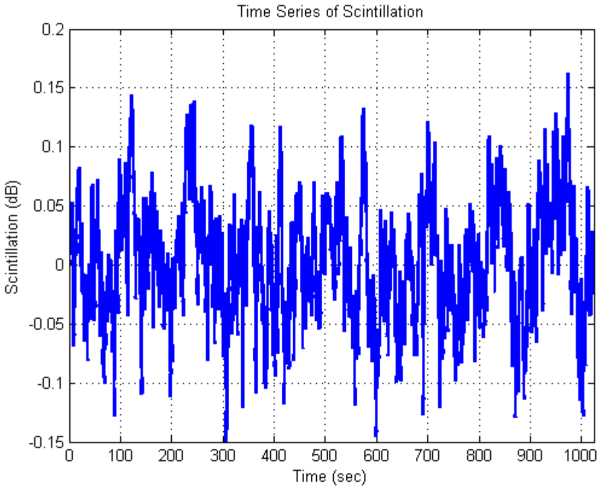

Εικόνα 1-27 Παράδειγμα παραγωγής χρονσειρών σπινθηρισμού

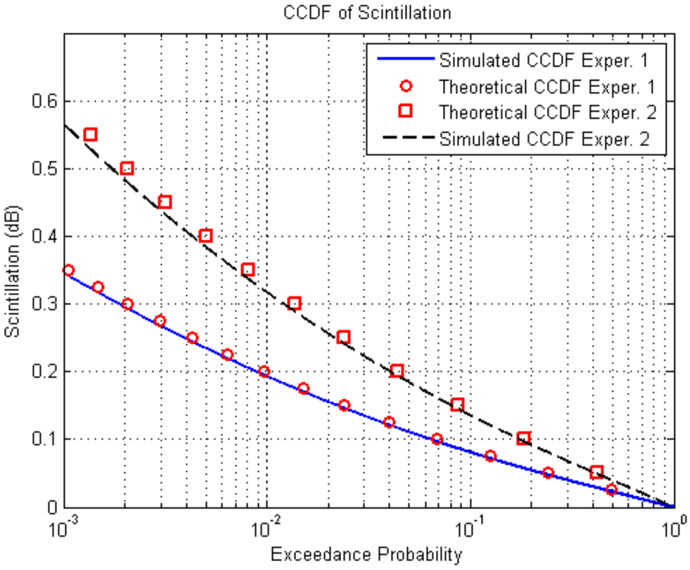

Εικόνα 1-28 Πιθανότητα υπέρβασης σπινθηρισμού από δεδομένα και χρονοσειρές

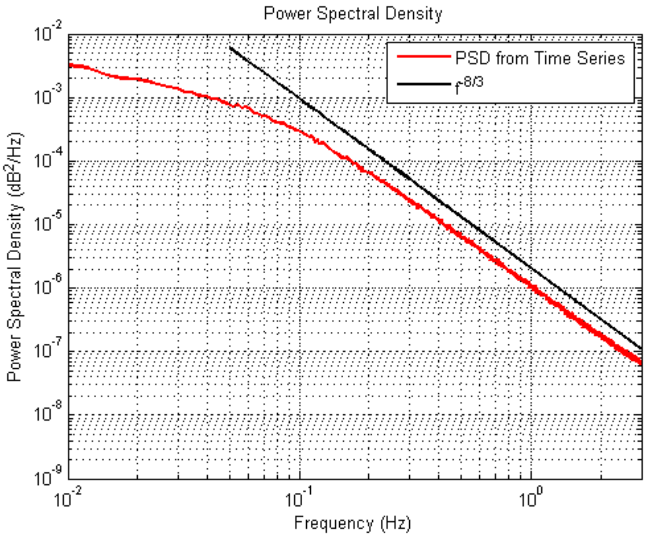

Εικόνα 1-29 Κατανομή φάσματος ισχύος με βάση τη θεωρία και τις παραγόμενες χρονοσειρές

1.4 Αξιολόγηση της Επίδοσης Γνωστικών Δορυφορικών Συστημάτων Επικοινωνιών και Συστημάτων Παρατήρησής Γης σε Συχνότητες άνω των 10 GHz

Στην παρούσα ενότητα παρουσιάζεται η αξιολόγηση της επίδοσης γνωστικών δορυφορικών συστημάτων επικοινωνιών μέσω της μοντελοποίησης των παρεμβολών σε συνθήκες βροχής και συστημάτων παρατήρησης Γης. Τα αποτελέσματα της παρούσας ενότητας αφορούν στις παρακάτω δημοσιεύσεις:

[J1] C. Kourogiorgas, P.-D. Arapoglou, A. D. Panagopoulos, “Statistical Characterization of Adjacent Satellite Interference for Earth Stations on Mobile Platforms Operating at Ku and Ka Band”, IEEE Wireless Communication Letters, vol. 4, issue 1, 2015.

[J2] Z. Katona, C. Kourogiorgas, A. D. Panagopoulos, N. Jeannin, “Capacity Analysis of High-Throughput Satellite Links for Earth Observation Missions”, accepted at International Journal of Satellite Communications and Networking.

[C1] C. Kourogiorgas, A. D. Panagopoulos, “Interference Statistical Distribution for Cognitive Satellite Communication Systems Operating above 10 GHz”, 7th Advanced Satellite Multimedia Systems Conference and the 13th Signal Processing for Space Communications Workshop, pp. 256-261, 8-10 September 2014, Livorno, Italy

[C2] C. Kourogiorgas, A. D. Panagopoulos, K. P. Liolis, "Cognitive Uplink FSS and FS Links Coexistence in Ka-band: Propagation based Interference Analysis", ICC 2015, London, UK, June 2015.

1.4.1 Στατιστική κατανομή παρεμβολών για δορυφορικά γνωστικά συστήματα που λειτουργούν σε συχνότητες άνω των 10 GHz

Η γεωμετρία του συστήματος το οποίο θεωρείται και αξιολογείται στην παρούσα υπο-ενότητα δίνεται στην Εικόνα 1-30. Αφορά σε δύο συστήματα τα οποία προσφέρουν διαφορετικές υπηρεσίες. Παρ' όλα αυτά για το διαμοιρασμό του φάσματος η μία υπηρεσία θεωρείται πρωτεύουσα και η άλλη δευτερεύουσα. Το παρόν σύστημα είναι ένα διπλό δορυφορικό σύστημα το οποίο λειτουργεί στις Ku και Ka ζώνες συχνοτήτων [Sharma13].

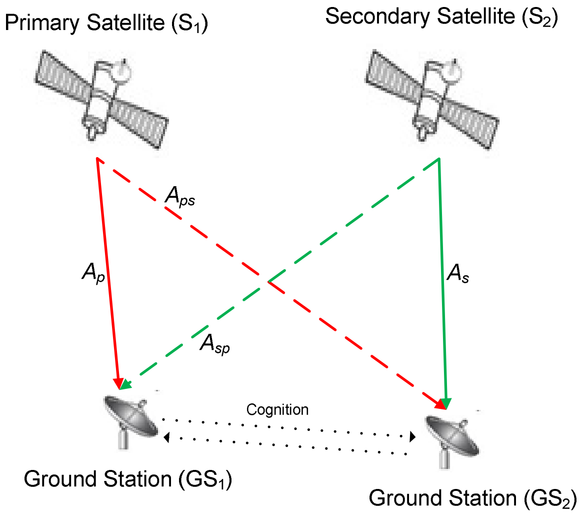

Εικόνα 1-30 Γεωμετρία διπλού δορυφορικού συστήματος

Για την αξιολόγηση της επίδοσης και της λειτουργίας οτυ παραπάνω συστήματος για την κάτω ζεύξη χρειάζεται η μοντελοποίηση της παρεμβολής από τη μία ζεύξη στην άλλη. Θέλοντας να αξιολογήσουμε μόνο την επίδραση των παρεμβολών χρησιμοποιούμε τη μετρική του λόγου ισχύς σήματος προς ισχύ παρεμβολών:

$$SIR = \frac{S}{I} \tag{1.56}$$

Για τον υπολογισμό του SIR και της πιθανότητας αποκοπής μπορούν να χρησιμοποιηθούν δύο τεχνικές είτε παράγοντας χρονοσειρές του SIR είτε μέσω θεωρητικών εκφράσεων οι οποίες λόγω πολυπλοκότητας των εξήχθησαν μόνο για ένα παρεμβάλλων δορυφόρο.

Για την πρώτη τεχνική, χρειάζονται χρονοσειρές απόσβεσης βροχής σε χωρικά διαχωρισμένες ζεύξεις και επομένως χωρικά συσχετισμένες. Για το λόγο αυτό χρησιμοποιείται η μέθοδος που παρουσιάζεται στο [Karagiannis12]. Για την εξαγωγή της θεωρητικής έκφρασης γίνεται χρήση της υπόθεσης ότι η απόσβεση λόγω βροχής ακολουθεί τη λογαριθμοκανονική κατανομή και επομένως η πιθανότητα αποκοπής για ένα χρήστη δίνεται από [Panagopoulos03b]:

$$P_{out,p} = P\left[SIR_p \le SIR_{th}, A_p \le A_{th,p} \right] \tag{1.57}$$

$$P_{out} = \frac{1}{2} erfc\left(\frac{u_r}{\sqrt{2}} \right) - \frac{1}{2} erfc\left(\frac{u_{th}}{\sqrt{2}} \right) - \int_{u_r}^{u_{th}} f_{U_1}(u_1) erfc\left(\frac{u_x - \rho_n u_1}{\sqrt{2(1-\rho_n^2)}} \right) du_1 \tag{1.58}$$

, όπου ρ_n ο συντελεστής συσχέτισης και

$$u_r = \frac{\ln\left(r / A_{m,j} \right)}{S_{A,j}} \tag{1.59}$$

$$u_{th} = \frac{\ln\left(A_{th} / A_{m,j} \right)}{S_{A,j}} \tag{1.60}$$

$$u_x = \frac{\ln\left(\left(A_{m,j} \exp\left(S_{A,j} u_1 \right) - r \right) / A_{m,ij} \right)}{S_{A,ij}} \tag{1.61}$$

$$f_{U_1}(u_1) = \frac{1}{\sqrt{2\pi}} \exp\left(-\frac{u_1^2}{2} \right) \tag{1.62}$$

με $r = SIR_{CS,dB} - SIR_{th}$ και $A_{m,j}$, $S_{A,j}$, $A_{m,ij}$, $S_{A,ij}$ οι παράμετροι της λογαριθμοκανονικής κατανομής.

Χρησιμοποιώντας τις παραμέτρους του Πίνακας 5, υπολογίζεται η πιθανότητα αποκοπής για δύο διαφορετικές συχνότητες για τον πρωτεύοντα χρήστη και δίνονται στην Εικόνα 1-31.

Πίνακας 5 Παράμετροι συστήματος

Parameters	Values
Frequency	20GHz, 14GHz
Incumbent Satellite (S_1)	22^{o}E
Cognitive Satellite (S_2)	20^{o}E
Satellite EIRP	54 dBW
G_{max}	32 dBi
Location of Ground Stations	Athens, Greece

Parameters	Values
Elevation angle S_1-GS_1	45.19°
Elevation angle S_2-GS_1	45.06°
Separation Angle for Incumbent Link	3.24°
Elevation angle S_1-GS_2	45.19°
Elevation angle S_2-GS_2	45.06°
Separation Angle for Cognitive Link	3.24°
Marginal Rain attenuation (Time Percentage Exceeded)	15.9 (0.01%)
Separation of Ground Stations	5 km

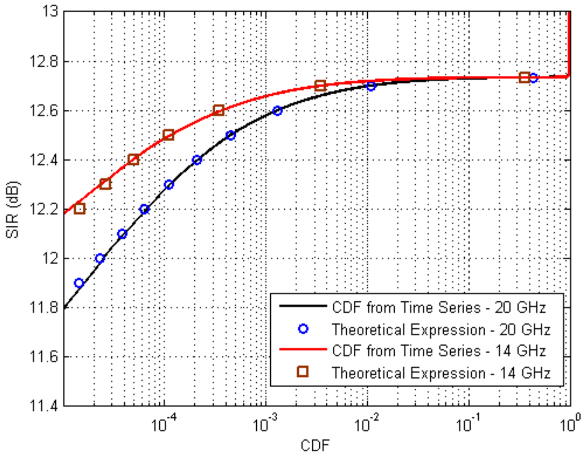

Εικόνα 1-31 Πιθανότητα αποκοπής λόγω παρεμβολών για τον πρωτεύοντα χρήστη

1.4.2 Στατιστικός χαρακτηρισμός των παρεμβολών από επικείμενους δορυφόρους για επίγειους σταθμούς σε κινητές πλατφόρμες που λειτουργούν σε συχνότητες άνω των 10 GHz

Αντικείμενο της παρούσας Διατριβής αποτέλεσε και η μοντελοποίηση του λόγου ισχύος φέροντος προς την ισχύ θορύβου και την ισχύ παρεμβολών (CNIR) για επίγειους σταθμούς οι οποίοι τοποθετούνται σε κινητές πλατφόρμες, όπως αεροπλάνα ή πλοία. Η αξιολόγηση της επίδοσης αυτών των συστημάτων έγινε μέσω της πιθανότητας αποκοπής τόσο στην άνω όσο και στην κάτω ζεύξη (η γεωμετρία του συστήματος δίνεται στην Εικόνα 1-32)και παρουσιάστηκαν δύο μεθοδολογίες:

α) μέσω παραγωγή χρονοσειρών του λόγου CNIR

β) μέσω θεωρητικών και αναλυτικών εκφράσεων

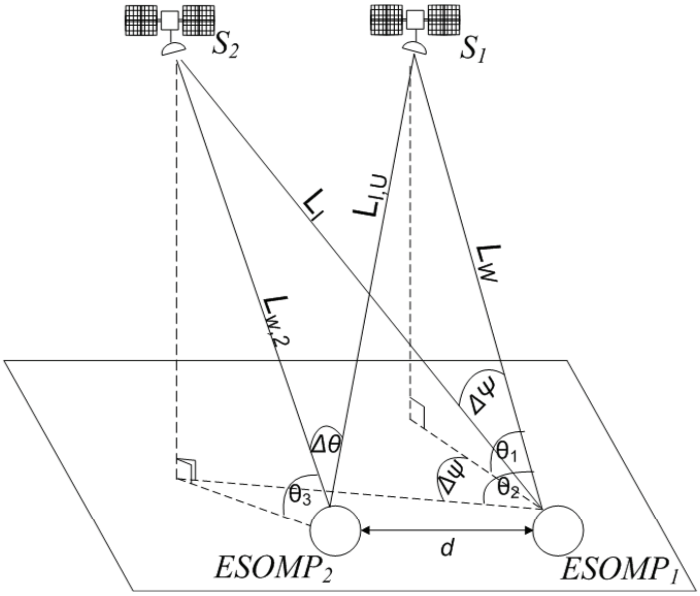

Εικόνα 1-32 Γεωμετρία συστήματος για τη μελέτη του λόγου CNIR

Για την πρώτη μεθοδολογία βασισμένοι στις υποθέσεις και τα αποτελέσματα των [Arapoglou12], [Matrriciani95a] και [Karagiannis12], μία πολυδιάστατη ΣΔΕ για την απόσβεση βροχής που εισάγεται σε κινητούς δέκτες αναπτύχθηκε:

$$dA_i(t) = A_i(t)\left[\frac{s_{ii}^2 + s_{ij}^2}{2} - \beta_i \ln\left(\frac{A_i(t)}{A_{mi}}\right)\right]dt + A_i(t)s_{ii}dW_t^i + A_i(t)s_{ij}dW_t^j, \qquad (1.63)$$

$$\{i = 1, 2,\ j = 2, 1, \text{respectively}\}$$

Για τη δεύτερη μεθοδολογία, αναλυτικές εκφράσεις δόθηκαν για τον υπολογισμό της αθροιστικής κατανομής του CNIR [J1].

Για την κάτω ζεύξη, δίνεται στην Εικόνα 1-33 η πιθανότητα αποκοπής για διάφορες τιμές του CNIR για ένα σύστημα που λειτουργεί στην Ku band για ένα και δύο δορυφόρους. Στην Εικόνα 1-34, δίνεται η πιθανότητα αποκοπής για ένα σύστημα που λειτουργεί στην Ka ζώνη συχνοτήτων, θεωρώντας ασυσχέτιστη την απόσβεση βροχής στις δύο ζεύξεις για διάφορες ταχύτητες της κινητής πλατφόρμας.

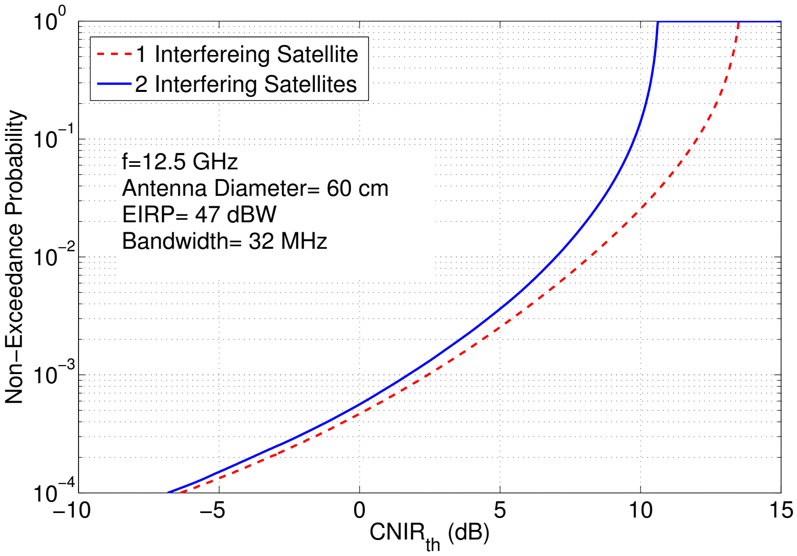

Εικόνα 1-33 Πιθανότητα αποκοπής για έναν και δύο παρεμβάλλοντες δορυφόρους

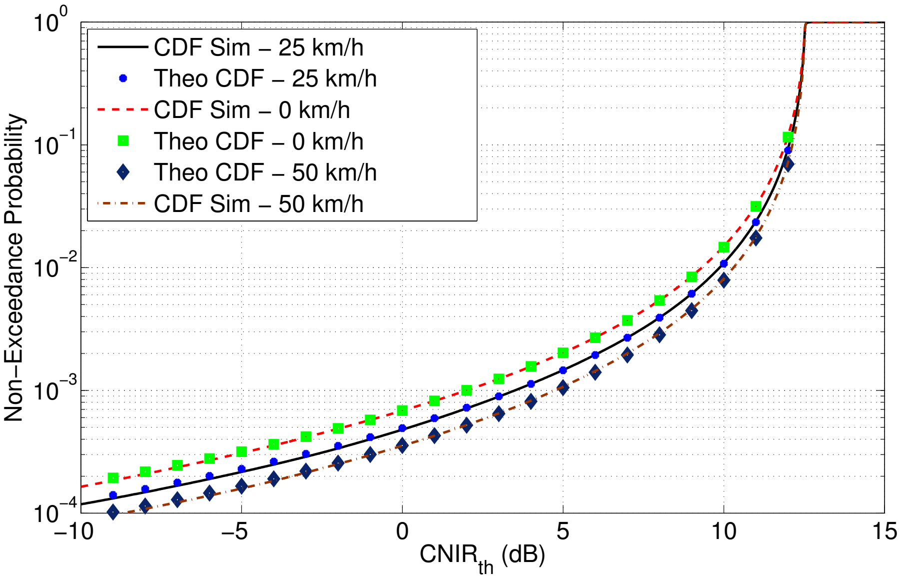

Εικόνα 1-34 Πιθανότητα αποκοπής της άνω ζεύξης για κινητούς δέκτες στην Ka ζώνη συχνοτήτων

1.4.3 Γνωστικό σύστημα συνύπαρξης άνω ζεύξης δορυφορικού συστήματος και επίγειας ασύρματης ζεύξης στην Ka ζώνη συχνοτήτων

Κατά τη Διατριβή μελετήθηκε ένα σενάριο συνύπαρξης ενός δορυφορικού δικτύου και μία ασύρματης ζεύξης με σταθερούς επίγειους σταθμούς. Ένα τέτοιο σενάριο γνωστικού συστήματος έχει περιγραφεί στο [CORASAT13]. Για την αξιολόγηση της απόδοσης ενός τέτοιου σεναρίου χρειάζεται η μοντελοποίηση των παρεμβολών. Όπως και στις προηγούμενες δύο υπο-ενότητες, παρουσιάστηκαν δύο μεθοδολογίες για τον υπολογισμό της πιθανότητας αποκοπής:

α) μέσω παραγωγής χρονοσειρών

β) μέσω αναλυτικών εκφράσεων.

Σκοπός της μελέτης ήταν η ανάλυση της επίδρασης των παρεμβολών από μία δορυφορική άνω ζεύξη η οποία αποτελεί τη δευτερεύουσα υπηρεσία σε μία ασύρματη ζεύξη, η οποία είναι και η πρωτεύουσα υπηρεσία. Η επίδραση της παρεμβολής μελετήθηκε τόσο από το λόγο SIR (ενότητα 1.4.3) όσο και με το λόγο της ισχύος σήματος προς την ισχύ θορύβου και την ισχύ παρεμβολών (SNIR).

Στον Πίνακας 6, δίνονται οι παράμετροι του συστήματος, οι οποίοι χρησιμοποιήθηκαν για τον υπολογισμό της αθροιστικής πιθανότητας του λόγου SNIR (Εικόνα 1-35) για την πόλη του Λουξεμβούργου για έναν παρεμβάλλων χρήστη και στην Εικόνα 1-36 για 1, 2 και 3 πολλαπλούς παρεμβάλλοντες χρήστες.

Πίνακας 6. Παράμετροι συστήματος

Parameter	Value
Operating frequency	29 GHz
Incumbent Link Path Length, L_{in}	3 km
Interfering Link Path Length, L_I	5 km
Bandwidth of Incumbent Link, B	28 MHz
FS Tx Antenna Gain, G_T	19 dBi
FS Rx Antenna Gain, $G_R(0^o)$	19 dBi
FS Tx Transmit Power, P_T	-6 dBW
$EIRP_{\mathrm{FSS}}$	See ITU-R. S. 524
FS Rx Antenna Gain, $G_R(\Delta\psi)$	See ITU-R. S. 465

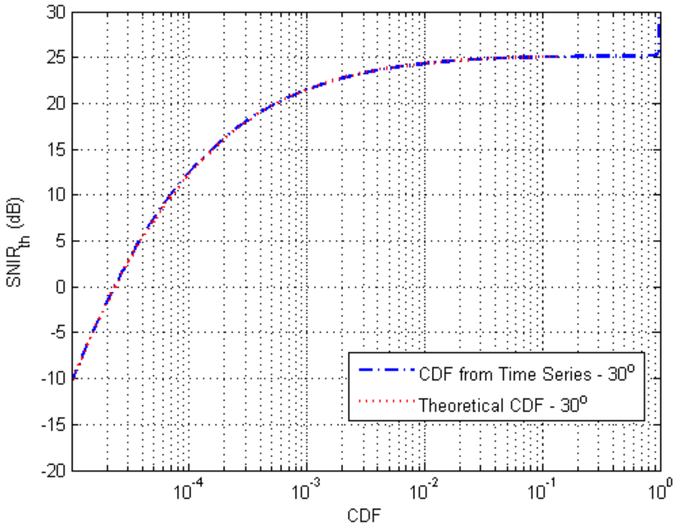

Εικόνα 1-35 Πιθανότητα αποκοπής για μία γωνία διαχωρισμού μεταξύ των ζεύξεων ίση με 30°

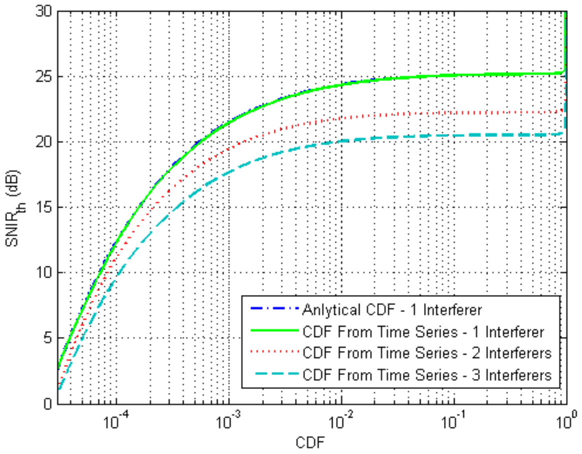

Εικόνα 1-36 Πιθανότητα αποκοπής για 1, 2 και 3 παρεμβάλοντες χρήστες

1.4.4 Απόδοση κάτω ζεύξης υψηλής μετάδοσης δεδομένων για συστήματα παρατήρησης Γης

Κατά τη συνεργασία στα πλαίσια του προγράμματος SatNEx III, αξιολογήθηκε η επίδοση δορυφορικών συστημάτων παρατήρησης Γης που λειτουργούν στις ζώνες συχνοτήτων Ka και Q και κάνουν χρήση της τεχνικής προσαρμοσμένης κωδικοποίηση και διαμόρφωσης. Στην [J2] δίνονται οι ισολογισμοί ισχύος και ο πίνακας με τις κωδικοποιήσεις και τις διαμορφώσεις. Χρησιμοποιώντας αυτές τις παραμέτρους και παράγοντας χρονοσειρές συνολικής απόσβεσης υπολογίστηκε η χωρητικότητα αποκοπής.

Η συνολική απόσβεση υπολογίστηκε από τη σύσταση ITU-R. P. 1853 [ITU-R.P.1853], χρησιμοποιώντας τη μεθοδολογία που αναπτύχθηκε προηγουμένως για την παραγωγή χρονοσειρών απόσβεσης σε LEO δορυφόρους. Επιπλέον, συγκρίθηκαν δύο περιπτώσεις για την εκτίμηση του καναλιού για την προσαρμοσμένη κωδικοποίηση και διαμόρφωση. Στην Εικόνα 1-37, δίνεται η χωρητικότητα αποκοπής για το σταθμό στη Matera, Ιταλίας για συχνότητα λειτουργίας 26.5 GHz ενώ στην Εικόνα 1-38 για συχνότητα λειτουργίας .

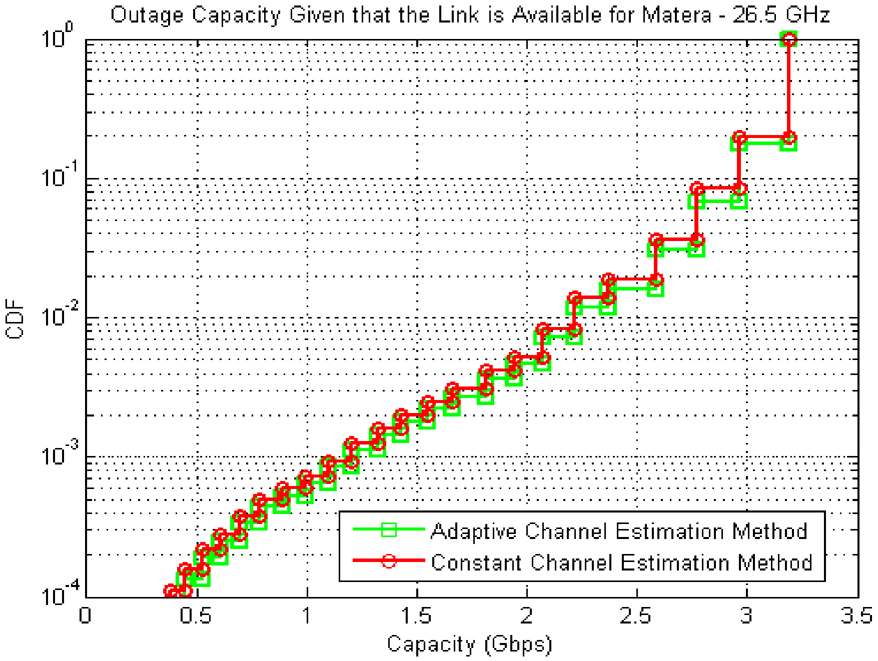

Εικόνα 1-37 Χωρητικότητα αποκοπής για τη Matera, Ιταλίας για συχνότητα 26.5 GHz

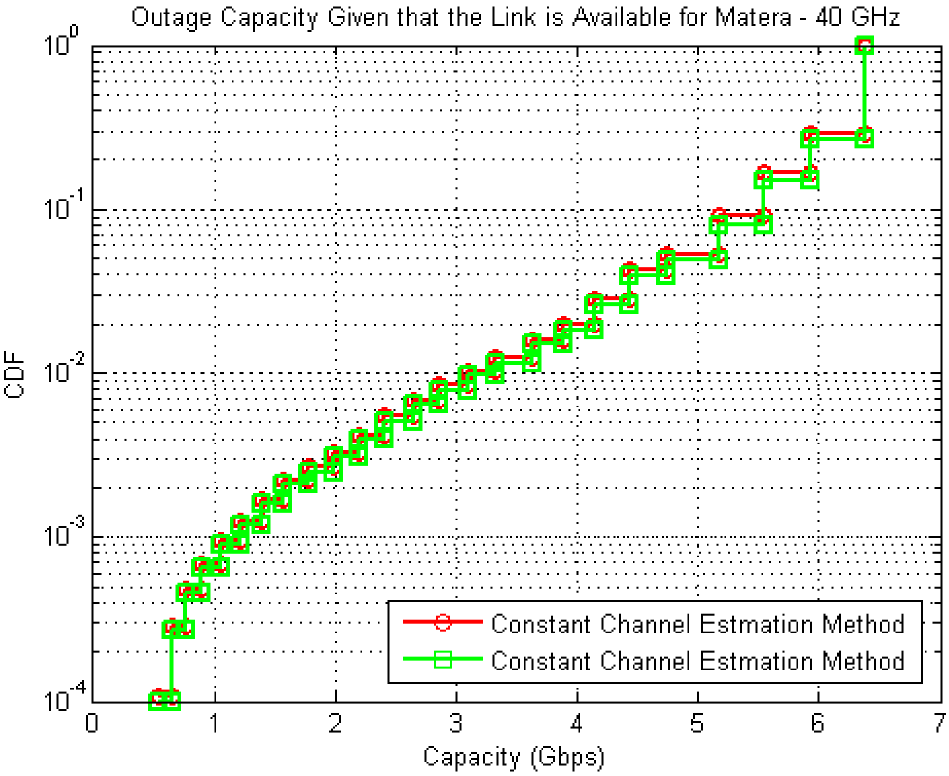

Εικόνα 1-38 Χωρητικότητα αποκοπής για τη Matera σε συχνότητα λειτουργίας 40 GHz

1.5 Συμπεράσματα

Συμπερασματικά από την παρούσα Διατριβή προέκυψαν τα εξής:

- Αξιολόγηση της κατανομής IG για τη μοντελοποίηση των στατιστικών χαρακτηριστικών πρώτης τάξης της έντασης βροχόπτωσης και της απόσβεσης
- Ανάπτυξη μοντέλου για τον υπολογισμό των στατιστικών χαρακτηριστικών της απόσβεσης λόγω βροχής σε ασύρματες επίγειες και δορυφορικές ζεύξεις
- Ανάπτυξη μοντέλου για τον υπολογισμό της από κοινού πιθανότητας απόσβεση για δορυφορικά συστήματα που κάνουν χρήση των τεχνικών διαφορισμού θέσης ή στο πεδίο του χρόνου
- Ανάπτυξη μοντέλου για τον υπολογισμό της πιθανότητα αποκοπής σε επίγεια ασύρματα συστήματα με χρήση του διαφορισμού διαδρομής
- Αξιολόγηση της χρήση συναρτήσεων copulas για τη μοντελοποίηση των από κοινού πιθανοτήτων υπέρβασης για συστήματα διαφορισμού χώρου και χρόνου
- Παρουσίαση έκφρασης για τον υπολογισμό της δυναμικής παραμέτρου της απόσβεσης
- Ανάπτυξη ΣΔΕ για την παραγωγή χρονοσειρών απόσβεσης λόγω βροχής σε ζεύξεις Γης με MEO/LEO δορυφόρους
- Ανάπτυξη μεθοδολογίας με χρήση συναρτήσεων copulas για την παραγωγή χρονοσειρών απόσβεσης βροχής
- Χρήση πολυδιάστατων ΣΔΕ για παραγωγή χρονοσειρών δισδιάστατων πεδίων βροχής
- Μέθοδο παραγωγής χρονοσειρών σπινθηρισμού πλάτους με χρήση ΣΔΕ
- Αξιολόγηση της επίδοσης σεναρίων συνύπαρξης:
    - Διπλού δορυφορικού συστήματος
    - Πολλαπλών υπηρεσιών με επίγειους σταθμούς σε κινητές πλατφόρμες

    - Επίγειας ζεύξης και δορυφορικού συστήματος
- Αξιολόγηση της επίδοσης της κάτω ζεύξης δορυφορικών συστημάτων παρατήρησης Γης νέας γενιάς

2 Introduction

It is estimated that the demand for Internet rates will be highly increased regarding the demands of current networks, according to the ISI strategic research and innovative agenda [ISI10]. Therefore, European Digital Agenda has set two targets: Firstly, fast broadband services by 2020 with a data rate greater than 30 Mbps or more for 100% of EU citizens and secondly the ultra-fast broadband subscription by 2020, according to which the 50% of European households should have subscriptions above 100 Mbps [DigAgenda10]. As it is indicated in the European Digital Agenda, the aim is to provide European citizens with a Paneuropean fast and ultra-fast broadband service. However, terrestrial wireline, such as fiber optics, and wireless networks will not be able to fulfill all the requirements and accomplish the targets of the European Digital Agenda, due to the high costs of providing broadband access to “difficult” areas. In particular, these areas will not be able to be served at all (unserved areas) or will not have access to services with data rates greater than 30 Mbps (under-served areas). Moreover, in a study conducted in [ITUTelW11], the percentage of households of the countries of European Union which will not have access to superfast broadband services via fixed line will be really high, especially in Greece. It was estimated that in the whole country coverage, the 68-98% of households will not have access to superfast broadband connections through a fixed line. On the other hand, wireless terrestrial connections and generally terrestrial infrastructure are very expensive for rural, insular and mountainous areas. Therefore, it seems that satellite connections will be a viable solution for the under-served and unserved areas, while wireless terrestrial and wireline networks in conjunction with satellite communications will be mainly used for urban environments.

The great advantage of satellite communications is that the whole European continent can be covered using one Geostationary (GEO) satellite. Satellite services have already been developed and they address a wide variety of applications for consuming, professional and institutional purposes. In [ISI10], apart from the current applications for Satellite Communication (SatCom) systems, future targeted applications are also provided. These include fast and ultra-fast broadband internet access, satellite internet applications in health and new service opportunities through Earth observation, among others. A concept, called “Terabit per second satellite” has already been introduced in [Gaurard09], in which the satellite communications offer very high data rates to the users. The idea of “Terabit per second” satellite, also addressed in [Thompson11], has gained a lot of interest among the research and industrial satellite community, with European Space Agency (ESA) funding researchers to work on this issue. Moreover, very recently, the company O3b has launched a satellite constellation at Medium Earth Orbit (MEO) in order to provide high data rates to the end-users. The company aims at 20 Mbps data rates with its most clients being internet service providers using the MEO system for supporting their backhaul system [O3b].

Apart from the broadband services which are provided by SatCom systems, satellite communications are used in Earth Observation (EO) systems. In EO systems, Low Earth Orbit (LEO) and GEO satellites are employed. The difference between a link with LEO and GEO satellites is that the first has a time variable elevation angle since it moves through the visibility area of the ground station, while the second a constant one. In the past, the links for the data transmission from the LEO satellite to ground station for EO applications were operating at X band. However, due to the increase of the data that have to be delivered at the ground stations, these links must operate at higher frequency bands [Toptsidis12].

Furthermore, ESA has introduced the idea of European Data Relay System (EDRS) [EDRS]. In EDRS, GEO satellites are employed in order to relay data to and from Earth stations or LEO satellites or other vehicles which are not able to communicate with each other. The need of EDRS, as this is also explained in [EDRS], lies on two facts: first, it has been estimated by ESA that the space telecommunication infrastructure will need to transmit a very high amount of data every day and second the conventional communication systems will not be able to serve the users of EO data. The services that benefit from the application of such systems are: EO applications of time-critical services such as floods and forest fires, government and security services, security forces and rescue teams.

However, for the design of the above mentioned systems, what is of primary importance is channel modeling. In particular, for the realization of these systems these must operate at Ka, i.e. frequencies from 20 to 30 GHz, Q, from 30 GHz to 50 GHz, V, from 50 GHz to 75 GHz and/or W, from 75 to 110 GHz, bands [ISI10], concerning Radio Frequencies (RF), and optical frequencies, since regulation issues forbid the use of lower frequency bands [Thompson11] and due to the fact that higher frequencies offer higher bandwidth hence higher data rates. In these high frequency bands, the signals are affected by atmospheric phenomena, such as precipitation, mainly rain, clouds and fog, atmospheric gases and molecules and atmospheric turbulence, having different effects on RF and optical frequencies. Modeling the impact of such tropospheric phenomena in the propagated electromagnetic waves of high frequency bands is currently under investigation with many research teams working on this field. Specifically, ESA has been focused on the propagation modeling for Ka, Q/V and W bands and COST Actions, such as IC0802, have also been carrying out studies on this field. Very recently, the ALPHASAT experiment has started in which the Aldo Paraboni payload is used for propagation experiments at Ka- and Q/V- bands [ALPHASAT15]. As for optical communication at least one COST Action, IC1102, have been devoted on this field and also there is the Optical Link Study Group with the cooperation of NASA and ESA, in which the inter-satellite and Earth-space satellite links are studied. However, until now, the largest part of the propagation models is developed for systems operating at Ku and Ka bands, while the most experimental campaigns are designed and executed at Ka band. NASA has announced a new propagation campaign in which new measurements will be obtained at Ka band.

This chapter is organized as follows: In the second section, the propagation impairments at Ka band and above are presented and various propagation models needed for the system design. Then, Fade Mitigation Techniques are briefly presented and finally, a description of the next generation wireless terrestrial and satellite communication systems is given.

2.1 Propagation Impairments and Propagation Modeling

It is known that larger bandwidth provide higher data rates and since the demand of broadband communications is increasing the use of higher than Ku bands is obligatory for future multimedia SatCom systems. Currently many commercial SatCom systems operate at Ka band and the operation of these systems in Q/V bands is planned. In these high frequency bands, the signal is affected by atmospheric phenomena. Atmospheric gases, i.e. water vapor and oxygen, clouds and fog, precipitation, mainly rain, tropospheric turbulence and ice cause the degradation of the quality of the link. In particular, atmospheric gases, precipitation and clouds attenuate the power of the signal while tropospheric turbulence causes the scintillation, i.e. rapid fluctuations, of the amplitude of the signal and ice causes the depolarization of the propagated electromagnetic waves. Although all the above mentioned phenomena must be taken into consideration for the system design of future SatCom systems, rain is the most dominant fading mechanism and the specific gaseous attenuation presents a local maximum at the frequency close to 60 GHz due to oxygen absorption.

Considering the atmospheric effects, a fixed power margin cannot compensate the propagation impairments due to the high losses that are introduced into the system by the atmospheric phenomena for a small, but crucial for the availability of the SatCom systems, time percentage. Therefore, Fade Mitigation Techniques (FMTs), or else Propagation Impairment Mitigation Techniques, must be designed and introduced into the system. Adaptive Coding and Modulation (ACM), downlink or uplink Power Control, reconfigurable on-board antennas of the satellite and diversity techniques, such as time diversity, site diversity, orbital diversity and frequency diversity are all considered as FMTs. Furthermore, the concept of complete or partial frequency reuse by applying dual polarization schemes in multi-beam satellite communication systems is studied in order to increase the number of beams without increasing the interference.

However, the evaluation of the performance and the design of the above mentioned concepts require the knowledge of first (Probability Density Function – PDF, Complementary Cumulative Distribution Function – CCDF) and second (Autocorrelation, Power Spectrum) order statistics, which affect the fade slope and fade and inter-fade duration statistics, of the total and excess in clear sky, i.e. rain and clouds, attenuation. Considering tropospheric turbulence, the parameters of the first and second order statistics are also of great importance and are also used for the evaluation of FMTs performance. Moreover, the prediction of the attenuation, long-term or instantaneously, at one frequency given the long-term statistics or the instantaneous value of the attenuation at a different frequency is needed for the prediction of downlink/uplink total or excess attenuation.

In diversity systems, an improvement factor is observed due to the exploitation of spatio-temporal inhomogeneity of the random processes of the atmospheric phenomena. It is essential for the design of the systems which apply diversity schemes for the mitigation of the fades to model this improvement gain or even the joint long-term statistics of the total attenuation and each attenuation component. For example, the joint CCDF of attenuation or the statistics of the improvement factor in site or time diversity systems can be used for the design of such systems since the separation distance of the ground stations can be derived from the statistics in order to succeed in having a certain marginal gain or the computation of the depth of the inter-leaver, which actually gives the time at which the data will be retransmitted (in case of time diversity). Therefore, the spatial correlation of total attenuation and each attenuation component is needed for the modeling of site diversity systems, while the temporal correlation for time diversity systems. Furthermore, the former is also useful for the design of efficient and highly available satellite systems in a large or even continental region as it can be used for the design and the application of the on-board reconfigurable antennas of multi-beam satellite. In case of dual polarization systems, the distribution of depolarization and cross-polarization are needed for the investigation of their design and availability, especially for non-spherical droplets, which seems to be closer to the shape of the rain particles under consideration.

In order to proceed to the simulation of a system for its performance evaluation and model the dynamics of the channel, time series must be generated for total attenuation and each attenuation components. This can be achieved either by directly modeling the time series of the attenuation components or by generating time series of the meteorological parameters which affect the signal and then proceed to the computation of the time series of each attenuation component. In the multi-beam satellite case which will be able to provide users with broadband services in a continental region, time series of attenuation components must be generated for a continental region which will take into account the spatio-temporal variations of the atmospheric phenomena.

This section is organized as follows: Firstly, the review of propagation models for the first order statistics is presented, then a review of models of the prediction of fade dynamics are presented and is divided in 3 subsections: the fade slope, fade and inter-fade duration and hitting times are analyzed. Then, the long-term and instantaneous frequency scaling models are given and later, the models for the prediction of the performance of diversity systems and in particular site diversity and time diversity. The models for the description of spatial correlation of total attenuation are briefly presented and then the space-time channel models for total attenuation

2.1.1 Review of Tropospheric effects and first order statistics modeling

In this subsection, the atmospheric effects and models for the prediction of first order statistics are given. As mentioned before, precipitation, atmospheric gases, clouds and fog cause the attenuation of the power of the signal, while tropospheric turbulence causes the scintillation of its amplitude [Panagopoulos04].

2.1.1.1 Gaseous Absorption

The atmospheric gases that mostly influence the signal in the frequencies of interest, close to 20 GHz, are the oxygen and water vapor [ESTECRep]. Liebe's Millimeter-Wave Propagation Model (MPM) [Liebe89] is the most accurate model for calculating the gaseous absorption. In this model, the atmosphere is divided into homogeneous layers and for each layer the specific attenuation due to water vapor and oxygen are calculated. The attenuation due to gases is the sum of the specific attenuation for the path on each layer. ITU-R proposes two models for the prediction of attenuation due to atmospheric gases in the range of frequencies less than 350 GHz [ITU-R. P.676]. Both models refer to oxygen and water vapor absorption and the first one is based on Liebe's methodology [Liebe89]. Both models require vertical profiles of pressure, temperature and water vapor density, which can be obtained from annual reference models of ITU-R. P. 835 [ITU-R. P.835].

However, these models are quite complicated and therefore, ITU-R has recommended in [ITU-R. P.676] a second model which can be used as an approximation. In this second model the approximation algorithms are used as well as surface meteorological data and maps of integrated water vapor content for various time percentages derived by ITU-R. P. 836 [ITU-R. P.836] for the calculation of the gaseous absorption.

2.1.1.2 Cloud attenuation

Clouds are containing liquid water particles whose size is considered less than the wavelengths at the Ka- and Q-bands. Rayleigh approximation may be used, as this is recommended in [ITU-R. P.840], for the calculation of cloud attenuation. According to this model, the specific attenuation due to clouds (γ_c) is obtained:

$$\gamma_c = K_l M, \quad \text{dB/km} \tag{2.1}$$

where K_l is the specific attenuation coefficient ((dB/km)/(g/m^3)) and M is the liquid water density in the clouds (g/m^3). The expressions for calculating the specific attenuation coefficient are given in [ITU-R. P.840] and it depends on the dielectric permittivity of the water and the temperature. Considering temperature equal to 0^{o}C, the specific attenuation coefficient for clouds can be obtained and it is shown in Figure 2.1 for various frequencies.

In order to compute cloud attenuation, in [ITU-R. P.840] the following expression is used:

$$A = \frac{K_l L}{\sin\theta}, \quad 5^o \le \theta \le 30^o \tag{2.2}$$

where K_l is shown in Figure 2.1, θ is the elevation angle of the link and L is the total columnar liquid water content and can be derived from the maps of ITU-R. An example of the exceedance probability of cloud attenuation for frequency equal to 20 GHz and 50 GHz for temperate climates is shown in Figure 2.2.

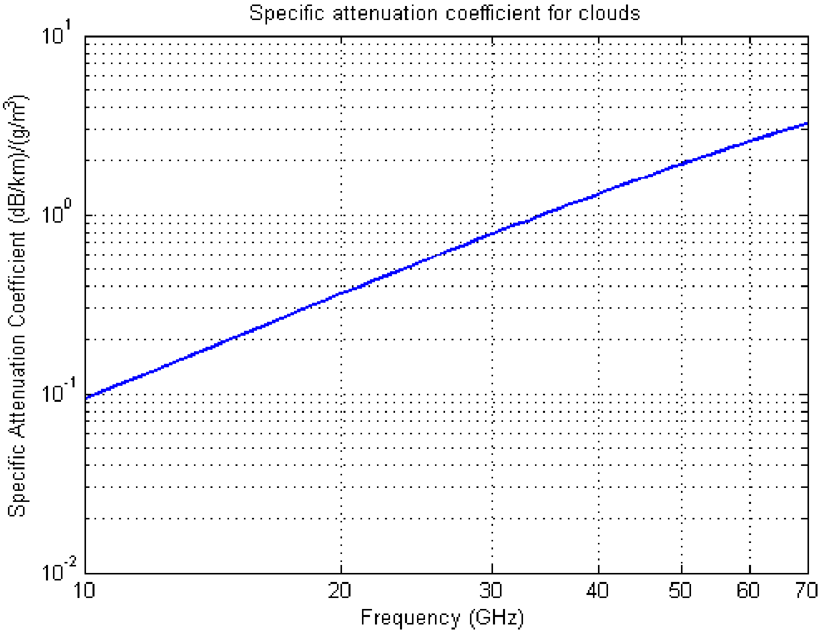

Figure 2.1 Specific attenuation coefficient vs. frequency

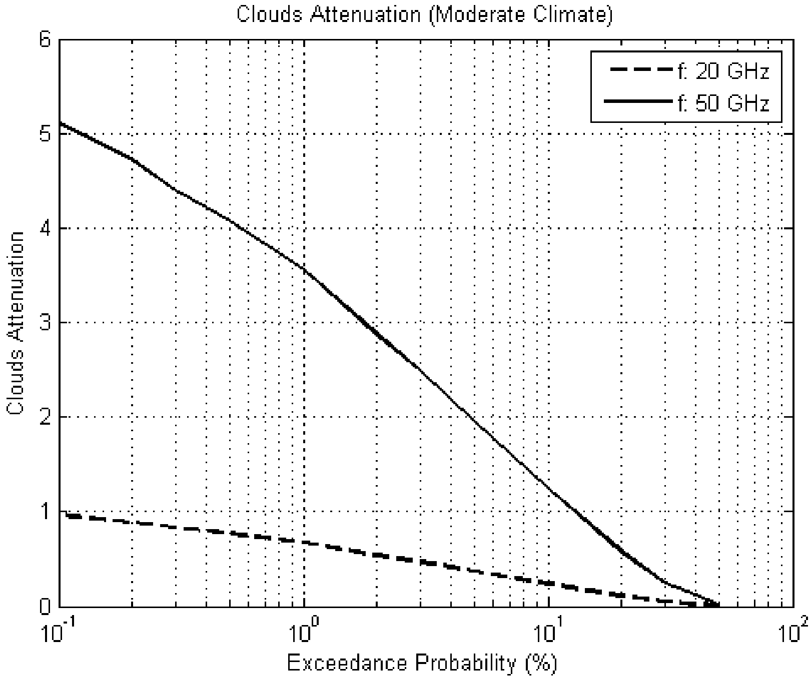

Figure 2.2. Cloud attenuation for a temperate climate

2.1.1.3 Rain Attenuation

Rainfall is the most dominant fading mechanism for the frequencies of interest for millimeter wave next generation radio communication networks. Due to the scattering and droplet absorption, rainfall causes the attenuation of the signal. The most approved expression for calculating the specific rain attenuation (A_o, dB/km) is the power law expression, which relates the rain rate (R, mm/h) with rain attenuation [Olsen78]:

$$A_o = aR^b \tag{2.3}$$

where a and b are two coefficients which depend on the elevation angle, frequency and polarization [ITU-R. P. 838]. In this case the rain attenuation along the radiopath can be calculated as:

$$A = \int_0^L A_0(x)dx \tag{2.4}$$

where L is the length of the path under rain.

Since, rainfall rate can be modeled as a random variable, rain attenuation induced on a radio path can be also considered a random variable. For the outage prediction of an Earth-space system, the exceedance probability, i.e. the Complementary Cumulative Distribution Function (CCDF) of rain attenuation can be used. There are numerous models in the literature for the prediction of the exceedance probability of rain attenuation.

Most of the propagation models require the long-term statistics of rain rate, which can be obtained either from measurements or from the ITU-R rainmaps in ITU-R Recommendation P. 837 [ITU-R. P. 837]. In Figure 2.3, the CCDF of rain rate derived from ITU-R. P. 837 is shown for two arbitrary regions one with moderate and one with tropical climate. As it is expected, in tropical regions higher rainfall rate values occur.

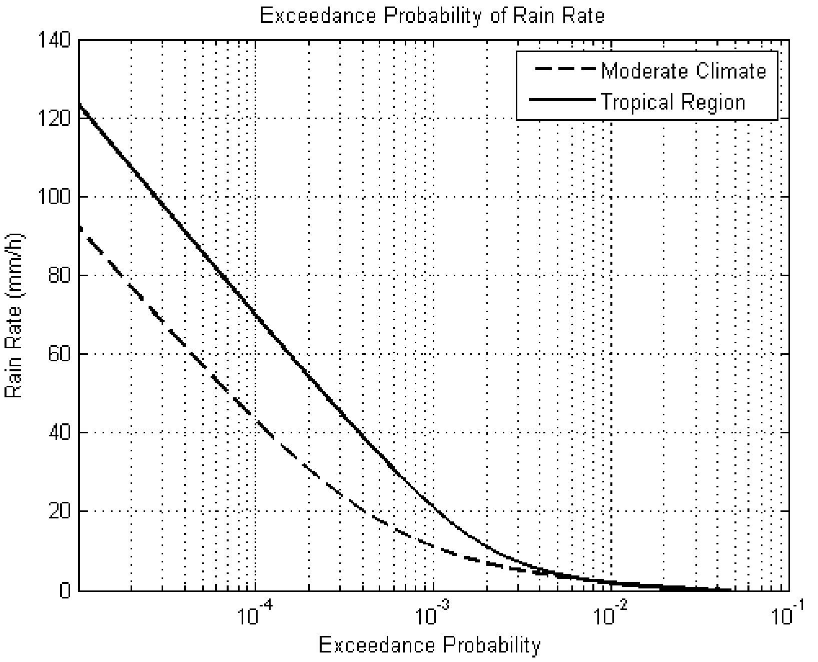

Figure 2.3. Exceedance probability of rain rate calculated with ITU-R. P. 837

The radio propagation models are classified into a) empirical, b) statistical and c) semi-physical models. The most known *empirical* model for the rain attenuation prediction is the ITU-R model in P. 618 [ITU-R P.618]. In this model a step-by step algorithm is given in order to compute the CCDF of rain attenuation given the electrical and geometrical characteristics of the satellite link as well as the rain height. As for the rain rate the value which is exceeded for 0.01% of time is needed. In Figure 2.4, the CCDF of rain attenuation calculated by the ITU-R model in [ITU-R P.618] is shown for an arbitrary region with a moderate climate for two frequencies, 20 and 40 GHz.

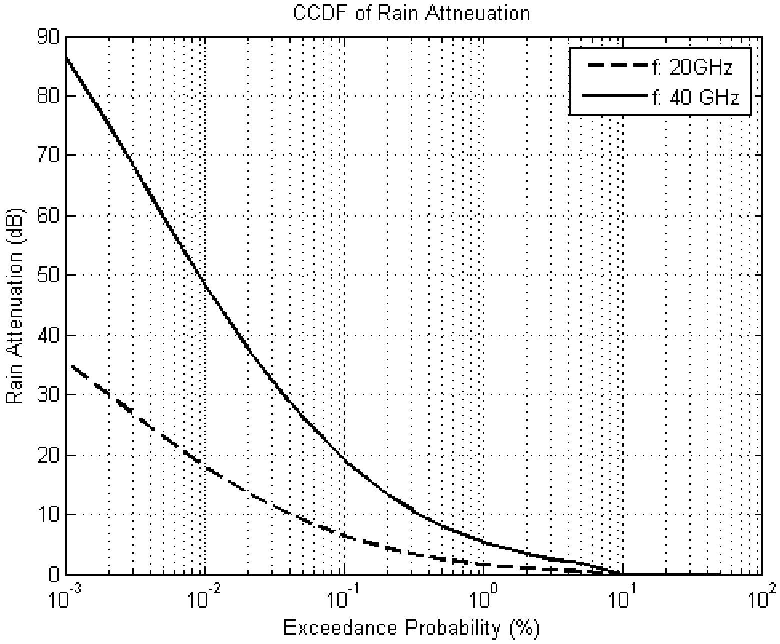

Figure 2.4. CCDF of rain attenuation

For the *statistical* models, rain attenuation and rainfall rate are assumed to follow specific probability distributions. Then adopting a spatial model for rainfall rate or specific rain attenuation, the statistical parameters of rain attenuation are calculated in terms of the statistical parameters of rain rate. A well accepted *statistical* model is presented in [Lin75]. In this methodology, rainfall rate and rain attenuation follow the lognormal distribution and the spatial distribution of specific rain attenuation shown in (2.5) is used for the calculation of the parameters of lognormal distribution of rain attenuation.

$$\rho_L = \frac{G}{\sqrt{G^2 + d^2}} \tag{2.5}$$

where G is a constant which can take values from 0.75 km to 3 km and depends on spatial homogeneity of rain rate which depends on the location and d is the distance between two points, x and x_1 of the radio path, i.e. $d=|x-x_1|$.

Another statistical model that extends Lin's methodology has been presented in [Kanellopoulos87]. The difference between this model and Lin's methodology is that the probability to rain on a specific point is equal to 1. Following this assumption the final expressions for calculating the CCDF of rain attenuation are different compared to [Lin75]. The CCDF of rain attenuation for a frequency of 20 GHz and two different elevation angles for a region with a temperate climate are calculated based on the methodology of [Kanellopoulos87] and shown in Figure 2.5.

For subtropical and tropical regions a different spatial coefficient has been proposed in [Morita76]:

$$\rho_G = \exp(-a_s\sqrt{d}) \tag{2.6}$$

where a_s take values from 0.2 to 0.3. A statistical model using the spatial coefficient of (2.6) has been presented in [Panagopoulos02a] for subtropical and tropical regions. In heavy rain climatic regions gamma distribution seems to be more appropriate for the modeling of rain rate and rain attenuation for the prediction of the exceedance probability of rain attenuation.

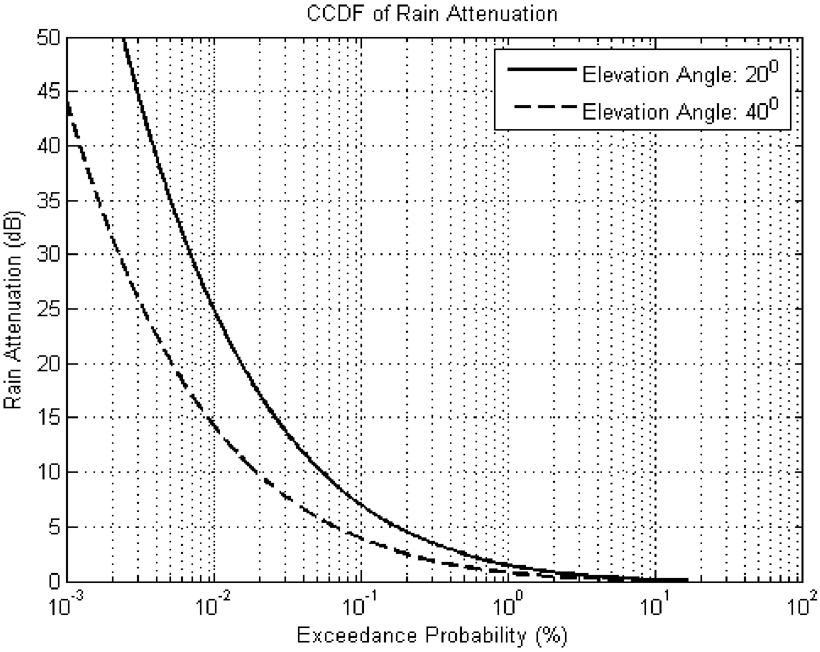

Figure 2.5. CCDF of rain attenuation

As a last category are the *semi-physical* models. In this category, the exceedance probability of rain attenuation is computed using the concept of rain cells. Rain cells are closed regions in which rain occurs, i.e. the rainfall rate is greater than 0. In [Capsoni87a], an exponential shape for the horizontal distribution of rain rate inside a rain cell is proposed, i.e.:

$$R = R_M e^{-\frac{\rho}{\rho_0}} \tag{2.7}$$

where R_M is the peak rain rate inside the cell, ρ is the distance from the peak and ρ_0 is the distance from the center of the cell in which the rain rate becomes $\frac{R_M}{e}$. The EXCELL model has been used for the prediction of the rain attenuation [Capsoni87b]. However, in [Capsoni06], the Lowered EXCELL model has been introduced as an improvement to the initial EXCELL model. According to [Capsoni06], using a probability of occurrence of a rain cell with specific radius and maximum value and knowing the distribution of rain rate, the CCDF of rain rate for stratiform and convective rain can be computed. Based on this methodology and adopting a model for the computation of the effect of melting layer, the CCDF of rain attenuation can be computed. The model is named Stratiform-Convective Excell (SC-EXCELL) and has been presented in [Capsoni09]. Finally, based on the methodology of the EXCELL modeling of rain cells a method for generating two-dimensional rain fields is proposed in [Luini11].

Another semi-physical model is the methodology of HYCELL [Feral03a], [Feral03a], [Feral06]. According to HYCELL, the horizontal structure of rain rate inside a rain cell can be described by the combination of a Gaussian and an exponential component:

$$R(x,y)=\begin{cases} R_G \exp\left[-\left(\dfrac{x^2}{a_G^2}+\dfrac{y^2}{b_G^2}\right)\right] & ,\ \text{if R } \geq \text{R}_1 \\ R_E \exp\left[-\left(\dfrac{x^2}{a_E^2}+\dfrac{y^2}{b_E^2}\right)^{1/2}\right] & ,\ \text{if } \text{R}_2 \leq \text{R} < \text{R}_1 \end{cases} \tag{2.8}$$

where R_G is the peak of the rain cell, a_G and b_G is the distances at the x- and y-axes, respectively, in which the rain rate is $\frac{R_G}{e}$ and R_E, a_E and b_E are the equivalent for the exponential component. According to the HYCELL methodology, in order to simulate two-dimensional rain fields, the size of the simulation area, the fractional area over which it is raining and the conditional exceedance probability of rain rate are required. The simulated rain field results from the conglomeration of rain cells inside the observation area. In order to put the rain cells inside the observation area, a random walk is followed. First results of the HYCELL methodology for calculating the CCDF of rain attenuation have been presented in [Kourogiorgas10].

2.1.1.4 Scintillation

Scintillation of the amplitude of the signal is caused by the tropospheric turbulence, i.e. small irregularities in time and space of the refractive index of the atmosphere. Scintillation becomes severe for low elevation links. One method for calculating the exceedance probability of the scintillation depth is the ITU-R. P.618 method [ITU-R. P.618]. According to this method, scintillation depends not only on the radio-electric and geometric characteristics of the link but also on the wet term of radio refractivity. It has been tested to experimental data with a range of frequencies from 7 to 14 GHz. However, its use is recommended for frequencies of at least up to 20 GHz. Moreover, the elevation angle must be greater than 4^o. An example is given in Figure 2.6 for a frequency of operation of 20 GHz and two different elevation angles 10^o and 40^o. The region that is selected is inside Europe. It can be observed that increasing the elevation angle the scintillation depth is decreasing while the opposite holds for frequency, that is with increasing frequency scintillation depth is increasing.

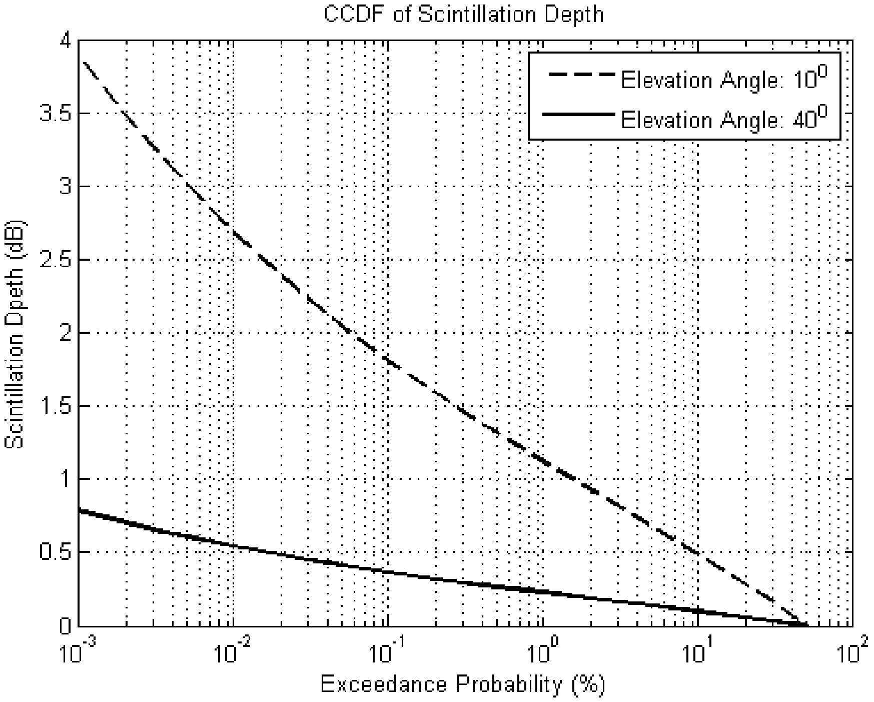

Figure 2.6. CCDF of scintillation depth

Another model is proposed for calculating the CCDF of scintillation depth using radiosonde data in order to obtain vertical profiles of temperature, pressure, humidity, wind speed and wind direction. In [Vasseur99], it is assumed that the probability density function (PDF) of the log-amplitude (x) of the signal can be computed by the following expression:

$$p_l(x) = \int_0^{+\infty} p_s\left(x \mid \sigma_x^2\right) p\left(\sigma_x^2\right) d\sigma_x^2 \tag{2.9}$$

where σ_x^2 is the variance of the log-amplitude which is assumed to follow the log-normal distribution, given in (2.10) and $p_s(x \mid \sigma_x^2)$ is the short-term pdf of x which follows the Gaussian distribution, given in (2.11).

$$p(\sigma_x^2) = \frac{1}{\sqrt{2\pi\sigma_x^2 s}} \exp\left(-\frac{\left[\ln\left(\sigma_x^2 / m\right)\right]^2}{2s^2}\right) \tag{2.10}$$

with m and s the mean value and standard deviation of the natural logarithm of σ_x^2.

$$p_s(x \mid \sigma_x^2) = \frac{1}{\sqrt{2\pi\sigma_x^2}} \exp\left(-\frac{x^2}{2\sigma_x^2}\right) \tag{2.11}$$

Then relating the variance of the scintillation with the structure parameter (see (2.12)) and using the mean structure parameter and its relationship with the parameters of temperature, humidity, pressure and wind as this is given in [Warnock85], the CCDF of scintillation depth can be calculated. However, for this method radiosonde data are needed.

$$\sigma_x^2 = 42.48 \frac{k^{7/6}}{(\sin\theta)^{11/6}} \int_{height} C_n^2(z) z^{5/6} dz \tag{2.12}$$

with θ the elevation angle of the link, k is the wavenumber and $C_n^2(z)$ is the structure parameter of the refractive index n at height z.

2.1.1.5 Total Attenuation

Although various models have been proposed for the evaluation of exceedance probability of each attenuation component, the combination of these phenomena for calculating the exceedance probability of total attenuation is a subject under investigation. Especially when the availability which must be guaranteed is low, apart from rain attenuation all the other effects must be taken into account. There are various methods for combining these effects considering if the effects are fully correlated or uncorrelated [COST255]:

1. Equiprobable summation:

In this method the attenuation predicted at a certain probability level *P%* are added. Therefore, if $A_1(P)$ and $A_2(P)$ are two attenuation values at *P* percentage of time then the total is:

$$A_{tot}(P) = A_1(P) + A_2(P)$$

(2.13)

2. Convolution method

In this case, the cumulative distribution of the total attenuation is calculated from:

$$P(A_t) = \int_{-\infty}^{A_t} p_1(A) P_2(A_t - A) dA \tag{2.14}$$

where $p_1(A)$ is the PDF of attenuation due to phenomenon 1 and $P_2(A)$ the CCDF of attenuation due to phenomenon 2.

3. Disjoint summation

The exceedannce probabilities of two phenomena can be added if these are disjoint. So, for example in case that the CCDF of attenuation in rainy and non-rainy time are available, the CCDF of total attenuation could be:

$$P(A_t > A) = P(A_{non-rain} > A) + P(A_{rain} > A) \tag{2.15}$$

However, to estimate the CCDF of disjoint attenuation due to different propagation phenomena is difficult.

4. Root-square summation

In this case the total attenuation is computed according to the following expression:

$$A_{tot}(P) = \sqrt{A_1^2(P) + A_2^2(P)} \tag{2.16}$$

5. Coherent summation

If the attenuation values are known simultaneously at a given time t_j then the total attenuation is computed by:

$$A_{tot}(t_i) = \sum_{j=1}^{n} A_j(t_i) \tag{2.17}$$

Therefore, if the attenuation components are known at a given period of time the distribution of the total attenuation can be calculated.

For the computation of total attenuation exceedance probability there are various methods which can be found in [COST255]. Among them is the ITU-R method which has been recommended in ITU-R. P.618 [ITU-R. P.618]. According to this methodology, the total attenuation can be calculated using the following expression:

$$A_T(P) = A_G(P) + \sqrt{\left(A_R(P) + A_C(P)\right)^2 + A_S^2(P)} \tag{2.18}$$

where A_T, A_G, A_R, A_C and A_S are the total attenuation, the gaseous attenuation, the rain and cloud attenuation and the scintillation fade depth, respectively, at a given probability. In Figure 2.7, the total attenuation has been computed following ITU-R. P. 618 for a region with a moderate climate and a frequency of 20 GHz for two different elevation angles 20^{o} and 40^{o}.

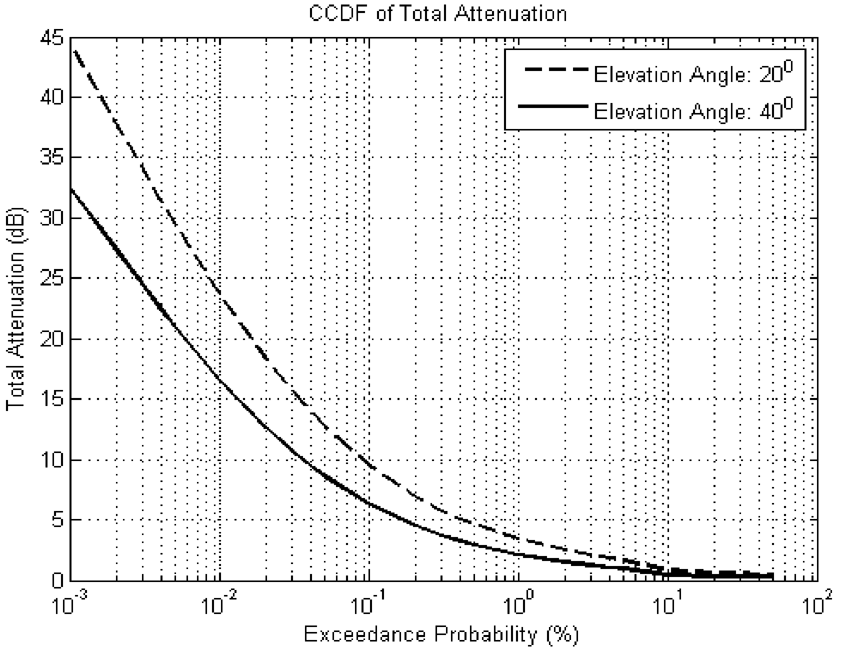

Figure 2.7. CCDF of total attenuation

2.1.2 Fade Dynamics

In this subsection fade dynamics, i.e. fade slope, fade duration and hitting time models are briefly examined.

2.1.2.1 Fade Slope

Fade slope $\zeta(t)$ is the rate of change of rain attenuation A(t) and is derived by the following expression:

$$\zeta(t) = \frac{A(t+\Delta t) - A(t)}{\Delta t} \tag{2.19}$$

Due to the importance of the modeling of fade slope for the implementation of the FMT control loop and short term prediction of attenuation, various models have been proposed for the characterization of the statistics of fade slope. An extended review of these models has been presented in [ESTECRep] and [ESTEC04]

2.1.2.2 Fade and Inter-Fade Duration

Fade duration is defined as the period of time between two consecutive crossings of the received signal on the same attenuation threshold, as this is defined in [ESTECRep]. Fade duration can be used for the calculation of the period of time when the link or the system is in outage and the calculation of a time period when the system is on service, inter-fade duration. Moreover, it can be used for the computation of time period in which a class of users are in outage in order to reallocate the resources to other users and for the choice of the system waveform as fade duration gives the duration of the block errors that incur due to propagation fadings.

1. Fade Duration

Since the European action COST 205 [COST205], two ways have been identified for the modeling of fade duration: 1) long fade duration (>32 s) caused by attenuation and 2) short fade duration due essentially to scintillation (with low attenuation level) and fast fluctuations during rain (associated with strong attenuation level).

Moreover, fade duration statistics can be described in various forms [ESTECRep], [Kamp02]:

- Statistics of the number of fade events in which the attenuation is higher than a given attenuation threshold and their duration is longer than a given fade duration. In this form the relative number of fades is defined as the number of fades relative to the total number of fades that a given duration is exceeded given an exceeded attenuation threshold.
- Statistics of the total duration of fade events with attenuation higher than a given attenuation threshold and duration longer than a given fade duration. Here the relative composite fade time is defined as the total fraction of fade time due to fades of duration longer than a specific duration threshold, given that the attenuation exceeds a specific threshold.
- Statistics of the fade duration with respect to the fraction of time during which impairments are higher than a given attenuation threshold.

The first and second forms of statistics of fade duration are of interest for testing prediction models, the third one is more suitable for system analysis. As denoted in [Kamp02] from the analysis of the OPEX experiment for fade duration statistics two conclusions can be drawn: 1) Statistical distribution obtained for both short and long fades are independent on the location and therefore on climatic parameters. 2) Statistical distribution obtained for both short and long fades are dependent on rain rate and therefore on the attenuation level. Moreover, since attenuation depends on the elevation angle and the operating frequency, fade duration statistics depend also on these parameters.

A large number of models have been developed for the prediction of fade duration statistics. Concerning the relative number of fades, the following models have been developed: the Goldhirsh model [Goldhirsh95], the COST205 [COST205], the Timothy [Timothy98] and Paraboni [Paraboni94] models. Moreover, there is the Lekkla model [Lekkla98] which has been developed using data derived by tropical regions.

Concerning the composite fade time using the same measurements, the Paraboni model has been also adopted by ITU-R. P. 1623 [ITU-R. P. 1623]. In this model the long fade durations are modeled with a lognormal distribution while a power law is used for the short fade durations. Moreover, in a recent model presented in [Cheffena08], it is assumed that the short fades duration due to scintillation follow the lognormal distribution as well as the long fades duration due to rain attenuation. Therefore, assuming that a fraction of fades are associated with short fade and (1-*a*) for long fades and using that attenuation is measured every second, the distribution of fade duration is:

$$P(d > D \mid A > A_{th}) = a\frac{Q\left(\dfrac{\ln(D/m_s)}{\sigma_s}\right)}{Q\left(\dfrac{\ln(1/m_s)}{\sigma_s}\right)} + (1-a)\frac{Q\left(\dfrac{\ln(D/m_r)}{\sigma_r}\right)}{Q\left(\dfrac{\ln(1/m_r)}{\sigma_r}\right)} \tag{2.20}$$

with

$$Q(x) = \frac{1}{\sqrt{2\pi}}\int_x^{+\infty} e^{-\frac{t^2}{2}}dt \tag{2.21}$$

the parameters m_s and σ_s are the parameters of the lognormal distribution for short fades duration and the parameters m_r and σ_r refer to the lognormal distribution for long fades durations.

2. Inter-Fade Duration

The statistics defined in fade durations can be also derived for the inter-fade durations. However, there are no developed models for these statistics [ESTECRep], [Castanet08].

2.1.2.3 Hitting times

A metric which may be proven essential for the FMTs is the hitting time distribution. Hitting time is the time at which a stochastic process reaches one value of the boundary (A_{min}, A_{max}) given that the initial value is A_0 with $A_{\min} < A_0 < A_{\max}$. Hitting time distribution reflects the dynamics of the process, given the SDE that describes it. For rain attenuation and the Maseng-Bakken model, the hitting time distribution has been presented in [Kanellopoulos07]. In Figure 2.8, the CCDF of hitting time distribution for a link in Europe with an operating frequency of 20 GHz is given. In the case of the figure the A_{max} was set infinite and so the hitting time distribution is the time needed for the process to reach $A_{th}=A_{min}$ starting from A_0. Hitting time distribution can be used for the estimation of the time needed for the FMT to change its state [Kourogiorgas12a]. In [Kanellopoulos13b], the hitting time distribution for a dynamic model of rain attenuation based on Weibull distribution is given.

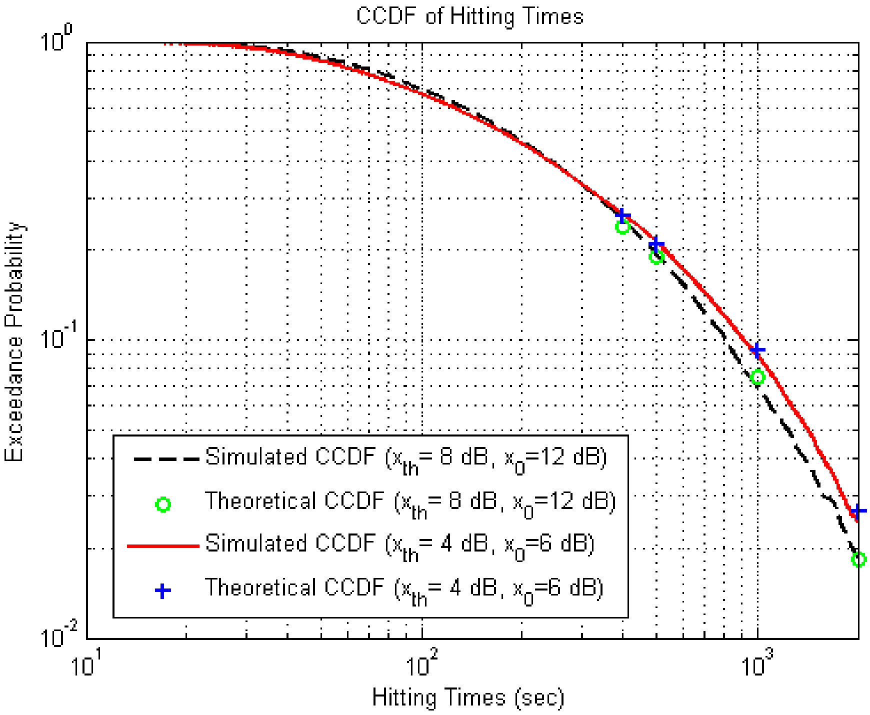

Figure 2.8. CCDF of hitting times

2.1.3 *Frequency Scaling*

The characteristics of propagation at a specific frequency exhibit similarities with the corresponding characteristics of propagation at another different frequency. Therefore, frequency scaling methods have been developed in order to estimate the magnitude of a propagation effect (attenuation, scintillation and depolarization) at a given frequency from the knowledge of its magnitude at another frequency, generally a lower one. This information can be used to identify the propagation characteristics of a higher frequency (e.g. Ka, V bands), taking into account measurements and characteristics of current systems that operate at lower frequency bands (e.g. Ku band) and to design Fade Mitigation Techniques (FMT), such as power control or site diversity, involving the estimation of the attenuation at a higher frequency from measurements at a lower frequency.

There are two kinds of frequency scaling methods: the long-term frequency scaling using the cumulative distributions of propagation effects at the same percentage of exceedence time and the instantaneous frequency scaling ratio at two different frequencies. The frequency scaling ratio exhibits strong variations during an event, especially for convective rain [Sweeney92], [OPEX94] and depends on dynamic variations of the drop size distribution (DSD) during a rain event [Dintelmann93]. In [Laster95], it is shown that the instantaneous and long-term frequency scaling ratios have the same order of magnitude and therefore the long-term ratio can be used as a rough estimation of the mean value of the instantaneous ratio in FMTs. A model which uses multi-dimensional Stochastic Differential

Equations for generating correlated time series of rain attenuation induced in links with different frequencies has been presented in [Karagiannis13].

A) Long-term frequency scaling ratio models

The long-term frequency scaling ratio (FSR) can be generally predicted using the following formula:

$$FSR(p) = \frac{A_2(p)}{A_1(p)} = \frac{g(F_{up})}{g(F_{down})} \tag{2.22}$$

where F_{down} is the lower frequency (generally the downlink frequency) and F_{up} the upper one (generally the uplink frequency), and p is the time percentage of exceedance. The $g(F)$ function is defined with empirical coefficients, and depends mainly on the frequency, but can also depend on attenuation or polarization. It can be calculated by different formulas depending on the considered method. In [Dintelmann93], CCIR [Drufuca74] and [Laster95], a power law function is used:

$$g(F) = F^n \tag{2.23}$$

where the power law exponent is a constant value depending on the method used.

In [ITU-R P.618] an empirical prediction method is proposed, where the long-term FSR varies with attenuation. In [COST205], the COST 205 Variable Effective Rain model is proposed where the ratio caused by an effective rain intensity increases with increasing attenuation.

B) Instantaneous frequency scaling ratio models

Concerning the Instantaneous FSR (IFSR), some empirical models of the mean and standard deviation are proposed [Laster95], while the standard deviation is considered to be constant. The impact of the stochastic temporal variations of the rain drop size distribution (DSD) on the standard deviation of the IFSR of rain attenuation, assuming a conditional gaussian distribution, is considered in [Gremont98]. Moreover, a linear variation of the standard deviation of the 50 GHz attenuation conditioned to the 40 GHz attenuation is derived in [Bolea-Alamañac04].

Another model has been presented in [Bertorelli05], [ESTECRep] and [Castanet06] assuming that the single frequency CDF of rain attenuation conditioned to rain follows a log-normal distribution and that the CDF of rain attenuation at one given frequency (uplink frequency) conditioned to the attenuation at another frequency (downlink frequency) follows a bi-dimensional joint log-normal form. Using the above assumptions, time series of attenuation at a given frequency knowing the attenuation at another frequency can be derived. A methodology presented in [Karagiannis13], takes into account the long-term correlation of rain attenuation for different frequencies and generates correlated time series of rain attenuation for the two links.

2.1.4 Diversity Systems

In this subsection the models for the prediction of improvement gain due to site and time diversity techniques are overviewed. In the first part the improvement gain for site diversity technique is examined while in the second part time diversity improvement gain is investigated.

2.1.4.1 Site Diversity

In site diversity systems applying the simplest combining technique, i.e. Selection Combining, two or more ground stations are communicating with the satellite and the Earth-space path with the least attenuation, i.e. higher SNR, is selected resulting to a selection combining scheme. Site diversity takes advantage of the decorrelation of rainfall rate with distance between the two radio paths. Therefore, the probability of simultaneous rain attenuation occurring on two or more network routes is less than the probability of rain attenuation occurring on each individual path.

In site diversity the joint cumulative distribution is of great importance, since the outage of a site diversity system can be calculated. However, there are two more metrics used for the evaluation of the performance of a site diversity system:

- Improvement factor, which is defined as the ratio of the single site time percentage and the multiple site time percentage, at which a given attenuation level is exceeded.
- Diversity gain defined as the difference between the single site attenuation threshold and multiple site attenuation threshold exceeded for a given time percentage.

There have been various models developed for the prediction and calculation of the three above-mentioned metrics: joint exceedance probability, improvement factor and diversity gain. More particularly, there has been a segmentation of these models into empirical and physical-based. In empirical models the following are included:

- Hodge model [Hodge82]: In this model the diversity gain is computed by modeling the effect of the frequency, baseline distance, elevation angle and baseline orientation in the diversity gain. It is an empirical model whose parameters have been derived after fitting the model expressions to data.
- ITU-R. P. 618-9, paragraph 2.2.4.2, [ITU-R. P. 618]: This model is used for the prediction of the diversity gain using a formula based on Hodge's model. This model has a limitation that the baseline distance must be less than 20 km and greater than 1.7km.
- NTUA simplified model [Panagopoulos05]: An empirical formula is proposed for the computation of the diversity gain, based on Hodge methodology but exhibits greater sensitivity to the variation of the distance.

More empirical models are reported in [ESTECRep], such as the Goldhirsh model [Goldhirsh82], Dissanayake model [Dissanayake00] and the Allnutt-Rogers model [Allnutt82]. However, models have been developed concerning site diversity attenuation prediction which are physically based:

- Paraboni-Barbaliscia model [Paraboni02]: In this model the joint CCDF of rain attenuation for an unbalanced system is computed assuming that rain attenuation follows the lognormal distribution and adopting a spatial correlation function derived from radar measurements. This model has been also adopted by ITU in ITU-R. P. 618.
- The EXCELL model has also used for the derivation of joint statistics of rain attenuation in [Bosisio98]. Joint rain attenuation statistics are computed through the isolated rain cells in which the horizontal distribution of rain rate is exponentially distributed.
- Matricciani model [Matricciani94] which is an extension of the well-know two-layer model. In this extension, the joint PDF of rain attenuation is considered asjoint-lognormal and the CDF of single site rain attenuation is computed through the two-layer model.
- NTUA physical model [Panagopoulos04] computes the unbalance joint CCDF of rain attenuation in which single site rain attenuation is assumed lognormal and the joint statistics of rain attenuation follow the joint lognormal distribution. The spatial correlation adopted for the specific rain attenuation is the one proposed by Lin.

More physical models have been proposed, such as Mass model [Mass87] which is based on a three-dimensional prediction of rain cells and the Crane model [Crane96], [Stafford01] based on the two-component model of Crane, which assumes that the rain cells are surrounded from a debris which corresponds to stratiform rain.

However, there have been other models developed in the last 5 years. Firstly, the MultiEXCELL model [Luini11] can be used for the derivation of the joint CCDF of rain attenuation. MultiEXCELL generates two-dimensional rain rate fields which are resulted from the conglomeration of rain cells whose horizontal rain rate is exponentially distributed. Also, HYCELL can be used for the computation of joint statistics of rain attenuation [Feral03a], [Feral03b] extending the methodology presented in [Kourogiorgas10]. Moreover, a space-time channel simulator which has been presented in [Jeannin12] can be also used for the derivation of joint statistics of rain attenuation, which however has not been tested against other models.

2.1.4.2 Time Diversity

Time diversity is an FMT which relies on the repetition of the already transmitted symbols in another time instance when the fades are not strong. Since there is a waiting time this technique must be applied in services which are delay tolerant such as data transfer and non-real time services. A great advantage in time diversity technique is that it does not need another receiver, as in site diversity, that makes it more cost effective.

In time diversity it is exploited that rain rate and rain attenuation of course are decorrelating in time and therefore, when the time instances of repetition are distanced in temporal domain, the probability to have high rain attenuation values in both time instances is less than the probability to have high rain attenuation values in one of the two instances. Therefore, the outage prediction in a time diversity system is:

$$P_{TD} = \Pr\left(A_1 = A(t) > a,\ A_2 = A(t+\Delta t) > a\right) = \int_a^\infty \int_a^\infty p_{A_1A_2}\left(A_1, A_2\right) dA_1\, dA_2 \tag{2.24}$$

An important metric in time diversity systems is the diversity gain for $p\%$ of time which is identified as:

$$G_{TD}\left(\Delta t, p\%\right) = A_{TD}\left(\Delta t = 0, p\%\right) - A_{TD}\left(\Delta t \neq 0, p\%\right) \tag{2.25}$$

Physically based techniques exist in which (2.24) is calculated and then (2.25) can be derived. The methods are based on the assumption that rain attenuation follows the lognormal distribution. As presented in [Arapoglou08] and [Fabbro09], the joint lognormal distribution is calculated using the appropriate correlation coefficient between the correlated lognormal variables $A(t)$ and $A(t+\Delta t)$. An empirical correlation coefficient has been presented in [Fabbro09] which was derived after processing the databases. The second approach is based on the Maseng-Bakken model and it has been presented in [Arapolgou08]. However, these models refer only to rain attenuation gain and not on other attenuation components.

2.1.5 Spatial Correlation of Total Attenuation

In the future satellite communications in which the cover area of a satellite is a whole continent, long-scale and mid-scale spatial correlation of total attenuation is important for the system design. Firstly, the spatial correlation of rain attenuation has been widely studied. In [Paraboni02] a correlation for the random variable of rain attenuation has been given which depend on the baseline distance between the two Earth stations. Moreover, in [Paraboni02] and [Jeannin12] from radar measurements a spatial correlation of rain rate has been extracted.

However, many models have been developed based on the spatial correlation of the rainfall rate which generate rain field in small-scale, mid-scale and large-scale areas. Most of these models are based on the modeling of rain cells, i.e. the horizontal distribution of rain rate inside a closed contour. For small-scale areas, i.e. the size of a rain cell, in [Capsoni87], it is recommended that the horizontal structure of rain rate inside a rain cell has an exponential shape. The model is known as EXCELL model. This model has been updated in [Capsoni06] for the discrimination between stratiform and convective rain and it has been used in [Capsoni09] for the prediction of exceedance probability of rain attenuation. Another model, presented in [Feral03a] assumes that the shape of a rain cell results from a combination of an exponential and Gaussian functions. The Gaussian part captures the convective part of the rain cell while the exponential simulates the stratiform rain.

For mid-scale rain fields, the above mentioned models of rain cells have been used. More particularly, the models presented in [Goldhirsh00] and [Luini11] are based on the EXCELL modeling of rain cells, while [Feral03b] is based on the HYCELL modeling of rain cells. In particular, [Feral03b] is presenting an iterative method for generating rain fields taking as input the lognormal distribution of rain rate and the fractional area, i.e area over which it is raining. Apart from these two models, the Bell methodology presented in [Bell87] is proposed for generating rain rate fields at mid-scale assuming that rain rate follows the lognormal distribution. As for large-scale rain fields, i.e. continental coverage, two models among others are [Feral06] and [Jeannin12]. In the first one the methodology of [Feral03b] has been used while in the second one the Bell's methodology is adopted.

Concerning the total attenuation fields there has not been an extensive research on their spatial correlation. However, in [ESTECRep] the spatial correlation of cloud liquid water and water vapour is examined from the ERA-40 database. Moreover, in [Jeannin11b] the spatial correlation of liquid water content and integrated water vapour content have been computed. Lastly, in [Luini12], a methodology is presented in order to calculate spatial fields of cloud attenuation based on the stochastic approach of [Bell87] and analyzing Earth-observation data.

2.1.6 Space-Time Channel Models

Apart from the temporal evolution of total attenuation in a single site (which is analyzed in detail in the next chapter), also the space-time variations on a continental area are of great importance for the design of the FMTs. More particularly, in the case of Terabit per second satellite systems, the European continent will be served by a multi-beam satellite. In order to evaluate the FMTs and so to design the system time series of total attenuation correlated in space are needed.

Research on this field has been growing since the last decade. First, in [Gremont04] a space-time series synthesizer is proposed based on the fact that point rain rate follows the lognormal distribution and so rain rate for multiple points follows the joint lognormal distribution. Moreover, the cross-correlation of the reduced Gaussian zero-mean and unit-variance variables which are obtained from the transformation of rain rate is modeled as an exponential function of the advection vector. However, in this model it is assumed that rain rate is homogeneous in the slant path in order to calculate the rain attenuation along the radio path.

A second model on space-time channel models is presented in [Bertorelli05a]. In this model it is assumed that rain attenuation on a single site follows the lognormal distribution and so for multiple sites the joint lognormal distribution. In order to generate rain attenuation time series an algorithm is followed. According to this algorithm, first a multivariate correlated Gaussian process is first generated in order to define the rainy and non-rainy sites. Then, again a correlated Gaussian vector is generated in order to calculate the 1-hour average of the natural logarithm of rain attenuation. Finally, for each site which is determined as a rainy site, time series of a period of 1-hour are extracted from ITALSAT data chosen so that the average attenuation of all samples matches the average value. The time series are then scaled in frequency, elevation angle and polarization.

Moreover, two models based on the Maseng-Bakken model have been proposed for the generation of time series of rain attenuation correlated in space for multiple sites. The first one presented in [Cheffena09]. In this work, the described model is a discrete-time model which can generate time-series of rain attenuation for multiple sites considering the Maseng-Bakken model and implementing it with a filtering method and has been applies in terrestrial networks. In [Karagiannis12], the theoretical formulation for multidimensional Stochastic Differential Equations (SDEs) is given as well as the multidimensional SDEs for generating rain attenuation in multiple sites.

Another space-time channel model for generating time series of spatially correlated two-dimensional rain fields has been presented in [Jeannin12]. This model is based on [Bell87] modeling of space-time evolution of rain fields and it is assumed that rain rate on space and time domains are assumed to be lognormal, whose statistical parameters can be extracted from rain rate measurements or the recommendation of ITU [ITU-R. P.837]. However, in this model time series of rainfall amount on a pixel of 250x250 km^2 with one sample every 6 hours are extracted from the ERA-40 database. Then the fractional area is computed for this pixel and using linear-piecewise interpolation scheme between two samples of the rainy fractional area, the time series of fractional area with one sample for every 6 minutes are calculated. Then rain fields are generated with Bell's methodology and rain attenuation is calculated for every 6 minutes. Time series of rain attenuation for every second are generated using stochastic interpolation, presented in [Carrie11]. The advantage of this model is that it is physically based.

All the presented models refer to space-time variations of rain rate or rain attenuation. Considering the other propagation effects such as atmospheric gases and cloud attenuation, a space-time synthesizer has been presented in [Jeannin11]. This model is based on the methodology presented in [Jeannin12] space-time fields of cloud liquid water content, integrated water vapour content are derived. Then, assuming that the oxygen concentration and absorption is constant, space-time total attenuation fields are generated. The rain rate and liquid water content are assumed to follow the lognormal distribution while the integrated water vapour content the Weibull distribution.

2.2 Fade Mitigation Techniques

As it was observed in the previous section total attenuation and mainly rain can exceed very high attenuation values for a small time percentage. Therefore, for a system which requires high availability the attenuation values exceeded for small time percentages are crucial. One solution in order to deal with the attenuation is to employ a fade margin. However, due to the high values of the fade margin which are required to compensate attenuation which is exceeded for a small time percentage, the sources of the system will remain unexploited for the most of the period of operation. So, in order that a system be efficient and operate under low fade margin, Fade Mitigation Techniques (FMTs) are required.

FMTs can be classified into three categories: a) Effective Isotropic Radiated Power (EIRP) control techniques, b) adaptive transmission techniques and c) diversity techniques. Most of the FMTs use a control loop in order to change their state. According to this loop, first the observation of the quality of the link must take place and then the state of the satellite channel and its duration on this state must be predicted.

The identification of the channel can be achieved by the measurements of the channel or by a short-term prediction. For the short-term prediction, the statistics of fade slope may be used. There are a number of models for the modeling of the long-term statistics of the fade slope, a review on which can be found in [ESTECRep] and [ESTEC04]. The Van de Kamp model, presented in [Kamp03] has been adopted by ITU in ITU-R. P. 1623 [ITU-R. P.1623]. Another method for the short-term prediction of fades at Ka band has been presented in [Gremont99] and it is assumed that attenuation is an autoregressive moving average process.

In the EIRP control techniques, in case of fades the power of the Earth station or the satellite can be changed or the antenna gain. In case of the adjustment of power at the Earth station, the technique is called Uplink Power Control (ULPC) while at the satellite Downlink Power Control (DLPC). The two drawbacks in the technique of ULPC is the adjacent channel interference due to the increased power sent at the sidelobes and the adjacent satellite interference. The adjacent satellite interference occurs due to the increased power that it is received by the satellites which are close to the receiver satellite. On the other hand, the implementation of DLPC is more difficult due to the limitations on satellite size and weight. Also, in DLPC adjacent channel interference may occur. One more drawback is the intersystem interference which is caused by the interference of the Earth-space system to terrestrial networks due to the increased power. Another EIRP control technique is the spot beam shaping by the adjustment of the antenna gain. A Geostationary satellite which covers a wide region may provide services using spot beam in order that the antenna beamwidth is reduced and the gain is increased. In this technique short-term weather predictions are needed which may be derived from satellite images or numerical weather products. Using these prediction the antenna gain may be changed in the region which is affected more by the atmospheric phenomena at the specific time instance. Given the meteorological conditions the optimization of the spot beams may be static or dynamic [Paraboni09].

The adaptive transmission techniques include the adaptive coding (AC), adaptive modulation (AM) and the data rate reduction (DRR). In AC technique bits are added into the transmitted symbol in order to detect and correct erroneous symbols. However, due to the increased size of the symbol the bandwidth have to be increased in order to keep the data rate the same. There are various coding schemes, as this is analyzed in [Panagopoulos04]. In case of short fades such as scintillation, the interleaving method is proposed. In case of strong fades complex coding schemes must be used. In AM technique the current modulation which is used is changing in order to have reduced BER for a given probability error. In this case, the spectral efficiency is reduced and so the data rate is reduced. In clear sky conditions highly efficient modulation schemes may be used, but under rain fading conditions schemes such as BPSK and QPSK shall be used. In DVB-s2, the ACM technique has been already incorporated. The last technique in the adaptive transmission techniques is DRR. In DRR, the data rate is decreased while the BER threshold and the bandwidth remain constant and so a reduced carrier –to-noise threshold is required.

The last category of the FMTs is the diversity techniques. The diversity techniques are: the site diversity, orbital (satellite) diversity, frequency diversity and time diversity. In Figure 2.9 a dual-site diversity system is shown. In these techniques, two Earth stations are communicating with the same satellite and the Earth-space path with the least attenuation is selected. This technique takes advantage of the fact that as the distance between two points is increased, the decorrelation of rain attenuation is also increased. In Figure 2.10, time series of rain attenuation correlated in space are shown for separate Earth-space stations, as well as the attenuation for the dual site diversity system. In orbital diversity instead of two Earth stations, there is only one Earth station (probably implemented with two receiving antennas) which communicates with two satellites, as shown in Figure 2.11, and as in site diversity the path with the least attenuation is selected. When the angular separation between the two radiopaths is increasing the decorrelation of rain attenuation also increases. In comparison to site diversity, it is less cost inefficient, since it does not require the installation of more than one Earth stations. However, it is less effective. Attenuation due to the atmospheric phenomena increases as the frequency increases. Therefore, in case that high attenuation values are observed, the system may operate at low frequencies while in clear sky conditions at high frequency. The last technique is time diversity technique. It takes advantage of the increased decorrelation of rain rate with time. Therefore, when in a time instance the attenuation values are high, the system may retransmit the same symbols when the meteorological conditions are such that the fades are weak. The time needed for the retransmission can be modeled with the concept of hitting time statistics (described previously), while the dynamics of attenuation are modeled with time series. In previous sections, models for predicting the joint exceedance probability of rain attenuation for two different time instances have been presented.

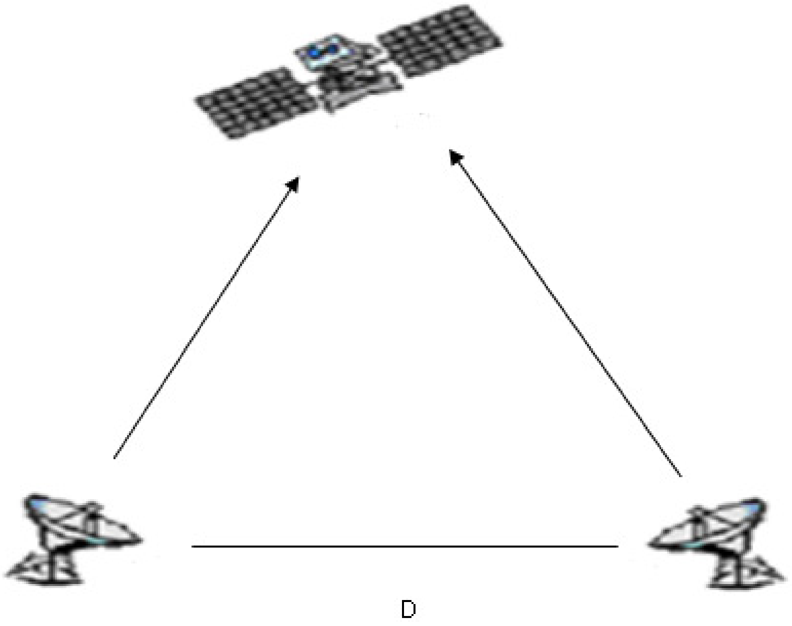

Figure 2.9. Dual-site diversity system

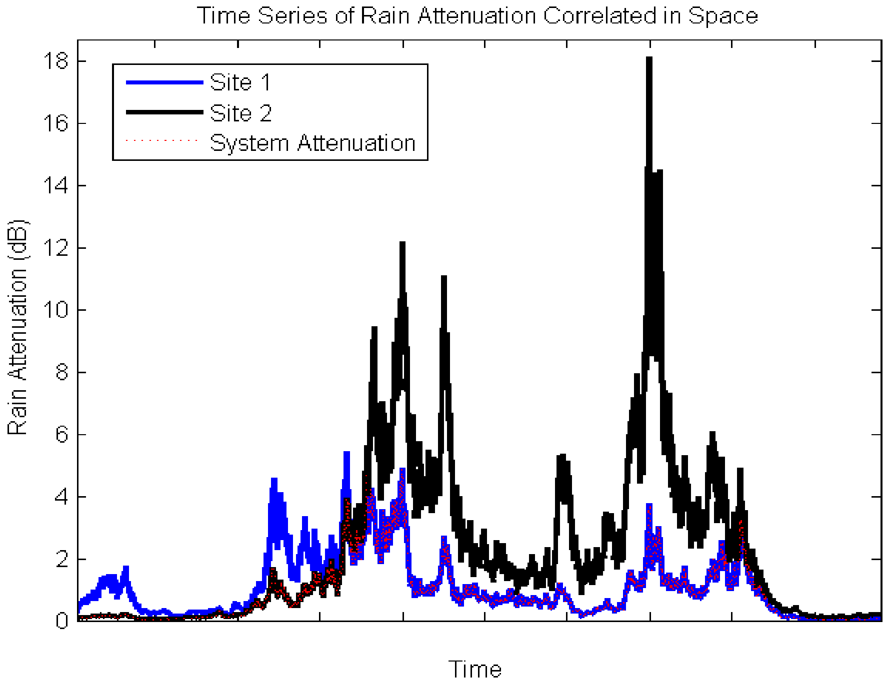

Figure 2.10. Rain Attenuation time series correlated in space for two sites and the attenuation for the dual site diversity system (selection combining)

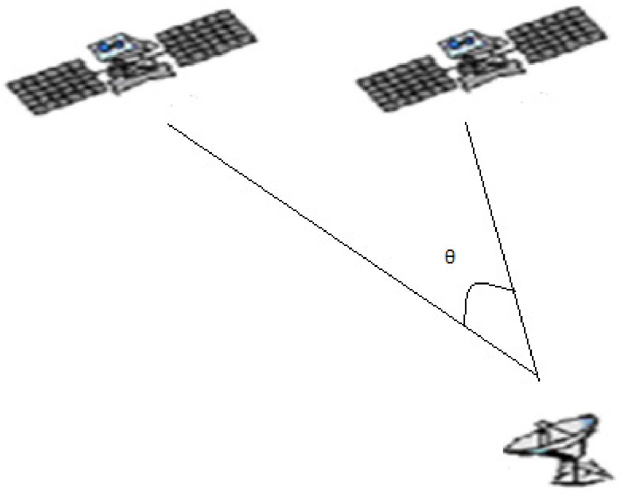

Figure 2.11. Orbital diversity system with two satellites

2.3 Future Wireless Terrestrial and Satellite Communication Systems

The ever increasing demand of high data rates and the spectrum scarcity at low frequency bands lead to the adoption of high microwave frequencies, such as Ka and Q/V bands for the operation of future satellite communication systems. Terabit per second satellite or the High Throughput Satellite (HTS) is a concept of using satellites operating at these high frequency bands for providing very high data rates [Thompson11]. In such systems one probable solution is the use of Q/V bands at the feeder link and the Ka band at the user link.

In HTS systems, multiple gateways are established in various regions of Europe which are connected to user beams. Since higher frequencies are used for the feeder link than the direct-to-user link, the problem of rain attenuation becomes more severe. The most effective PIMT is the site diversity since it exploits the spatial decorrelation of rain rate and rain attenuation which increases as the separation distance of the Earth stations is increasing. As in the case of Terabit/s satellite, in future satellite communications, a number of Gateways (GW) may be deployed on the ground, thus making feasible the gateway diversity techniques. Moreover, in multi-beam satellite such as Terabit/s satellite systems each gateway serves a number of user beams. In multi-beam satellites, transmit or receive diversity can be implemented [Thompson11]. In order to reduce the complexity of the procedures which hold on the satellite, transmit diversity can hold for the forward link. The receive diversity techniques that may be used are the Maximal Ratio Combining (MRC), the Selection Combining (SC), the Equal Gain Combining (EGC) [Skraparlis]. As for the transmit diversity techniques these are described in [Ismail11] and [Lo99]. More particularly in [Lo99] and [Paulraj03] the MRT is described in more detail. However, very recently other gateway diversity techniques have been identified in [Ritchie11] and [Jeannin11], in which the gateways deployed across Europe are communicating via a network center.

On the other hand, Multiple-Input Multiple-Output (MIMO) technology has recently emerged as one of the most significant technical breakthroughs in modern digital communications due to its promise for very high data rates at no cost of extra spectrum and transmitted power [Arapoglou11]. The application of MIMO technology in Satellite Communication Systems (fixed and mobile) is under investigation by the Research community [Arapoglou11]. Broadband Satellite communication can be benefited from MIMO [Liolis07], [Knopp10] signaling in two different ways: spatial multiplexing and diversity. In the spatial multiplexing concept, independent data are transmitted by separate antennas in order to maximize throughput (i.e., linear capacity growth can be achieved by increasing the number of antennas). In the diversity configurations, the same signal is transmitted along multiple fading paths with low correlation in order to improve the robustness of the link in terms of each user BER performance. These advantages have already led to the success of MIMO both as a research topic and as a commercially viable technology in terrestrial communications, while they offer a promising perspective for satellite communications.

Multiple Input Multiple Output (MIMO) antenna techniques have been recently proposed in Satellite communication systems in order to increase the transmission rates, the availability and generally to enhance the capacity and to exploit the interference. Moreover, Mobile Satellite Systems are able to provide large coverage at mobile users and also achieving high data rate transmission at low cost [Arapoglou11] in navigation, communications and broadcasting applications. Moreover, cooperative techniques, which can be seen as virtual MIMO systems, have been extensively used to increase the system performance of terrestrial wireless networks [Laneman04] offering spatial diversity. Cooperation can be applied to LMS and high frequency satellite communications in terms of hybrid satellite-terrestrial systems [Sakarellos14] where terrestrial relays forward the information broadcasted by the satellite to the final destination [Paillassa11], operating as assisted gap-filers. The cooperative relaying scenarios between sources and destinations incorporating satellite part are analytically described in [Paillassa11].

Apart from the MIMO techniques defined in spatial domain, i.e. multiple antennas at the transmitter and/or receiver side, the polarization domain has been exploited as a resource for achieving multiplexing gain in highly correlated satellite channels ([Arapoglou11], [Arapoglou11b], [Oestges08], [King06]). In [Arapoglou11b], [King06] the dual polarization has been identified as a potential solution for the increase of throughput in mobile satellite system in L- or S-bands. In [Liolis10] a model is proposed for dual polarization Land Mobile Satellite channels. For the case of multi-beam satellite systems, the dual polarization can be used along with a more intense frequency re-use factor in order to increase the offered throughput.

As aforementioned, the use of high frequency bands for wireless terrestrial and satellite communications systems is qualified as a solution for future broadband communications mostly due to the high bandwidth which is offered. However, the congestion of services in the Ku- and Ka-bands has recently started to appear. In [CORASAT13], [Liolis13], [Sharma13], [Sharma13b], cognitive aspects are studied with a view to their possible implementation in next generation satellite communications. More particularly, in [CORASAT13] the Cognitive aspects and scenarios for the satellite communications networks are analytically described.

In cognitive radio systems, at least two users or services may be identified. The users of the first service are considered as incumbent users while for the second one, the users are identified as cognitive. In cognitive radio systems, the cognitive users firstly have to sense if an incumbent user transmits in the same frequency. If the cognitive user does not sense any communications activity at these frequencies, then the user will start to communicate. In Cognitive radio systems generally the spectrum sharing techniques can be divided in the spectrum interweave, spectrum underlay and spectrum overlay approaches. In the first approach, the cognitive users are allowed to transmit their data only in the absence of incumbent users' transmission, whereas in the spectrum underlay approach, the cognitive are allowed to transmit at the same time with the incumbent users guaranteeing specific interference constraints. Finally, in the spectrum overlay approach the cognitive users are allowed to transmit simultaneously with the incumbent users but they are obligated to help them and relay their messages so as to offset the caused interference. An important scenario identified for the cognitive satellite communication systems is the dual cognitive SatComs [Sharma13]. In this cognitive system, two Geostationary Earth Orbit (GEO) satellites operating mainly at Ku-band and above are communicating with two different ground satellite terminals. One GEO satellite network is considered as the incumbent satellite network and the second one as the cognitive satellite network. Another important scenario for the realization cognitive satellite networks is the coexistence of satellite communication systems with wireless terrestrial communications [Sharma13b].

The commercial satellite market is witnessing a surge in Ku- and Ka- High Throughput Satellite (HTS) systems -including Intelsat's Epic, Inmarsat's Global Express, O3b, Viasat 2- aiming at providing broadband services to ships, airplanes, trains and land vehicles [Lobao13]. The broadband mobile represents a fast growing market for satellite operators, which cannot be addressed by the Mobile Satellite Service (MSS) spectrum allocated to these bands mostly on a secondary basis. In search for additional spectrum, service providers have coined the term Earth Stations on Mobile Platforms (ESOMP) for mobile terminals, allowing them to exploit also Fixed Satellite Service (FSS) spectrum and the use case has been backed up by regulatory support (see e.g. at ITU-R level [ITU-R. M.1643] for aeronautical services over Ku-band and [ITU-R. S.2223] for the regulatory status in Ka-band).

The major technical challenge for this convergence between FSS and MSS in Ku- and Ka-frequency bands is adjacent system interference both satellite and terrestrial.

Focusing on the adjacent satellite case, ESOMPs need to fully comply with FSS rules, including the same off-axis EIRP (Effective Isotropically Radiated Power) as typical uncoordinated FSS earth stations. This stresses particularly the (open- or closed-loop) antenna tracking mechanisms of ESOMPs, but also contradicts the commercial driven incentive to reduce antenna size. For an accurate system and waveform design of mobile HTS, the statistical characterization of adjacent satellite interference (ASI) is necessary. The statistical nature of the total carrier-to-noise plus ASI ratio (CNIR) is due to the differential impact of the troposphere (predominantly rain fading) over the two (wanted and interfering) slant paths [Panagopoulos04].

3 Review on Tropospheric Attenuation Time Series Synthesizers

As explained analytically in previous chapter, due to the very high values of attenuation for a small time percentage, static fade margins are not the most efficient technique for attenuation compensation and the reach of a certain availability or capacity threshold. Therefore, Fade Mitigation Techniques have been developed and technologically proposed, such as site diversity, time diversity, adaptive coding and modulation, power control and data rate adjustment (Panagopoulos et al., 2004) for the cost reduction of the communications. These techniques require apart from the knowledge of first order statistics of the satellite channel, i.e. Probability density functions, the dynamics of channel in order to be able to proceed to end-to-end simulations and evaluation methods of a system's performance.

Therefore, time series synthesizers and channel models are used for the next generation satellite systems reliable design at high frequencies (Ku-band and above). Moreover, time series synthesizers can be used in case that there are no measurements for various link characteristics and for various climatic regions, which is the usual case. Since, measurements of attenuation need at least a year (a very optimistic estimation in terms of time consumption) and these can be obtained for a certain elevation angle, frequency and ground position, synthesizers can be used (of course with caution) for generating attenuation time series. Such synthesizers must be able to generate time series of attenuation which reproduce first-order statistics of attenuation and then the dynamics of attenuation. Here, it must be noted that the term 'dynamics' in the literature has been translated in many ways. Here, dynamics are considered the second-order statistics of attenuation, i.e. temporal correlation, or the fade slope or fade duration statistics.

Propagation community has been drawing a lot of attention on the development of synthesizers for attenuation. In Ku- and Ka-bands, rain attenuation plays the most significant role and therefore, the number of synthesizers for generating rain attenuation time series is higher than the other attenuation factors. However, as the Q/V bands are planned to be used, time series generators are needed for the other attenuation factors, since their effect on signal power and amplitude is increasing, in order to optimize the system's performance. It must be noted that very recently, ITU-R. has published the Recommendation P.-1853 in which synthesizers of attenuation factors and total attenuation are presented.

In this chapter, tropospheric attenuation time series synthesizers found in the literature are presented and briefly explained. In Section 2, rain attenuation time series synthesizers are given, while in section 3 for integrated liquid water content and in section 4 for integrated water vapor content from which clouds and water vapor attenuation, respectively, can be derived. In Section 5, scintillation time series generators are presented and in section 6 two methods for synthesis of the total tropospheric impairments time series.

At this point it must be noted that from this chapter the methodologies for generating time series of tropospheric attenuation based on space-time fields are excluded.

3.1 Rain Attenuation Synthesizers

Rain attenuation has the greatest impact for satellite links at Ku-, Ka- and Q/V bands. Therefore, the number of synthesizers developed for the generation of time series of rain attenuation are numerous. A simple classification is the following:

a) Filter-based models

b) Models based on Stochastic Differential Equations (SDEs)

c) Synthetic Storm Technique

d) Models based on conditional probabilities

e) Models based on Markov Chains

f) Data-based models

Every category will be briefly explained on the following.

3.1.1 Filter-based Models

In this category of models the synthesizer depends on the creation of a filter from which uncorrelated Gaussian noise is passing in order to create temporal correlated Gaussian samples which then are transformed to random variables of specific theoretical distribution.

3.1.1.1 Maseng-Bakken Model

A well accepted model of this category is the Maseng-Bakken (M-B) model [Maseng81]. Although, in the M-B model, a Stochastic Differential Equation was mainly introduced (which will be explained later), the stochastic process of rain attenuation was generated using a low-pass filter. The main assumptions of the model are:

1) Rain attenuation follows the lognormal distribution

2) The rate of change of rain attenuation is proportional to the instantaneous value of rain attenuation

3) Rain attenuation can be described as a 1st order Markov process

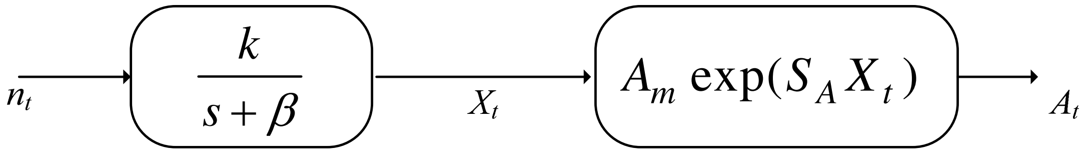

Figure 3.1. Block Diagram of the M-B model

In Figure 3.1, the block diagram for the generation of rain attenuation time series according to the M-B model is given. The input in the first block (n_t) are independent samples of a zero mean and unity variance Gaussian stochastic process. The first block is a low-pass filter with a cut-off frequency equal to the dynamic parameter of rain attenuation (β_A). The output of the filter is correlated samples of a Gaussian stochastic process which then pass through the non-linear transformation:

$$A_t = A_m \exp(S_A X_t) \tag{3.1}$$

where A_m and S_A are the statistical parameters of the lognormal distribution of rain attenuation. In the aforementioned model, it is considered that rain attenuation follows the unconditional exceedance probability, i.e. the probability to rain on a specific point of the slant path is equal to one and therefore, the probability that rain attenuation exceeds the zero dB value is also equal to one. In Figure 3.2, a snapshot of the time series of rain attenuation considering a Ground Station in Athens, frequency of 30GHz and elevation angle of 30°.

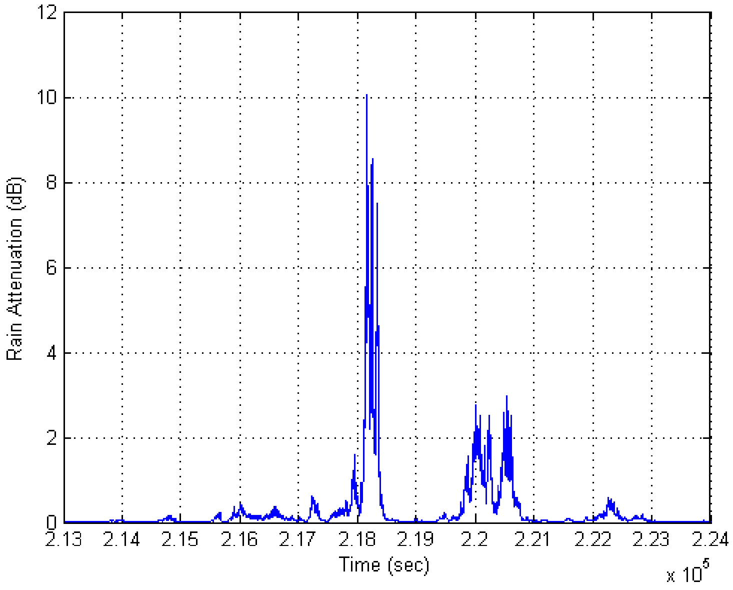

Figure 3.2. A snapshot of rain attenuation time series

From the M-B model, the autocorrelation of the output of the low-pass filter is:

$$\rho_X(t) = e^{-\beta_A t} \tag{3.2}$$

and its spectrum is:

$$S_X(f) = \frac{1}{1+\left(\frac{2\pi f}{\beta_A}\right)^2} \tag{3.3}$$

In [Lacoste05], a first attempt to consider the intermittency of rain attenuation is attempted by introducing an offset parameter. This offset parameter takes into account the exceedance probability of the zero-dB threshold for rain attenuation. The model relies on the M-B assumptions and uses the M-B model. In Figure 3.3, the block diagram of the enhanced M-B model is given.

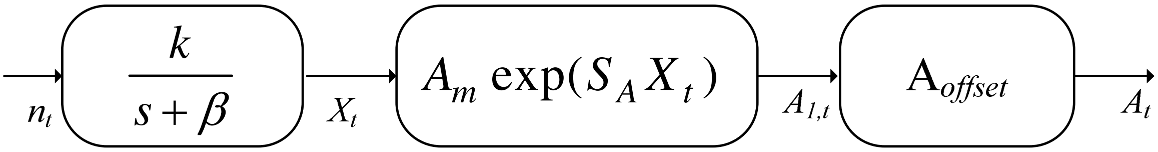

Figure 3.3. Block Diagram of the Enhanced Maseng-Bakken model

The difference with the M-B model is that rain attenuation is obtained through the expression:

$$A_t = \max\left[A_{1,t} - A_{offset}, 0\right] \tag{3.4}$$

with

$$A_{offset} = A_m \exp\left(S_A Q^{-1}\left[\frac{P_0}{100}\right]\right) \tag{3.5}$$

where Q(.) is the CCDF of a zero mean unity variance Gaussian variable (Gaussian Q-function) and P_0 is the probability to rain on a point and can be computed through the Recommendation of ITU-R. P. 837 [ITU-R. P.837]. In Figure 3.4, a snapshot of rain attenuation is given using the EMB model. The above methodology has been also adopted in the first version of ITU-R. P. 1853 [ITU-R. P.1853, 2012].

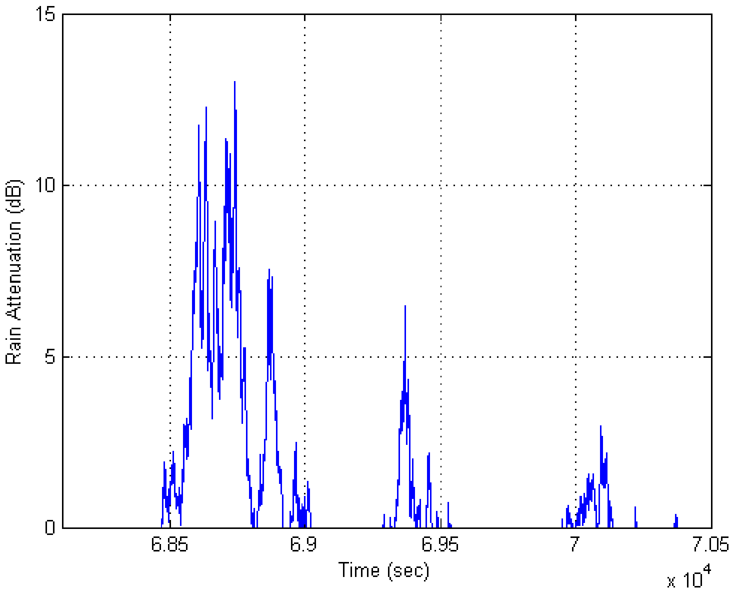

Figure 3.4. A snapshot of rain attenuation time series with EMB

However, in [Boulanger13], it is explained that the synthesizer in [Lacoste05], [ITU-R. P.1853], does not give as an output a process following a lognormal distribution for the rain attenuation, given that it is raining somewhere on the slant path. Therefore, a new synthesizer is proposed as a result of a mixed law between a Dirac and a Lognormal distribution. Moreover, an algorithm is presented for generating rain attenuation time series for different correlation coefficient expressions and not be restricted in the one of (3.2).

The step-by-step algorithm of the synthesizer is the following:

1. Generate zero mean unity variance Gaussian random variables ($G(t)$) with arbitrary temporal correlation on Fourier domain (details in [Boulanger13])
2. Calculate:

$$G_0 = \sqrt{2}erfc^{-1}\left(2\left(\frac{P_0}{100}\right)\right) \tag{3.6}$$

3. Calculate rain attenuation time series through the expression:

$$A(t) = \exp\left(erfc^{-1}\left(erfc\left(\frac{G(t)}{\sqrt{2}}\right)/(P_0/100)\right)\cdot\sqrt{2}\cdot\sigma + m\right) \quad for \quad G(t) > G_0$$

$$A(t) = 0 \quad for \quad G(t) \le G_0$$

(3.7)

3.1.2 Models based on SDEs

The stochastic differential equations have been used in the propagation framework for the generation of rain attenuation. Firstly, the MB model introduced a first-order SDE for the description of rain attenuation [Maseng81]. The SDE was of the form:

$$da(t) = K_1\left(a(t)\right)\cdot dt + \sqrt{K_2\left(a(t)\right)}dW(t) \tag{3.8}$$

with K_1 the drift coefficient and K_2 the diffusion coefficient and dW, the Brownian increments. In (Maseng and Bakken, 1981), it is assumed that the rate of change of rain attenuation is proportional to the instantaneous value of rain attenuation. Therefore, by definition of the diffusion coefficient [Karlin81], [Karatzas05], it is assumed that $K_2 \sim A_t^2$ So, given that:

- the static pdf of a stochastic process described by (3.8), is given by:

$$p_{st}(a) = \frac{C}{K_2(a)}\exp\left\{2\int\frac{K_1(y)}{K_2(y)}dy\right\} \tag{3.9}$$

C normalization constant

- rain attenuation is assumed to follow lognormal distribution

, the SDE which describes rain attenuation is:

$$dA_t = \beta_A A_t\left[S_a^2 - \ln\left(\frac{A_t}{a_m}\right)\right]dt + \sqrt{2\beta_A}S_a A_t dW_t \tag{3.10}$$

Now, using the following transformation:

$$X_t = \mathrm{M}\left[A_t\right] = \ln\left({}^{A_t}\!\big/_{A_m}\right)/\,S_a \tag{3.11}$$

the SDE which describes the process X_t is:

$$dX_t = -\beta_A X_t dt + \sqrt{2\beta_A}dW_t \tag{3.12}$$

The analytical solution of (3.12) is given in [Kanellopoulos07]:

$$X_t = e^{\beta_A t}\left(X_0 + \sqrt{2\beta_A}\int_0^t e^{-\beta_A s}dW_s\right) \tag{3.13}$$

with X_0 the initial value of the process X_t. The process X_t is the Ornstein-Uhlenbeck process which is a Gaussian zero mean unity variance stochastic process with an autocorrelation function given by (3.2). Therefore, for the generation of rain attenuation using the above model the following step-by-step algorithm can be used:

1) Generate time series of X_t process through (3.13).

2) Calculate rain attenuation through the following transformation:

$$A_t = A_m \exp(S_A X_t) \tag{3.14}$$

Apart from the lognormal distribution, the Weibull and Gamma distributions have been identified for the description of rain attenuation. In [Kanellopoulos13a], a synthesizer based on SDEs is proposed for Gamma distributed rain attenuation based on the assumption that $K_2 \sim A_t^2$, as in the M-B model. Given that the PDF of Gamma distribution is:

$$p_A(a)=\frac{w_a^{v_a}}{\Gamma(v_a)}\cdot a^{v_a-1}\cdot\exp(-w_a\cdot a) \tag{3.15}$$

where w_a, v_a are the two positive parameters of the gamma distribution, which can be calculated by regression fitting on experimental data or prediction models data and Γ(.) is the gamma function. The proposed SDE is:

$$dA_t=\beta_{AG}\cdot A_t\cdot\left(\frac{v_a}{w_a}+\frac{1}{w_a}-A_t\right)\cdot dt+\sqrt{(2/w_a)\cdot\beta_{AG}\cdot A_t^2}\,dW(t) \tag{3.16}$$

where β_{AG} is the dynamic parameter of rain attenuation. The solution of (3.16) is:

$$a(t)=\frac{a_0\cdot e^{\sqrt{\frac{2\beta_{AG}}{w_a}}\cdot W(t)+\beta_{AG}\cdot\frac{v_a}{w_a}\cdot t}}{\left(1+\beta_{AG}\cdot a_0\int_0^t e^{\sqrt{\frac{2\beta_{AG}}{w_a}}\cdot W(s)+\beta_{AG}\cdot\frac{v_a}{w_a}\cdot s}\,ds\right)} \tag{3.17}$$

where a_0 is the initial value of rain attenuation and W the Brownian motion.

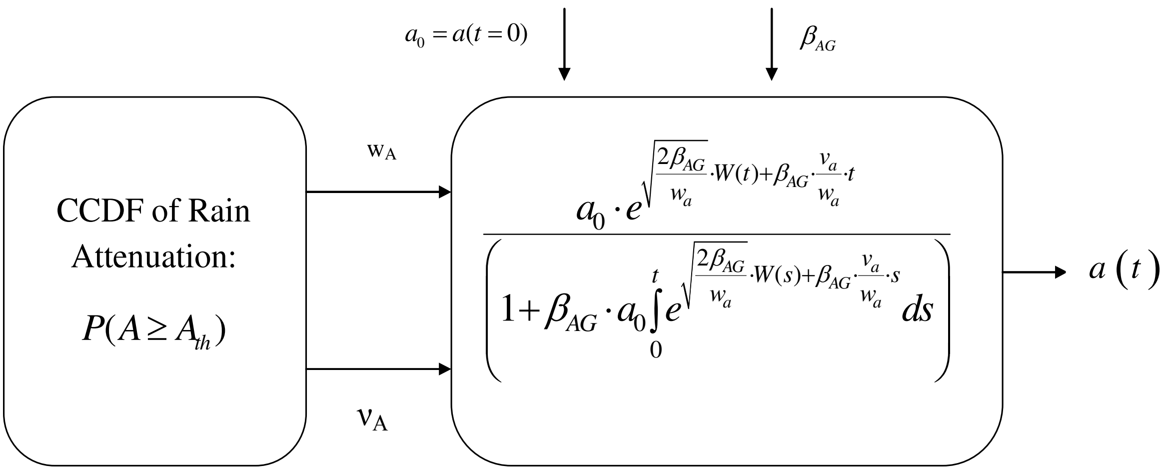

Figure 3.5. Block Diagram of rain attenuation time series synthesizer for Gamma distributed rain attenuation

A block diagram for generating rain attenuation time series for Gamma distributed rain attenuation is given in Figure 3.5. The first block is required in order to obtain the two statistical parameters of rain attenuation.

In [Kanellopoulos13b], an SDE is proposed for Weibull distributed rain attenuation. Similarly to the two previously presented models, it is assumed that $K_2 \sim A_t^2$. The PDF of a Weibull distribution is:

$$p_X(x) = \frac{\nu}{w} x^{\nu-1} e^{-\frac{x^\nu}{w}}, \;\; x>0 \tag{3.18}$$

where *v* and *w* is the two parameters of Weibull distribution which must be greater than 0. The proposed SDE is of the form of (3.8) with drift coefficient of the proposed synthesizer:

$$K_1(A(t)) = \beta_a A(t)\left(w + \frac{w}{\nu} - A^\nu(t) \right) \tag{3.19}$$

with β_A the dynamic parameter of rain attenuation. The diffusion coefficient is:

$$K_2(A(t)) = \frac{2\beta_a w}{\nu} A^2(t) \tag{3.20}$$

Rain attenuation time series are then obtained through the solution of the SDE:

$$A(t) = \frac{A_0 \cdot e^{\sqrt{\frac{2\beta_a w}{\nu}} \cdot B(t) + \beta_a \cdot w \cdot t}}{\left(1 + \nu\beta_a \cdot A_0^\nu \int\limits_0^t e^{\nu\sqrt{\frac{2\beta_a w}{\nu}} \cdot B(s) + \nu \cdot \beta_a \cdot w \cdot s} ds \right)^{1/\nu}} \tag{3.21}$$

Apart from the previous models, the model developed in [Manning90] is based on SDEs, considering a second-order SDE for the description of rain attenuation. More particularly, it is considered that rain rate is described by the following SDE:

$$dR_t = \beta_R R_t \left[S_R^2 - \ln\left(\frac{R_t}{R_m} \right) \right] dt + \sqrt{2\beta_R} S_R R_t dW_t \tag{3.22}$$

where β_R is the dynamic parameter of rain rate, R_m is the median value of rain rate and S_R the standard deviation of ln*R*. The SDE of (3.22) is the same as the MB for rain attenuation. The assumptions of the SDE of (3.22) for rain rate have been also tested in [Burgueno90] and [Kourogiorgas13] showing that rain rate fulfills the same assumptions. Therefore, from (3.22) the SDE which describes the underlined Gaussian process $x_R = \frac{\ln R - \ln R_m}{S_R}$ is:

$$dx_{R,t} = -\beta_R X_{R,t} dt + \sqrt{2\beta_R} dW_t \tag{3.23}$$

According to [Manning90], the underlined Gaussian process of the specific rain attenuation (*Γ*) is:

$$dx_{\Gamma,t} = -\beta_\Gamma X_{\Gamma,t} dt + \sqrt{2\beta_\Gamma} dW_t \tag{3.24}$$

Given a very short path, the underlined Gaussian process for rain attenuation also follows the expressions of (3.23) and (3.24):

$$dX_{A,t} = -\beta_A X_{A,t} dt + \sqrt{2\beta_A} dW_t \tag{3.25}$$

However, as stated in [Manning90], in case that the slant path increases, (3.25) cannot be used, firstly, because rain attenuation is not any more proportional to the specific rain attenuation and also due to the increased path through rain, the process dW_t is smoothed. Therefore, a smoothed process ($\zeta(t)$) is considered:

$$\zeta(t) = \frac{1}{T_S} \int_{-\infty}^{t} \exp\left(-\frac{t'-t}{T_S}\right) \xi'(t') dt' \tag{3.26}$$

where $\xi'(t')$ is white Guassian noise. So, (3.26) is described through:

$$d\zeta_t = -\gamma_S \zeta_t dt + \gamma_S dW_t \tag{3.27}$$

with $\gamma_S = (T_S)^{-1}$. The smoothed process is now used for driving rain attenuation dynamics, i.e. the SDE which describes the underlined Gaussian process for rain attenuation is:

$$dX_t = -\beta X_t dt + \sqrt{2\beta} d\zeta_t \tag{3.28}$$

Using (3.27) and (3.28), the following second order SDE for the description of rain attenuation is used:

$$\frac{d^2 X_A}{dt^2} = -\gamma(1 + \frac{\gamma_S}{\gamma}) \frac{dX_A}{dt} - \gamma\gamma_s X_A + \gamma_s \sqrt{2\gamma}\xi(t) \tag{3.29}$$

with $\xi(t)$ zero mean unity variance Gaussian noise.

Moreover, the SDEs have been used for generating rain attenuation time series at links with mobile receivers [Arapoglou12]. More particularly, in [Arapoglou12] a rain attenuation synthesizer is developed and combined with the attenuation caused by power arches in order to have a channel model for railways. This model is based on the theoretical modeling of exceedance probability of rain attenuation for mobile receivers presented in [Matricciani95a]. In the later reference it is found that the CCDF of rain attenuation for a mobile receiver ($P_M(A)$) is connected to this of a fixed receiver ($P_F(A)$) through:

$$P_M(A) = \xi P_F(A) \tag{3.30}$$

where

$$\xi = \frac{\upsilon_R}{|\upsilon_M - \upsilon_R \cos\varphi|} \tag{3.31}$$

with υ_R the wind speed, υ_M the speed of the mobile receiver and φ the angle between the storm's velocity and the receiver's velocity.

Now, in [Arapoglou12], it is assumed that rain attenuation induced in a mobile receiver follows lognormal distribution and that rain attenuation temporal variations are proportional to the instantaneous value of rain attenuation. Therefore, the MB model can describe the rain attenuation time series. So, the following SDE describes the rain attenuation induced on a slant path with a mobile ground station:

$$dA_{M,t} = \beta_{A,M} A_{M,t} \left[S_{M,a}^2 - \ln\left(\frac{A_{M,t}}{a_{M,m}}\right) \right] dt + \sqrt{2\beta_{A,M}} S_{M,a} A_{M,t} dW_t \tag{3.32}$$

with $S_{M,a}$ and $a_{M,m}$ the lognormal parameters of rain attenuation induced in a link with mobile terminal and the dynamic parameter of the mobile case is related to this of the fixed case through:

$$\beta_M = \frac{1}{\xi}\beta_F \tag{3.33}$$

3.1.3 Synthetic Storm Technique

The Synthetic Storm Technique (SST), given in [Matricciani96], is a methodology for generating rain attenuation time series given as input apart from the electrical characteristics, rain rate time series. In SST, the Taylor's hypothesis is used in order to translate the time series of rain rate to spatial domain and calculate the rain attenuation along the path. Therefore, the SST uses as input parameter the mean wind speed of the location in which time series are obtained. In [Matricciani96], for the vertical structure of rain rate, the two-layer model (shown in Figure 3.6) is taken into account [Matricciani91] for generating rain attenuation time series.

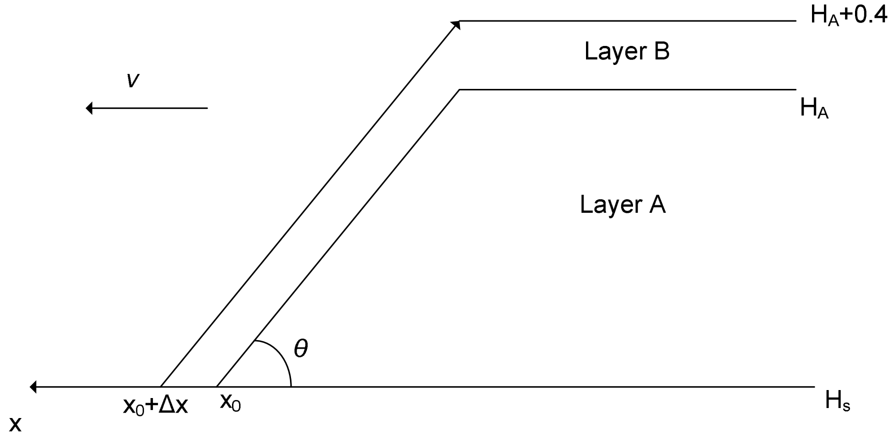

Figure 3.6. Vertical structure of rain rate in the two-layer model

3.1.4 Models Based on Data

In [Bertorelli08], a methodology for generating time series of rain attenuation based on rain attenuation events from large datasets with obtained measurements is presented. Given that the rain attenuation events have been extracted by a given database for a ground station and specific link, rain attenuation is generated through the appropriate scaling for another link with different climatic and/or electrical, geometrical characteristics. The first version of the model was developed with ITALSAT data in order to reproduce, fade duration, fade slope and the first-order statistics of rain attenuation.

The database used as input to the model needs to include only rain attenuation. Therefore, the effect of atmospheric gases must have been removed, while with rain gauges the true rain events can be derived. Firstly, according to the model the attenuation events of the databases are classified into 10 classes according to the attenuation peak. As noted in [Bertorelli08], it is important that each class contains a significant number of events. Then for each class the ccdf normalized to the total duration is calculated. The later are called “base functions”.

After the calculation of “base functions”, the unconditional ccdf of rain attenuation (“objective function”) is calculated by prediction models from literature. For the objective function, although the ccdf must take into account the climatology of the site in which time series are required through the ccdf of rain rate, the elevation angle, frequency, polarization and rain height must remain the same with these of the reference database. However, in case that for the site under investigation the rain attenuation ccdf is available but not time series, then the measured ccdf is scaled to this of the reference site for which time series database exists through the following scaling factor:

$$F=\frac{H_{r1}-h_1}{H_{r2}-h_2}\frac{\sin(\theta_2)}{\sin(\theta_1)}\left(\frac{f_1}{f_2}\right)^{1.72} \tag{3.34}$$

where H_r is the rain height, h the altitude amsl of station, θ elevation angle and f the operating frequency of links 1 and 2.

Now given that the objective function ($P(A)$) and the base functions ($P_j(A)$, $j=1,\ldots,10$) are known the weights (W_j) of each base function are needed such that:

$$P(A)=\sum_{j=1}^{10}W_jP_j(A) \tag{3.35}$$

Multiplying the weights with the total observation period, the duration of each class is calculated. Then, from the classes, a subset of the rain events is chosen in the manner that the duration of these events is the same with the one calculated from the weights. Finally, the time series of rain attenuation is scaled using (3.34).

3.1.5 Models based on conditional probabilities

In this category of synthesizers, the conditional probabilities of rain attenuation are used. More particularly, in [Carrie11], the assumptions of the EMB model presented in Section 2.1.1 are used in order to synthesize rain events on-demand for FMTs evaluation. The on-demand characterization of the synthesizer occurs due to the main input parameters of the model which are the max value of rain attenuation for the specific event, i.e. A_{max}, the duration of the event (D) and the time instance when the maximum occurs, i.e. D_{peak}. These parameters are needed in order to have the on-demand generation of rain attenuation for a rain event.

The methodology and framework of the ‘on-demand’ synthesizer relies on the M-B assumptions and the EMB model. From these latter models, the conditional probability of rain attenuation given the values of rain attenuation at a past time instance and a future time instance is needed. The latter conditional probability, assuming that rain attenuation is a first order Markov process is given by:

$$p(A(t)\,|\,A(t-\Delta t_1),A(t+\Delta t_2))=\frac{p(A(t+\Delta t_2)\,|\,A(t))\times p(A(t)\,|\,A(t-\Delta t_1))}{p(A(t+\Delta t_2)\,|\,A(t-\Delta t_1))} \tag{3.36}$$

Based on the MB model the transitional probability density funciton of rain attenuation follows a lognormal distribution with a PDF:

$$p(A(t+\Delta t)\,|\,A(t)) = \frac{1}{A(t+\Delta t)\sigma_{|A(t)}\sqrt{2\pi}}\exp\left(-\left[\frac{\ln\left(A(t+\Delta t)-m_{|A(t)}\right)}{\sigma_{|A(t)}\sqrt{2}}\right]^2\right)$$

(3.37)

with

$$\begin{aligned} m_{|A(t)}(\Delta(t)) &= m(1-\exp(-\beta\,|\,\Delta t\,|) + \ln(A(t))\exp(-\beta\,|\,\Delta t\,|) \\ \sigma^2_{|A(t)}(\Delta(t)) &= \sigma^2(1-\exp(-2\beta\,|\,\Delta t\,|) \end{aligned} \qquad (3.38)$$

Since the TPDF of rain attenuation is a lognormal distribution, it follows that (3.36) follows a lognormal distribution with parameters:

$$m_{\Delta t_1,\Delta t_2} = \left\{\begin{matrix} (1-\exp(-2\beta\Delta t_1))\times\exp(-2\beta\Delta t_2)\times\ln(A(t+\Delta t_2) \\ +(1-\exp(-2\beta\Delta t_2))\times\exp(-2\beta\Delta t_1)\times\ln(A(t-\Delta t_1) \\ +m\times(1-\exp(-2\beta\Delta t_1))\times(1-\exp(-2\beta\Delta t_2)) \\ \times(1-\exp(-2\beta(\Delta t_1+\Delta t_2))) \end{matrix}\right\} / \,(1-\exp(-2\beta(\Delta t_1+\Delta t_2)))$$

(3.39)

$$\sigma^2_{\Delta t_1,\Delta t_2} = \sigma^2\times\frac{(1-\exp(-2\beta\Delta t_1))\times(1-\exp(-2\beta\Delta t_2))}{1-\exp(-2\beta(\Delta t_1+\Delta t_2))} \qquad (3.40)$$

In order to take into account the offset parameter for the rain attenuation intermittency, the following expression is used:

$$P_{L-C}\left(A(t)\,|\,A(t-\Delta t_1),A(t+\Delta t_2)\right) = P\left(A(t)+A_{offset}\,|\,A(t-\Delta t_1)+A_{offset},A(t+\Delta t_2)+A_{offset}\right)$$

(3.41)

For the generation of rain attenuation events, the duration *D* of the rain event is needed, the maximum attenuation (A_{max}) and the temporal position D_{peak} of the maximum attenuation are needed. So, the algorithm starts with the initial values of attenuation [0, A_{max}, 0] :

- Add the A_{offset} to the initial values of attenuation
- The interpolation starts from the middle and at (3.39) and (3.40) use the value of A_{offset} at time t_0 and A_{max}+A_{offset} at time t_0+D_{peak}. If T_s is the sampling period of the desired time series then in (3.39) and (3.40) $\Delta t_1 = T_s$ and $\Delta t_2 = D_{peak} - T_s$
- Generate zero mean and unity variance Gaussian noise
- Transform exponentially using the log-normal parameters at (3.39) and (3.40)

Another model based on conditional probabilities is the ONERA-Van de Kamp two state model [Kamp03a]. The model is based on the use of conditional probability of rain attenuation given the knowledge of two previous samples of rain attenuation. The pdf of rain attenuation given the two previous samples is given by:

$$p(A \mid A_0, A_{-1}) = \frac{m_A}{2A\sigma_A} \sec h \left[\frac{\pi m_A \ln\left(A / m_A \right)}{2A\sigma_A} \right] \tag{3.42}$$

where m_A and σ_A are given by:

$$\begin{aligned} m_A &= A_0 \left(\frac{A_0}{A_{-1}} \right)^{a_2} \\ \sigma_A &= A_0 \sqrt{\beta_2 \delta t} + A_0 \gamma_2 \left(1 - e^{-\left| \ln\left(\frac{A_0}{A_{-1}} \right) \right|} \right) \end{aligned} \tag{3.43}$$

The values of the above parameters have been extracted from measurements [Kamp03a).

The generation of rain attenuation time series occurs from the conditional pdf of rain attenuation and in [Kamp03a], it is recommended that the synthesizer be used for generation of separate events. In case that a specific maximum attenuation is needed, then the time series are scaled with a multiplication factor such that the peak of the event is equal to the desired value.

3.1.6 Markov Chain Models

Markov chains have been used for the generation of rain attenuation time series. In [Drougas08], a verification of the first-order Markovian property of rain attenuation is presented. The first model presented here is the N-state Markov ONERA model [Castanet03]. This model is used to generate either event-on-demand or long time series. The method contains three parts. The first one is the "macroscopic model" and it is a Markov chain with two states of rain and no rain. As explained in [Castanet03], two probabilities are needed: the probability to rain (p_1) and the probability of transition from state of rain to the state of no rain (p_{10}). The other probabilities of the transition matrix of the two-state Markov chain can be found through:

$$p_{01} = \frac{p_1}{1 - p_1} p_{10} \tag{3.44}$$

where p_{01} is the probability from state of no rain to state of rain. The probability of no rain is equal to 1-p_{01}. The probability from rain state to no rain state can be obtained through fade duration models, as explained in [Castanet03].

The second part of the model is the microscopic model in which propagation events are generated. Firstly, a maximum rain attenuation is assumed, i.e. A_{max}=X, with X an integer and a minimum value of rain attenuation of 0 dB. The interval between minimum and maximum rain attenuation is discretized into the number of the states of the Markov Chain:

$$N = \frac{A_{\max} - A_{\min}}{da} + 1 \tag{3.45}$$

with da the distance in dBs between the two states of attenuation. So the following transition matrix has to be defined and its elements to be calculated:

$$P = \begin{bmatrix} p_{11} & p_{12} & \cdots & & p_{1N} \\ p_{21} & \ddots & & & \vdots \\ \vdots & & p_{ij} & & \\ & & & \ddots & p_{N-1N} \\ p_{N1} & & & p_{NN-1} & p_{NN} \end{bmatrix} \tag{3.46}$$

where p_{ij} is the probability of transition from state i to state j. The computation of transition probabilities is based on the fade slope (ζ) statistics. Therefore, given a time series resolution of δt, it holds that:

$$p_{ij} = p\left(s\left(t+\delta t\right) = s_j \mid s\left(t\right) = s_i\right) = p\left(\zeta = \frac{s_j - s_i}{\delta t} \mid s(t) = s_i\right) \tag{3.47}$$

So:

- To stay in the same state, it must hold: $|\zeta \delta t| < \frac{\delta a}{2}$
- To go from state i to state i±k: $|\zeta \delta t| < \frac{\delta a}{2} \pm k\delta a$

From (56) and the rules above, it holds that:

$$p_{i,i\pm k} = \int_{k\delta\alpha - \frac{\delta\alpha}{2}}^{k\delta\alpha + \frac{\delta\alpha}{2}} p(\zeta \mid A_i)\, d\zeta \tag{3.48}$$

where $p(\zeta | A_i)$ is the pdf of fade slope. The fade slope statistics can be derived from the ITU-R P. Recommendations [ITU-R. P. 1623].

Another model based on Markov chains is the DLR channel model [Fiebig02]. DLR channel model or second-order Markov chain model is described in [Fiebig02] in which it is assumed that rain attenuation is a 2nd order Markov process. The model can be discrete-valued or continuous-time valued. In this model the attenuation values are quantized and the value of rain attenuation at time t depends on the segment of the previous tow samples, i.e. constant segment the previous two values are equal, up-segment the rain attenuation is increasing and down-segment rain attenuation is decreasing. For every segment a Gaussian PDF is formulated from which the new value is derived.

Therefore, although a 2nd order Markov chain is described by the N^3 transition probabilities, using the segmentation and the fact that the Transition probabilities can be described by a Gaussian distribution, the states are characterized by 3N transition probabilities. Now depending on whether rain attenuation increased, decreased or remained equal on the previous two samples, three different Gaussian distributions are used for the description of the transition probabilities at the final state.

3.2 Clouds Attenuation Time Series

Although, at frequencies close to 20GHz, rain attenuation is the dominant fading mechanism, clouds also affect the signal and the attenuation caused by clouds is increasing as the operating frequency gets higher and higher. One synthesizer for generating time series of clouds attenuation is the one proposed in [ITU-R. P.1853]. More particularly, the synthesizer generates time series of Integrated Liquid Water Content (ILWC) which then are transformed to clouds attenuation time series using the methodology proposed in [ITU-R. P. 840].

The main assumption of the synthesizer is that the exceedance probability of ILWC (*L*) is given by:

$$P(L \geq L_{th}) = P\left(L > 0\right) \cdot P(L \geq L_{th} \mid L > 0) \tag{3.49}$$

The probability that ILWC exceeds the 0mm value is taken from ITU-R. P.840. Moreover, the conditional probability $P(L \geq L_{th} \mid L > 0)$ is considered to follow the lognormal distribution [Jeannin08] with statistical parameters *m, s* again derived from the database ITU-R. P.840. The methodology for generating ILWC time series is similar to the one proposed by [Boulanger13] for rain attenuation.

Firstly, a Gaussian white noise *n*(*t*) is generated and then the following Gaussian stochastic processes are calculated at the time instants kT_s for T_s the sampling period:

$$\begin{aligned} X_1(kT_S) &= \rho_1 X_1(\left(k-1\right)T_S) + \sqrt{1-\rho_1^2}\, n\left(kT_S\right) \\ X_2(kT_S) &= \rho_2 X_2(\left(k-1\right)T_S) + \sqrt{1-\rho_2^2}\, n\left(kT_S\right) \end{aligned} \tag{3.50}$$

with

$$\rho_i = \exp(-\beta_i T_S), i = 1,2 \tag{3.51}$$

Then the following Gaussian time series are calculated:

$$G_C\left(kT_S\right) = \gamma_1 X_1(kT_S) + \gamma_2 X_2(kT_S) \tag{3.52}$$

i.e. the weighted sum of the processes X_1 and X_2. Since ILWC follow a conditional distribution, a truncation threshold is calculated:

$$a = Q^{-1}(P(L > 0)) \tag{3.53}$$

where *Q* is the Gaussian exceedance probability. The time series of ILWC are generated through:

$$L(t) = \exp\left(erfc^{-1}\left(erfc\left(\frac{G_C(t)}{\sqrt{2}} \right) / \left(P\left(L > 0\right)/100\right) \right) \cdot \sqrt{2} \cdot s + m \right) \quad for \quad G(t) > a$$

$$L(t) = 0 \quad for \quad G(t) \le a \tag{3.54}$$

The synthesizer as aforementioned generates ILWC time series assuming lognormal distribution for the conditional probability. Considering a ground station in Athens, Greece, the theoretical CCDF, as well as the CCDF resulted from time series are shown in Figure 3.7a . The time series of ILWC are derived and shown in Figure 3.7b. Moreover, the underlined Gaussian processes are considered to have an exponentially decaying with time autocorrelation function. Therefore, the autocorrelation function of the underlined Gaussian process of ILWC is given by (Boulanger et al., 2011) :

$$R_{G_C}(\tau) = A\exp(-\beta_1\tau) + (1 - A)\exp(-\beta_2\tau) \tag{3.55}$$

It must be noted that in ITU-R. P. 1853 the noise used for the filtering methods of rain attenuation and ILWC time series is the same, thus introducing a correlation for the two phenomena.

As aforementioned from the ILWC time series the clouds attenuation time series can be derived from the Recommendation of ITU-R. P. 840. In Figure 3.7b,c a snapshot of ILWC time series are shown for Athens, Greece and the clouds attenuation time series for an operating frequency of 40 GHz and elevation angle of 30^{o}.

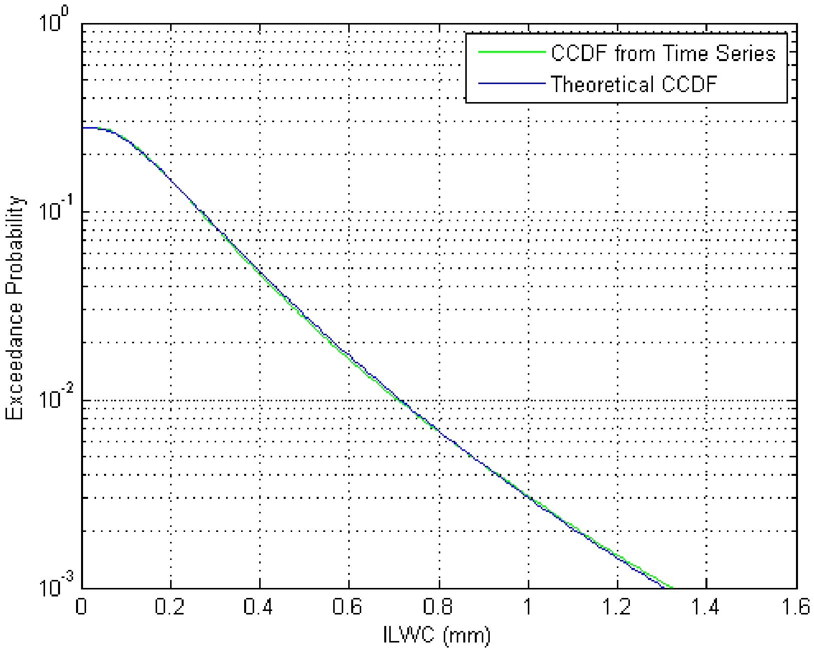
CCDF from Time Series
Theoretical CCDF
Exceedance Probability
10^0
10^-1
10^-2
10^-3
0
0.2
0.4
0.6
0.8
1
1.2
1.4
1.6
ILWC (mm)

(a)

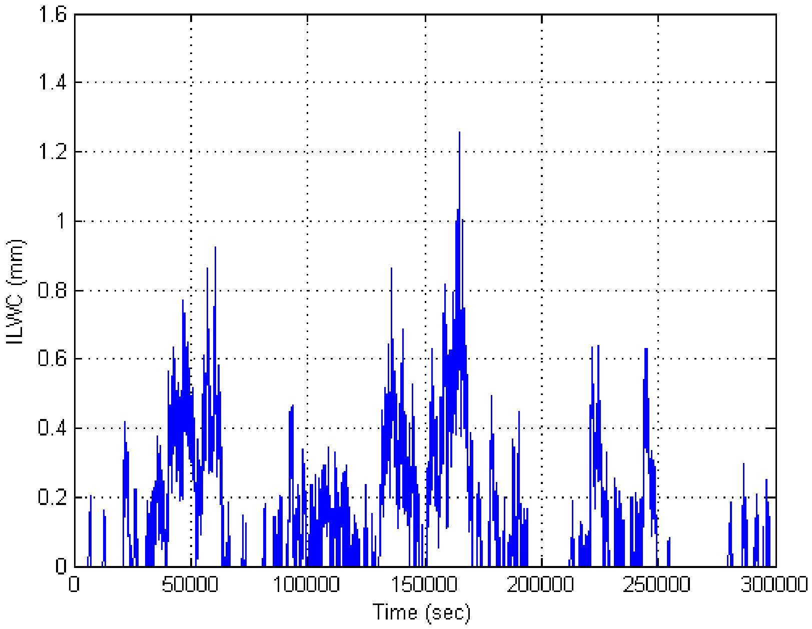
ILWC (mm)
1.6
1.4
1.2
1
0.8
0.6
0.4
0.2
0
0
50000
100000
150000
200000
250000
300000
Time (sec)

(b)

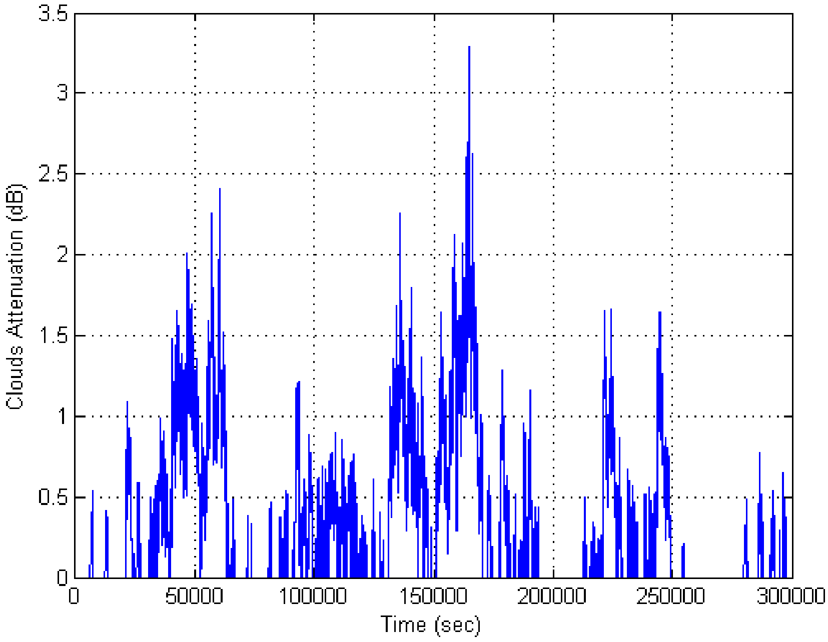

(c)

Figure 3.7. (a)CCDF of ILWC for Athens from Time series and theoretical, (b) Snapshot of ILWC time series, (c) Snapshot of clouds attenuation

Moreover, in [Boulanger11], a simpler synthesizer has been proposed in order to have a unified synthesizer for clouds and rain attenuation. The approach is motivated by the fact that the separation of rain attenuation in the presence of clouds from clouds attenuation is difficult and therefore a synthesizer which generates rain plus clouds attenuation is required. Therefore, time series of rain plus clouds attenuation are modeled. The first order statistics are conditional with the conditioned PDF following a lognormal distribution:

$$P(A_{R+C} \geq A_{th}) = P\left(A_{R+C} > 0\right) \cdot \frac{1}{2} erfc\left(\frac{\ln\left(A_{th}\right) - m_{R,C}}{\sqrt{2} s_{R,C}}\right) \tag{3.56}$$

Then starting from Gaussian noise again two parallel low pass filters are used and then their output is summed in order to obtain a Gaussian process with autocorrelation function a decaying double-exponential function, similarly with the ILWC time series generator methodology.

Another methodology for generating ILWC time series has been presented in [Resteghini14]. The methodology is based on the ILWC time series derived from databases. The ILWC daily time series are classified into frames of 24 hours and then into classes based on the maximum value of ILWC for every day. The methodology can be extended to sites without any measurements through objective function and using the following scaling factor:

$$SF_L = \frac{P(L)_{OBF}(p)}{P(L)_{DB}(p)} \tag{3.57}$$

where $P(L)_{OBF}(p)$ is the CCDF of ILWC derived, e.g. ITU-R. P. 840, for a desired site and $P(L)_{DB}(p)$ the CCDF from the database for a probability level $p\%$, e.g. 0.1%. The scaling factor is then applied to the time series of the database. Now using, the time series of every class a base function is calculated as the CCDF of ILWC for every class. Every base function has a weight such that their sum gives the CCDF for the desired site and this weight multiplied by the observation period (in number of days) will give the number of days a certain class has been observed in the database. For the generation of time series of ILWC, since there is a seasonal variation, the database is classified into months and the time series of this month are ordered randomly.

In [Resteghini14], an algorithm is introduced for the classification of the cloud type according to the vertical extent of the cloud and for every cloud type the probability to rain is derived from database. Therefore, a dependence between ILWC and rain attenuation is introduced and can be used for the generation of ILWC and rain attenuation time series.

3.3 Time Series of Attenuation due to Atmospheric Gases

A synthesizer proposed for atmospheric gases is presented in [Boulanger11] and ITU-R. P. 1853-1. According to the methodology, it is assumed that oxygen attenuation is constant. Considering the attenuation due to water vapour, firstly time series of Integrated Water Vapour Content (IWVC) are generated and then through the use of the simplified method of the calculation of water vapor attenuation, the attenuation time series are obtained. For IWVC it is assumed that it is always present and that it follows the Weibull distribution [Jeannin08]:

$$P\left(IWVC \geq IWVC_{th}\right) = \exp\left(-\left(\frac{IWVC_{th}}{\lambda}\right)^{\kappa}\right) \tag{3.58}$$

As in the other time series generators of ITU-R. P. 1853, an underlined Gaussian process is assumed which follows a decaying exponential autocorrelation function. After the generation through low-pass filtering of the later Gaussian process a non-linear device is used for obtaining the Weibull distribution of IWVC.

The block diagram for generating IWVC time series is shown in Figure 3.8. The last non-linear device is actually transforming the Gaussian time series to time series which follow the Weibull distribution.

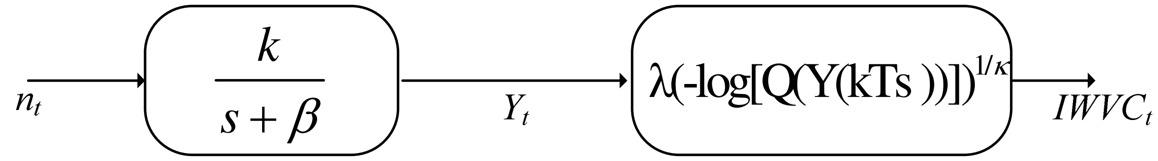

Figure 3.8. Block diagram of generating IWVC time series

The correlation between ILWC, rain and IWVC time series in ITU-R. P. 1853-1 is taken into account through the Gaussian noise used as input. More particularly, for clouds and rain the same noise is used while for IWVC, the covariance between the input noise of IWLC and IWVC is equal to 0.8. Therefore, through the correlation on the input noise, a correlation is introduced in the IWVC time series. From the IWVC time series the simplified model given in [ITU-R. P. 676] is used for generating time series of attenuation due to water vapor.

Similarly with ILWC time series, the IWVC time series are generated using the methodology based on database [Resteghini14]. In the latter reference, a method is proposed for generating IWVC time series for different sites using a single database, as very briefly explained in the previous section. However, in [Resteghini14], since the IWVC and ILWC are classified into different classes, then the probability of simultaneous occurrence of the various classes between IWVC and ILWC is computed. Then a joint optimization procedure is used in order to have the weights of the joint base functions and preserve the number of the days when each joint class is observed equal to this given by the database. Then through random ordering based on seasonal variation the joint time series of IWVC and ILWC are generated.

3.4 Scintillation Time Series

Turbulent eddies that are shaped into the troposphere cause the scintillation of the amplitude of the signal. Although, the effect is not so severe in terms of fades as in rain attenuation, ARQ schemes and dynamic FMTs have been identified for the compensation of scintillation.

Therefore, time series of scintillation have been studied in the literature. More particularly, four synthesizers have been developed in literature, two filtering methods have been identified [ITU-R. P.1853], [Kassianides03], one using the fractional Brownian Motion [Celadroni99] while a synthesizer has been developed for LEO slant paths [Liu12].

The first filtering method proposed in [ITU-R. P.1853], for the generation of time series of scintillation is based on low-pass filtering of Gaussian zero mean and unity variance noise. The low pass filter has a decreasing slope of -80/3 dB/decade which is also the decreasing slope of the power spectrum of scintillation at high frequencies. The resulted time series are following Gaussian distribution with zero mean and unity variance and the power spectrum has the same shape of the low pass filter. The cut-off frequency of the filter is considered equal to 0.1 Hz. For the long-term statistics, the time series are multiplied by the variance of scintillation which as it will be analyzed later depends on the kind of scintillation, i.e. wet and dry.

In the second filtering method [Kassianides03], the Gaussian noise passes through a low-pass filter and then through a non-linear memory-less device as shown in Figure 3.9. The low pass filter gives the appropriate shape at the power spectrum of scintillation, i.e. low pass with a -80/3 roll-off factor and the non-linear device the appropriate shape at the pdf of the generated time series. The low-pass filter has a characteristic function given in

(3.59). The y(t) signal at Figure 3.9 is determined by the x(t) signal through the expression in (3.60). The parameters of (3.60) are determined in [Kassianides03].

$$T(z)=\frac{0.1810+0.0791z^{-1}+0.0371z^{-2}}{1-0.4574z^{-1}+0.1990z^{-2}} \tag{3.59}$$

$$y(t)=a_1x(t)+a_3x^3(t)+a_5x^5(t)-a_6x^6(t)+a_7x^7(t) \tag{3.60}$$

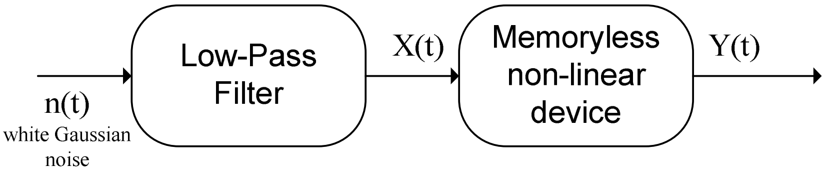

Figure 3.9. Block diagram of scintillation time series synthesizer

In [Celadroni99], the fractional Brownian motion is proposed for the modeling of scintillation time series. According to the analysis on the physical characterization of scintillation, a difference process is defined $W(t_1, t_2)=A(t_2)- A(t_1)$, with A the attenuation values and for sufficient small $t=t_2-t_1$, is the difference process of scintillation. This difference process is assumed to be a function of rain attenuation, since scintillation variance depends on scintillation. It is stated in [Celadroni99] that the process $W(t,A)$ is assumed to be normal with zero mean and variance of σ_W^2 which is also validated through chi-square tests. Therefore, scintillation is modeled as a fBm process with variance:

$$\sigma_W^2 = Vt^{2H} \tag{3.61}$$

with H (the Hurst parameter) and V depending on the rain attenuation values. For the spectrum analysis, the power spectrum indicated in [Karasawa91] is assumed, which gives that in log-log scale the power spectrum of scintillation follows a f^{1}slope followed by $f^{8/3}$. The corner frequency (f_c) is found to depend on the Hurst index and so to rain attenuation. The dependence of hurst index to corner frequency is: H=0.83-1.7f_c.

In [Liu12], a synthesizer based on low-pass filters with time varying parameters for generating scintillation time series for different LEO satellite passes is proposed. In the proposed model, the spectrum of scintillation time series is the one proposed by Tatarskii, i.e. constant at low frequencies and a slope of -80/3 dB^2/Hz for high frequency components, as already described in this chapter. However, in [Liu12], the corner frequency of the power spectrum is considered time dependent since it depends on the turbulent layer height and the satellite velocity, for a constant operating frequency. More particularly, the corner frequency (f_c) is equal to 1.43f_0, where:

$$f_0=\frac{\upsilon_t}{\sqrt{2\pi\lambda z}} \tag{3.62}$$

where υ_t is the transverse velocity perpendicular to Earth-space path, λ the wavelength and z the length of the slant path between the Earth station and the turbulent layer. The height of the turbulent layer is considered to be Rician-distributed and its thickness lognormally distributed [Vasseur98]. The short-term log-amplitude of the signal is considered as

Gaussian random variable with zero mean and the standard deviation of scintillation on the long-term as lognormally distributed or Gamma distributed. The wet and dry scintillation is considered through the correlation of the standard deviation of scintillation with rain attenuation, as will explained later on this subsection. For the generation of the short-term scintillation, time varying parameters are used in low-pass filter. The low-pass filter is of fourth order and uses as input white Gaussian noise. However, its parameters are calculated for every sample.

One factor that has been studied in literature is the correlation between rain and scintillation, or the wet (in presence of rain) and dry scintillation. In [Matricciani08], it was found that in presence of rain, the standard deviation of scintillation is equal to:

$$\sigma_{\chi} = CA^{5/12} \tag{3.63}$$

when rain attenuation (A) is greater than 1 dB. However, in [ITU-R. P. 1853], the scintillation is modeled considering not only dependence to rain attenuation but also to clouds and water vapor.

3.5 Total Tropospheric Attenuation Time Series Generation

Two main methodologies have been developed for generating time series of tropospheric attenuation. One is based on ITU-R. P. 1853-1 methodology and the other is proposed in [Resteghini14].

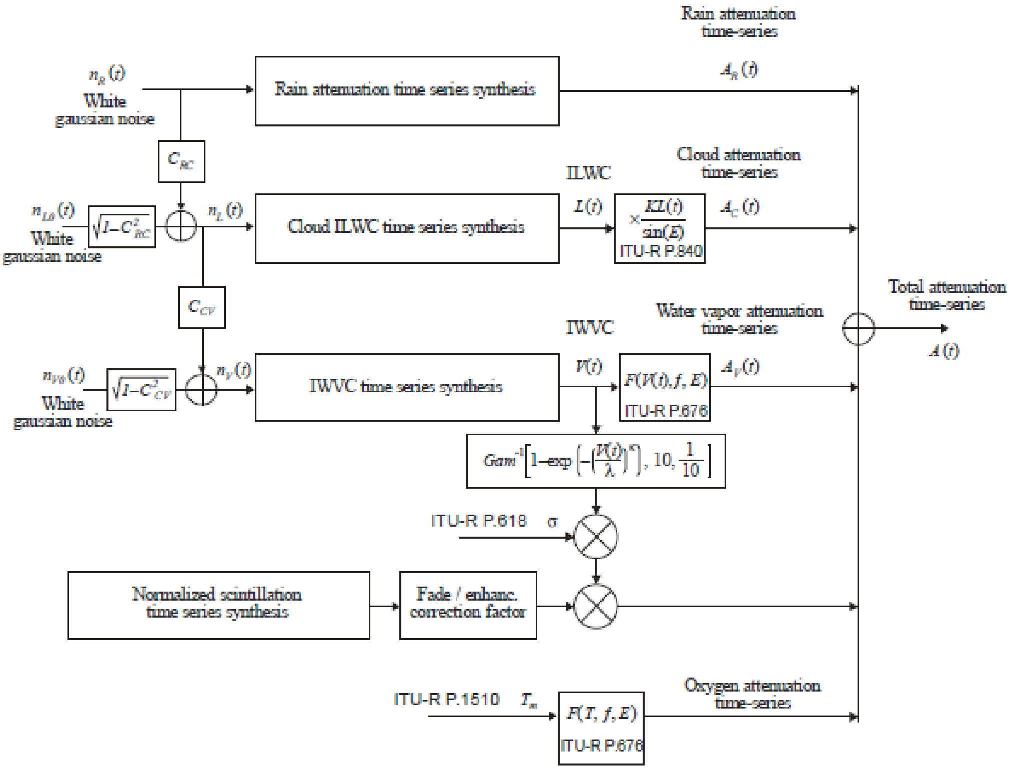

(a)

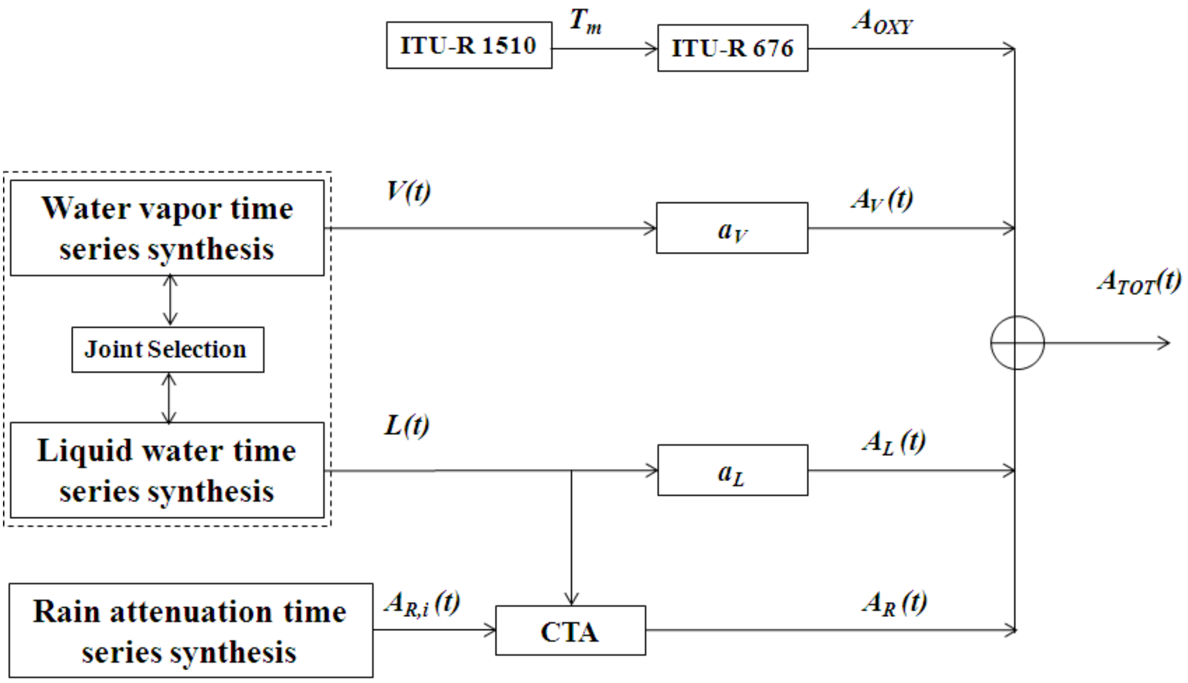

(b)

Figure 3.10. Block diagram for generating total tropospheric attenuation time series a) ITU-R. P. 1853 and b) Resteghini method derived from (ITU-R. P. 1853, 2012) and (Resteghini, 2014), respectively.

Starting from ITU-R. P. 1853-1, the block diagram is shown in Figure 3.10, a directly derived from the Recommendation. In the previous subsections, the generators for every attenuation factor and their interdependencies have been explained. The recommended synthesizer adds the time series of all the effects in order to calculate the time series of total attenuation, as:

$$A(t) = A_R(t) + A_C(t) + A_V(t) + Sci(t) + A_O \tag{3.64}$$

where A_R, A_C, A_V, Sci and A_O are the rain attenuation, clouds attenuation, water vapor attenuation, scintillation and oxygen attenuation time series. The oxygen attenuation is considered constant.

The second synthesizer proposed in [Resteghini14] is based on the generation of time series from database including the appropriate scaling to take into account the difference in the geometric and electrical characteristics of the link. Although, the synthesizers of each attenuation factor for this specific synthesizer have been briefly presented in previous sections, the generation of total tropospheric attenuation time series is based on the block diagram of Figure 14b. Firstly, since the variations of the oxygen attenuation are very slow, attenuation due to oxygen is considered constant. Then as briefly explained in section 4, time series of ILWC and IWVC are derived, after the appropriate scaling, jointly from the input database in order to have correlated/dependent ILWC and

IWVC time series. Using ITU-R. P. 840 and ITU-R. 676, clouds attenuation and attenuation due to water vapor is calculated for every sample of ILWC and IWVC time series, respectively.

Moreover, using the cloud type algorithm (CTA) in [Resteghini14], the cloud types, associated with the ILWC time series, with the higher probability to rain are identified. Then, identifying the clouds intervals, i.e. time period in which ILWC is greater than zero, a rainy mask is considered equal to the 50% of the clouds interval during which is considered that is raining, giving priority of presence of rain to the cloud types with the highest probability to rain. Then in the rain mask a rain attenuation event is superimposed with equal length. In this way, the rain attenuation and clouds attenuation are presented inter-dependent.

4 Long Term Outage Prediction Modeling of Wireless Systems Operating above 10 GHz

In this Chapter, firstly, the Inverse Gaussian (IG) distribution ([Al-Hussaini81], [Chikkara89], [Seshardi93]) is investigated for the modeling of long-term first order statistics (Probability Density Function – PDF, Complementary Cumulative Distribution Function – CCDF) of rain rate and slant paths and terrestrial links rain attenuation. Then two novel methods are proposed for predicting rain attenuation exceedance probability, one for terrestrial links and one for slant path links, based on the assumption that both rain rate and rain attenuation follow the IG distribution.

The IG distribution has been previously reported for the description of shadowing phenomena [Chatzidiamantis11a] and turbulence-induced phenomena in free-space optical systems operating in weak turbulence conditions [Chatzidiamantis11b]. Also, in [Kedem90], the IG distribution is used for modeling the conditional distribution of rain rate for meteorological applications, due to the fact that IG distribution is a skewed distribution. For the above reasons we have been motivated to use the IG distribution for the prediction and modeling of single and joint exceedance of rain rate and rain attenuation statistics.

Moreover, in this Chapter the validity of modeling joint statistics of rain attenuation for time diversity and site diversity system using Copulas theory is examined showing that the Copulas function can be used for capturing first order joint statistics of rain attenuation on temporal and spatial domain. Finally, for time diversity systems the joint statistics of rain attenuation are modeled using the solution of Fokker-Planck partial differential equation for the Transitional Probability Density Function of rain attenuation.

In the first Section of the Chapter, the IG distribution is examined for capturing the exceedance probability of rain rate and slant path and terrestrial links induced rain attenuation. This Section is based on the papers of [C1], [C2]. In Section 3.2, a methodology of predicting rain attenuation first order statistics is proposed based on the assumption that both rain attenuation and rain rate follow IG distribution [J1], [J2]. In 3.3, a model for predicting joint statistics of rain attenuation on spatially separated parallel links is proposed based on [J3], [C3] and in 3.4 for converging terrestrial paths as well as the modeling of outage probability for Selection Combining and Maximal Ration Combining systems [J4], [C4]. In 3.5, copulas theory is examined for modeling joint statistics of rain rate and rain attenuation on spatial domain, results presented in [C5]. Finally, in 3.6, on the one hand, a model for predicting joint exceedance probability of rain attenuation for time diversity based on Maseng-Bakken assumptions is proposed [J5], [C6] and on the other hand, copulas are testing for capturing first order statistics of rain attenuation on temporally domain separated links [C7].

[J1] C. Kourogiorgas, A. D. Panagopoulos, J. D. Kanellopoulos, "*An Engineering Method for the Prediction of Outage Probability of LOS Terrestrial Links Operating above 10 GHz*", IEEE Antennas and Wireless Propagation Letters, vol. 12, pp. 516-519, 2013.

[J2] C. Kourogiorgas, A. D Panagopoulos, "*A Physical-Mathematical Model for Predicting Slant Path Rain Attenuation Statistics*", IET Microwave, Antennas and Propagation, vol. 7, no. 12, pp. 970-975, 2013.

[J3] C. Kourogiorgas, A. D. Panagopoulos, J. D. Kanellopoulos, "*On the Earth-space Site Diversity Modeling: A novel physical mathematical model*", IEEE Transactions on Antennas and Propagation, vol. 60, no. 9, pp. 4391-4397, November 2011

[J4] C. I. Kourogiorgas, A. D. Panagopoulos, "*Outage Performance of Dual Branch Diversity Techniques in Broadband Fixed Wireless Access Networks*", IET Communications, vol. 8, no. 9, pp. 1648-1653, June 2014.

[J5] C. Kourogiorgas, A. D. Panagopoulos, et al, , "*On the Outage Probability Prediction of Time Diversity Scheme in Broadband Satellite Communication Systems*", Progress In Electromagnetics Research C, vol. 44, pp. 175-184, 2013

[C1] C. Kourogiorgas, A. D. Panagopoulos, G. K. Karagiannidis, J. D. Kanellopoulos, "On the modeling of rain rate and of slant path and terrestrial links rain attenuation with Inverse Gaussian distribution", MCM6 COST Action IC0802, 28-30 September 2011, Prague, Czech Republic.

[C2] C. Kourogiorgas, A. D. Panagopoulos, G. K. Karagiannidis, J. D. Kanellopoulos, "*On the Inverse Gaussian Modeling of Rain Rate and Slant Path and Terrestrial Links Rain Attenuations*", EuCAP 2012, 26–30 March, Prague, Czech Republic.

[C3] C. Kourogiorgas, A. D. Panagopoulos, J. D. Kanellopoulos, "Site Diversity Performance Using Two-Dimensional Inverse Gaussian Distribution", ESA Workshop on Radiowave Propagation 2011, 30 November–2 December, Noordwijk, Netherlands.

[C4] C. Kourogiorgas, A. D. Panagopoulos, "*On the Route Diversity Improvement Modeling for Broadband Radio Access Networks*", EuCAP 2013, 8-12 April 2013, Gothenburg, Sweden.

[C5] C. Kourogiorgas, S. N. Livieratos, A. D. Panagopoulos, G. E. Chatzarakis, "*Modeling of Joint Rainfall Rate and Rain Attenuation Statistics Using Archimedean Copula Functions*", EuCAP 2014, 6-11 April 2014, The Hague, The Netherlands.

[C6] C. Kourogiorgas, A. D. Panagopoulos, et al., "*Modeling of Joint Rain Attenuation for Time Diversity Satellite Communication Systems*", 2013 Joint Conference: 19th Ka and Broadband Communications, Navigation and Earth Observation Conference and 31st AIAA ICSSC, 14-17 October 2013, Florence, Italy.

[C7] C. Kourogiorgas, A. D. Panagopoulos, S. N. Livieratos, G. E. Chatzarakis, "*Time Diversity Prediction Modeling Using Copula Functions for Satellite Communication Systems Operating Above 10 GHz*", 2014 XXXIth URSI General Assembly and Scientific Symposium, 16-23 August 2014, Beijing, China

4.1 Modeling of Rain Rate and Terrestrial Link and Slant Path Rain Attenuation with the Inverse Gaussian Distribution

The first study undertaken considering the modeling of the long term statistics of rain attenuation is the suitability of the IG distribution to model the CCDF of rain rate, the CCDF of terrestrial link and slant path rain attenuation.

4.1.1 Modeling of Rain Rate

It is assumed that the CCDF of rain rate, i.e. the probability that rain rate (R) is greater than a threshold value (R_{th}) can be written as:

$$P\left[R \geq R_{th}\right] = P_o P\left[R \geq R_{th} / R > 0\right] \tag{4.1}$$

The P_o value is the probability of rain or else the probability that rain rate is higher than 0 mm/h and can be calculated by the recommendation of ITU-R. P. 837-6 [ITU-R.P.837]. Moreover, for this study we make the further assumption that the conditional CCDF of rain rate is given by the CCDF of IG distribution (Appendix A):

$$P\left[R \geq R_{th} / R > 0\right] = 1 - Q\left(\sqrt{\frac{\lambda_R}{R_{th}}}\left(1 - \frac{R_{th}}{\mu_R}\right)\right) - e^{2\frac{\lambda_R}{\mu_R}} Q\left(\sqrt{\frac{\lambda_R}{R_{th}}}\left(1 + \frac{R_{th}}{\mu_R}\right)\right) \tag{4.2}$$

where λ_R and μ_R are the two statistical parameters of IG distribution, are referred to the stochastic process of rain rate and they are both positive and Q(.) is the Gaussian Q-function (CCDF of zero mean variance 1 normally distributed random variable).

In order to evaluate the performance of the modeling of CCDF of rain rate with the IG distribution, experimental data derived from the database of study group 3 of ITU [DBSG3] have been used as well as the predicted CCDF of rain rate by the recommendation ITU-R. P. 837-6. The predicted and experimental data are used for the fitting of the theoretical IG distribution given in (4.1) and (4.2). Moreover, the accuracy of the modeling of the CCDF of rain rate with lognormal distribution is examined.

In Figure 4.1, Figure 4.2, Figure 4.3 and Figure 4.4, the CCDFs of rain rate for four different places (Prague, Czech Republic, Tokyo, Japan, Athens, Greece and Rio de Janeiro, Brazil) are shown, respectively. In these figures, the IG CCDF and the lognormal CCDF were fitted to the predicted exceedance probability of rain rate from ITU-R. P. 837-6. As it can be observed by these figures, the IG distribution has a better performance than lognormal distribution especially for the low time percentages. Moreover, it must be remarked that the IG distribution can model the first order statistics of rain rate not only for temperate regions such as Prague and Athens but also heavy rain climatic regions, Tokyo and tropical regions, Rio de Janeiro.

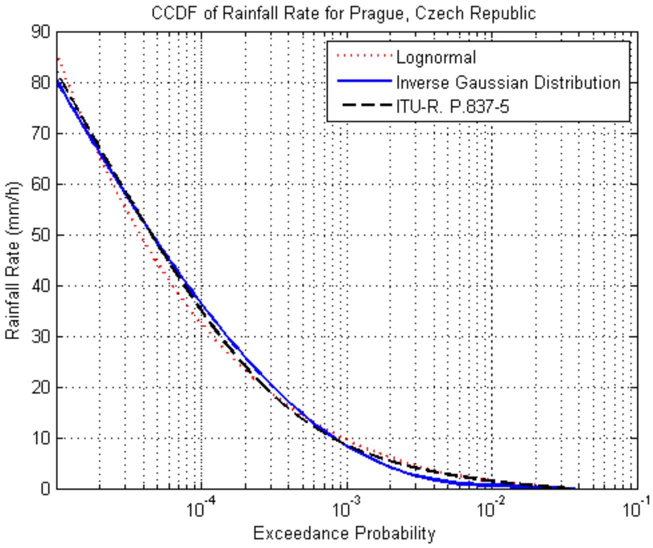

Figure 4.1. CCDF of Rain Rate for Prague, Czech republic

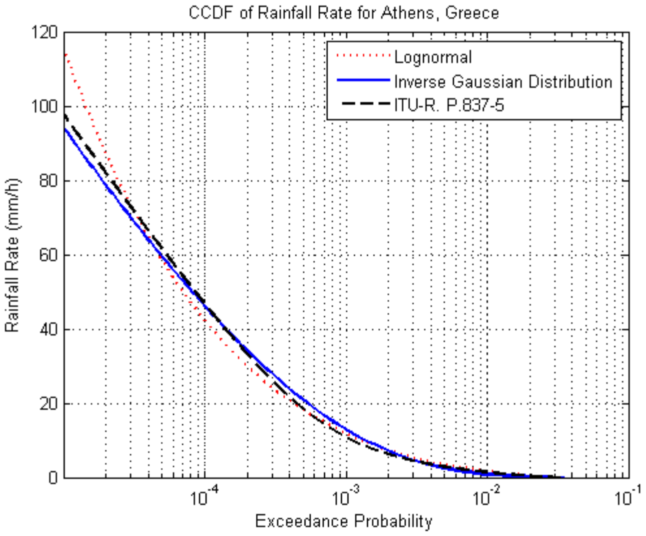

Figure 4.2. CCDF of Rain Rate for Athens, Greece

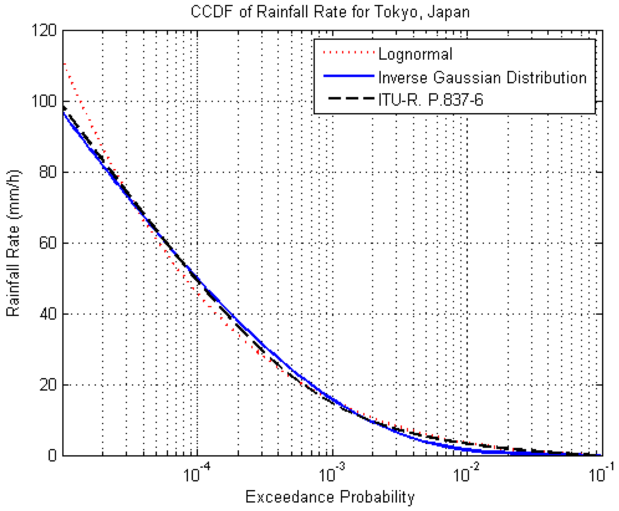

Figure 4.3. CCDF of Rain Rate for Tokyo, Japan

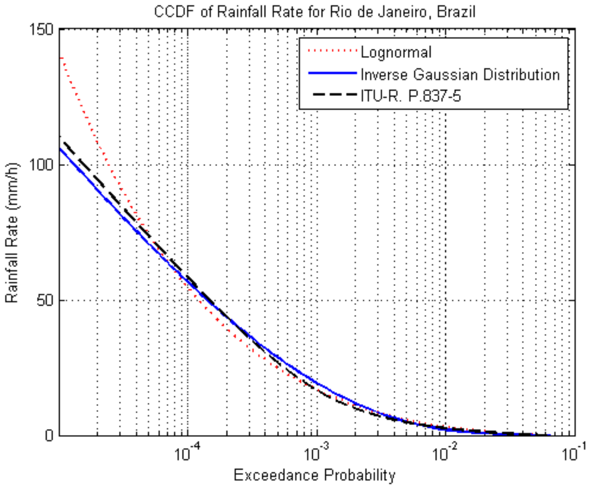

Figure 4.4. CCDF of Rain Rate for Rio de Janeiro, Brazil

In Figure 4.5 and Figure 4.6, the IG distribution is tested against measured CCDF of rain rate derived from DBSG3 database for two sites, in Austin of U.S. and Yamaguchi of Japan, respectively. In these two figures it is clearer that the IG distribution captures better the CCDF of rain rate for low probabilities (Figure 4.5) and is accurate for the temperate region of Austin, U.S. and for a heavy rain climatic region, Yamaguchi, Japan.

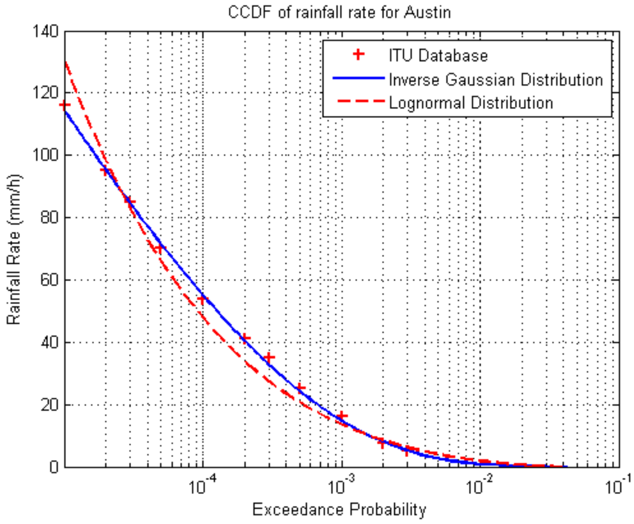

Figure 4.5. CCDF of Rain Rate for Austin, U.S.

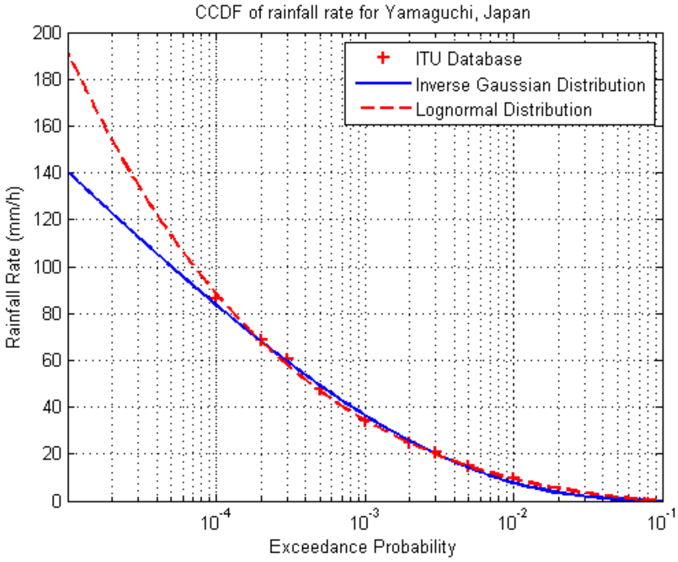

Figure 4.6. CCDF of Rain Rate for Yamguchi, Japan

4.1.2 Modeling of Slant Path and Terrestrial Link Rain Attenuation

Rain attenuation, as already mentioned, is the most dominant fading mechanism for operating frequency above 10 GHz. Therefore, the modeling of the exceedance probability of rain attenuation is of paramount importance. As in Modeling of Rain Rate, we assume that the exceedance probability of rain attenuation is equal to the probability that rain attenuation along the path is greater than zero dB multiplied by the conditional CCDF of rain attenuation:

$$P\left[A \geq A_{th}\right] = P[\mathrm{A} > 0] \cdot P\left[A \geq A_{th} / A > 0\right] \tag{4.3}$$

Since there is no accurate modeling of the probability that rain attenuation is greater than zero dB, we make the further assumption that $P[\mathrm{A} > 0]$ is equal to the probability to rain (P_o). The latter is derived from [ITU-R.P.837]. Furthermore for the evaluation of the IG distribution, it is supposed that:

$$P\left[A \geq A_{th} / A > 0\right] = 1 - Q\left(\sqrt{\frac{\lambda_A}{A_{th}}}\left(1 - \frac{A_{th}}{\mu_A}\right)\right) - e^{2\frac{\lambda_A}{\mu_A}} Q\left(\sqrt{\frac{\lambda_A}{A_{th}}}\left(1 + \frac{A_{th}}{\mu_A}\right)\right) \quad (4.4)$$

with λ_A and μ_A the statistical parameter of rain attenuation.

4.1.2.1 Slant Path Rain Attenuation

In this subsection, the IG distribution is evaluated with slant path rain attenuation statistics derived from experimental data of [DBSG3] database for Earth space links. As in the case of rain rate the theoretical exceedance probability of rain attenuation given in (4.3) and (4.4) is fitted to the measured statistics of rain attenuation.

In Figure 4.7 the CCDF of rain attenuation for Clarksburg of US (Latitude: 45.4°, Longitude: 9.5°) is given as this is derived from DBSG3 database. The frequency of the link is 28.6 GHz and the elevation angle 41°. Another fitting example is shown in Figure 4.8 for an Earth-space link with the Earth station located at Spino d'Adda (Latitude: 39.2°, Longitude: 282.7°) of Italy, with a frequency of the link 11.6 GHz and the elevation angle 32°. Both sites refer to mid-latitude regions and can be seen that the IG distribution can model accurately the first order statistics of rain attenuation.

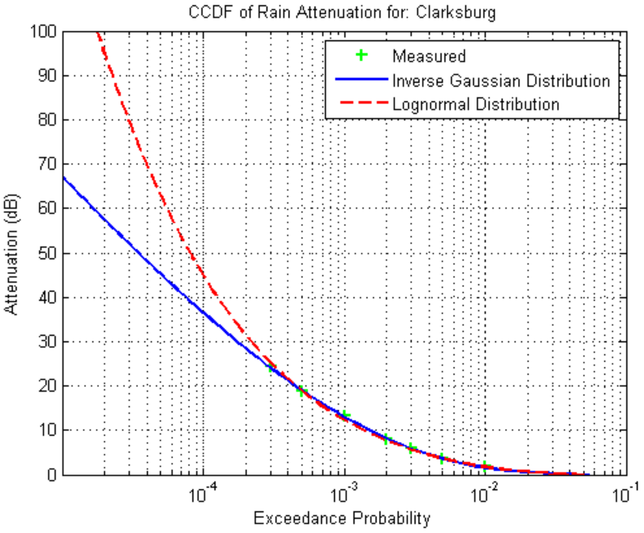

Figure 4.7. CCDF of rain attenuation for Clarksburg, U.S.

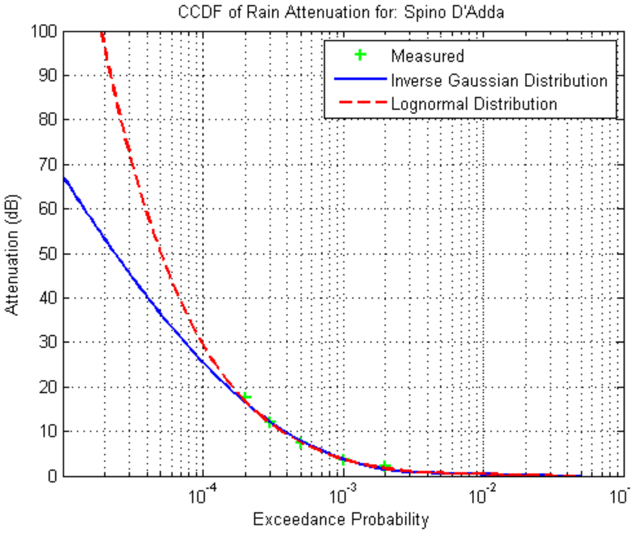

Figure 4.8. CCDF of rain attenuation for Spino d'Adda, Italy.

The performance of IG modeling of slant path rain attenuation for a tropical region is shown in Figure 4.9. In this case, the Earth station is located at UniTech Lae (Latitude: -6.45°, Longitude: 147°) of Papua New Guinea, the operating frequency of the link is 12.69 GHz and the elevation angle 72.8°. From Figure 4.9, it can be referred that the IG distribution can also model accurately the CCDF of rain attenuation for tropical regions also.

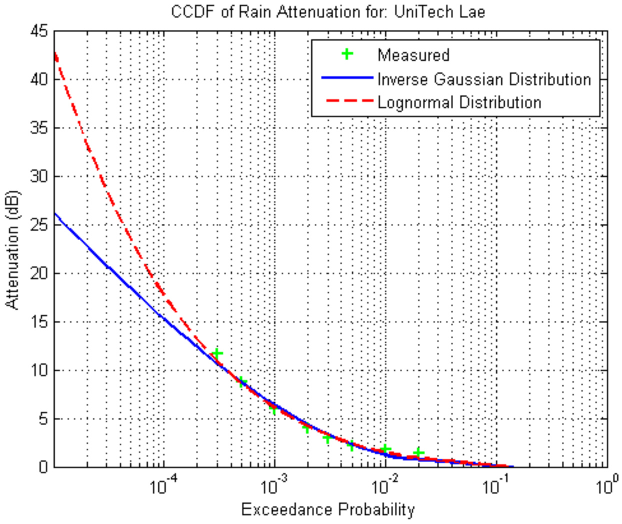

Figure 4.9. CCDF of rain attenuation for UniTech Lae, Papua New Guinea.

4.1.2.2 Terrestrial Link Rain Attenuation

The IG distribution is also used to fit the experimental CCDF of rain attenuation for LOS terrestrial links derived from [DBSG3] database. In Figure 4.10, the CCDF of rain attenuation for a LOS terrestrial link is shown with the stations located at Mendlesham

((Latitude: 52.26°, Longitude: 1.1°) of Great Britain for an operating frequency of 20.1 GHz and path length of 16.6 km. In Figure 4.11 and the same curves as in Figure 4.10 are presented for stations located at Darmstadt (Latitude: 49.87°, Longitude: 8.625°) of Germany and Tokyo, Japan, respectively. More particularly, for the former link the operating frequency is 12.4 GHz and the path length 20 km while for the latter one 34.5 GHz and 1.3 km. The same conclusions can be derived as in the previous Sections, i.e. IG distribution models well the CCDF of rain attenuation for LOS terrestrial links for both temperate and heavy rain climatic regions.

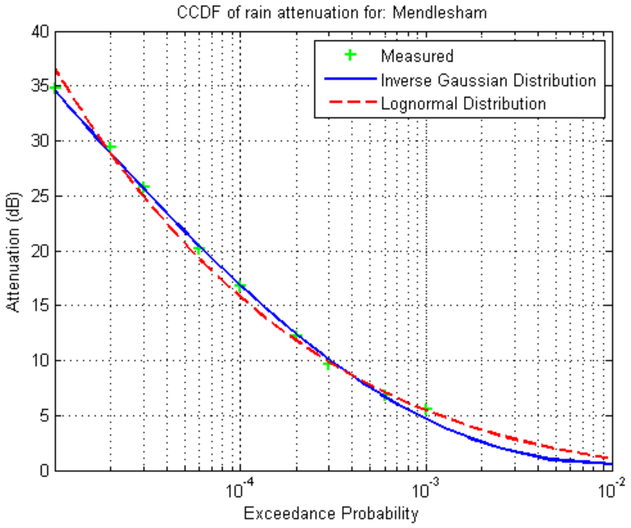

Figure 4.10. CCDF of rain attenuation for a LOS terrestrial link at Mendlesham, GB.

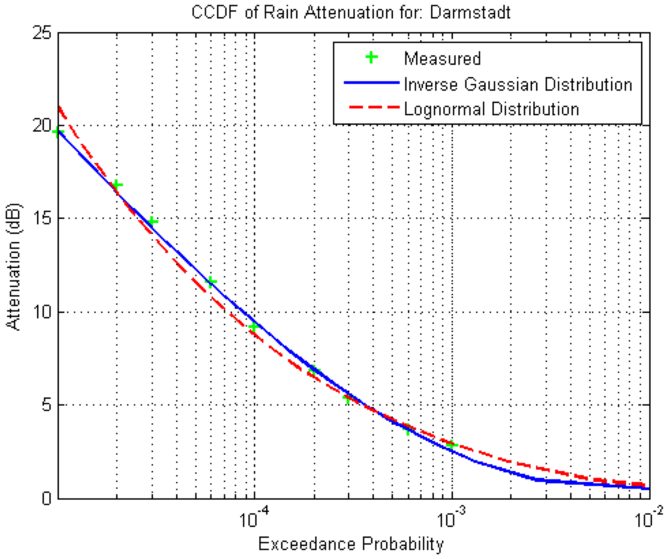

Figure 4.11. CCDF of rain attenuation for a LOS terrestrial link at Darmstadt, Germany

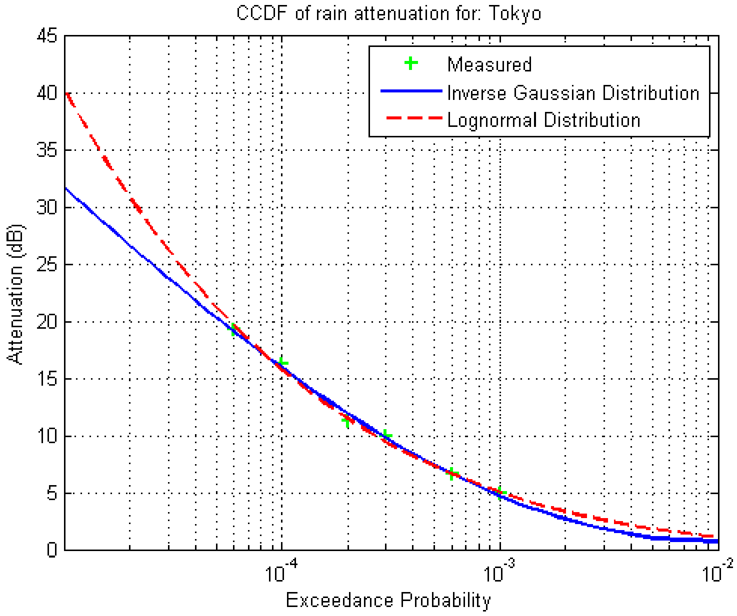

Figure 4.12. CCDF of rain attenuation for a LOS terrestrial link located at Tokyo, Japan

4.2 Outage Prediction Models for LOS Terrestrial and Satellite Links operating above 10GHz

For the calculation of a system margin for high microwave frequencies at single terrestrial and satellite links, the exccedance probability of the losses is of great importance. At frequencies above 10 GHz, rain attenuation cause the highest degradation of the signal and therefore, the prediction of CCDF of rain attenuation for various link configurations around the globe is necessary. In this Section of this Chapter a methodology is presented for the prediction of exceedance probability of rain attenuation and can be applied at LOS terrestrial and Earth-space links. Considering the analysis presented in preliminary Section 1, the main assumption of the model is that rain rate and rain attenuation for both kind of links follow the IG distribution.

4.2.1 Rain Rate Statistics

As already mentioned we assume that rain rate follow the IG distribution. We also make a further assumption that the probability to rain on a point of an area is always equal to 1. Therefore, the exceedance probability of rain rate is:

$$P\left[R \geq R_{th}\right] = 1 - Q\left(\sqrt{\frac{\lambda_R}{R_{th}}}\left(1 - \frac{R_{th}}{\mu_R}\right)\right) - e^{2\frac{\lambda_R}{\mu_R}} Q\left(\sqrt{\frac{\lambda_R}{R_{th}}}\left(1 + \frac{R_{th}}{\mu_R}\right)\right) \tag{4.5}$$

with λ_R and μ_R the statistical parameters of the IG distribution of rain rate. Although, the assumption that the probability to rain is set equal to one is not physical feasible, it can be considered through a mathematical modeling, since system engineers are interested in low probabilities, less than 0.1%. However, in Figure 4.13 the exceedance probability of rain rate predicted by ITU-R. P. 837-6 and in Figure 4.14 the CCDF of rain rate derived from the [DBSG3] database have been used to fit the theoretical CCDF of rain rate, given in (4.5). As it can be observed by these two figures, the unconditional distribution, assumed hereafter, can model accurately the long term first order statistics for the low probabilities which are of interest to the calculation of system margins.

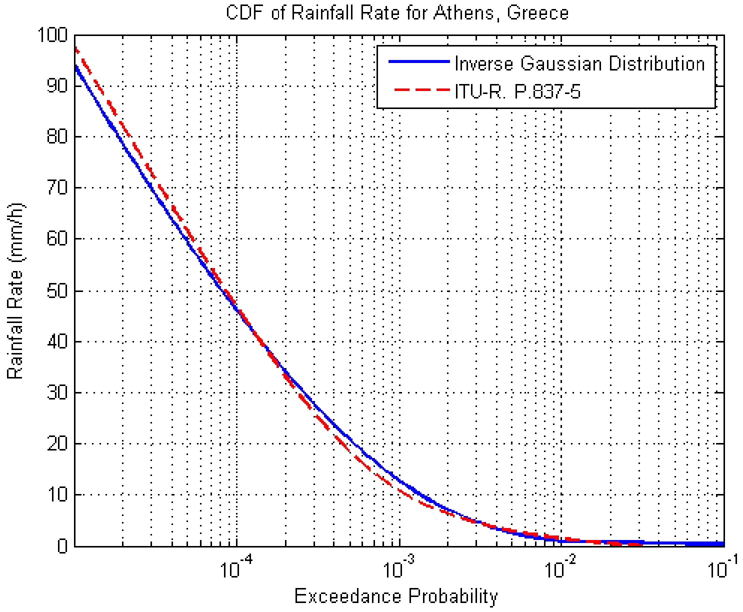

Figure 4.13. CCDF of rain rate for the region of Athens, Greece, derived from ITU-R. P. 837-6 (red dashed line) used for the fitting of IG distribution (blue solid line).

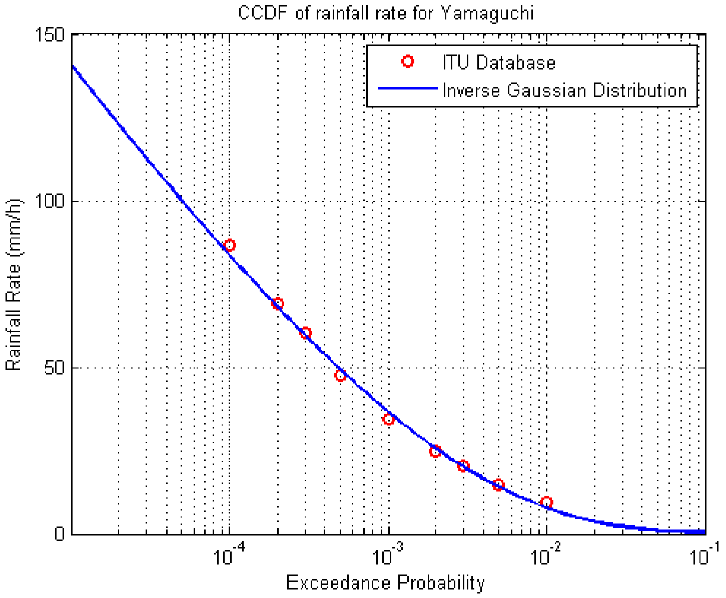

Figure 4.14 CCDF of rain rate for the region of Yamaguchi, Japan, derived from DBSG3 (red circles) used for the fitting of IG distribution (blue solid line).

4.2.2 Outage Prediction Methodology

As already mentioned the methodology refers not only to Earth-space links but also to LOS terrestrial links. In this methodology, the statistical parameters of rain attenuation will be given as a function of the statistical parameters of rain rate. Generally, rain attenuation (*A*) along a path is given by the following expression:

$$A(t)=\int_0^L \Gamma(x,t)dx=\int_0^L a\cdot R(x,t)^b dx \tag{4.6}$$

where *L* is the path of the link, *Γ*(*x*,*t*) is the specific rain attenuation (dB/km) on the point *x* of the path at time *t* which is equal to $a\cdot R(x,t)^b$ [Olsen78]. The specific attenuation coefficients *a* and *b* depend on the elevation angle, the frequency and the polarization of the link and can be derived from ITU-R. P. 838-3 [ITU-R.P.838].

More particularly, considering an Earth space link as this is shown in Figure 4.15, the path along which it may rain is the slant path (L_S) between the transmitter antenna and the 0° isotherm. So, considering an elevation angle (θ) of the link, it holds that:

$$L_S=\frac{H_R-H_S}{\sin(\theta)} \tag{4.7}$$

where H_s is the Earth station's antenna height above mean sea level and H_R is the height above mean sea level of the 0° isotherm. H_R can be computed from the ITU-R. P. 839-3 [ITU-R.P.839] model and H_S from the ITU-R. P. 1511 [ITU-R. P. 1511] model.

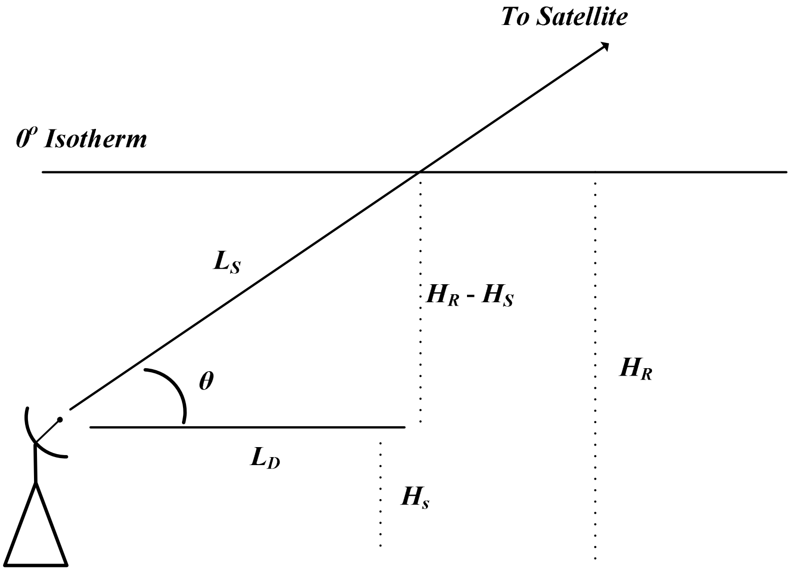

Figure 4.15. Earth-space link geometry

Firstly, for Earth-space links the Crane's assumption for uniform vertical profile of rain rate is employed [Crane80]. Therefore, assuming a satellite link with elevation angle φ the rain attenuation of the slant path (A_s) with effective average path length link L_s is connected to the rain attenuation of the projection of the slant path on the ground (A) with projected path length L_D:

$$A = A_s \cos\varphi \tag{4.8}$$

As a matter of fact, the probability that rain attenuation of the satellite link exceeds a threshold value (x_s) is equal to the probability that rain attenuation of the projected on the ground link exceeds a threshold value (x_D) with $x_D = x_s \cos\varphi$:

$$P[A_s \geq x_s] = P[A \geq x_D] \tag{4.9}$$

The connection between the length of the projection of the slant path on ground and the effective path length of the slant path is:

$$L_D = L_S \cos\varphi \tag{4.10}$$

For terrestrial links, the elevation angle can be approximated with 0° $\left(L_D = L_S\right)$. Consequently, the above analysis holds only for Earth-Space links.

The expression which connects the rain attenuation (A) of the projected on the ground link and rain rate (R) is:

$$A(t) = \int_0^{L_D} \Gamma(x,t)dx = \int_0^{L_D} a \cdot R(x,t)^b dx \tag{4.11}$$

where $\Gamma(x,t)$ is the specific rain attenuation concerning a point x at time t and is equal to $aR(x,t)^b$, also defined in (4.6).

Assuming that IG approximates the rain attenuation the unconditional CCDF of rain attenuation is given:

$$P\left[A \geq A_{th}\right] = 1 - Q\left(\sqrt{\frac{\lambda_A}{A_{th}}}\left(1 - \frac{A_{th}}{\mu_A}\right)\right) - e^{2\frac{\lambda_A}{\mu_A}} Q\left(\sqrt{\frac{\lambda_A}{A_{th}}}\left(1 + \frac{A_{th}}{\mu_A}\right)\right) \tag{4.12}$$

It is obvious that for the calculation of (4.12), we have to compute the statistical parameters λ_A and μ_A of the IG rain attenuation distribution in terms of the known parameters λ_R and μ_R of rain rate distribution for the specific location. The mean value of rain attenuation is the parameter μ_A of the IG distribution:

$$\mu_A = E\left[A(t)\right] \tag{4.13}$$

and the variance of rain attenuation is (see Appendix A):

$$\sigma_A^2 = E\left[A(t)^2\right] - E\left[A(t)\right]^2 = \frac{\mu_A^3}{\lambda_A} \tag{4.14}$$

From (4.14) the λ_A parameter of IG distribution is obtained:

$$\lambda_A = \frac{\mu_A^3}{\sigma_A^2} \tag{4.15}$$

Further, we calculate the mean value ($m_{\Gamma,1}$) and the variance (σ_Γ^2) of the specific rain attenuation in terms of the moments of rain rate of order b ($m_{R,b}$) and $2b$ ($m_{R,2b}$), as follows:

$$m_{\Gamma,1} = E\left[\Gamma(x,t)\right] = aE\left[R(x,t)^b\right] = a \cdot m_{R,b} \tag{4.16}$$

$$\begin{aligned}\sigma_\Gamma^2 &= E\left[\Gamma(x,t)^2\right] - m_{\Gamma,1}^2 = a^2 E\left[R(x,t)^{2b}\right] - m_{\Gamma,1}^2 = \\ &= a^2\left(m_{R,2b} - m_{R,b}^2\right)\end{aligned} \tag{4.17}$$

The two moments of rainfall rate statistics can be computed using Appendix A, since the coefficient *b* is almost always not an integer.

From (4.13) and (4.14) the mean value ($m_{A,1}$) and the variance (σ_A^2) of rain attenuation concerning the whole microwave path are, respectively:

$$m_{A,1} = E[A(t)] = \int_0^{L_D} E[\Gamma(x,t)]dx \tag{4.18}$$

$$\begin{aligned}\sigma_A^2 &= E[A(t)^2] - E[A(t)]^2 = \\ &= \int_0^{L_D}\int_0^{L_D} E\left[\Gamma(x,t)\Gamma(x',t)\right]dxdx' - \left(\int_0^{L_D} E[\Gamma(x,t)]dx\right)^2\end{aligned} \tag{4.19}$$

Hereafter it is assumed that the statistical parameters of the IG distribution of rain rate are notated as λ_R and μ_R and are assumed constant with space, which follows from the assumption that the mean value and variance of rain rate are constant.

Therefore, the mean value of *A* can be computed from (4.18) as:

$$m_{A,1} = m_{\Gamma,1}L_D = am_{R,b}L_D \tag{4.20}$$

For (4.19) the first integral must be calculated. Therefore, a horizontal spatial correlation coefficient (ρ) is introduced:

$$\rho\left(x,x'\right) = \frac{E[\Gamma(x,t)\Gamma(x',t)] - m_{\Gamma,1}^2}{\sigma_\Gamma^2} \tag{4.21}$$

where $m_{\Gamma,1} = a \cdot m_{R,b}$ is the mean value of specific rain attenuation and $\sigma_\Gamma^2 = a^2\left(m_{R,2b} - m_{R,b}^2\right)$ its variance with $m_{R,2b}$ the moment of rain rate of order 2*b*. From (4.19), the expressions of the mean value and variance of specific rain attenuation and the assumption that the statistical parameters of rain rate are constant it follows that:

$$\sigma_A^2 = \sigma_\Gamma^2 H_1 = a^2\left(m_{R,2b} - m_{R,b}^2\right)H_1 \tag{4.22}$$

with

$$H_1 = \int_0^{L_D}\int_0^{L_D} \rho(x,x')dxdx' \tag{4.23}$$

For the calculation of the above double integral of (4.23), we use the convective raincell model and the semi-empirical formula of Lin [Lin75] for modeling the specific rain attenuation spatial coefficient is also adopted:

$$\rho = \frac{G}{\sqrt{G^2 + \left(d = |x - x'|\right)^2}} \tag{4.24}$$

where d is the distance between the two points x, x'. G is a constant which depends on the local characteristics of rainfall medium and expresses the distance for which $\rho = 1/\sqrt{2}$. G is usually chosen 1.5km which is a good approximation for USA and Europe as will be shown in the numerical results Section. For terrestrial links and from extended tests performed on the DBSG3, it is recommended that the parameter G takes the value of 5km for the Japan area [Morita76], i.e. Latitudes ranging from 30^o N to 40^o N and Longitudes from 113^o East to 142^o East. In all the other cases the value of 1.5km is taken. The result of the double integral using (4.24)is:

$$H_1 = 2L_D G \sinh^{-1}\left(\frac{L_D}{G}\right) + 2G^2\left[1 - \sqrt{\left(\frac{L_D}{G}\right)^2 + 1}\right] \tag{4.25}$$

To conclude the above analysis, we have that:

$$\mu_A = a m_{R,b} L_D \tag{4.26}$$

and:

$$\lambda_A = \frac{\left(a m_{R,b} L_D\right)^3}{a^2\left(m_{R,2b} - m_{R,b}^2\right) H_1} \tag{4.27}$$

Where from Appendix A:

$$m_{R,b} = 2\sqrt{\frac{\lambda_R}{2\pi}} e^{\lambda_R/\mu_R} \left(\mu_R^2\right)^{\frac{b-1/2}{2}} K_{b-1/2}\left(\frac{\lambda_R}{\mu_R}\right) \tag{4.28}$$

and

$$m_{R,2b} = 2\sqrt{\frac{\lambda_R}{2\pi}} e^{\lambda_R/\mu_R} \left(\mu_R^2\right)^{\frac{2b-1/2}{2}} K_{2b-1/2}\left(\frac{\lambda_R}{\mu_R}\right) \tag{4.29}$$

Summarizing the procedure, the IG statistical parameters λ_R, μ_R of rainfall rate can be calculated through regression fitting analysis either on experimental data or on ITU-R rainmaps and the IG rain attenuation statistical parameters are given in equations (23)-(24). Then, the CCDF of rain attenuation in terrestrial links and Earth-space links can be calculated for any threshold. The fundamental assumptions on which the model is based are: a) point rain rate and rain attenuation follow the Inverse Gaussian distribution due to its skewness, b) the statistical parameters of rain rate, i.e. the mean value and standard deviation, are constant along the radiopath and c) the spatial correlation of specific rain attenuation is modeled with (4.24).

4.2.3 Numerical results

4.2.3.1 Terrestrial Links

The proposed methodology will be validated with the DBSG3 database, in which LOS terrestrial links are included. From the 89 available experiments in the DBSG3 database, 57 have been selected according to the quality of rain rate data and the concurrency of the rain rate exceedance probability and the rain attenuation exceedance probability. The range of frequency of these experiments is from 7 GHz to 81.8 GHz, the path length is from 1.2 km to 43.8 km and the absolute value of the latitude ranges from 2^o to 60^o.

The error criterion which is used is the one recommended in ITU-R. P.311-13[ITU-R. P. 311]. The statistics of the error, i.e. mean value, standard deviation and RMS error, are computed for every time percentage and for all the errors. The same approach is used for the model of ITU-R. P.530-14 [ITU-R. P.530]. In Table I, the overall statistics are presented for both models taking into account the overall error. In Figure 4.16, Figure 4.17 and Figure 4.18, the mean value, the standard deviation and the rms error for both models is given for every time percentage.

TABLE I

Mean, Standard Deviation and RMS Error (%) for Terrestrial Links

	ε_{mean} (%)	ε_{std} (%)	ε_{rms} (%)
IG model	-7.69	21	22.36
ITU-R. P.530-14	-9.53	20.64	22.7

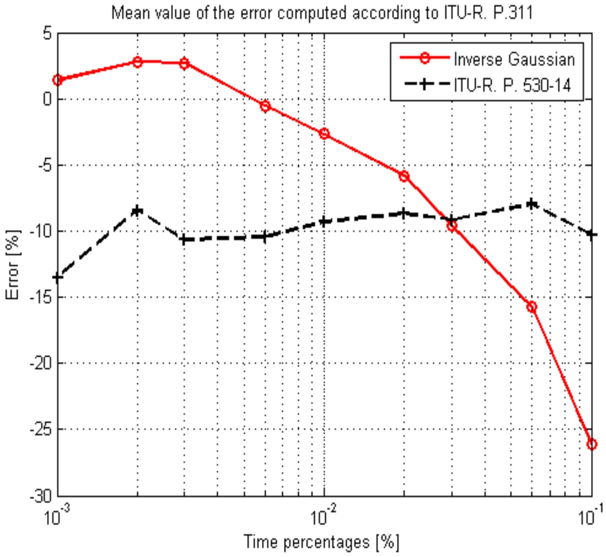

Figure 4.16 Mean error of IG model (red circles) and ITU-R. P. 530-14 (black crosses)

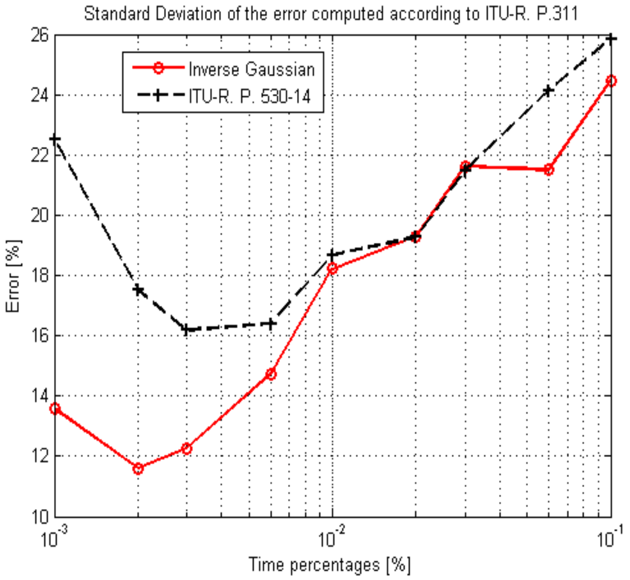

Figure 4.17 Standard deviation of the error of IG model (red circles) and ITU.R P. 530-14 (black crosses)

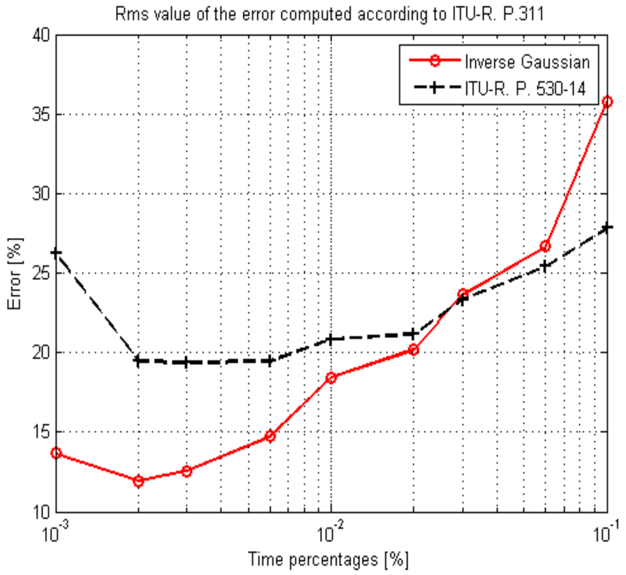

Figure 4.18 RMS error of IG model (red circles) and ITU-R. P. 530-14 (black crosses)

As it can be observed from the above Figures the proposed model is more accurate for the biggest part of time percentages according to the error criterion of ITU-R. P.311. Moreover, from the Table and particularly the RMS error, it is observed that the performance of the model is slightly better than this of ITU-R. P. 530. Here, it must be noted that the ITU-R model is an empirical one and its parameters are derived and refined after a fitting process of the model to the experimental data of DBSG3. Therefore, for terrestrial links with technical and climatic characteristics not included in the database, the model may have much worse behavior. However, the proposed model, since it is derived after physical and mathematical assumptions, it is expected that its performance will follow the above error statistics and will still have the same good performance.

4.2.3.2 Earth-Space Experiments

The proposed method is first tested against the DBSG3 database of ITU-R and the mean value the standard deviation and the RMS errors are computed for two cases: for every time percentage, in Figure 4.19, Figure 4.20 and Figure 4.21, respectively and the statistics of total error, Table II. The error is computed according to ITU-R. P. 311. The same approach was used for the computation of the error of ITU-R. P.618-10. As it is observed from the three Figures the performance of the model is better comparing to the one from ITU-R. P.618-10. More particularly, as shown in Table II the RMS error of the proposed model is less than this of ITU-RP.618-10. Here we have to note, that if we have used a different experimental database, it is expected that the new model will have much better performance comparing to ITU-R, since the ITU-R model is based on fitting process of the DBSG3 data. The proposed model is flexible and can be used for any location of world with very good accuracy.

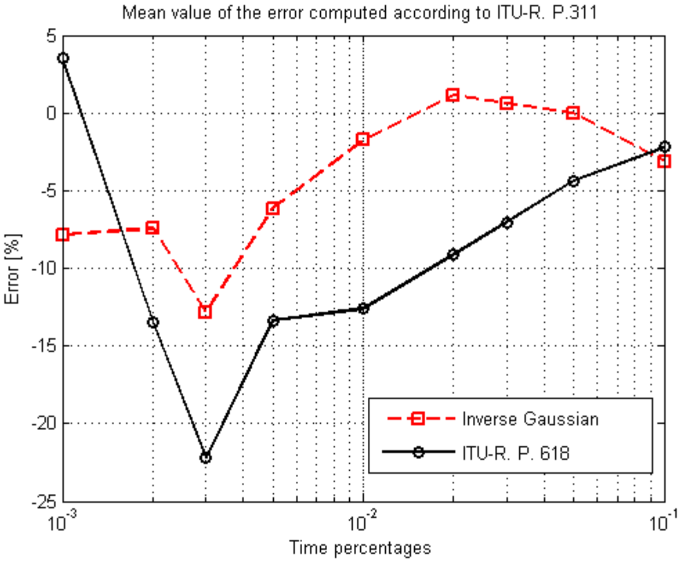

Figure 4.19 Mean value of the error for the IG model and the ITU-R. P. 618 model

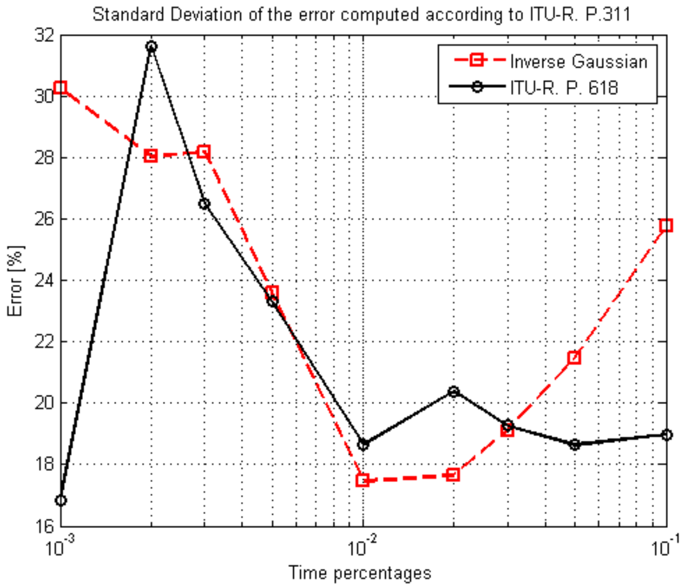

Figure 4.20 Standard deviation of the error for the IG model and the ITU-R. P. 618 model

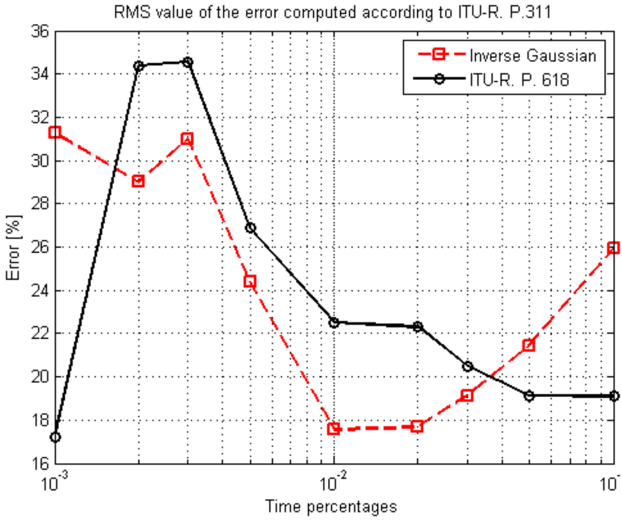

Figure 4.21 RMS value of the error for the IG model and the ITU-R. P. 618 model

TABLE II

Mean value, standard deviation and RMS value of the error for IG model and ITU-R. P. 618 model, considering all the errors

	ε_{mean} (%)	ε_{std} (%)	ε_{rms} (%)
IG model	-1.55	21.53	21.59
ITU-R. P.618	-7.68	20.42	21.81

Next the proposed model and the recommendation ITU-R. P. 618-10 are compared to the CCDF computed from synthesized rain attenuation time series. The time series are derived after the application of the SST ([Matricciani96]) on rain rate time series measured inside the NTUA campus in Athens, Greece. One reason why these time series are used are first to show the performance of the proposed model and its comparison to ITU-R. P. 618 with data apart from these of the DBSG3 databank, as these data have already been used for the derivation of the parameters of ITU-R. P. 618-10. A second one is that the exceedance probability calculated by the SST applied on measured rain rate time series has been validated with various experimental data ([Matricciani96], ([Matricciani05]. A great advantage of the SST is that time series of rain attenuation can be generated for the whole period in which measured time series of rain rate are available, taking into account all the events with high rain rate values or low ones.

For the case presented in this Section, two tipping buckets were placed in the campus of NTUA with a separation distance of 387 m. Although there are data measured for a period of 15 months, presented recently in [Kourogiorgas12], only one year measured rain rate time series were used, started from 18th of June 2010, as the random variable of rain rate seems to be cycloperiodic. The data were processed in the same way as presented in [Kourogiorgas12].

In order to apply the SST on rain rate measurements, there was a change in the formulation of the SST. In [Matricciani96] it refers that the rain height is 5 km and the depth of the melting layer was assumed to be 0.4 km. To be consistent with the ITU-Recommendation and the description of the proposed model, the rain height is derived from the map of ITU-R. P. 839 and the depth of the melting layer was considered equal to 0.36 km, as this is considered in [ITU-R. P.839]. For comparing the two models two links were considered, one for every measured rain rate time series. For the first site the elevation angle of the link has been set equal to 30^o and the operating frequency equal to 12 GHz (Ku band), while for the second site the elevation angle of the link was chosen 43.2^o and the frequency 20 GHz (Ka band). In Figure 4.22, three curves of the CCDF of rain attenuation for site 1 are shown derived from the SST, ITU-R. P. 618-10 and the proposed model, while in Figure 4.23, the same curves are shown for site 2.

Moreover, the mean error, the standard deviation and the rms value of the error are shown in Table III for site 1 and in Table IV for site 2. These errors were calculated for the time percentages from 10^{-3}% to 10^{-1}% to be consistent with the comparison made in DBSG3 case.

From Figure 4.22 and Figure 4.23, it can be observed that the prediction made by the proposed model based on the IG distribution is close to the one derived from the time series, while the recommendation of ITU-R. P. 618 behaves much worse than the proposed model. This can be also pointed from the two tables (Table III and Table IV) which present the statistics of the error. For site 1 the mean error of the proposed model is greater than this of ITU-R. P. 618. However, the standard deviation of the IG model is much less than this of ITU and so the rms value of the error for the proposed model is much less (actually the half) than this of ITU. In site 2, all the statistics of the error of the proposed model are less than these of ITU-R. P. 618, with a final rms error of 26.85% and 50.01 % for the IG model and the ITU model, respectively.

The poor prediction made by the ITU-R. P. 618 and the great difference between the statistics of the error at the comparison with DBSG3 and NTUA site are due to the fact that its parameters were derived from the data of DBSG3, as this has been also pointed before and this gives a credit to the fact that for any new data ITU-R model may not have the same behavior, probably worse, comparing with the DBSG3 data. The proposed model which is based on a very few basic assumptions for the physical process of rain rate and has inputs the long-term statistics of rain rate is expected to have generally very good performance since it as physical-mathematical one.

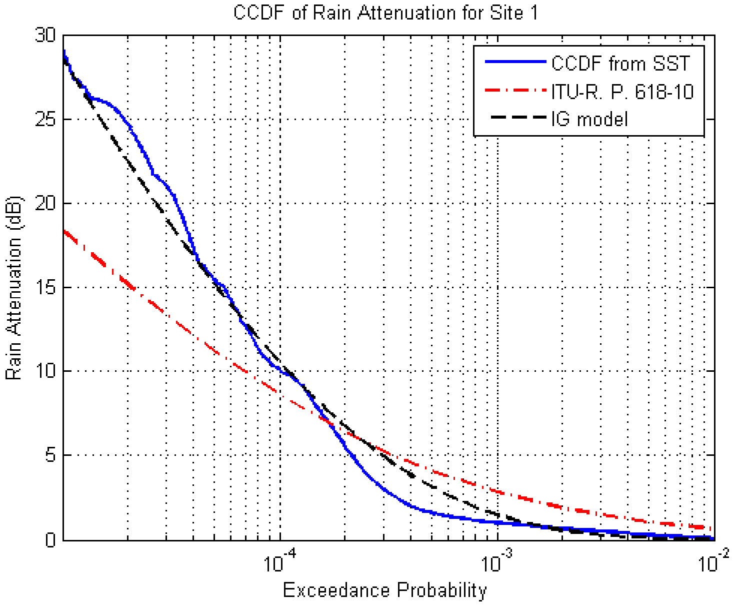

Figure 4.22 CCDF of rain attenuation derived from the application of SST (solid line) on measured rain rate times series in NTUA, site 1 (Ku band), from the IG model (dashed line) and ITU-R. P. 618-10 (dash-dotted line).

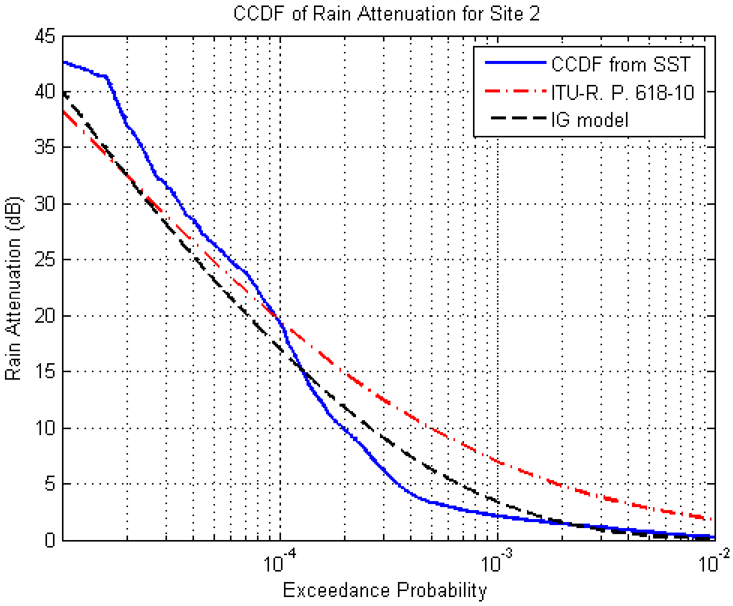

Figure 4.23 CCDF of rain attenuation derived from the application of SST (solid line) on measured rain rate times series in NTUA, site 2 (Ka band), from the IG model (dashed line) and ITU-R. P. 618-10 (dash-dotted line).

TABLE III

Mean, Standard Deviation and RMS Error (%) for Site 1

	ε_{mean}	ε_{std}	ε_{rms}
IG model	11.91	20.5	23.71
ITU-R. P.618-10	-1.10	47.40	47.41

TABLE IV

Mean, Standard Deviation and RMS Error (%) for Site 2

	ε_{mean}	ε_{std}	ε_{rms}
IG model	8.91	25.35	26.87
ITU-R. P.618-10	26.01	42.73	50.02

4.3 On the Earth-Space Site Diversity Modeling: A Novel Physical-Mathematical Outage Prediction Model

In this Section, a novel model for predicting the joint exceedance probability of rain attenuation for a dual site diversity system is presented using the single and the bivariate Inverse Gaussian (IG) distribution [Chikkara89]. The general unbalanced diversity configuration is considered since different statistical inputs for the single slant path distributions are used.

4.3.1 Outage Prediction Model

It is assumed that the unconditional single-site rain attenuation can be modeled with IG distribution. So the rain attenuation exceedance probability of a rain attenuation threshold $A_{th}(\mathrm{dB})$ from Appendix A is given:

$$P\left[A \geq A_{th}\right] = 1 - Q\left(\sqrt{\frac{\lambda_A}{A_{th}}}\left(1-\frac{A_{th}}{\mu_A}\right)\right) - e^{2\frac{\lambda_A}{\mu_A}} Q\left(\sqrt{\frac{\lambda_A}{A_{th}}}\left(1+\frac{A_{th}}{\mu_A}\right)\right) \tag{4.30}$$

The term unconditional that is used, means that there is no separation between rainy and non-rainy periods for modeling the rain attenuation distribution. The use of the unconditional CCDF for rain attenuation modeling overcomes the problem of the knowledge of probability of the existence of rain attenuation (P[A>0]). However, the probability of rain, that means that rainfall rate R is greater than zero (P_0= P[R>0]) can be derived for every location of the world using the ITU-R rainmaps P. 837-5 . This does not take into account the year variations of the probability to rain in a single point. The value of P_0 can also be used for the rain attenuation case with precaution. An expression that relates the P_0 value with the probability that rain attenuation exceeds zero dB value (P[A>0]) along the slant path is needed. Summing up, using the unconditional complementary cumulative density function the P_0 value and the relationship between P[A>0] and P_0 are not required.

The unconditional IG CCDF of rain attenuation approximates very well the rain attenuation distribution for probability levels less than 1%. So the 'tail' of a given rain distribution can be modeled very well with IG model. Two examples are given here in Figure 4.24 and Figure 4.25. In both figures the parameters μ_A and λ_A of the CCDF of IG rain attenuation distribution (4.30) were computed through a non linear regression fitting process with data points of rain attenuation. Data derived from ITU-R. P. 618-10 for the city of Bangkok considering a link with operating frequency (f) equal to 20GHz and elevation angle θ=30^{o} in Thailand were used for the first Figure. Experimental data points from La Conception in Canada from DBSG3 database with f=13GHz and θ=18^{o} were used for Figure 4.25. The computed parameters of the IG distribution are μ_A=0.2656 dB and λ_A=8.4$\cdot$10^{-3} dB for Figure 1 and μ_A=0.0209 dB and λ_A=2.99$\cdot$10^{-4} dB for Figure 2.

From Figure 4.24 and Figure 4.25, it can be observed the fitting of rain attenuation exceedance probability using IG distribution is very good. However, the relative error between the fitted values of the CCDF of IG distribution and the experimental exceedance probability was computed for both figures. The mean value, the standard deviation and the rms value of the error are -1.8 %, 13.75 %, 13.87 %, respectively, for the first figure and -1.7 %, 13.4 %, 13.54 % for the second figure. Lognormal [Panagopoulos04] and Weibull [Panagopoulos05] distributions have also very good behavior in single-site rain attenuation data. A comparative test of them with IG distribution on an experimental database is out of scope of this study.

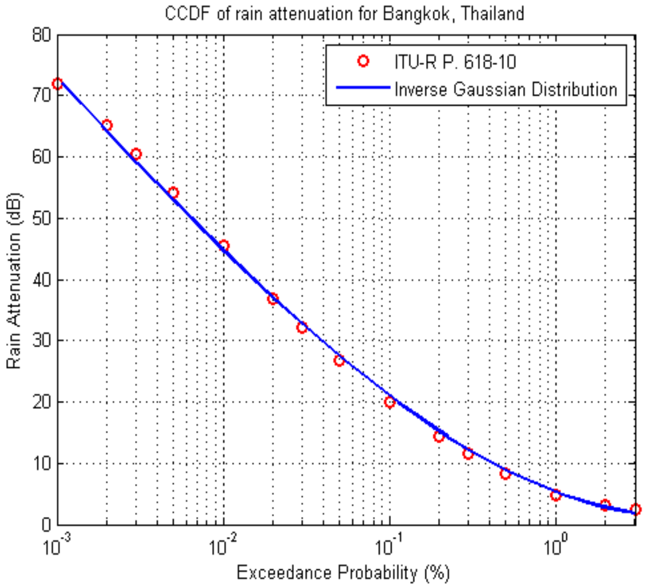

Figure 4.24 CCDF of rain attenuation for Bangkok, Thailand with f=20GHz and θ=30° curve from ITU-R. P. 618 (o) and the IG fitted curve (solid line) with parameters μ_A=0.2656 dB and λ_A=8.4·10^{-3} dB

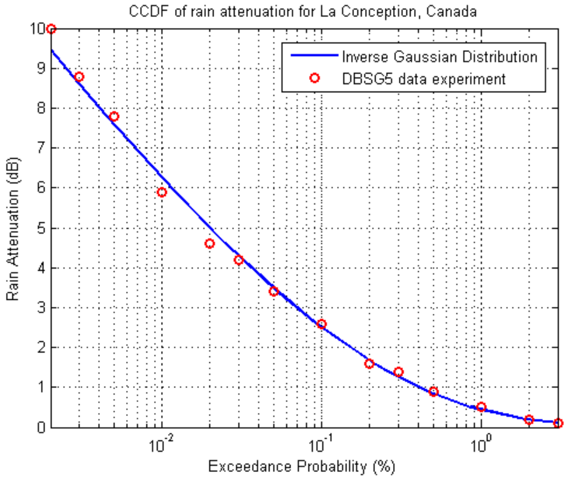

Figure 4.25 CCDF of rain attenuation for La Conception, Canada for f=13GHz and θ=18° with curve from DBSG3 database (o) and the IG distribution (solid line) with parameters μ_A=0.0209 dB and λ_A=2.99$\cdot 10^{-4}$ dB

As it was previously referred, the parameters of the IG exceedance probability must be greater than 0. Therefore, a nonlinear least-squares fitting problem subject to bounds is solved to compute the statistical parameters of the IG distribution. The trust-region-reflecting algorithm was used for solving the problem based on the interior-reflective Gauss-Newton method as this is described in [Coleman94], [Coleman96]. Then, using the preconditioned conjugate method the normal equations of the Gauss-Newton method are solved. As, the parameters of the CCDF of IG distribution must be greater than zero the bounds were selected 10^{-6} dB and 100 dB for both the parameters. The lower bound is close to zero dB and much smaller than the expected values of the parameters. The upper bound is much greater than the expected values of the parameters and can approximate for our case the infinite. The algorithm which is used has been already adopted from Matlab software [MATLAB].

Our objective is to calculate the joint exceedance probability of a dual unbalanced site diversity scheme which is defined:

$$P_{out} = P\left[A_1 \geq A_{th1}, A_2 \geq A_{th2}\right] \tag{4.31}$$

That means that we have to calculate:

$$P_{out} = \int_{A_{th1}}^{\infty} \int_{A_{th2}}^{\infty} f_{A_1A_2}\left(A_1, A_2\right) \cdot dA_1 \cdot dA_2 \tag{4.32}$$

where $f_{A_1A_2}\left(A_1, A_2\right)$ is the bivariate IG distribution (see expressions in Appendix B). From [22] we have an expression that gives the joint exceedance probability (CCDF) in term of the joint CDF and the single CDFs:

$$P_{out} = P\left[A_1 \geq A_{th1}, A_2 \geq A_{th2}\right] = 1 - P\left[A_1 \leq A_{th1}\right] - P\left[A_2 \leq A_{th2}\right] + P\left[A_1 \leq A_{th1}, A_2 \leq A_{th2}\right] \tag{4.33}$$

As far as the correlation coefficient is concerned, we employ the Paraboni-Barbaliscia expression [11] that also has been used in ITU-R physical-mathematical model [7]:

$$\rho_a = 0.94e^{-d/30} + 0.06e^{-(d/500)^2} \tag{4.34}$$

where d is the baseline distance of the two Earth terminals in km. If there are experimental data for the horizontal variation of the rainfall medium for the specific region of the site diversity system, the proposed model is flexible and the experimental correlation coefficient is recommended for the model.

Concluding the methodology, the outage probability can be calculated of a dual site diversity scheme using the following step-by-step procedure:

- Calculate the IG rain attenuation parameters for every single slant path using either experimental data or by fitting on the ITU-R P.618 prediction curve. Then we will have μ_1, λ_1 and μ_2, λ_2.
- Calculate the long-tem rain attenuation correlation coefficient using expression (4.34) and
- Finally calculate the outage probability using the final close formula derived from expression (4.33) and the CDFs from Appendix A and B.

Now we will present two characteristic comparison examples of the proposed methodology with experimental data from the ITU-R Databank.

In Figures 3 and 4 the joint rain attenuation exceedance probability taken from DBSG3 database and calculated from the expressions (12)-(14) are shown for two experiments. For Figure 3 the first base station is located at La Conception in Canada and the second one at Vernet in Canada. Their distance is 22.7 km with f=13GHz and θ=18°. The parameters of the individual CCDF of IG distributions are μ_1=0.0209dB, λ_1=$2.99\cdot10^{-4}$dB for the first slant path and μ_2=0.0206dB, λ_2=$3.013\cdot10^{-4}$dB for the second slant path at Vernet. For the second figure, the two base stations are located in Austria at Graz and Michelbachberg with their distance equal to 10.9 km. The operating frequency of the link is 11.4GHz and the elevation angle of both Earth stations is 33°. The parameters of the two IG distributions are μ_1=0.0253 dB, λ_1=$7.66\cdot10^{-4}$ dB, and μ_2=0.029dB, λ_2=$8.11\cdot10^{-4}$dB respectively. The error between the predicted values of the joint exceedance probability and the measured values has been computed for both Figures. For Figure 3, the mean value, standard deviation and rms value of the error are 1.27 %, 4.79 % and 4.95 %, respectively, while for figure 4 they are 7.06 %, 4.38 % and 8.31 %.

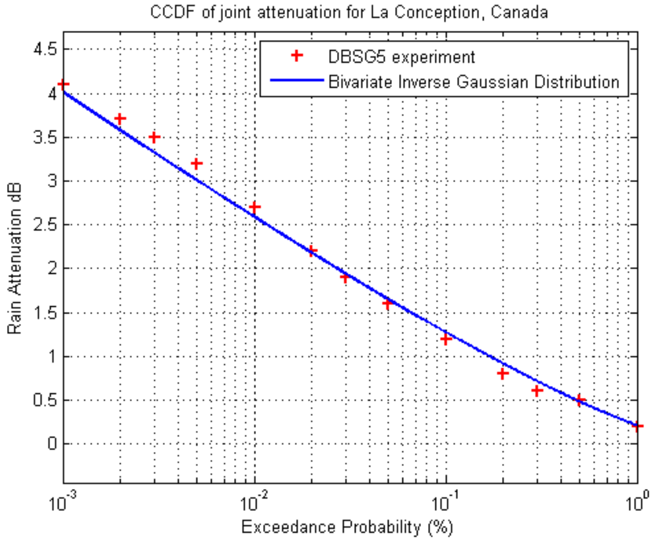

Figure 4.26. Experimental data (+) and simulated (solid line) joint CCDF of rain attenuation for two Earth stations with a distance 22.7 km, f=13GHz and θ=18° located at La Conception and Vernet, in Canada.

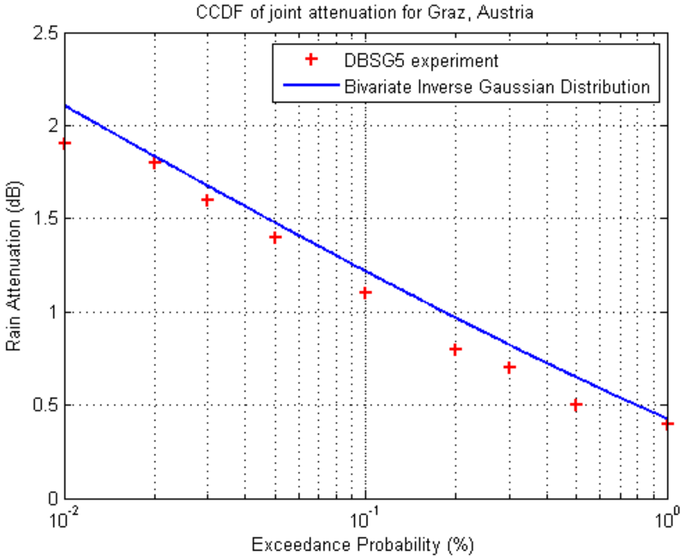

Figure 4.27 Experimental (+) and simulated (solid line) joint CCDF of rain attenuation for two Earth stations with a distance 10.9 km, operating frequency 11.4GHz and elevation angle 33° located at Graz and Michelbachberg, in Austria.

4.3.2 Numerical Results and Comparison Tests

In this Section, the proposed model will be validated with the Earth-space path experimental database of ITU-R, Study Group 3, DBSG3. The experimental joint rain attenuation exceedance probability will be compared with the resulted one from the new model using bivariate IG distribution. The error will be computed for all the experiments for two cases: first, for every time percentage and second, for all time percentages. For the first case the mean value, standard deviation and rms value of the error were computed for every time percentage considering all the experiments, while for the second case the statistical parameters of the error were computed considering all the errors for all data points, i.e. all time percentages and all experiments. The error is computed according to ITU-R. P. 311-13 error criterion [ITU-R. P.311]:

For the computation of the mean value, standard deviation and rms value of the error, the errors are weighted according to the duration of the experiment as this is noted in [ITU-R. P.311]. The error for the same experiments will be computed according to the error criterion of ITU-R. P.311 for the predicted values using ITU-R. P. 618-10 (in §2.2.4.1) [ITU-R. P.618], in order to compare the results of the proposed model against the ITU-R Recommendation.

The inputs for the new model are the parameters μ_1, λ_1 and μ_2, λ_2 of the individual exceedance probabilities for every Earth-space path (calculated from the experimental curve) and the baseline distance between the two base stations. For ITU-R. P. 618-10 model apart from the parameters of the lognormal fitting to the individual experimental CCDF of rain attenuation and the distance between the two base stations, the probability of rain for the two regions where the Earth stations are located is required. The latter vales are obtained from ITU-R. P.837-5 [ITU-R. P.837].

The presenting error was computed using 44 experiments from Earth-space path DBSG3 database for the time percentages that available data exist. These experiments were chosen for two reasons. First, they are the only experiments of the database which include all the required data to validate the proposed model and compare it to the ITU-R. P. 618. Second, they include a sufficient number (greater than four) of experimental data points for the single-site induced rain attenuation, in order to obtain accurate results from the nonlinear regression fitting process of IG (for the proposed model) and lognormal distribution (for ITU-R. P. 618) to the single-site rain attenuation experimental data points. The required data are the latitude, longitude, the baseline length and single-site rain attenuation of the two Earth stations and the joint rain attenuation. Most of the experiments took place in moderate climates and only one in Brazil at Latitude -3.1^o, the operating frequency of the links is between 11.4GHz and 30GHz, the minimum elevation angle is 6^o and the maximum 83^o. The separation distance between the two base stations varies from 1.7 km to 213 km.

The mean (ε_{mean}), the standard deviation (ε_{std}) and the rms (ε_{rms}) value of the error were computed for every time percentage and for all time percentages for all the experiments. In Figure 4.28, Figure 4.29 and Figure 4.30, the mean value, the standard deviation and the rms value of the error for every time percentage for all the experiments are shown. In Table V the same statistical parameters of the error are shown for all time percentages for all the experiments.

It is observed from Figure 4.28 that the mean error of the proposed model is much less comparing to the one from ITU-R P.618 recommendation for almost all time percentages. It is obvious that the new model behaves better in terms of mean error for every time percentage and for the overall error, as this is shown in table V. The mean error of the proposed model is -0.75 % and for ITU-R. P.618 is -16.31 %.

As for the standard deviation, it is observed that ITU-R. P.618 model behave better in almost every time percentage (see Figure 4.29). However, in overall the proposed model is statistically slightly more stable than ITU-R. P. 618 as from Table V the standard deviation of the error of the proposed model is 29.19% and for ITU-R P.618 30.25%. Furthermore, the performance of a model is evaluated via the rms value of the error. From Figure 4.30 it can be referred that the proposed model has a lower rms error than ITU-R. P. 618 for every time percentage apart from 0.001%-0.003% time percentages. The overall rms error for the proposed model is 29.2% and for the recommendation of ITU 34.37%, as this is shown in Table V. Therefore, the overall performance of the proposed model is better comparing to the ITU-R. P. 618. We can conclude that the prediction made by the new model based on bivariate IG distribution is accurate and closer to the experimental data than the prediction of ITU-R. P. 618.

TABLE V

Mean, Standard Deviation and RMS Error (%) for the Proposed Model and ITU-R. P. 618 for DBSG3 Database

	Proposed Model	ITU-R. P. 618
ε_{mean} (%)	-0.75	-16.31
ε_{std} (%)	29.19	30.25
ε_{rms} (%)	29.2	34.37

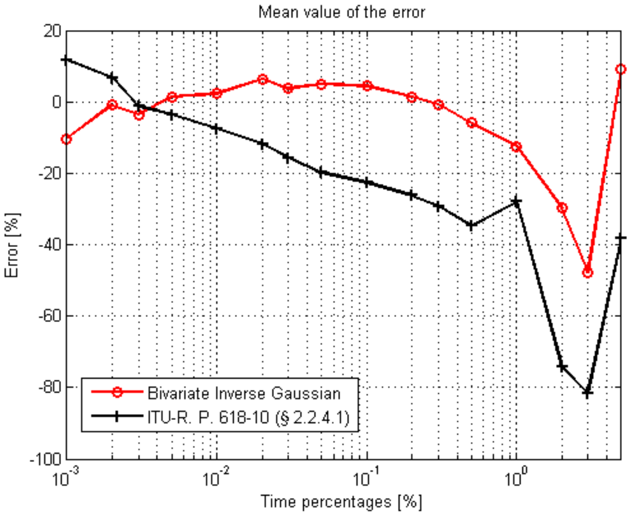

Figure 4.28 Mean value of the error (%) for every time percentage for the proposed model (o) and ITU-R. P. 618 (+).

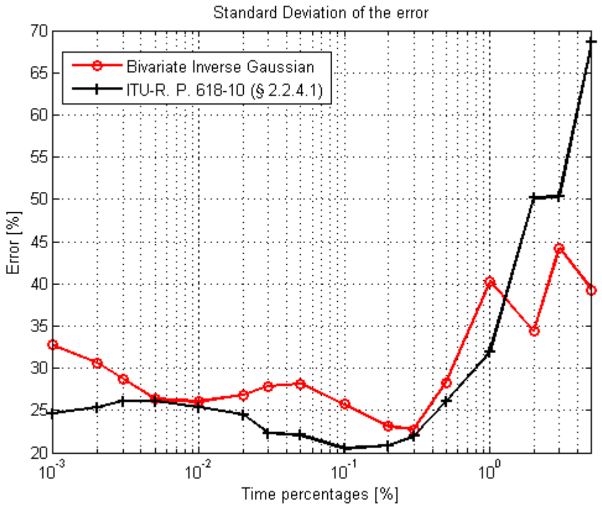

Figure 4.29 Standard deviation of the error (%) for every time percentage for the proposed model (o) and ITU-R. P. 618 (+).

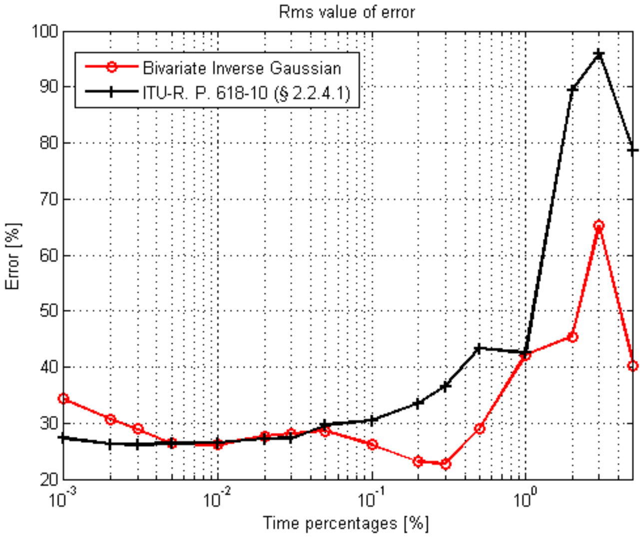

Figure 4.30 RMS value of the error (%) for every time percentage for the proposed model (o) and ITU-R. P. 618 (+).

4.4 Outage Performance of Broadband Fixed Wireless Access Diversity Networks

4.4.1 System Model

In this Section analytical expressions for the prediction of outage probability for Selection combining (SC) and Maximal Ratio Combining (MRC) diversity schemes are presented. First of all, the geometry of the site diversity system in fixed wireless access networks is described. In such system, a receiver (R) with two highly directive collocated antennas, is communicating with two base stations (BS$_1$ and BS$_2$), as this is shown in Figure 1. L_1 and L_2 are the path lengths of the LOS links between R-BS$_1$ and R-BS$_2$, respectively. The two links are converging and their separation angle is considered θ.

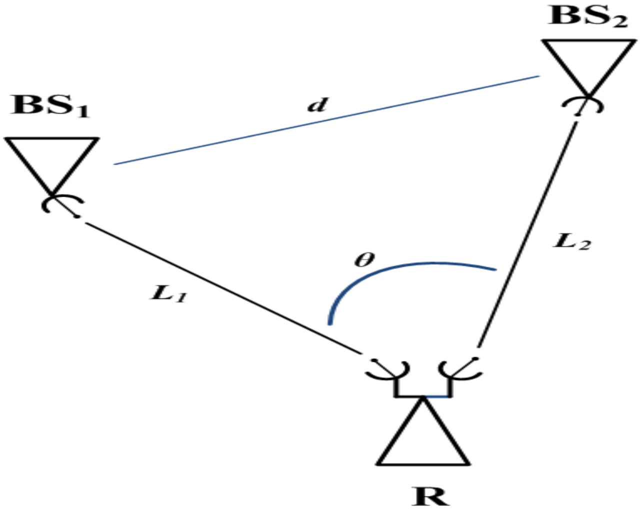

Figure 4.31 Geometry of a site diversity system

In the SC scheme, the link with the highest SNR is selected from the receiver in order to communicate, while in MRC scheme the receiver combines the two signals received at the two antennas of the receiver, in order that the Signal to Noise Ratio (SNR) of the received signal is the sum of the SNR of the two signals. The latter summation holds considering the SNR in linear terms. Another difference between the MRC and SC diversity techniques is that for the former technique (MRC), the sum of the SNR of the two signals received at the antennas on the receiver side takes place after co-phasing these two signals at the receiver side, while in the latter one, there is no need for co-phase of the two signals. . The received SNR$_r$ in linear terms, i.e. Watts, can be calculated, as:

$$SNR_r = \begin{cases} \max\left(SNR_1, SNR_2\right), \text{ SC} \\ SNR_1 + SNR_2, \text{ MRC} \end{cases} \tag{4.35}$$

with SNR_1 is the SNR of the signal transmitted from BS$_1$ and received by R and SNR_2 is the SNR of the signal transmitted from BS$_2$ and received in R, both in linear terms. For both SNR_1 and SNR_2 holds that:

$$SNR_i = 10^{\frac{SNR_{cs,i} - A_i}{10}}, \ \left(i = 1, 2\right) \tag{4.36}$$

where $SNR_{cs,i}$ is the SNR in dB of the received signal in path L_i under clear sky conditions and A_i is the rain attenuation in dB induced in link with path length L_i. The SNR under clear sky conditions can be computed as:

$$SNR_{cs,i} = P_i + G_{i,tr} + G_{i,rec} - PL_i - N_i, \quad \left(i = 1, 2\right) \tag{4.37}$$

where P_i (dBW) is the transmitted power from transmitter S_i, $G_{i,tr}$ is the antenna gain of transmitter BS_i and $G_{i,rec}$ is the antenna gain of the receiver R in link L_i, all in dBi. PL_i is the path loss in dB of link L_i and is equal to $PLi = 20\log\left(4\pi L_i / \lambda\right)$, with λ the wavelength and N_i in dB is equal to $N_i = 10\log\left(kT_iB\right)$The constant k is $k = 1.38\times 10^{-23}\left(J/K\right)$, T_i the antenna temperature of the receiver in link L_i and B is the bandwidth of the system.

An outage occurs when the received SNR is below a certain threshold. Consequently, the outage probability of both SC and MRC systems is given by:

$$P_{out} = P\left[SNR_r \le SNR_{th}\right] \tag{4.38}$$

For the case of the SC scheme, from (4.35) the outage probability is:

$$P_{out,SC} = P\left[\max\left(SNR_1, SNR_2\right) \le SNR_{th}\right] = P\left[SNR_1 \le SNR_{th}, SNR_2 \le SNR_{th}\right] \tag{4.39}$$

Using (4.39), the outage probability for a SC system after straightforward algebra becomes:

$$P_{out,SC} = P\left[A_1 \ge a_{1,th} = SNR_{cs,1} - SNR_{th,dB}, A_2 \ge a_{2,th} = SNR_{cs,2} - SNR_{th,dB}\right] \tag{4.40}$$

where $SNR_{th,dB}$ is the SNR_{th} in dB values, i.e. 10log (SNR_{th}).

For the MRC scheme the outage probability is given:

$$P_{out,MRC} = P\left[SNR_1 + SNR_2 \le SNR_{th}\right] = P\left[SNR_1 \le SNR_{th}, SNR_2 \le SNR_{th} - SNR_1\right] \tag{4.41}$$

Using the expression in (4.36), the outage probability for the MRC scheme is:

$$P_{out,MRC} = P\begin{bmatrix} A_1 \ge SNR_{cs,1} - SNR_{th,dB}, \\ A_2 \ge SNR_{cs,2} - 10\log\left(10^{\frac{SNR_{th,dB}}{10}} - 10^{\frac{SNR_{cs,1}-A_1}{10}}\right) \end{bmatrix} = P\left[A_1 \ge SNR_{cs,1} - SNR_{th,dB}, A_2 \ge g\left(A_1\right)\right] \tag{4.42}$$

4.4.2 Outage Performance Prediction Final Formulas

For the calculation of the of the above outage probabilities, we employ the fundamental assumption that the rain induced attenuations on the terrestrial links A_1, A_2 both following the IG distribution with parameters λ_1, μ_1 and λ_2, μ_2 , respectively, their joint PDF is given by [Al-Hussaini81] (see Appendix B):

$$f_{A_1,A_2}\left(A_1, A_2\right) = f_{A_1}(A_1)\cdot f_{A_2}(A_2)\cdot\left[1 + \rho_d \cdot \Psi(A_1, A_2)\right] \tag{4.43}$$

where ρ_d is the correlation coefficient of the random variables and $f_{A_1}(A_1)$, $f_{A_2}(A_2)$ are the PDF of the univariate IG distribution and

$$\Psi\left(A_1,A_2\right)=8\sqrt{\lambda_1\lambda_2/\mu_1^3\mu_2^3}\cdot\left(A_1-\mu_1\right)\cdot\left(A_2-\mu_2\right)\cdot\exp\left[-\left(\frac{\lambda_1\left(A_1-\mu_1\right)^2}{2\mu_1^2A_1}\right)+\left(\frac{\lambda_2\left(A_2-\mu_2\right)^2}{2\mu_2^2A_2}\right)\right] \quad (4.44)$$

The following spatial correlation coefficient is employed:

$$\rho_d=\frac{D_r}{\sqrt{D_r^2+d^2}}\left(d=\sqrt{L_1^2+L_2^2-2L_1L_2\cos(\theta)}\right) \quad (4.45)$$

with d the separation distance between the two transmitters and the coefficient D_r, also in km, is derived from [ITU-R. P.1410]:

$$D_r=0.644\ln\left(\left|Latitude\right|\right)-1.02,\quad 5^0\le\left|Latitude\right|\le 90^0 \quad (4.46)$$

The final expression (4.39) for the outage probability of a SC diversity system is given:

$$P_{out,SC}=P\left[A_1\ge a_{1,th},A_2\ge a_{2,th}\right]=1-P\left[A_1\le a_{1,th}\right]-P\left[A_2\le a_{2,th}\right]+P\left[A_1\le a_{1,th},A_2\le a_{2,th}\right] \quad (4.47)$$

where the CDF of single links are given:

$$P\left[A_i\le a_{i,th}\right]=Q\left(\sqrt{\frac{\lambda_i}{a_{i,th}}}\left(1-\frac{a_{i,th}}{\mu_i}\right)\right)+e^{2\frac{\lambda_i}{\mu_i}}Q\left(\sqrt{\frac{\lambda_i}{a_{i,th}}}\left(1+\frac{a_{i.th}}{\mu_i}\right)\right)\quad\left(i=1,2\right) \quad (4.48)$$

where Q is the Gaussian Q-function and the joint CDF is calculated trough the following expressions (see Appendix B):

$$P[A_1\le a_{1,th},A_2\le a_{2,th}]=P[A_1\le a_{1,th}]\cdot P[A_2\le a_{2,th}]+\rho_d\cdot H\left(a_{1,th},a_{2,th}\right) \quad (4.49)$$

with

$$\begin{aligned}H\left(a_{1,th},a_{2,th}\right)&=\int_0^{a_{1,th}}\int_0^{a_{2,th}}\Psi(A_1,A_2)f_{A_1}\left(A_1\right)f_{A_2}\left(A_2\right)dA_2dA_1=\\&16\sqrt{\frac{\lambda_1\lambda_2}{\mu_1\mu_2}}\exp\left[4\left(\frac{\lambda_1}{\mu_1}+\frac{\lambda_2}{\mu_2}\right)\right]Q\left(C_1\right)Q\left(C_2\right)\end{aligned} \quad (4.50)$$

$$\left.\begin{aligned}C_i&=\left[2\left(\frac{4\lambda_i}{\mu_i}+z_i^2\right)\right]^{1/2}\\z_i&=\frac{\sqrt{\lambda_i}(a_{i,th}-\mu_i)}{\mu_i\sqrt{a_{i,th}}}\end{aligned}\right\}\left(i=1,2\right) \quad (4.51)$$

For the MRC case (see (4.42)), the joint CCDF is more complex, considering that the threshold value of the one of two random variables depends on the value of the other, The computation of this joint CCDF using the bivariate IG distribution is not straightforward and an analysis must be done. The novel mathematical framework is presented here:

From (4.42), we have:

$$P_{out,MRC} = P\left[A_1 \geq a_{1,th}, A_2 \geq g\left(A_1\right)\right] = \int_{a_{1,th}}^{+\infty} \int_{g\left(A_1\right)}^{+\infty} f_{A_1,A_2}(A_1, A_2) dA_2 dA_1 =$$

$$= \int_{A_1}^{+\infty} \int_{g\left(A_1\right)}^{+\infty} f_{A_1}(A_1) \cdot f_{A_2}(A_2) dA_2 dA_1 + \rho_d \int_{A_1}^{+\infty} \int_{g\left(A_1\right)}^{+\infty} f_{A_1}(A_1) \cdot f_{A_2}(A_2) \Psi(A_1, A_2) dA_2 dA_1 = I_1 + I_2$$

(4.52)

From Appendix-B, it is obtained that:

$$P_{out,MRC} = P\left[A_1 \geq A_1, A_2 \geq g\left(A_1\right)\right] = \int_{a_{1,th}}^{+\infty} f_{A_1}(A_1) \cdot P\left[A_2 \geq g\left(A_1\right)\right] dA_1$$
$$+4\rho_d \sqrt{\frac{\lambda_2}{\mu_2}} e^{4\frac{\lambda_2}{\mu_2}} \int_{a_{1,th}}^{+\infty} f_{A_1}(A_1) \Psi_1\left(A_1\right) Q(C_2) dA_1 \tag{4.53}$$

where the function Ψi(.) is:

$$\Psi_i(x) = \sqrt{8} \sqrt{\frac{\lambda_i}{\mu_i^3}} \left(x - \mu_i\right) \exp\left[-\left(\frac{\lambda_i \left(x - \mu_i\right)^2}{2\mu_i^2 x}\right)\right] \tag{4.54}$$

Q(.), the Gaussian Q-function and

$$C_2 = \left[2\left(\frac{4\lambda_2}{\mu_2} + y_2^2\right)\right]^{1/2}$$
$$y_2 = \frac{\sqrt{\lambda_2}\left(g\left(A_1\right) - \mu_2\right)}{\mu_2 \sqrt{z_2}} \tag{4.55}$$

The numerical calculation of the final expressions is straightforward and the corresponding integral converges quickly. Here it must be noted that the complexity of the calculation of MRC and SC techniques for dual diversity systems based on the IG distribution or lognormal distribution, i.e. the model presented in ITU-R. P. 1410-5 [ITU-R. P.1410] is similar. However, the presentation and use of the proposed expressions are motivated by the accurate modeling of rain attenuation long-term first order statistics with the IG distribution. Moreover, (4.47) and (4.53) refer only to dual branch site diversity systems and therefore cannot be used for higher order diversity techniques. The whole analysis for the calculation of the performance of dual diversity systems can be extended in diversity systems with more branches, considering the assumptions that the spatial correlation is considered only between the two links. The concept of n-dimensional IG distribution with correlated links is considered as a future work,

4.4.3 Numerical Results and Discussion

In this Section some brief numerical results are presented regarding the outage probability of diversity systems in order to validate the proposed models. For the computation of clear sky SNR we consider a transmitted power of P_t=-10dBW and transmitter antenna gains of 19dBi for each transmitter. The antenna gains at the two receiver antennas are 34 dBi and the antenna temperatures are considered 300°K. The bandwidth is set equal to 28 MHz, typical values from IEEE 802.16 Standard

[IEEE802.16]. In order to proceed to a fair comparison of the performance of the diversity systems with the single link, we consider that the transmitted power at the case of single link is -7 dBW. The rain attenuation prediction is derived from ITU-R. P. 530-14 [ITU-R. P.530].

Firstly, we consider the diversity scheme in Athens, Greece. In Figure 4.32, the outage probability for the SC and MRC systems are shown, as well as the outage probability for the single link. The frequency of the link is considered 25 GHz and the path lengths (L_1, L_2) are 4 km. Two configurations of cell site diversity were considered in which the separation angle between the two links (θ) was 60^o and 90^o.

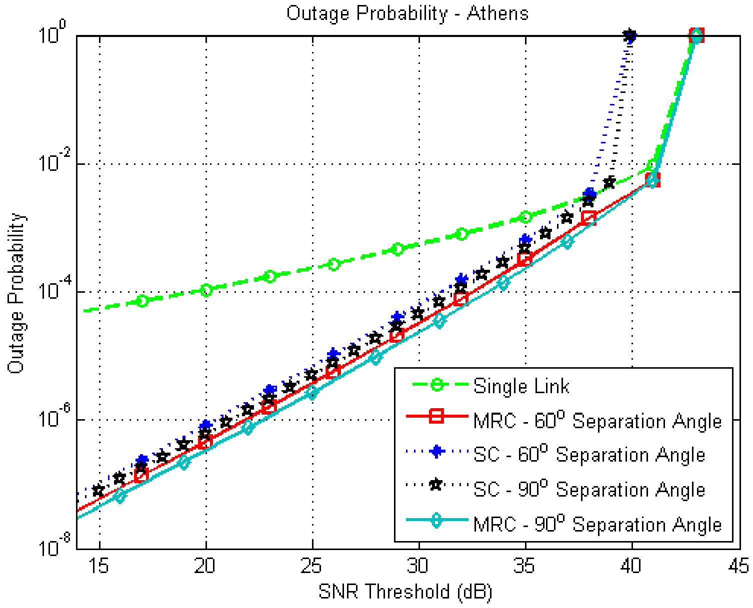

Figure 4.32 Outage probability for MRC and SC diversity systems with 60^o and 90^o separation angle and the corresponding single link, in Athens, Greece.

The same curves as in Figure 4.32 are shown in Figure 4.33 but considering that the stations are located at Seoul with operating frequency of 27 GHz and path lengths equal to 3 km. Again, two configurations are considered with separation angles of 120^o and 80^o. It can be observed from Figure 4.32 and Figure 4.33 that the performance of MRC systems is better than this of SC and single link for all the SNR thresholds. However, it is noted that MRC technique requires to co-phase the signals, while SC does not. Furthermore, SC has a higher performance than single link for low probability levels. The latter is due to the fact that we proceed to a fair comparison, i.e. the total transmitted power is equal for the case of single links and the diversity systems. Moreover, the minimum SNR thresholds above which the system is in a permanent outage are the SNR_{cs} values for the SC technique ($SNR_{cs,SC}$) and the case of single link ($SNR_{cs,SL}$) which in linear terms the former is half of this of SC technique. This occurs due to the fact that if the SNR threshold required for the realization of the communications is larger than the obtained SNR in case of clear sky conditions and considering that the losses in clear sky conditions are present for 100% of time, the system will be permanently in outage. Now, considering the threshold for MRC case, this is twice of the $SNR_{cs,SC}$ in linear terms due to the sum of the SNRs of the signalsreceived by the two different radiopaths. For higher order diversity techniques it is expected that the performance will be further improved for both techniques. The relative diversity gain will decrease with the increase of the number of the branches. However, the costs will be increased since more stations will be needed for the realization of the multi-branch diversity, the receiver will be more complex and the Channel State Information at the receiver side (CSIR) required will be also increased. Moreover, it can be observed that increasing the separation angle, the outage probability is decreasing, since rain attenuation on the two links is less and less correlated.

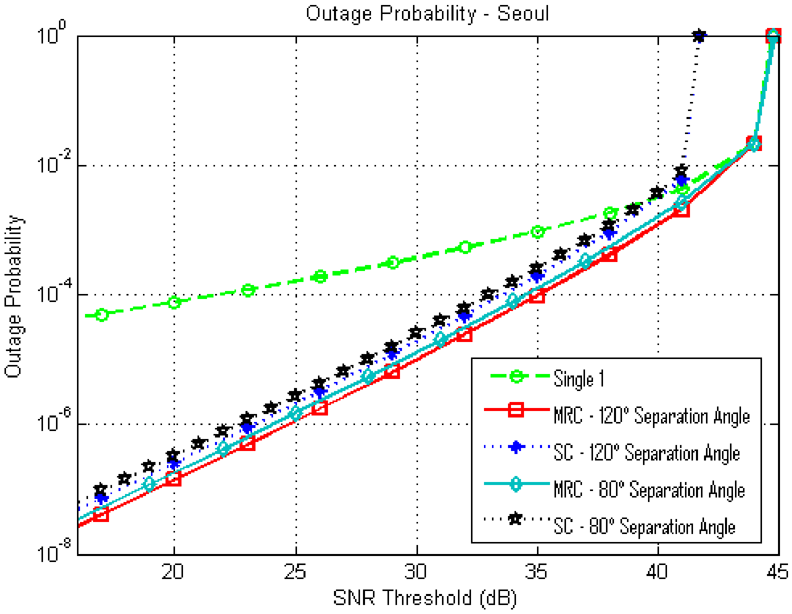

Figure 4.33 Outage probability for MRC and SC diversity systems with 80° and 120° separation angle and the corresponding single link in Seoul, South Korea.

Moreover, we may consider the diversity gain for the evaluation of the improvement of the performance of a diversity system. The diversity gain for the MRC system is greater comparing to the SC system for all the paths and that for higher path lengths, the diversity gain of the system is increasing.

4.5 Outage Prediction Modeling Using Archimedean Copula Functions

Copulas are used for coupling random variables in order to calculate their joint statistics. More details in the Copulas theory is given in Appendix C and in [Nelsen06]. Here, in this Section and after extended test the following Copula functions will be considered:

$$C(u,v)=\left(u^{-\theta}+v^{-\theta}-1\right)^{-1/\theta},\theta\in\left(0,+\infty\right)\ (5) \tag{4.56}$$

$$C(u,v)=\exp\left\{1-\left[(1-\ln u)^{\theta}+(1-\ln v)^{\theta}-1\right]^{\frac{1}{\theta}}\right\}\ (6) \\ ,\theta\in(0,+\infty) \tag{4.57}$$

$$C(u,v)=\frac{\theta}{\ln\left(e^{\frac{\theta}{u}}+e^{\frac{\theta}{v}}-e^{\theta}\right)},\theta\in\left(0,+\infty\right)\ (7) \tag{4.58}$$

$$C(u,v)=\left[\ln\left(e^{u^{-\theta}}+e^{v^{-\theta}}-e\right)\right]^{-1/\theta},\theta\in\left(0,+\infty\right)\ (8) \tag{4.59}$$

4.5.1 Rain Rate Modeling

Following the Appendix C and assuming that the exceedance probability of rain rate is known for two points and noted as:

$$P\left[R_1\geq R_{th}\right]=1-u \tag{4.60}$$

$$P\left[R_2\geq R_{th}\right]=1-v \tag{4.61}$$

where u and v are uniformly distributed in [0,1] interval random variables and they are equal to the CDF of the point rainfall rate. Therefore, from Appendix C, we have:

$$P[R_1\geq R_{th},R_2\geq R_{th}]=1-u-v+C(u,v) \tag{4.62}$$

From (4.60) and (4.61) the variables u and v can be computed from the known CCDFs of rain rate for given thresholds (R_{th}) and then choosing an appropriate Copula function, the CCDF of rain rate can be computed.

Considering the modeling of joint statistics of rain rate, data from British Atmospheric Data Center (BADC) [BADC] were used. More particularly, in BADC, close to 7 years of time series of rain rate data are available measured at Sparsholt and Cholbolton at UK, simultaneously. The recorded rain rate time series from rain gauge tipping buckets were selected. In Figure 4.34 the single rain rate statistics and joint statistics for the year of 2003 are shown. In the same Figure, the fitted expressions of Copula functions (4.56) - (4.59) are shown. It can be observed that the Copula functions fit well to the joint rain rate statistics. In Figure 4.35 the joint statistics for the same sites but for multiple years (7 years) are shown. Again it can be observed that the Copulas fit well the experimental joint statistics.

The last comparison with joint rain rate statistics is shown in Figure 4.36. For this comparison rain rate time series measured at Athens were used [Kourogiorgas12]. The two sites are separated with a distance of 387 meters. From the Figure it can be observed that Copulas do behave well but worse regarding the BADC data. Especially, Copula of (4.58) has the worst behavior. This probably comes due to the very small distance of the two separation sites in comparison to Chilbolton and Sparsholt.

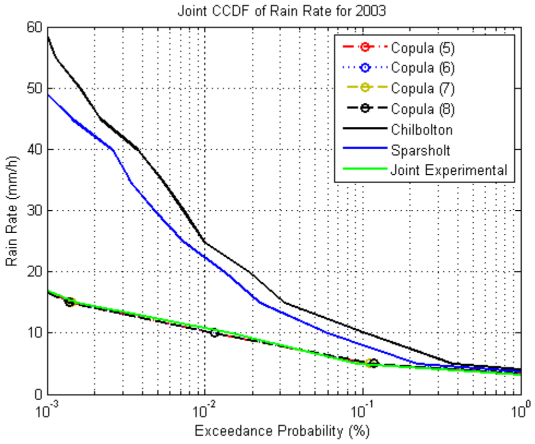

Figure 4.34. Joint and single statistics of rain rate from experiments at UK and the fitted Copula expressions for a single year 2003

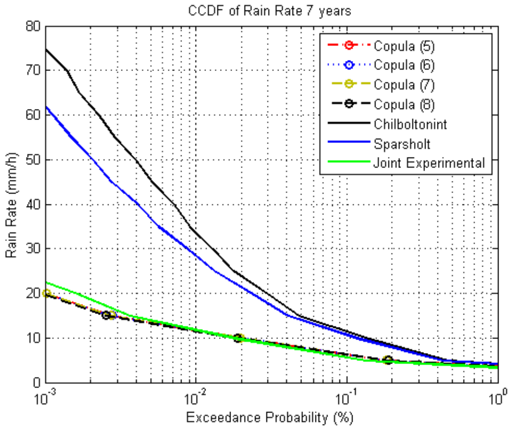

Figure 4.35 Joint and single statistics of rain rate from experiments at UK and the fitted Copula expressions for 7 years (2003-2009)

Finally, the RMS value of the relative error for the three Figures for the four Copulas given in (5)-(8) is shown in Table VI. In the Table it can be observed that Copulas (4.56) and (4.57) give the least error while copula (4.58) may have a difficulty in representing joint statistics at very low distances. However, for small distances there may be other Copula functions that can fit better. For this reason in Figure 4.36, the Gumbel-Hoogard Copula has been added [Nelsen06]. As it is observed it has a very good behavior and its rms error is 5.21%. The expression of the Copula function Gumbel-Hoogard is:

$$C(u,v)=\exp\left[-\left(\left(-\ln u\right)^{\theta}+\left(-\ln v\right)^{\theta}\right)^{1/\theta}\right] \tag{4.63}$$

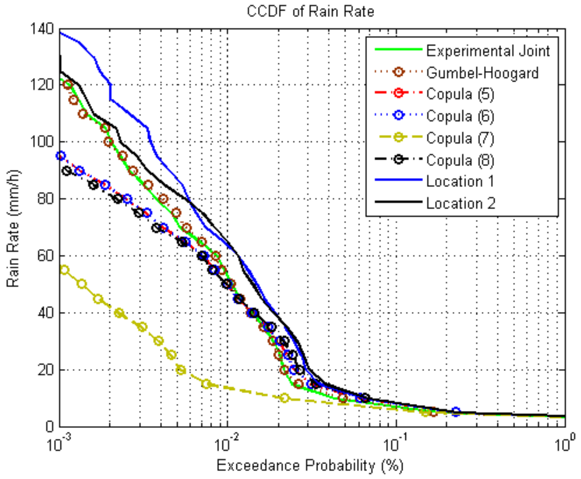

Figure 4.36. Joint and single statistics of rain rate from experiment at Athens and the fitted Copula expressions for 1 year (2010-2011)

TABLE VI

RMS value of relative error of Copula functions for Rain Rate

Exp. / Copulas	Single Year UK	Multiple Years UK	Athens
(5)	17.48 %	34.27 %	18.62 %
(6)	17.43 %	34.14 %	18.62 %
(7)	17.52 %	34.39 %	80.69 %
(8)	20.57 %	38.68 %	24.17 %

4.5.2 Rain Attenuation Modeling Using Copulas

Similarly with rain rate, if the exceedance probability of rain attenuation at two different links is known the following random variables *u* and *v* can be computed for given attenuation thresholds:

$$P\left[A_1 \geq A_{th}\right] = 1 - u \tag{4.64}$$

$$P\left[A_2 \geq A_{th}\right] = 1 - v \tag{4.65}$$

Then similarly with previous subsectionSection, the joint exceedance probability of rain attenuation can be computed through:

$$P[A_1 \geq A_{th}, A_2 \geq A_{th}] = 1 - u - v + C(u,v) \tag{4.66}$$

The expression given in (4.66) is firstly fitted to experimental joint CCDF derived from the databank of ITU's study group 3 [DBSG3]. Figure 4.37, experimental joint CCDF of rain attenuation is shown for two links with a separation distance of 18 km. The two Earth stations are located at St. Jovite and Arundel of Canada. The frequency of the link is 13 GHz. It can be observed that all the copula functions considered, i.e. (4.56)-(4.59), give a low error. In Figure 4.38, the same curves are shown for another experiment at Palmetto of US. The Earth stations have a separation distance of 16 km and the links have operating frequency of 17.8 GHz. In Figure 4.39, the Copula functions are tested with a third experimental joint CCDF derived at Atlanta of US. The separation distance is 37.5 km and operating frequency of 12 GHz. The same observations with the previous experimental CCDFs are made for this case, too.

Furthermore, the Copula functions are tested with synthesized data using the Synthetic Strom Technique for Gera Lario of Italy for a micro-scale diversity system for which the separation distance is only 1.5 km [Matricciani03]. The results are shown in Figure 4.40. The operating frequency of the link is 19.77 GHz. As in the rain rate statistics, also in this case for small separation distances the four chosen Copula functions do not give the best estimation of the experimental joint CCDF. However, the Copula Gumbel-Hoogard, whose expression is given in (4.63) is also tested and it is found that it gives much better prediction.

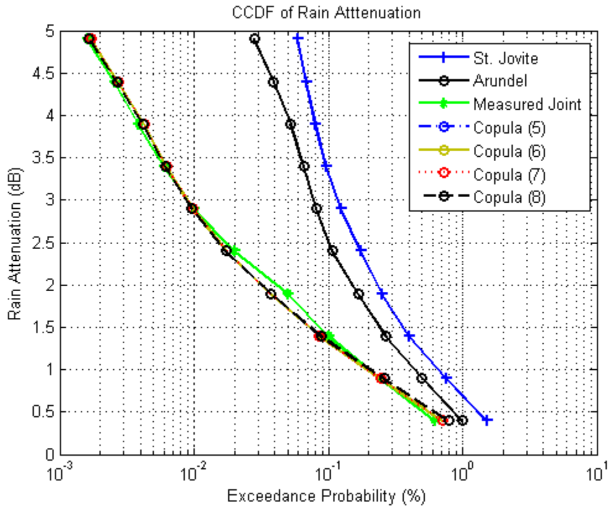

Figure 4.37 Joint and single statistics of rain attenuation from experimental data for two Earth stations at St. Jovite and Arundel of Canada

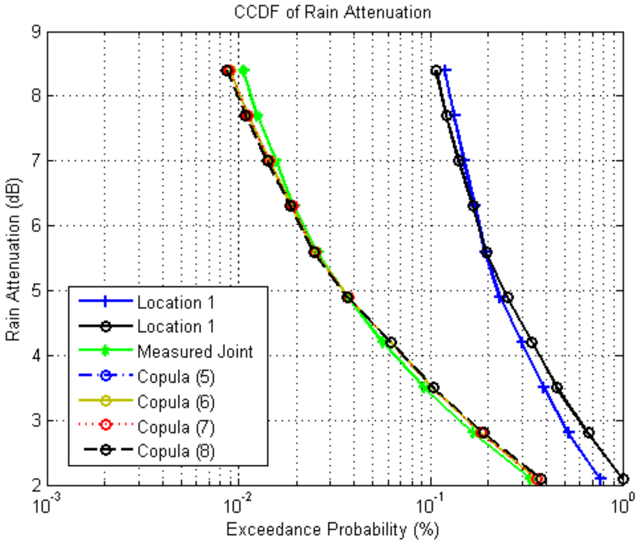

Figure 4.38 Joint and single statistics of rain attenuation from experimental data for two Earth stations at Palmetto of US.

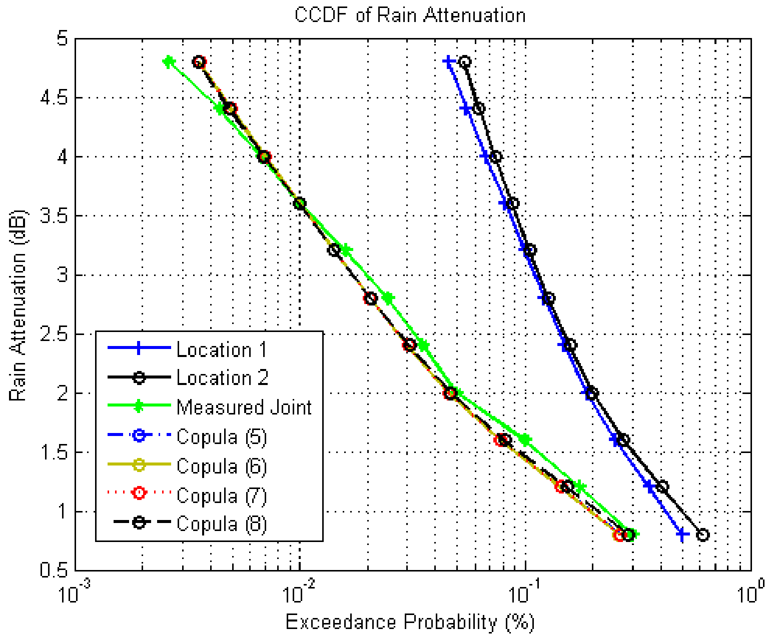

Figure 4.39 Joint and single statistics of rain attenuation from experimental data for two Earth stations at Atlanta of US.

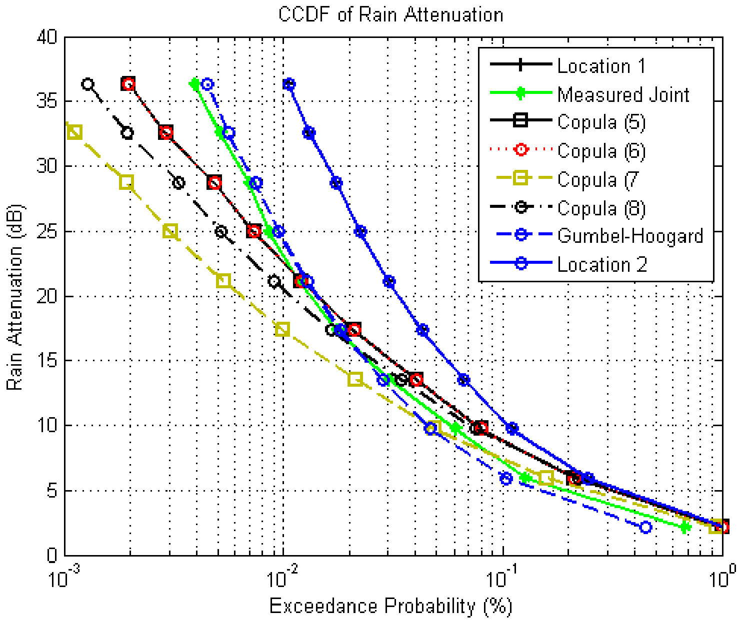

Figure 4.40 Joint and single statistics of rain attenuation from synthesized data using SST for Gera Lario of Italy.

Finally, the rms relative error is found for the above four cases and it is presented in Table II. The Copulas with expressions shown in (4.56) and (4.57) have the best performance which is similar to one another. The worst performance is this of Copula (4.59) with the exception of Atlanta experimental joint CCDF. Furthermore, for the last experiment the Gumbel-Hoogard copula function has the best performance with rms error of 17.20%.

TABLE VII. RMS value of relative error of Copula functions for Rain Attenuation Experiments

Site / Copulas	St. Jovite	Palmetto	Atlanta	Gera Lario
(5)	12.66 %	9.19 %	17.71%	40.01%
(6)	12.64 %	9.07%	17.77%	39.99%
(7)	12.67 %	9.31%	17.65%	56.58%
(8)	14.21 %	11.67%	15.51%	49.43%

4.6 Performance of Time Diversity Satellite Systems

4.6.1 Model based on Lognormal Distribution

The main assumptions of the Maseng-Bakken model [Maseng81] is that rain attenuation follows the lognormal distribution and that the rate of change of rain attenuation is proportional to the instantaneous value of rain attenuation. Therefore, we adopt that the Probability Density Function (PDF) of the rain attenuation on every time instant is:

$$p_A(A) = \frac{1}{\sqrt{2\pi} S_A A} \exp\left\{ -\frac{(\ln A - \ln A_m)^2}{2S_A^2} \right\} \tag{4.67}$$

with S_A the standard deviation of $\ln(A_t)$ and A_m the median value of the lognormal distribution of rain attenuation.

Next, by adopting the Maseng-Bakken model, rain attenuation (A_t) can be modelled as a stochastic process and be described by the following Stochastic Differential Equation:

$$dA_t = A_t \beta_A \left[S_A^2 - \ln(A_t / A_m) \right] dt + \sqrt{2\beta_A} A_t S_A dW_t \tag{4.68}$$

where β_A (sec^{-1}) is a parameter on which the dynamics of rain attenuation depend and hereafter will be named as the dynamic parameter of rain attenuation and dW_t are the Brownian increments [Karatzas05].

It is known that for a S.D.E. of the form:

$$dA_t = f\left(A_t, t\right)dt + g\left(A_t, t\right)dW_t \tag{4.69}$$

with $f\left(A_t, t\right)$ the drift coefficient and $g\left(A_t, t\right)$ the diffusion coefficient, the Transition Probability Density Function (TPDF), i.e. $p\left\{A(t), t \mid A(t_0), t_0\right\}$ is the solution of the differential equation:

$$\frac{\partial p\left\{A(t), t \mid A(t_0), t_0\right\}}{\partial t} + \frac{\partial}{\partial A}\left[f\left(A(t), t\right)\cdot p\left\{A(t), t \mid A(t_0), t_0\right\}\right] - \\ -\frac{1}{2}\frac{\partial^2}{\partial A^2}\left[g^2\left(A(t), t\right)\cdot p\left\{A(t), t \mid A(t_0), t_0\right\}\right] = 0 \tag{4.70}$$

The TPDF describes the evolution of the stochastic process by giving the probability of the stochastic process in time $t = t_0 + \Delta t$ given the initial value of the process at time t_0.

The solution of the above differential equation is [16]:

$$p\left\{A(t), t \mid A(t_0), t_0\right\} = \frac{1}{\sqrt{2\pi}\, S_{a0}(\Delta t) A(t)} \exp\left\{-\frac{\left[\ln A(t) - \ln A_{m0}(\Delta t)\right]^2}{2S_{a0}^2(\Delta t)}\right\} \tag{4.71}$$

where

$$A_{m0}(\Delta t) = A_m^{\left[1-\exp(-\beta_A \Delta t)\right]} A(t_0)^{\exp(-\beta_A \Delta t)} \tag{4.72}$$

and

$$S_{a0}(\Delta t) = S_a\sqrt{1-\exp\left(-2\beta_A \Delta t\right)} \tag{4.73}$$

Therefore, the outage probability, joint exceedance probability of rain attenuation for a time diversity system can be calculated by:

$$P_{TD} = \Pr\left\{A(t) \geq a_{thr},\, A(t_0) \geq a_{thr}\right\} = \int_{a_{thr}}^{\infty}\int_{a_{thr}}^{\infty} p\left\{A(t), t \mid A(t_0), t_0\right\}\, p\left\{A(t_0), t_0\right\} dA(t)\, d\left(A(t_0)\right) \tag{4.74}$$

with $p\left\{A(t), t \mid A(t_0), t_0\right\}$ derived from (4.71) and $p\left\{A(t_0), t_0\right\}$ from (4.67). The double integral of (4.74) can be reduced to a single integral, since the TPDF $p\left\{A(t), t \mid A(t_0), t_0\right\}$ is a lognormal PDF with median value $A_{m0}(\Delta t)$ and standard deviation of the natural logarithm $S_{a0}(\Delta t)$. Therefore, (4.74) becomes:

$$P_{TD} = \int_{a_{thr}}^{\infty} P\left\{A(t) \geq a_{thr}, t \mid A(t_0), t_0\right\} p\left\{A(t_0), t_0\right\} d\left(A(t_0)\right) \tag{4.75}$$

where

$$P\left\{ A(t) \geq a,\, t \mid A(t_0),\, t_0 \right\} = \frac{1}{2} erfc\left(\frac{\ln A(t) - \ln A_{m0}(\Delta t)}{\sqrt{2} S_{a0}(\Delta t)} \right) \tag{4.76}$$

The final expression (4.76) for the calculation of the outage probability in a time diversity scheme is easily calculated numerically and converges very fast due to the monotonically decreasing nature of the integrand functions. The long-term parameters A_m and S_A are derived through fitting procedure on the latest version ITU-R P.618 [ITU-R. P.618] and the dynamic parameter β_A (sec^{-1}) is either considered by ITU-R P.1853 [ITU-R. P.1853] or the physical-mathematical model in [Panagopoulos01], [Panagopoulos03].

From here, numerical results are given and the proposed model is tested against experimental data. Firstly, the proposed expression given in (4.75) is tested against the joint CCDF derived from the time series of rain attenuation generated by the Maseng-Bakken model. For this purpose, a hypothetical Earth space link with the ground station located at Athens, Greece and operating frequency of 40 GHz and elevation angle of 40^o is considered. The dynamic parameter is set equal to 2x10^{-4} sec^{-1} as this is recommended in [ITU-R. P.1853]. In Figure 4.41, the single link CCDF of rain attenuation for the above link as well as the simulated and proposed joint CCDF of rain attenuation for a time diversity system are given. The time lag was set equal to 10 min and the lognormal CCDF which was given as an input to the time series was derived after the fitting of theoretical CCDF to the prediction of ITU-R. P. 618-10 model. As it can be observed from Figure 4.41, the theoretical results coincide with the simulated ones.

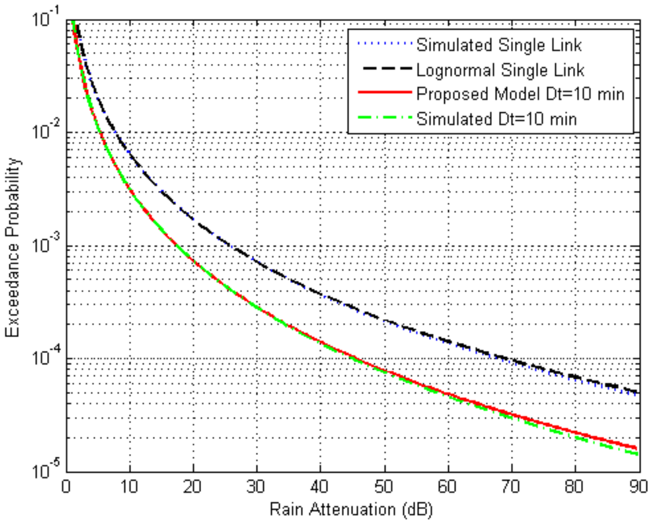

Figure 4.41 CCDF of rain attenuation for a single link with and without time diversity derived from the proposed model and from simulations.

In Figure 4.42, for the same hypothetical link, the CCDF of induced rain attenuation for a system without time delay and for a system with various time delays are shown. Apart from the joint exceedance probability the diversity gain is of paramount importance for the design of time diversity SatCom systems. The diversity gain $G_{TD}\left(\Delta t, p\%\right)$ for $p\%$ time percentage and a TD system with time lag Δt is defined as:

$$G_{TD}\left(\Delta t, p\%\right) = A_{TD}\left(\Delta t = 0, p\%\right) - A_{TD}\left(\Delta t \neq 0, p\%\right) \tag{4.77}$$

where $A_{TD}\left(\Delta t = 0, p\%\right)$ is the attenuation exceeded for $p\%$ in case that there is no TD adopted and $A_{TD}\left(\Delta t \neq 0, p\%\right)$ is the attenuation exceeded for $p\%$ for a TD system with time delay Δt. In Figure 4.43, the achieved diversity gain is given for probability levels 1% and 0.01%. As it can be observed from Figure 4.42 and Figure 4.43, increasing the time delay of the diversity system the joint CCDF of rain attenuation is decreasing. This is very obvious since with the increase of time delays the radiopaths are less correlated thus resulting to lower joint exceedance probability. However, the gain is increasing less and less with the increase of time delays, as this can be seen in Figure 4.43.

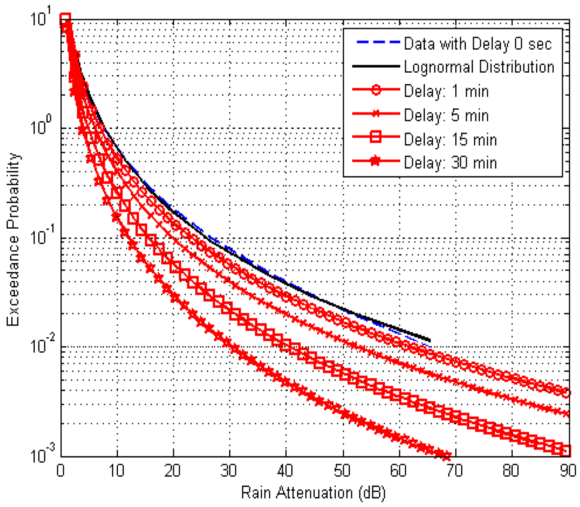

Figure 4.42 CCDF of rain attenuation for a link without time delay and for various delays.

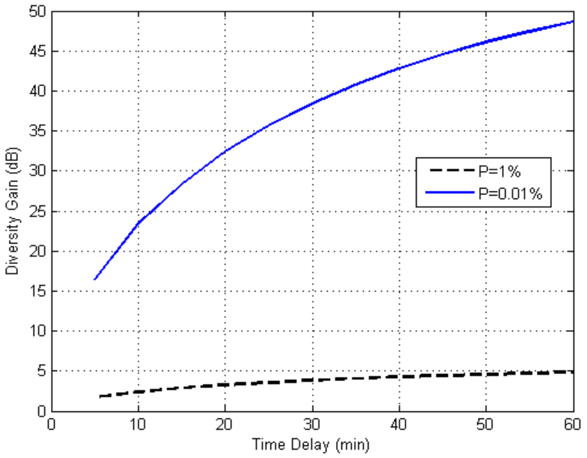

Figure 4.43. Gain achieved with the adoption of time diversity for 0.01% and 1% time percentages

In Figure 4.44 and Figure 4.45, for data derived from measurements at Spino d'Adda at frequencies 19 GHz and 40 GHz, respectively. The experimental curves were derived from [Fabbro09]. In [Fabbro09], as this is mentioned in the paper, the statistics presented refer to in-excess attenuation. However, in this Section due to the lack of measurements for time diversity systems, we compare the proposed model with these data. For the derivation of the theoretical exceedance probabilities, we computed the parameters of lognormal distribution of the system without time diversity (delay equal to 0 sec) through a non-linear regression process. The value of the dynamic parameter was set equal to 10^{-4} sec^{-1} for both experiments, as this has been measured for these experiments [Arapoglou08]. From the figures it can be easily observed that the method proposed can be considered accurate for both experiments.

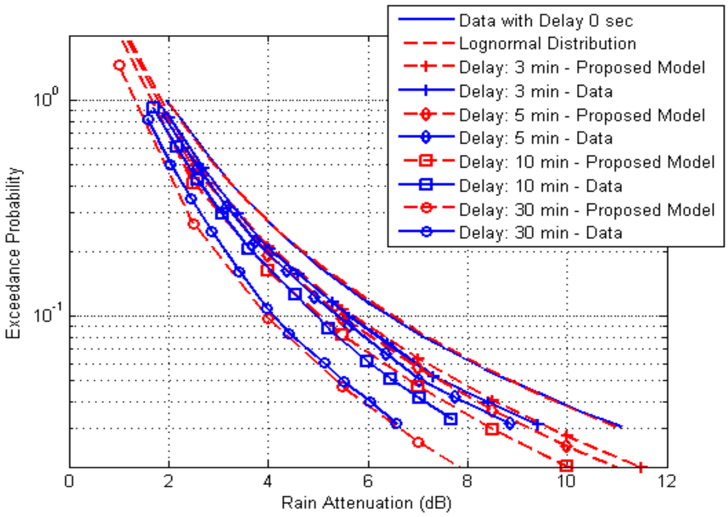

Figure 4.44. CCDF of rain attenuation with and without TD derived from data and the proposed model for Spino d'Adda at 19 GHz

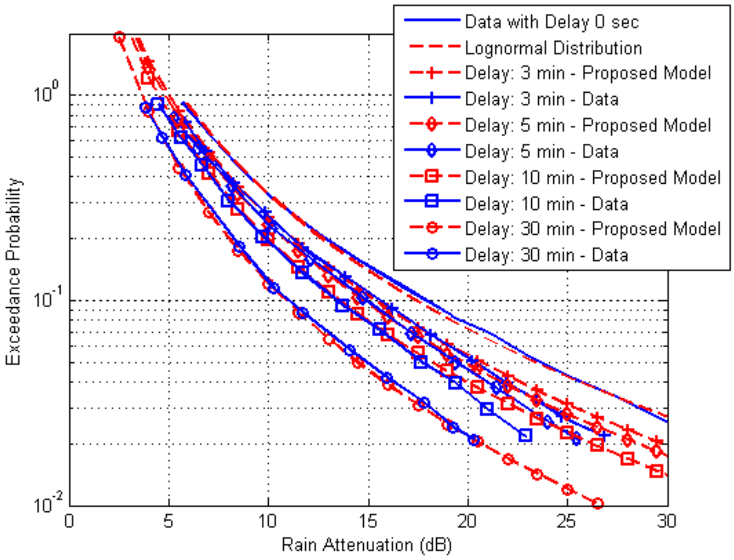

Figure 4.45. CCDF of rain attenuation with and without TD derived from data and the proposed model for Spino d’Adda at 40 GHz

Finally, the time diversity gain achieved for 0.01% for various elevation angles and various time delays is computed. It has been observed and shown that the dynamic parameter of rain attenuation depends on the dynamics of rain rate and the characteristics of the link, i.e. frequency, elevation angle etc [Panagopoulos01], [Panagopoulos03]. Therefore, we assessed the performance of time diversity systems for various elevation angles using the methodology presented in [Panagopoulos01] for the computation of the dynamic parameter of rain attenuation for various elevation angles. In Figure 4.46, the time diversity gain is shown for 0.01% of time for time delays between 5 min and 60 min for various elevation angles. The Earth station was considered to be at Paris, France and the frequency of the link was set equal to 30 GHz. In Figure 4.47, the same curves are shown but for an Earth station located at Tampa of Florida and 20 GHz operating frequency of the link. The dynamic parameter of rain rate was set equal to 10^{-3} sec, considering the measurements presented in [Kourogiorgas12]. It can be easily observed that higher gains are achieved as the elevation angle gets lower.

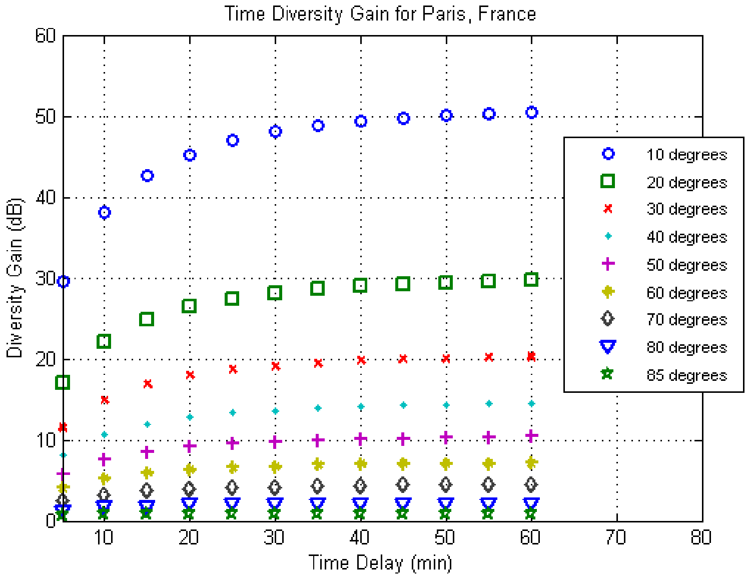

Figure 4.46. Time diversity gains for Paris, France for various elevation angles

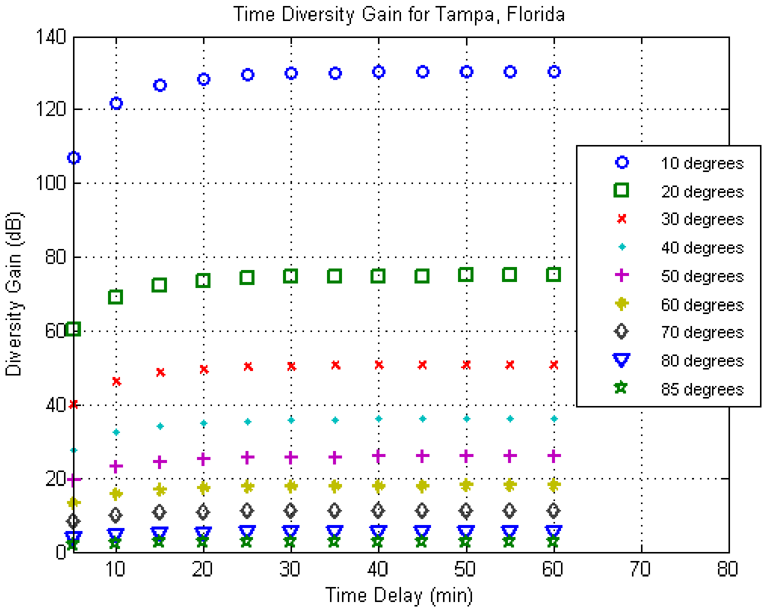

Figure 4.47. Time diversity gains for Tampa, Florida for various elevation angles

4.6.2 Model Based on Copulas

In this Section, the expressions for modeling of joint rain attenuation statistics for time diversity systems using Copulas theory are presented. Copulas are used in order to couple the single marginal distributions of two dependent random variables. For the bivariate case, it holds for the Cumulative Distribution function (CDF) of two rain attenuation random variables $A(t)$ and $A(t+\Delta t)$ of the same slant path in two time instants that:

$$P\left(A(t) \le A_{th}, A(t+\Delta t) \le A_{th}\right) = C(u,v) \tag{4.78}$$

where C(.) is the Copula function and *u* and *v*, are two random variables which are uniformly distributed in [0,1] and they can be considered equal to the marginal distributions of random variable $A(t)\left(F\left(A_{th}\right)\right)$ and $A\left(t+\Delta t\right)\left(G\left(A_{th}\right)\right)$, respectively.

In (4.78), the joint CDF is given. The expressions for the computation of the joint Complementary CDF (CCDF) is given :

$$P\left(A(t) \ge A_{th}, A(t+\Delta t) \ge A_{th}\right) = 1-u-v+C(u,v) \tag{4.79}$$

Details are given in Appendix C.

The functions of the Copulas that are investigated here are all included in the category of Archimedean Copulas and are given in [14]:

$$C(u,v) = \left(u^{-\theta} + v^{-\theta} - 1\right)^{-1/\theta}, \theta \in \left(0,+\infty\right) \tag{4.80}$$

$$C(u,v) = \exp\left[-\left(\left(-\ln u\right)^{\theta} + \left(-\ln v\right)^{\theta}\right)^{1/\theta}\right], \theta \in [1,+\infty) \tag{4.81}$$

The performance of the above Copulas is going to be investigated firstly using the joint exceedance probability of rain attenuation for different time lags for the Spino d'Adda experiment, as these are given in [Fabbro09]. The excedance probability of rain attenuation shown in Figure 4.48 and Figure 4.49 refer to the experiment which took place at Spino d'Adda, Italy for two different frequencies, at 19GHz and 40GHz, respectively. The joint CCDFs are considered for time lags of 1 min and 60 min. It can be observed that for 1 min and 60 min time lags the Copula of the expression shown in (4.80) gives a better performance comparing to the Copula of (4.81). In Figure 4.50, the experimental CCDFs are derived from data in Kuala Lumpur of Malaysia for frequency of the link equal at 12GHz and the elevation angle, 77.43^{o} and the joint statistics are given for time delays of 3 and 10 min [Ismail00]. It can be referred that for the 3 min delay Copula of (4.81) has a better performance than this of (4.80), while for the 10 min delay the Copula function given in (4.80) has a better performance than this of (4.81). The same observations can be made from Table VIII, in which the rms value of the relative error is given.

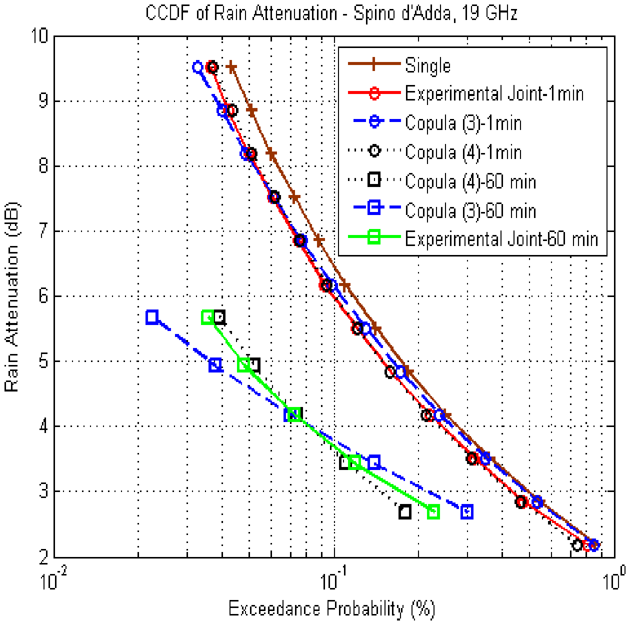

Figure 4.48 Time diversity prediction performance in Spino d’Adda at 19GHz

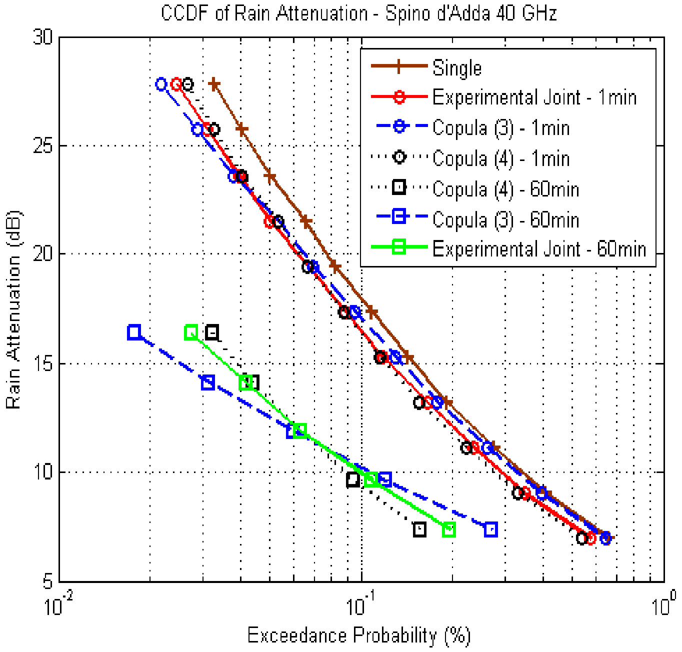

Figure 4.49Time diversity prediction performance in Spino d’Adda at 40GHz

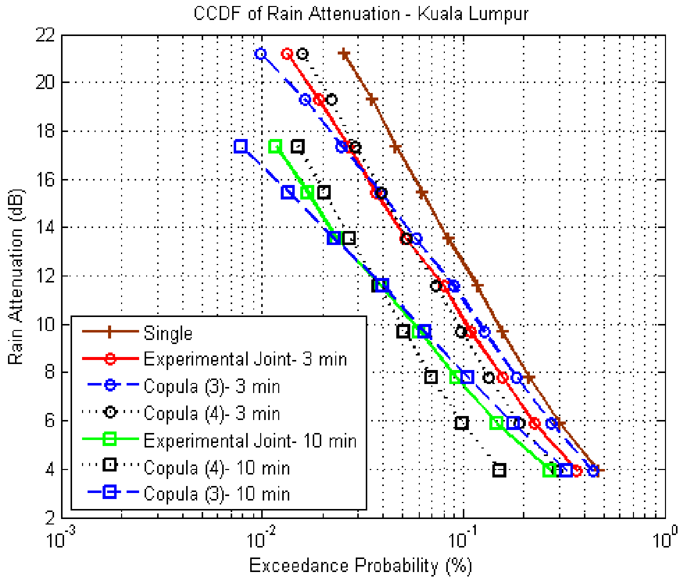

Figure 4.50 Time diversity prediction performance in Kuala Lumpur, at 12GHz

TABLE VIII. RMS value of relative error for the two copulas for the three experiments

Experiment Copula	Spino d'Adda 19GHz	Spino d'Adda 40GHz	Kuala Lumpur 12GHz
Copula (3)	16.87 %	19 %	17.72 %
Copula (4)	8.62 %	11 %	23.25 %

Appendix A: Single Variable IG Distribution

Suppose that the random variable X, X>0, follows the IG distribution. The PDF of X is given by [Chikkara89]:

$$f_X(x) = \sqrt{\frac{\lambda}{2\pi}} x^{-3/2} \exp\left(-\frac{\lambda (x-\mu)^2}{2\mu^2 x} \right) \tag{A.1}$$

where, λ and μ are the two parameters of the IG distribution, both positive. The n-th moment, with n an integer of the IG distribution is [Chikkara89]:

$$E\left[x^n\right] = \mu^n \sum_{k=0}^{n-1} \frac{(n-1+k)!}{k!(n-1-k)!} \left(2\frac{\lambda}{\mu} \right)^{-k} \tag{A.2}$$

where E[.] denotes the expectation operator. From (A.2), the mean value and the variance of random variable X are:

$$m_{x,1} = E\left[x\right] = \mu \tag{A.3}$$

$$\sigma_x^2 = E\left[x^2\right] - E\left[x\right]^2 = \frac{\mu^3}{\lambda} \tag{A.4}$$

In case that a moment of X of a non-integer order b is required, this can be calculated from:

$$m_b = E\left[x^b\right] = \int_0^{+\infty} x^b f_X(x)dx = 2\sqrt{\frac{\lambda}{2\pi}} e^{\lambda/\mu} \left(\mu^2\right)^{\frac{b-1/2}{2}} K_{b-1/2}\left(\frac{\lambda}{\mu}\right) \tag{A.5}$$

where $K_n(x)$ is the modified Bessel function of second kind of order n. Equation (A.5), has been derived considering the definition of the moment of an IG random variable and the integral 9, in page 368 of [Gradshteyn07]. Finally from [Chikkara89] the CDF and CCDF of X are:

$$P\left[X \le x_{th}\right] = Q\left(\sqrt{\frac{\lambda}{x_{th}}}\left(1 - \frac{x_{th}}{\mu}\right)\right) + e^{2\frac{\lambda}{\mu}} Q\left(\sqrt{\frac{\lambda}{x_{th}}}\left(1 + \frac{x_{th}}{\mu}\right)\right) \tag{A.6}$$

$$P\left[X \ge x_{th}\right] = 1 - P\left[X \le x_{th}\right] \tag{A.7}$$

where Q(.) is the Gaussian Q-function:

$$Q(x) = \frac{1}{\sqrt{2\pi}} \int_x^{+\infty} e^{-\frac{t^2}{2}} dt = \frac{1}{2}\operatorname{erfc}\left(\frac{x}{\sqrt{2}}\right) \tag{A.8}$$

Appendix B: Bivariate IG Distribution

Assuming that two variables X_1 and X_2 which are greater than zero each of them follows the IG distribution with parameters μ_1, λ_1 and μ_2, λ_2, and PDFs $f_{X_1}(X_1)$ and $f_{X_2}(X_2)$, respectively, the bivariate PDF is constructed as follows [Chikkara89], [Al-Hussaini81]:

$$f_{X_1,X_2}(X_1, X_2) = f_{X_1}(X_1) \cdot f_{X_2}(X_2) \cdot \left[1 + \rho \cdot \Psi(X_1, X_2)\right] \tag{B.1}$$

with

$$\begin{aligned} \Psi(X_1, X_2) = {} & 8\sqrt{\lambda_1\lambda_2 / \mu_1^3\mu_2^3} \cdot \left(X_1 - \mu_1\right) \cdot \left(X_2 - \mu_2\right) \\ & \cdot \exp\left[-\left(\frac{\lambda_1\left(X_1 - \mu_1\right)^2}{2\mu_1^2 X_1}\right) + \left(\frac{\lambda_2\left(X_2 - \mu_2\right)^2}{2\mu_2^2 X_2}\right)\right] \end{aligned} \tag{B.2}$$

and ρ is the correlation coefficient between the random variables X_1 and X_2. In order that the PDF be positive, it must hold that: $-a \le \rho \le b$ with

$$-a = \max(-1, -\frac{1}{M}),\ b = \min(\frac{1}{N}, 1) \text{ and } M = \max_{x_1,x_2>0} \Psi\left(x_1, x_2\right),\ -N = \min_{x_1,x_2>0} \Psi\left(x_1, x_2\right)$$

The joint CDF of the two variables X_1 and X_2 is given [Chikkara89], [Al-Hussaini81]:

$$P[X_1 \le x_1, X_2 \le x_2] = P[X_1 \le x_1] \cdot P[X_2 \le x_2] + \rho \cdot H(x_1, x_2) \tag{B.3}$$

where

$$\begin{aligned} H(x_1,x_2) &= \int_0^{x_1}\int_0^{x_2}\Psi(X_1,X_2)f_{X_1}(X_1)f_{X_2}(X_2)dX_2dX_1 \\ &= 16\sqrt{\frac{\lambda_1\lambda_2}{\mu_1\mu_2}}\exp\left[4\left(\frac{\lambda_1}{\mu_1}+\frac{\lambda_2}{\mu_2}\right)\right]Q(C_1)Q(C_2) \end{aligned} \tag{B.4}$$

with Q( ) is the Gaussian Q-function and is related to the complementary error function erfc() as shown in (A.8) and

$$\left.\begin{aligned} C_i &= \left[2\left(\frac{4\lambda_i}{\mu_i}+z_i^2\right)\right]^{1/2} \\ z_i &= \frac{\sqrt{\lambda_i}(x_i-\mu_i)}{\mu_i\sqrt{x_i}} \end{aligned}\right\}(i=1,2) \tag{B.5}$$

In case that in joint CDF or CCDF of bivariate IG distribution the one threshold value depends on the other random variable (MRC case of 3.4 subsectionSection), the following expressions are used:

$$\begin{aligned} &P\left[X_1\geq x_1, X_2\geq g(X_1)\right]=\int_{x_1}^{+\infty}\int_{g(X_1)}^{+\infty}f_{X_1,X_2}(X_1,X_2)dX_2dX_1= \\ &=\int_{x_1}^{+\infty}\int_{g(X_1)}^{+\infty}f_{X_1}(X_1)\cdot f_{X_2}(X_2)dX_2dX_1+\rho\int_{x_1}^{+\infty}\int_{g(X_1)}^{+\infty}f_{X_1}(X_1)\cdot f_{X_2}(X_2)\Psi(X_1,X_2)dX_2dX_1=I_1+I_2 \end{aligned} \tag{B.6}$$

The calculation of I_1 is straightforward:

$$I_1=\int_{x_1}^{+\infty}f_{X_1}(X_1)\cdot P\left[X_2\geq g(X_1)\right]dX_1 \tag{B.7}$$

where

$$P\left[X_2\geq g(X_1)\right]=1-P\left[X_2\leq g(X_1)\right] \tag{B.8}$$

and $P\left[X_2\leq g(X_1)\right]$ is given by (A.6).

For the computation of I_2 we denote the function $\Psi_i(.)$, with

$$\Psi_i(x)=\sqrt{8}\sqrt{\frac{\lambda_i}{\mu_i^3}}(x-\mu_i)\exp\left[-\left(\frac{\lambda_i(x-\mu_i)^2}{2\mu_i^2x}\right)\right] \tag{B.9}$$

such as $\Psi(X_1,X_2)=\Psi_1(X_1)\cdot\Psi_2(X_2)$. Now it holds for I_2 that:

$$I_2=\rho\int_{x_1}^{+\infty}f_{X_1}(X_1)\Psi_1(X_1)\int_{g(X_1)}^{+\infty}f_{X_2}(X_2)\Psi_2(X_2)dX_2dX_1 \tag{B.10}$$

The inner integral of (B.10) is :

$$\int_{g(X_1)}^{+\infty}f_{X_2}(X_2)\Psi_2(X_2)dX_2=\sqrt{8}\sqrt{\frac{\lambda_2}{\mu_2}}\frac{1}{\sqrt{2\pi}}\int_{g(X_1)}^{+\infty}\frac{1}{x}\frac{\sqrt{\lambda_2}(x-\mu_2)}{\mu_2\sqrt{x}}e^{-\frac{\lambda_2(x-\mu_2)^2}{\mu_2^2x}}dx \tag{B.11}$$

Making the substitution $y = \frac{\sqrt{\lambda_2}(x-\mu_2)}{\mu_2\sqrt{x}}$, (B.11) becomes:

$$I_3 = \sqrt{8}\sqrt{\frac{\lambda_2}{\mu_2}}\frac{2}{\sqrt{2\pi}}\int_{y_{th}}^{+\infty}\frac{y}{\sqrt{4\frac{\lambda_2}{\mu_2}+y^2}}e^{-y^2}dy \tag{B.12}$$

with $y_{th} = \frac{\sqrt{\lambda_2}(g(X_1)-\mu_2)}{\mu_2\sqrt{g(X_1)}}$.

Finally, making a last substitution $w = \sqrt{2\left(4\frac{\lambda_2}{\mu_2}+y^2\right)}$, I_3, (B.12), becomes:

$$I_3 = 4\sqrt{\frac{\lambda_2}{\mu_2}}e^{4\frac{\lambda_2}{\mu_2}}Q(C_2) \tag{B.13}$$

with Q, the Gaussian Q-function and

$$\begin{gathered} C_2 = \left[2\left(\frac{4\lambda_2}{\mu_2}+y_2^2\right)\right]^{1/2} \\ y_2 = \frac{\sqrt{\lambda_2}\left(g(X_1)-\mu_2\right)}{\mu_2\sqrt{z_2}} \end{gathered} \tag{B.14}$$

Consequently, from all the above (B.6) becomes:

$$\begin{aligned} P\left[X_1 \geq x_1, X_2 \geq g(X_1)\right] = \int_{x_1}^{+\infty} f_{X_1}(X_1)\cdot P\left[X_2 \geq g(X_1)\right]dX_1 + \\ 4\rho\sqrt{\frac{\lambda_2}{\mu_2}}e^{4\frac{\lambda_2}{\mu_2}}\int_{x_1}^{+\infty} f_{X_1}(X_1)\Psi_1(X_1)Q(C_2)dX_1 \end{aligned} \tag{B.15}$$

Appendix C: Copulas Theory

Copula functions are used to couple the single marginal distributions in order to derive the joint marginal distributions of two dependent random variables. More particularly, as given in [Nelsen06], for the bivariate case, it holds that:

$$H(x,y) = P\left(X \leq x, Y \leq y\right) = C\left(F(x), G(y)\right) \tag{C.1}$$

where $F(x)$ and $G(y)$ denote the marginal distributions, i.e. $P\left[X \leq x\right] = F(x)$ and $P\left[Y \leq y\right] = G(y)$, C(.) the Copula function. Assuming two random variables, *u* and *v*, which are uniformly distributed in [0,1], they can be considered equal to $F(x)$ and $G(y)$, respectively. Therefore, (C.1) becomes:

$$H\left(F^{-1}(u), G^{-1}(v)\right) = C(u,v) \tag{C.2}$$

The most studied Copula functions refer to the bivariate case and a part of them have been identified in [Nelsen06]. A problem that arises is that most of Copulas are given in order to compute the joint Cumulative Distribution Function (CDF) of two correlated variables. In the case of rain attenuation, what is needed and used in the system evaluation procedure is the Complementary CDF (CCDF). For the latter case, it holds that [Papoulis02]:

$$\begin{aligned} P[X \geq x, Y \geq y] = 1 - P[X \leq x] - P\left[Y \leq y\right] \\ + P\left[X \leq x, Y \leq y\right] \end{aligned} \tag{C.3}$$

Using (C.1) and (C.2) to (C.3), the joint CCDF becomes:

$$P[X \geq x, Y \geq y] = 1 - u - v + C(u,v) \tag{C.4}$$

Therefore we can relate the Copula functions to CCDF of random variables.

5 Rain Attenuation and Scintillation Dynamics Modeling

In this Chapter, the second order statistics of rain attenuation and scintillation are studied and time series synthesizers are proposed. Firstly, starting from the model proposed by Maseng-Bakken [Maseng81], the dynamic parameter of rain attenuation is modeled as a function of the dynamic parameter of rain rate, the electrical and geometric characteristics of the link. The methodology has been presented in [J1]. Then, a time series synthesizer for rain attenuation time series induced at MEO/LEO slant paths is proposed extending the Maseng-Bakken model introducing time dependent parameters. Moreover, a model for predicting of first order statistics of fade slope is proposed for a LEO/MEO link. The results of the first two Sections have been presented in [J1] and [C1], [C2], [C3].

Secondly, a synthesizer based on Copula functions is described assuming that the temporal joint statistics of rain attenuation can be described through Gaussian Copulas. The synthesizer takes into account the difference in rainy conditions for temperate and tropical climates and reproduces the first order statistics of rain attenuation and the temporal Kendall's τ correlation. The synthesizer has been presented in [C4]. Further on this Chapter, multi-dimensional stochastic differential equations are used for developing a space-time rain rate field generator in order to synthesize two-dimensional fields of rain rate correlated also on temporal domain. Using the time series of two-dimensional fields and numerical expressions, rain attenuation time series can be generated from the rain rate fields for single and spatially separated links. The generator has been presented in [C5].

Finally, a scintillation time series synthesizer is proposed based on SDEs driven by fractional Brownian motion (fBm) and reproduces the first order and second order statistics of scintillation. The synthesizer has been presented in [C6].

[J1] C. I. Kourogiorgas, A. D. Panagopoulos, "A Rain Attenuation Stochastic Dynamic Model for LEO Satellite Systems Operating at Frequencies above 10 GHz", IEEE Transactions on Vehicular Technology, vol. 64, issue 2, Feb. 2015.

[C1] C. Kourogiorgas, A. D. Panagopoulos, J. D. Kanellopoulos, "Synthesizing Rain Attenuation Time Series for an Earth-LEO Satllite Link", MCM7 COST Action IC0802, 16-18 April 2012, Portsmouth, Great Britain.

[C2] C. Kourogiorgas, A. D. Panagopoulos, J. D. Kanellopoulos, P.-D. M. Arapoglou, "Rain Attenuation Time Series Synthesizer for LEO Satellite Systems Operating at Ka Band", ASMS/SPSC 2012, 5-7 September 2012, Baiona, Spain.

[C3] C. Kourogiorgas, A. D. Panagopoulos, P.-D. M. Arapoglou,"Rain Attenuation Time Series Generator for Medium Earth Orbit Links Operating at Ka Band and above", EuCAP 2014, 6-11 April 2014, The Hague, The Netherlands.

[C4] C. Kourogiorgas, G. A. Karagiannis, A. D. Panagopoulos, "Space-Time Rain Rate Field Generator for Multi-Antenna Satellite Communication Applications", EuCAP 2013, 8-12 April 2013, Gothenburg, Sweden.

[C5] C. Kourogiorgas, A. D. Panagopoulos, "A Tropospheric Scintillation Time Series Synthesizer based on Stochastic Differential Equations", 2013 Joint Conference: 19th Ka and Broadband Communications, Navigation and Earth Observation Conference and 31st AIAA ICSSC, 14-17 October 2013, Florence, Italy.

[C6] C. Kourgiorgas, A. Kelmendi, A. D. Panagopoulos, S. N. Livieratos, A. Vilhar, G. E. Chatzarakis, "Rain Attenuation Time Series Synthesizer based on Copula Functions", EuCAP 2015, Lisboa, April 2015.

5.1 Modeling of dynamic parameter of rain attenuation

Point rainfall rate (R_t) and rain attenuation (A_t) stochastic processes are assumed to follow the lognormal distribution and the first-order stochastic differential equations, [Panagopoulos03], [Manning90] and [Lin75]. Therefore, both rain rate and rain attenuation can be described by the model in [Maseng81]. The Transition Probability Density Functions (TPDF) of A_t and R_t are lognormal distributions with parameters $A_{m,T}$, $R_{m,T}$ the median values of the TPDF of rain attenuation and rain rate, that are given from the following relationships:

$$\left.\begin{aligned} A_{m,T} &= A_m^{(1-\exp(-\beta_A|\Delta t_A|))} A_0^{\exp(-\beta_A|\Delta t_A|)} \\ R_{m,T} &= R_m^{(1-\exp(-\beta_R|\Delta t_R|))} R_0^{\exp(-\beta_R|\Delta t_R|)} \end{aligned}\right\} \tag{5.1}$$

and $S_{A,T}$ and $S_{R,T}$ the standard deviation of the natural logarithm of the random variables A_T and R_T, respectively:

$$\left.\begin{aligned} S_{A,T}^2 &= S_A^2(1-\exp(-2\beta_A|\Delta t_A|)) \\ S_{R,T}^2 &= S_R^2(1-\exp(-2\beta_R|\Delta t_R|)) \end{aligned}\right\} \tag{5.2}$$

We consider that the two lognormal random variables A_T and R_T, referring to rain attenuation and rain rate, respectively, are related with a power law expressions similar to rain rate and rain attenuation [ITU-R. P.838]:

$$A_T = \int_0^{L(\theta)} k R_T^b(x)dx \tag{5.3}$$

with $L(\theta) = L_s \cdot \cos(\theta)$ being the projection of the slant path under rain on ground. From (5.3) and following the assumption that the long-term statistics of rain rate are constant on a slant path (more details can be found in [Crane03] and [Panagopoulos03]) the mean value of A_T is:

$$\mu_{A_T} = E\{A_T\} = k m_{R_T,b} L(\theta) \tag{5.4}$$

where E{ } is the expectance operator in time domain and $m_{R_T,b}$ is the statistical moments of R_T of order b

The second moment of A_T is:

$$E\{A_T^2\} = \int_0^L \int_0^L E\{kR_T^b(x) kR_T^b(x')\} dx dx' \tag{5.5}$$

Employing now the same correlation coefficient (ρ) of the specific rain attenuation $\Gamma_T(x) = kR_T^b(x)$, for the transition probability distributions case, it holds that [Panagopoulos03] and [Lin75]:

$$\rho = \frac{g}{\sqrt{g^2 + d^2}} \tag{5.6}$$

From (5.6) and assuming that the 2b moment of R_T ($m_{R_T,2b}$) is also constant along the path, standard deviation of A_T becomes:

$$\sigma_{A_T}^2 = k^2 \left(m_{R_T,2b} - m_{R_T,b}^2 \right) H_1 \tag{5.7}$$

where $H_1 = \int_0^{L(\theta)} \int_0^{L(\theta)} \rho(x, x') dx dx'$ and in analytical form is:

$$H_1(\theta_t) = 2L(\theta_t) g \sinh^{-1}\left(\frac{L(\theta_t)}{g} \right) + 2g^2 \left[1 - \sqrt{\left(\frac{L(\theta_t)}{g} \right)^2 + 1} \right] \tag{5.8}$$

Since A_T follows the lognormal distribution from (5.4) and (5.7) holds that:

$$S_{A,T} = \sqrt{\ln\left\{ 1 + \frac{H_1}{L^2} \left[\exp\left(b^2 S_{R,T}^2 \right) - 1 \right] \right\}} \tag{5.9}$$

and replacing them in (5.1) and (5.2) the following expression is obtained:

$$\beta_A(\theta, |\Delta t_A|) = -\frac{1}{2|\Delta t_A|} \ln\left\{ 1 - \frac{1}{S_A^2} \ln\left\{ 1 + \frac{H_1(\theta)}{L(\theta)^2} \left[\exp\left(b^2 S_R^2 (1 - \exp(-2\beta_R |\Delta t_R|)) \right) - 1 \right] \right\} \right\}$$

(5.10)

Firstly, we investigate the sensitivity of the elevation angle and time dependent dynamic parameter of rain attenuation as this is calculated from (5.10) for the region of Athens, Greece. The rain rate dynamic parameter of is considered equal to 0.001 sec^{-1}, a value obtained from experimental measured rain rate time series in Athens [Kourogiorgas12]. In Figure 5.1, the values of the dynamic parameter of rain attenuation are given for different elevation angles and different values of the parameter *g* of the spatial correlation of the specific rain attenuation. From this first Figure we can observe that the dynamic parameter of rain attenuation is smaller than this of rain rate. This occurs due to the fact that rain attenuation is the integral over the slant path of the specific rain attenuation and so an averaging over the path is performed. Therefore, the temporal autocorrelation of rain attenuation is higher than this of rain rate. Moreover, the dynamic parameter of rain attenuation is increasing as the elevation angle increases. The latter point results from the fact that the effect of averaging becomes less as the slant path decreases and so the temporal autocorrelation of rain attenuation is decreasing. Furthermore, as the elevation angle tends to 90° the dynamic parameter of rain attenuation tends to the value of this of rain rate and it results from the fundamental Crane's assumption that the vertical profile of rain rate is uniform [Crane03]. From the same Figure, it can be also observed that increasing the parameter *g* and the frequency of the link the rain attenuation dynamic parameter is also increasing.

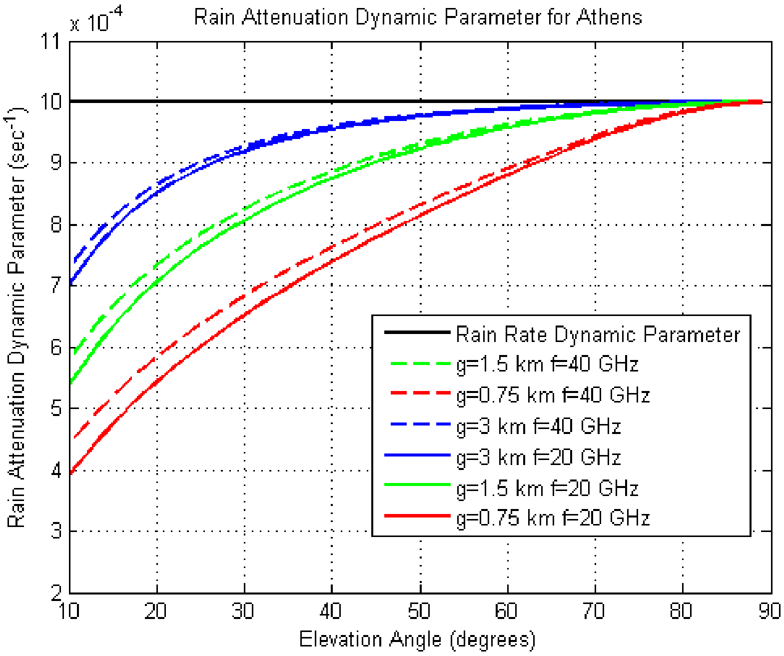

Figure 5.1 Rain attenuation dynamic parameter vs elevation angle for Athens, Greece for different values of *g* parameter and frequency of the link.

Moreover, the autocorrelation of rain attenuation is investigated for various elevation angles using the expression of β_{α} derived previously. Here, considering that rain attenuation at a given elevation angle follows the M-B model, the autocorrelation function of rain attenuation is calculated as [Maseng81]:

$$R_a(\tau) = A_m^2 \exp\left(S_{\ln A}^2 \left(1+\rho(\tau)\right)\right) \tag{5.11}$$

with

$$\rho(\tau) = \exp\left(-\beta_\alpha \, |\, \tau \,|\right) \tag{5.12}$$

Using the previous two expressions and the methodology presented in [Panagopoulos03] for the calculating the parameters A_m and $S_{\ln A}$ the autocorrelation function of rain attenuation for various time intervals and frequency of 25 GHz was calculated and shown in Figure 5.2.

In Figure 5.3, the autocorrelation function is shown for different frequencies, while in Figure 5.4 for various values of g parameter. g parameter gives the distance between two points, where the spatial correlation of specific rain attenuation is reduced by a factor $1/\sqrt{2}$. The higher the g parameter, the more stratiform rain is the dominant type of rain, since in stratiform rain, rainfall rate has a higher spatial correlation. It can be observed that the autocorrelation function always decreases as the elevation increases and/or the increase of time delay. Moreover, as the frequency is increasing, the autocorrelation increases. A similar observation is also made in [Luini13] with the processing of radar data, for the spatial correlation of rain attenuation. Following the Taylor's hypothesis, the calculated autocorrelation can be translated also into the spatial domain. Finally, as expected, the more stratiform rain occurs the higher the autocorrelation of rain attenuation.

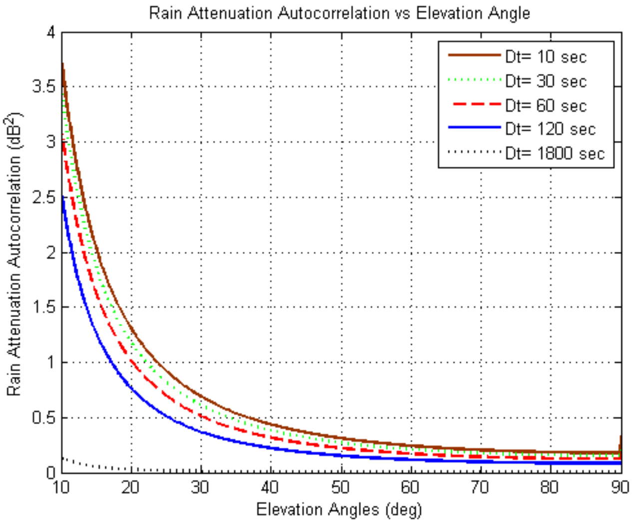

Figure 5.2 Rain attenuation autocorrelation functions for various time delays and elevation angles.

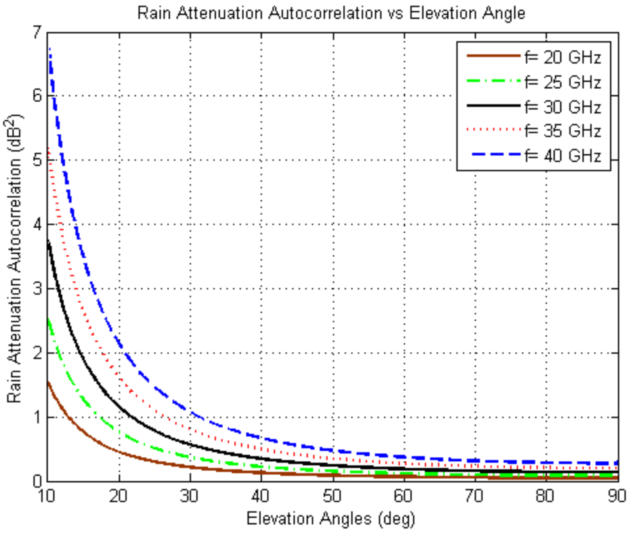

Figure 5.3 Rain attenuation autocorrelation functions for various frequencies and elevation angles

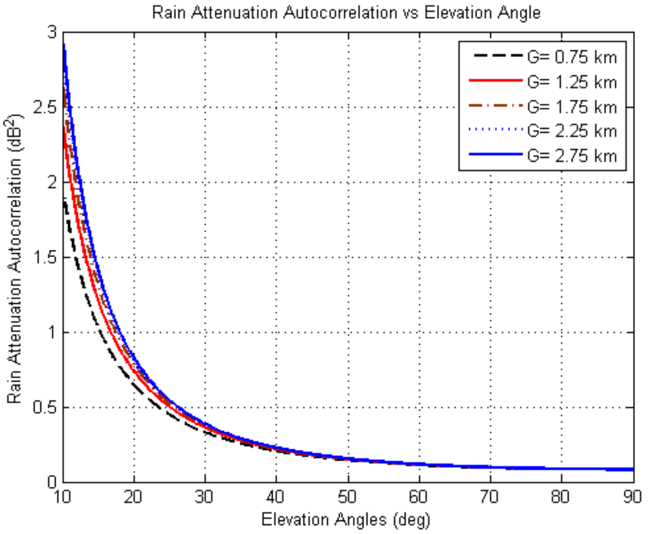

Figure 5.4 Rain attenuation autocorrelation functions for various values of *G* parameter and elevation angles

5.2 Stochastic Dynamic MEO/LEO Channel Model Operating Above 10GHz

5.2.1 The Dynamic Model

Lognormal distribution is a well-accepted distribution to model long-term the rain attenuation exceedance probability for fixed satellite communication links (with given elevation angles) [Panagopoulos03], [Panagopoulos04a]. We also consider the assumption for unconditional lognormal distribution in order to model the rain attenuation induced on a fixed elevation angle slant path [Panagopoulos03]. In view of the lack of available measurements of rain attenuation for LEO channels, we properly modify the M-B model in [Maseng81] to take into account the time-dependent elevation angle $\theta_t = \theta(t)$ of LEO satellite. In the proposed modification and given that rain attenuation depends on the elevation angle, the parameters of the SDE proposed in [Maseng81] are time-dependent and therefore, the following SDE for the rain attenuation (A_t^{LEO}) of a LEO satellite channel operating above 10GHz is proposed:

$$dA_t^{LEO} = A_t^{LEO}\beta_A(\theta_t)\left[S_A^2(\theta_t) - \ln\left(A_t^{LEO} / A_m(\theta_t)\right)\right]dt + \sqrt{2\beta_A(\theta_t)}A_t^{LEO}S_A(\theta_t)\,dW_t \tag{5.13}$$

In (5.13), the following four parameters must be defined: $A_m(\theta_t), S_A(\theta_t)$, $\beta_A(\theta_t)$ and dW_t. The parameters $A_m(\theta_t)$ and $S_A(\theta_t)$ are the statistical rain attenuation parameters of lognormal distribution for every elevation angle at every time instant. More particularly, $S_A(\theta_t)$ is the standard deviation of the natural logarithm of rain attenuation and $A_m(\theta_t)$ the median value of rain attenuation, both referring to a specific elevation angle θ_t. These parameters can be calculated in terms of rainfall rate by employing the described rainfall rate model described in [Panagopoulos03].

Moreover, from (5.13), $\beta_A(\theta_t)$ is the dynamic parameter of rain attenuation for a given time and that corresponds to an elevation angle of the LEO satellite channel. dW_t are the Brownian increments, i.e. Gaussian process with zero mean and variance equal to dt. In the previous Section, a novel analytical methodology for the calculation of $\beta_A(\theta_t)$ in terms of resolution time delay lag ($|\Delta t_A|$) was calculated and the simple following closed form was obtained:

$$\beta_A(\theta_t, |\Delta t_A|) = -\frac{1}{2|\Delta t_A|}\ln\left\{1 - \frac{1}{S_A^2}\ln\left\{1 + \frac{H_1(\theta_t)}{L^2(\theta_t)}\left[\exp\left(b^2 S_R^2\left(1 - \exp\left(-2\beta_R(|\Delta t_R|)\cdot|\Delta t_R|\right)\right)\right) - 1\right]\right\}\right\} \tag{5.14}$$

In (5.14), β_R is the dynamic parameter of rainfall rate and it has been computed in [Kourogiorgas12] and [Burgueno90], b the power parameter of the power law expression between rain rate (R) and specific rain attenuation ($\Gamma = kR^b$) [ITU-R. P.838]. Here it must be noted that the parameters of k and b of specific rain attenuation depend on the polarization, frequency and elevation angle of the link. Moreover, S_R is the standard deviation of the natural logarithm of rain rate ($\ln R$), considering that rain rate follows the lognormal distribution, Δt_R the temporal resolution of rain rate time series, $L(\theta_t)$ is the projection of the slant path on the ground for elevation angle equal to θ_t and

$$H_1(\theta_t)=2L(\theta_t)\,g\sinh^{-1}\left(\frac{L(\theta_t)}{g}\right)+2g^2\left[1-\sqrt{\left(\frac{L(\theta_t)}{g}\right)^2+1}\right] \tag{5.15}$$

with g a parameter on which the spatial correlation of specific rain attenuation depends, as also described in Section 4.1.

An advantage of (5.15) is that it requires as input the link characteristics, i.e. elevation angle, polarization and frequency of the link, as well as the lognormal parameters and the dynamic parameter of rainfall rate, thus making the need of rain attenuation experimental time series unnecessary for the calculation of the dynamic parameter of rain attenuation.

At this point, we present the analytical method for the solution of (5.13). Firstly, we define the transformed stochastic process of rain attenuation for a fixed elevation angle $X_t=\dfrac{\ln\left(A_t/A_m(\theta)\right)}{S_A(\theta)}$ and we are leading to the following equation [Manning90]:

$$dX_t=-\beta_A(\theta)\,X_t dt+\sqrt{2\beta_A(\theta)}dWt \tag{5.16}$$

The above equation describes the transformed process X_t for a constant elevation angle. In case of LEO satellites the elevation angle θ is time dependent (θ_t) and using the general expression of the dynamic parameter $\beta_A(\theta_t,|\Delta t_A|)$ and consequently we have:

$$dX_t^{LEO}=-\beta_A(\theta_t,|\Delta t_A|)\,X_t^{LEO}dt+\sqrt{2\beta_A(\theta_t,|\Delta t_A|)}dWt \tag{5.17}$$

Equation (5.17) can be also written as:

$$X_t^{LEO}=X_0^{LEO}+\int_0^t\left(-\beta_A(\theta_s,|\Delta t_A|)\right)X_s^{LEO}ds+\int_0^t\sqrt{2\beta_A(\theta_s,|\Delta t_A|)}dW_s \tag{5.18}$$

where X_0^{LEO} is the initial value of the process X_t^{LEO}. Considering the time dependent process $Y_t^{LEO}=\int_0^t-\beta_A(\theta_s,|\Delta t_A|)ds$ with 0 initial value and using the transformation process $f(x)=e^{-x}$ on the process Y_t^{LEO} we obtain the process $F_t^{LEO}=e^{-Y_t^{LEO}}$ which is described by $F_t^{LEO}=1+\int_0^t\beta_A(\theta_s,|\Delta t_A|)F_s^{LEO}ds$. Then applying the transformation with two variables $g(x_1,x_2)=x_1\cdot x_2$ over the process F_t^{LEO} and X_t^{LEO} and using the two-dimensional Itô's formula [Karatzas05] we obtain the solution of (5):

$$X_t^{LEO}=e^{-\int_0^t\beta_A(\theta_s,|\Delta t_A|)ds}\left(X_0^{LEO}+\int_0^t\sqrt{2\beta_A(\theta_s,|\Delta t_A|)}\exp\left(\int_0^s\beta_A(\theta_{s'},|\Delta t_A|)ds'\right)dW_s\right) \tag{5.19}$$

where X_0^{LEO} is the initial value of the transformed process X_t^{LEO}. The rain attenuation time series for an Earth-LEO link can be calculated using (7) and employing the following inverse transform:

$$A_t^{LEO} = A_m(\theta_t)\exp\left[X_t^{LEO} S_A(\theta_t)\right] \tag{5.20}$$

Here, it must be noted that the proposed rain attenuation synthesizer does not describe a stationary stochastic process [Karatzas05]. This results from the fact that the input parameters are time dependent due to the temporal variations of the elevation angle of the LEO slant path. Given that the elevation angle is a non-stationary process, the autocorrelation function of rain attenuation will also depend on the time instance on which this is calculated. However, experimental results are needed to verify the non-stationarity property of rain attenuation at LEO slant paths. A flow diagram for the generation of rain attenuation time series for LEO satellite links is presented in Figure 5.5.

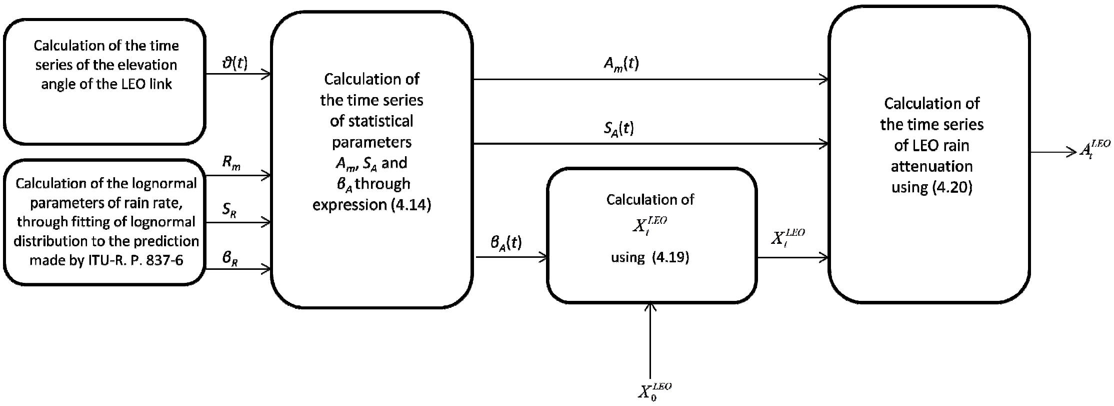

Figure 5.5 Flow diagram for the generation of time series of rain attenuation for LEO links.

5.2.2 *Fade Slope of LEO Channel Prediction Model*

In this Section, we present an analytical prediction model for the calculation of Fade Slope statistics based on the theoretical assumptions of LEO satellite channel model for operation at frequencies above 10GHz. More particularly, we investigate the conditional case of fade slope, that means for a given rain attenuation value at specific instant. For given elevation angles at time instances t (θ_1) and t+Δt (θ_2), we are interested in the LEO satellite fade slope statistics:

$$P\left(\zeta\middle|\theta_1,\theta_2\right) = P\left(\frac{\left|A(t)-A(t+\Delta t)\right|}{\Delta t}\middle| A(t)\right) \tag{5.21}$$

where $A(t)$, $A(t+\Delta t)$ are lognormal random variables with median values $A_m(\theta_1)$ and $A_m(\theta_2)$, respectively and the standard deviation of their natural logarithms $S_A(\theta_1)$ and $S_A(\theta_2)$, respectively. The correlation coefficient between their reduced variables

$u_1 = \dfrac{\ln\left(A(t)/A_m(\theta_1)\right)}{S_A(\theta_1)}$ and $u_2 = \dfrac{\ln\left(A(t+\Delta t)/A_m(\theta_2)\right)}{S_A(\theta_2)}$ is considered $\rho_n = \exp(-\beta_A(\theta_1)\cdot\Delta t)$, where $\beta_A(\theta)$ is the previously given dynamic parameter. Although, the synthesizer given in (5.19) and (5.20) does not generate stationary rain attenuation time series, for the prediction of long-term statistics of fade slope, rain attenuation is approximated as a stationary process (ρ_n expression), in order to facilitate and make feasible the prediction of fade slope statistics through a closed-form expression.

For the LEO satellites, the CCDF of the fade slope can be calculated as:

$$P(\zeta) = \int_{\theta_{\min}}^{\theta_{\max}} \int_{\theta_{\min}}^{\theta_{\max}} P(\zeta \mid \theta_1, \theta_2) p_{\theta_1\theta_2}(\theta_1, \theta_2) d\theta_2 d\theta_1 \tag{5.22}$$

where $P(\zeta|\theta_1,\theta_2)$ is given by (5.21), θ_{min} and $\theta_{\max}$ represent the minimum and the maximum observed elevation angles for the specific LEO satellite, and $p_{\theta_1\theta_2}(\theta_1,\theta_2)$ is the joint PDF of elevation angles at time instances t (θ_1) and t+Δt (θ_2) for the specific LEO satellite link. The fade slope statistics in (5.22) for a ζ greater than zero, is calculated following the analytical model below:

$$P\left(\zeta|\theta_1,\theta_2\right) = P\left(A(t+\Delta t) \geq A(t) + \zeta\Delta t \mid A(t)\right) + P\left(A(t+\Delta t) \leq A(t) - \zeta\Delta t \mid A(t)\right) \tag{5.23}$$

However, the term $P\left(A(t+\Delta t) \leq A(t) - \zeta\Delta t \mid A(t)\right)$ is defined only for $A(t)>\zeta\Delta t$. Employing the bivariate lognormal distribution for the random variables $A_1=A(t)$ and $A_2=A(t+\Delta t)$, we can calculate the terms $P\left(A(t+\Delta t) \geq A(t) + \zeta\Delta t \mid A(t)\right)$ and $P\left(A(t+\Delta t) \leq A(t) - \zeta\Delta t \mid A(t)\right)$ after some simple probabilistic algebra:

$$P\left(A(t+\Delta t) \geq A(t) + \zeta\Delta t \mid A(t)\right) = \int_{u_{2,th}}^{+\infty} \frac{1}{\sqrt{2\pi}\sqrt{1-\rho_n^2}} \exp\left\{-\frac{1}{2}\left[\frac{u_2 - \rho_n u_1}{\sqrt{1-\rho_n^2}}\right]^2\right\} du_2 \tag{5.24}$$

where $u_{2,th} = \dfrac{\ln\left(\left(A(t)+\zeta\Delta t\right)/A_m(\theta_2)\right)}{S_A(\theta_2)}$.

Consequently, (5.24) is the CCDF of a normal distribution with mean value $\rho_n u_1$ and standard deviation $\sqrt{1-\rho_n^2}$. Similarly, for the term $P\left(A(t+\Delta t) \leq A(t) - \zeta\Delta t \mid A(t)\right)$, defined only for A(t)>ζΔt, we have:

$$P\left(A(t+\Delta t) \leq A(t) - \zeta\Delta t \mid A(t)\right) = \int_{-\infty}^{u_{2,th1}} \frac{1}{\sqrt{2\pi}\sqrt{1-\rho_n^2}} \exp\left\{-\frac{1}{2}\left[\frac{u_2 - \rho_n u_1}{\sqrt{1-\rho_n^2}}\right]^2\right\} du_2 \tag{5.25}$$

where $u_{2,th1} = \dfrac{\ln\left(\left(A(t)-\zeta\Delta t\right)/A_m(\theta_2)\right)}{S_A(\theta_2)}$

Also, (5.25) is the CDF of a normal distribution with mean value $\rho_n u_1$ and standard deviation $\sqrt{1-\rho_n^2}$. The single integrals in (5.24) and (5.25) are converging fast due to the descending nature of the integrant functions

5.2.3 Numerical Results and Discussion

The first scenario concerns communication satellite downlinks employing the IRIDIUM LEO satellite. For this second scenario two Earth stations are considered, one in Athens (GR) and one in Paris (FR), and two different radio frequencies will be investigated, 20 GHz (Ka band) and 40 GHz (Q/V band). For both scenarios we consider that the communication between the LEO satellite and the Ground station occurs for elevation angles higher than 10^o.

Hereafter, we may make the simplifying assumption that the dynamic parameter of rain rate is considered constant for all the places around the globe. The motivation of such an assumption comes from the comparison of the value of the estimated value of dynamic parameter of rain rate from measurements in Athens [Kourogiorgas12] and in Barcelona [Burgueno90]. However, different values can be given as input to (5.14) conditioned that there are local rain rate time series measurements in the desired area. In Figure 5.6, a snapshot of rain attenuation time series for a link between a Ground station in Athens and the IRIDIUM LEO satellite at 20 GHz (Ka band) during one orbit of the satellite is shown. From the simulated time series the exceedance probability of rain attenuation has been calculated. More particularly, in Figure 5.7, the theoretical and the simulated LEO CCDF of rain attenuation are shown. As it can be observed the simulated exceedance probability is almost identical to the theoretical one. Therefore, it can be remarked that the time series synthesizer reproduces the first order statistics of rain attenuation for a LEO slant path. However, the model needs to be tested against experimental data which are not available yet at the research satellite propagation community.

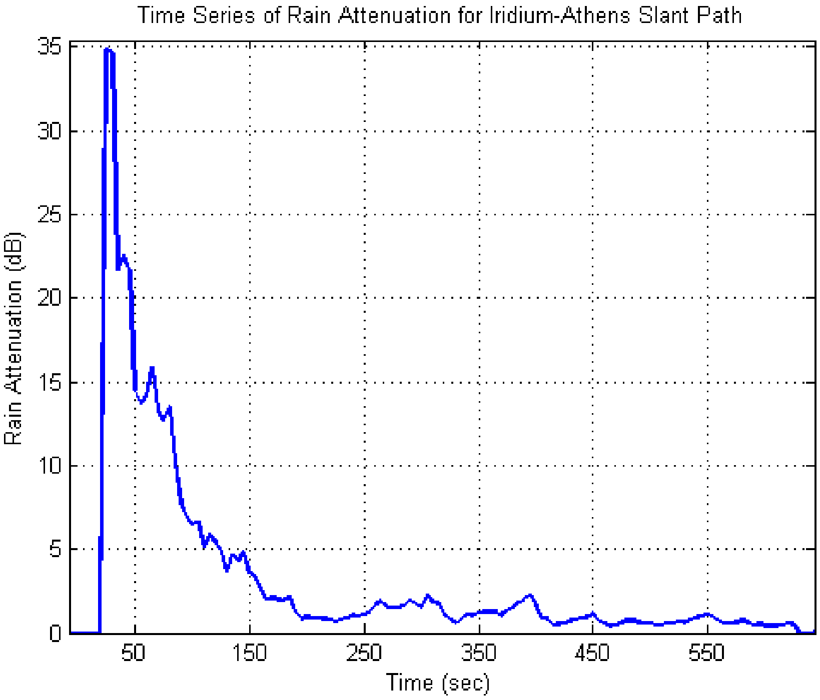

Figure 5.6 Snapshot of time series of rain attenuation during one orbit of the IRIDIUM, in Athens, at 20GHz

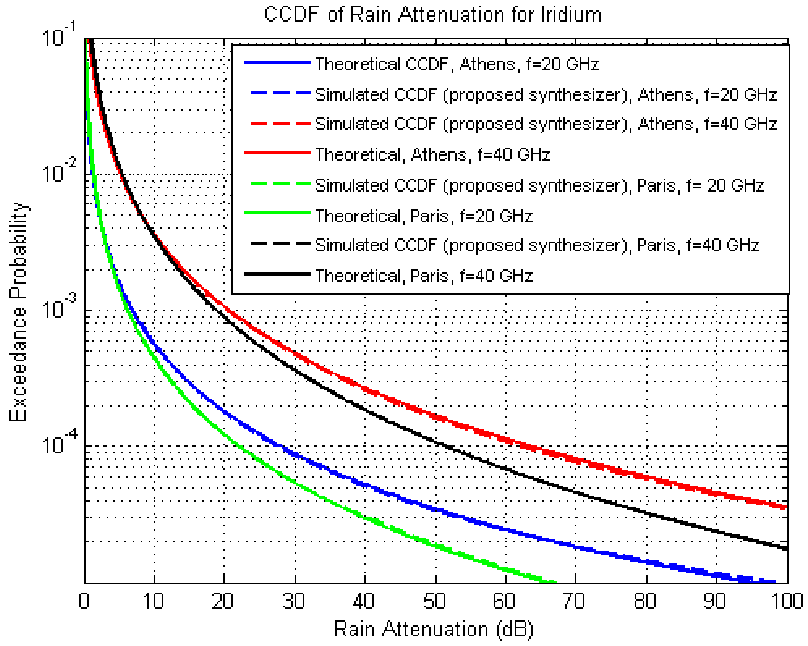

Figure 5.7 CCDF of rain attenuation for LEO links between IRIDIUM satellite and ground stations Athens, Paris, for *f*=20GHz (blue lines and green lines, respectively) and *f*=40GHz (red lines and black lines, respectively) derived from theoretical calculations (solid lines) and from time series (dashed lines)

Furthermore, considering the validation of the proposed rain attenuation synthesizer, an Earth station located in Athens and one MEO satellite from the O3b constellation are considered [O3b]. The time series of the elevation angles were obtained from AGI's STK using a satellite with altitude of 8062 km, circular orbit with inclination angle less than 0.1^{o}. In Figure 5.8, time series of a pass of the MEO satellite over the visibility area of the Earth station are shown. In Figure 5.9, the theoretical CCDF of rain attenuation and the one obtained by the synthesizer are depicted for two different frequencies, 20 GHz and 30 GHz. For both frequencies, the synthesizer reproduces the first order statistics. Finally, in Figure 5.11, the rain attenuation CCDF of a MEO slant path with the Earth station located at Kuala Lumpur is shown. The frequency of the link is 35 GHz. As in the case of Figure 5.9, also in this case, the synthesizer reproduces the theoretical first order statistics of rain attenuation.

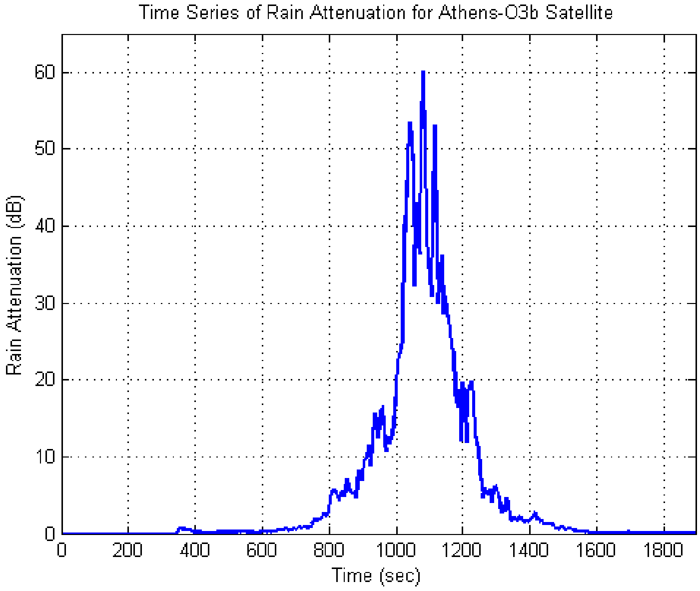

Figure 5.8. Rain attenuation time series snapshot for a pass of the MEO satellite of O3b constellation with the Earth station located at Athens, Greece

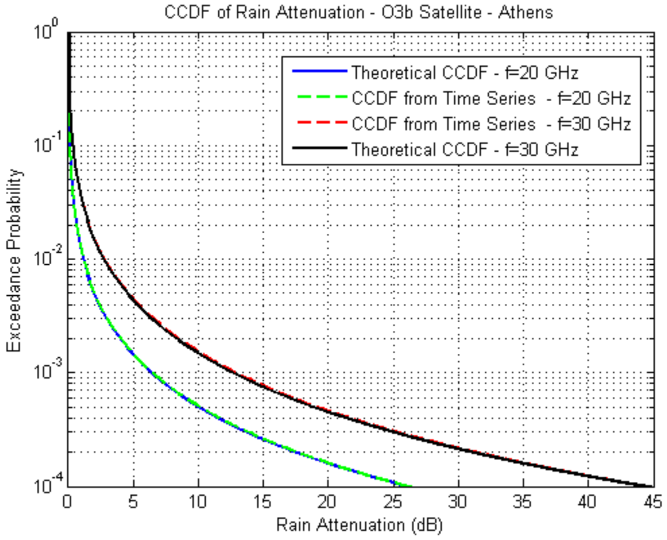

Figure 5.9. CCDF of rain attenuation for an Earth-MEO link with the Earth station located at Athens, Greece.

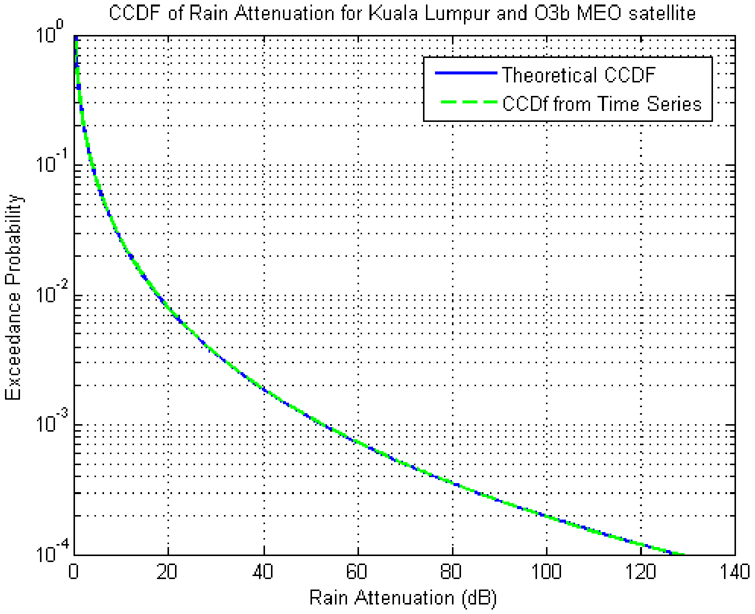

Figure 5.10. CCDF of rain attenuation for an Earth-MEO link with the Earth station located at Kuala Lumpur, Malaysia.

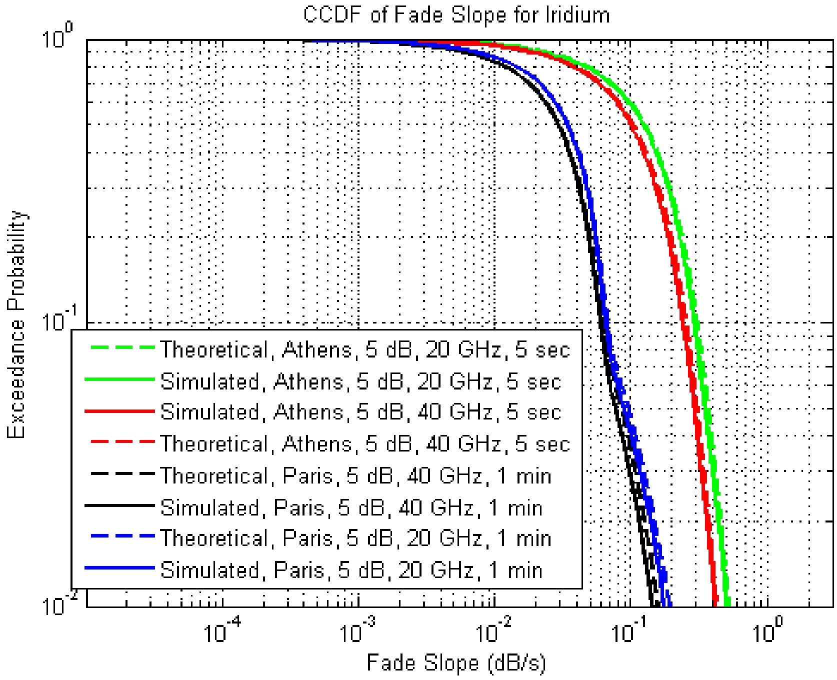

Figure 5.11. CCDF of fade slope (dB/s) for links between IRIDIUM satellite and ground stations in Athens and Paris for rain attenuation threshold 5 dB and two different frequencies 20 GHz and 40 GHz. For Athens Δt= 5 sec and for Paris Δt= 1 min.

Considering the fade slope statistics, for the communications downlink scenario we calculate for the two links between IRIDIUM satellite and the ground stations at Athens and Paris the CCDF of fade slope for attenuation threshold equal to 5 dB and time lag of 5 seconds for Athens and 1 minute for Paris. In Figure 5.11, the exceedance probability of fade slope is presented for the previous configuration for both ground stations. The theoretical values were calculated from (5.22). It can be observed that the theoretical modeling of fade slope is close enough to the CCDF of fade slope resulted from the time series synthesizer proposed. Moreover it can be seen that with the increase of the frequency of the LEO satellite link and/or the decrease of time delay the fade slope decreases.

5.3 Time Series Synthesis of Rain Attenuation Using Copula Functions

The use of copula for modeling joint statistics of rain attenuation has been firstly used in [Kourogiorgas14a], [Livieratos14] for capturing the spatial dependence of rain attenuation and rain rate. Moreover, the study has been extended for temporal dependence and in particular for the joint statistics of rain attenuation for various time delays [Kourogriorgas14b]. It was found that from the Archimedean Copulas the Gumbell Hougard and the Clayton Copula give the least relative error.

5.3.1 Joint Statistics of Rain Attenuation on Temporal Domain Using Gaussian Copula

However, in this Section, the Gaussian Copula will be evaluated for the modeling of joint statistics of rain attenuation on the temporal domain. Generally, Copula functions couple the marginal distributions of two or more random variables. More particularly, given two random variables *X* and *Y* with marginal distributions, i.e. Cumulative Distribution Function (CDF), $F_X(X)=u$ and $G_Y(Y)=v$, with *u*, *v* in the interval [0,1], a bivariate Copula function (C(:,:)) with input the marginal distribution is equal to the joint CDF of the two random variables [Nelsen06]:

$$P(X \leq x, Y \leq y) = C(F_X(x), G_Y(y)) = C(u,v) \tag{5.26}$$

Here the Gaussian copula is tested. The expression of the Gaussian copula for *n* random variables is [Nelsen06]:

$$C(\mathbf{u}) = \Phi_R^n\left(\Phi^{-1}(u_1),\ldots,\Phi^{-1}(u_n)\right) \tag{5.27}$$

where Φ_R^n is the normal mlultivariate CDF of gaussian distribution with zero mean variables and correlation matrix **R**. The function Φ^{-1} is the inverse CDF of the standard gaussian distribution.

Firstly, the Gaussian Copula is tested for modeling the joint first order statistics of rain attenuation on temporal domain. For this reason data from [Fabbro09], [Ismail00], [Kuhar14] have been used and the expression of (5.27) has been fitted considering two variables for various time delays. The joint exceedance probabilities for 15 min and 60 min time delays from Ljubljana are shown in Figure 5.12. The relative error has been calculated and the results are shown in Table I. It can be observed that the error remains small and it can be remarked that the Gaussian copula can be used for the modeling of joint statistics on temporal domain.

TABLE I.

Statistics of Relative Error from fitting of Gaussian Copula

Experiment	Mean error	Std	RMS
Spino 19GHz	-0,5%	4,88%	4,9%
Spino 40 GHz	-0,91%	6,3%	6,3%
Ljubljana	-1%	9,9%	9,9%
KLM	-2,9%	13,4%	13,7%

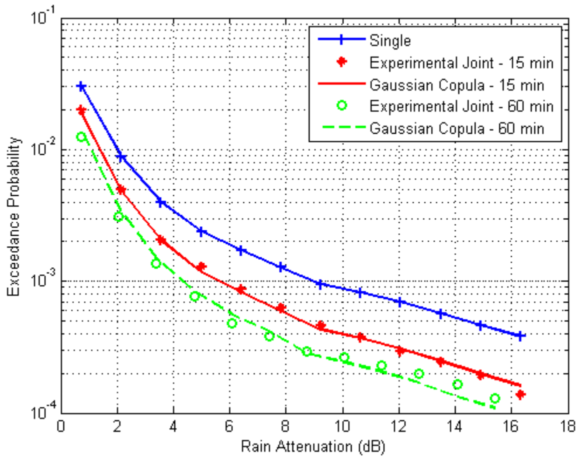

Figure 5.12 CCDF of rain attenuation for a ground station at Ljubljana from experiments and from copula fitting for 15 and 60 min time delays

From these experiments, the correlation parameter of the Gaussian copula has been extracted for the experiments shown in Table I and the various time delays. Figure 5.13, these parameters are shown for the experiments included in Table I. It can be seen that increasing the time delay the parameter is decreasing since the dependence of the variables is also decreasing. Moreover, from Figure 5.13, it can be seen that for the three experiments at Europe, the parameter is similar, while at Kuala Lumpur, the parameter changes a lot. Therefore, for the modeling of the parameter of Gaussian copula, two models will be used, one for temperate regions and one for tropical regions.

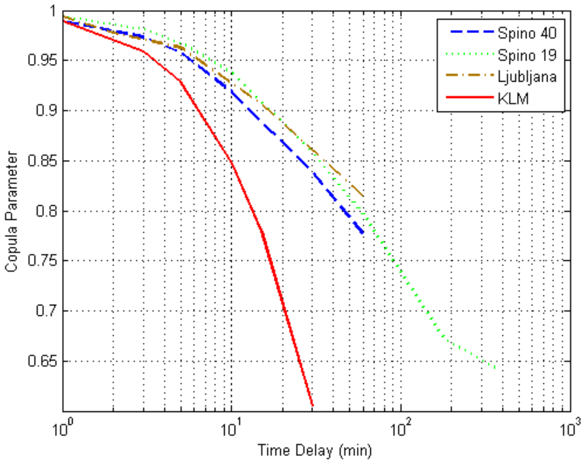

Figure 5.13 Copula parameter as a function of time delay

For the copula parameters from the experiments in European region the following expression has been extracted:

$$\rho(\Delta t) = 0.31e^{-\left(\frac{\Delta t}{52}\right)} + 0.69e^{-\left(\frac{\Delta t}{1390}\right)^2} \tag{5.28}$$

The above expression is similar to the one given in for rain attenuation linear correlation. The comparison of the resulted parameters from (5.28) and from the experimental results are shown in Figure 5.14.

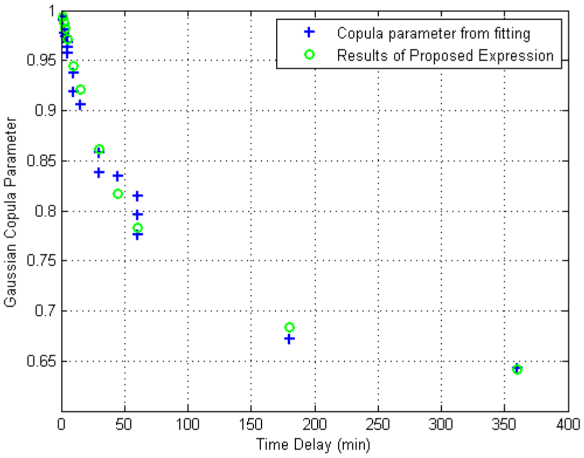

Figure 5.14. Copula parameter from (5.28) and from the experiments

Now, as aforementioned for the experiment in Kuala Lumpur, the copula parameters are much less probably, due to the more convective nature of rain. So, the expression given in (5.28) is highly probable that will overestimate the dependence between the variables. Therefore, a new model is proposed for tropical regions:

$$\rho(\Delta t) = e^{-\left(\frac{\Delta t}{60.1}\right)} \tag{5.29}$$

The results of the expression of (5.29) are shown in Fig. 4 along with the experimental values.

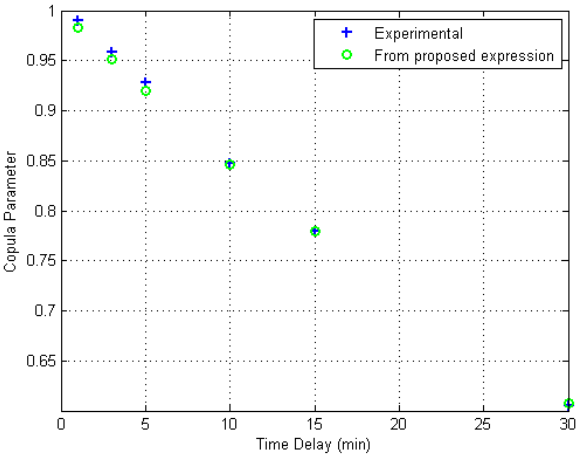

Figure 5.15 Copula parameter from (4) and from the experiments.

From the definition of Gaussian copula, it is found that the if two random variables follow jointly the Gaussian Copula with parameter ρ then the Kendall's τ correlation is calculated from [Nelsen06]:

$$\tau = \frac{2}{\pi}\sin^{-1}\left(\rho\right) \tag{5.30}$$

Therefore, using (5.28) and (5.29), one can have the Kendall's τ correlation modeled for temperate and tropical areas. The use of Kendall's τ correlation for the measure of the dependence between random variables has the advantage that it is a distribution free test, i.e. it does not require a hypothesis on the distribution of random variables. In the previous works most synthesizers use the Pearson correlation coefficient which is optimally derived for normally distributed random variables. Therefore, when considering various distributions, Kendall's τ correlation can be used.

Moreover, the Kendall's tau correlation has a straight interpretation. Starting from the definition of the coefficient, Kendall's tau is the difference between the number of concordant pairs (*C*) and the number of discordant pairs (*D*) divided by the number of observations (*N*) [Nelsen06]:

$$\tau = \frac{C-D}{N} \tag{5.31}$$

A concordant pair is when $\left(x_i > x_j \text{ and } y_i > y_j\right)$ or $\left(x_i < x_j \text{ and } y_i < y_j\right)$and a discordant pair is $\left(x_i < x_j \text{ and } y_i > y_j\right)$ or $\left(x_i > x_j \text{ and } y_i < y_j\right)$. So, as interpretation this coefficients measures the relation of the order of the random variables.

5.3.2 Proposed Time Series Synthesizer

In this Section, the time series synthesizer is proposed for generating time series of rain attenuation based on the Gaussian copula modeling of joint statistics of rain attenuation. The proposed synthesizer is used in order to generate time series of rain attenuation for whatever Kendall's tau rank correlation and long-term Probability Distribution Function (PDF).

Such synthesizer has been used for Nakagami channels [Sakarellos14] and here it is extended for rain attenuation. The expression in (5.27) actually couple multiple variables. In case that the tau corelation is known, here modeled in previous Section, for various time delays and the marginal distributions one can define the joint statistics at temporal domain.

Since the Kendall's tau rank corelation is related to the parameter of Gaussian copula through (5.30), if the tau correlation is identified for the various time delays the correlation matrix at (5.27) can be identified. Therefore, starting from the generation of multiple zero mean Gaussian variables with correlation matrix **R**, the values $\Phi^{-1}(u_i)$ are obtained. Then, calculating the normal cdf of the variables $\Phi^{-1}(u_i)$, the marginal distributions of every time sample is calculated. Finally, taking the inverse cdf of a distribution one obtains the rain attenuation time series for the various time samples. The step-by-step algorithm is given briefly in the following:

- Generate multiple normal zero mean Gaussian variables with correlation matrix **R**
- Take the normal CDF of the generated variables

- Proceed to the calculation of the inverse cdf of the desired distribution on the variables obtained in step 2

In Figure 5.16, an example is given for a ground station in Ljubljana. The frequency of the link is considered 20.2 GHz and elevation angle equal to 36.3^o. The input CCDF of rain attenuation is taken after fitting Weibull distribution to the experimental CCDF of rain attenuation.

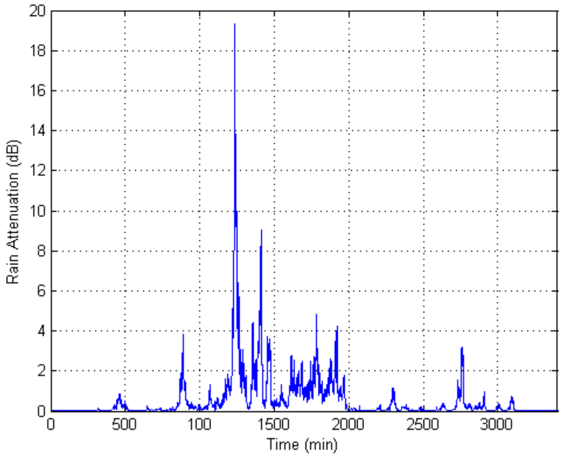

Figure 5.16 Time series of rain attenuation for a ground station in Ljubljana using the proposed synthesizer

5.3.3 Numerical Results

In the numerical Section, the synthesizer is validated considering the first order statistics and the second order statistics. Firstly the model is tested for the ground station at Ljubljana. The expression for the Gaussian Copula parameter is obtained from (5.28) and for the CCDF of rain attenuation the weibull distribution is used. For the first order statistics, the results are shown in Figure 5.17. In this figure, the theoretical CCDF and the one obtained from time series are shown for 1-min delay and for no delay. It can be observed that the synthesizer reproduces the CCDF given as input for joint statistics on temporal domain and for the single link with no delay. The parameters of the Weibull distribution have been extracted after fitting of Weibul on the single link CCDF of Ljubljana ground station.

Proceeding to the second order statistics, given that the Kendall's τ correlation given as input to the synthesizer is the one obtained from (5.30) using (5.28), time series of rain attenuation are obtained. The Kendall's τ correlation from the time series is then calculated and the results are shown in Figure 5.18 along with the one given as input. Therefore, it can be observed that the synthesizer reproduces the Kendall's τ correlation.

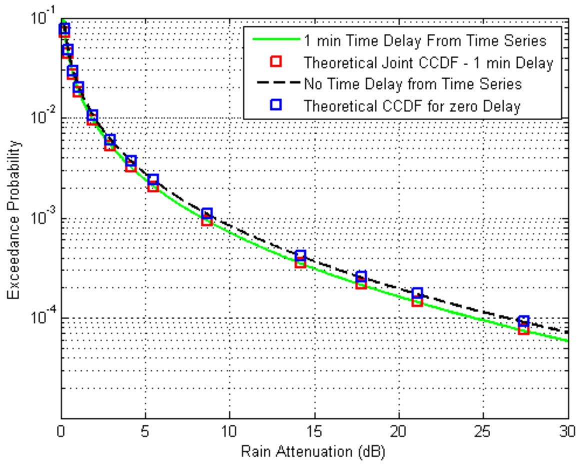

Figure 5.17 CCDF of rain attenuation for zero time delay from time series synthesizer and the theoretical values and the joint CCDF of rain attenuation for 1 min time delay

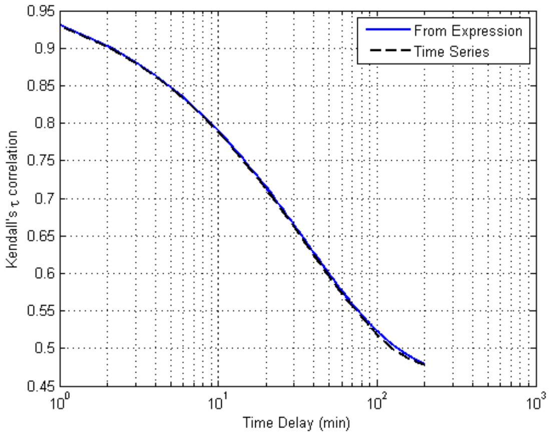

Figure 5.18 Kendall's τ correlation from time series and theoretical expression

5.4 Space-Time Rain Rate Field Generator for Multi-Antenna Satellite Communication Applications

5.4.1 Rain Rate Field Generator

In [Manning90], it has been shown that the SDE of the form of the Maseng-Bakken model can be also used for the generation of time series of rain rate. Using this specific SDE, time series of a stochastic process, whose long-term static distribution follows the lognormal one and has an exponential decaying autocorrelation function of the reduced variable, are generated. Such properties are also met in the rain rate process. Therefore, the same SDE can be used for the description of rain rate.

However, with the specific SDE only point rainfall rate time series can be generated. In order to simulate time series of rain rate fields over a specific area, multi-dimensional SDEs shall be used, treating the rain rate on every point as a stochastic process. However, the various point rainfall rates are found to be correlated due to the spatial correlation found in the rain rate process. This spatial correlation can be derived using the expression presented in [Paraboni].

The form of the multi-dimensional SDE shall be of the following form:

$$d\mathbf{R}_t = \mathbf{F}\left(\mathbf{R}_t\right)dt + \mathbf{Z}\left(\mathbf{R}_t\right)d\mathbf{W}_t \tag{5.32}$$

where $\mathbf{R}_t = \left[R_t^1,...,R_t^n\right]^T$ is the vector of rain rate processes $R_t^i, i = 1,...,n$. The nx1 $\mathbf{F}\left(\mathbf{R}_t\right)$ vector is the drift vector and the nxn $\mathbf{Z}\left(\mathbf{R}_t\right)$ matrix is the diffusion matrix. Following the methodology presented in [Karagiannis12], these coefficients can be computed in order that the each element of the vector follow the lognormal distribution, with median value R_m^i and the standard deviation of the natural logarithm of rain rate $S_{\ln R}^i$. The other properties that shall be met and followed for the computation of drift vector and diffusion coefficient are based on properties of the reduced variable $X_t^i = \ln\left(\dfrac{R_t^i}{R_m^i}\right)$:

- Every reduced variable must have an exponential decaying autocorrelation function
- The spatial correlation of the reduced variables shall be given by this of [Paraboni].

Fulfilling these requirements, the elements of the drift vector and diffusion coefficient can be calculated. So from the above described methodology and the theoretical framework of SDEs for rain attenuation [Karagiannis12], time series of rain rate fields can be generated. In Figure 5.19, three instances, at time t_0, t_0+1 min, t_0+5 min, of a rain rate field are shown. The rain rate field was generated for the region of Athens, in Greece. The statistical parameters of the rain rate field were computed from a nonlinear regression process with which the theoretical lognormal distribution is fitted to the one predicted by ITU-R. P. 837-5 [ITU-R. P.837]. Here it must be noted that the probability to rain on a single point is taken equal to 1 for every point. The size of the area was considered (50km x50km). In order to simulate the rain rate fields, the dynamic parameter of every stochastic process was set equal to a typical value of 10^{-3} sec^{-1}.

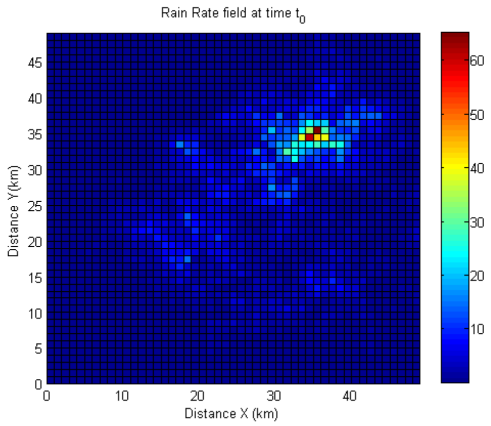

(a)

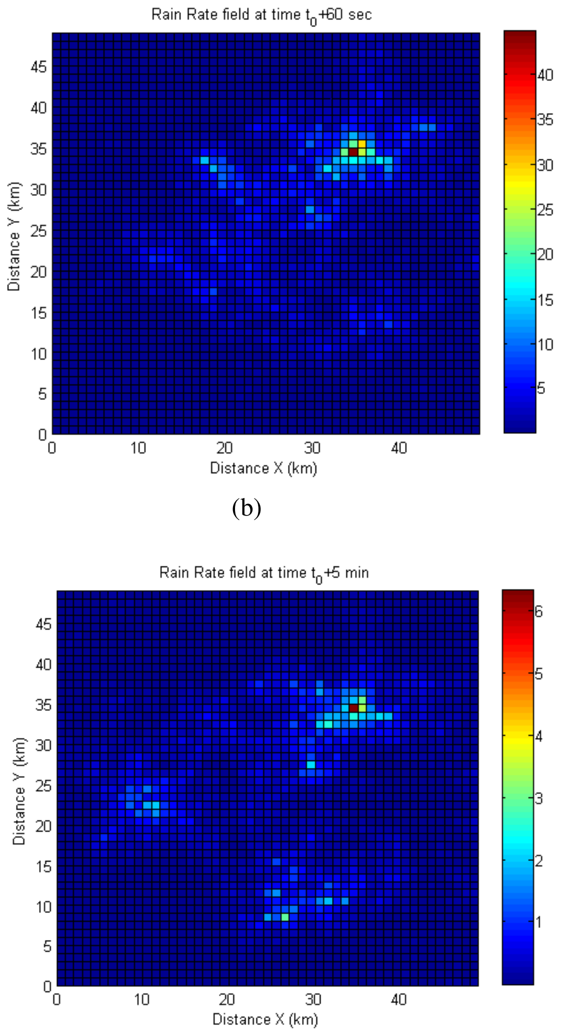

(b)

(c)

Figure 5.19. Rain rate fields at time t_0 (a), t_0+60 sec (b) and t_0+5 min

In Figure 5.20, the long-term statistics of point rain rate are depicted as these were derived from the simulated rain rate fields. Also, the theoretical lognormal distribution which was taken as an input to the model is also shown. Moreover, two point rainfall rates were chosen to compute the joint CCDF of rain rate. As it can be seen this coincides with the theoretical bivariate lognormal distribution. So, the model reproduces the first order statistics of rain rate, as well as the theoretical joint statistics on spatial domain assuming that the joint PDF of rain rate is the bivariate lognormal distribution.

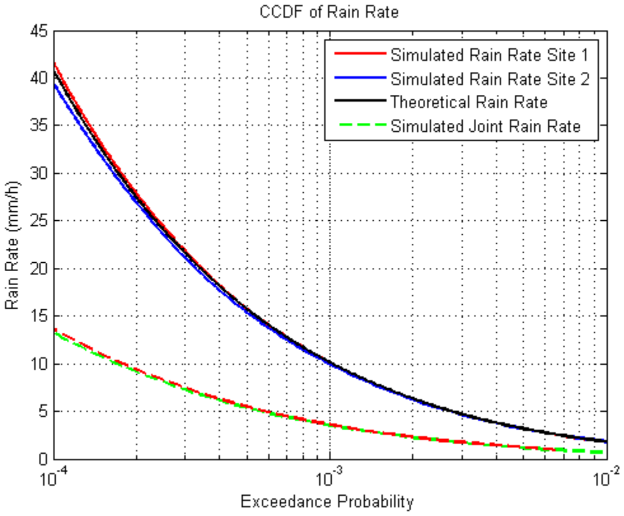

Figure 5.20 CCDF of rain rate and joint CCDF of rain rate

5.4.2 *Computation of Rain Attenuation*

In the previous Section the methodology for generating time series of rain rate fields simulated over an area was given. From every instance of a rain rate field the specific rain attenuation (A_0) can be calculated on every point:

$$A_0(x,y) = aR(x,y)^b \tag{5.33}$$

where a and b are two coefficients which depend on the polarization, frequency and elevation angle of the link. They can be calculated from ITU-R. P. 838 [ITU-R. P.838]. Rain attenuation on a link with projected effective slant path L at a given instance is calculated by:

$$A = \int_0^L A_0\left(z = \sqrt{x^2 + y^2}\right) dz \tag{5.34}$$

Consequently, from a numerical integration and assuming that rain rate has a vertical uniform profile, rain attenuation time series can be derived. In Figure 5.21, the CCDF of rain attenuation is computed with the proposed methodology for an Earth-space link. The Earth station is located in Vienna, Austria, the elevation angle is 30^o and the operating frequency is 25 GHz. In the same figure the prediction made by ITU-R. P. 618 is also depicted.

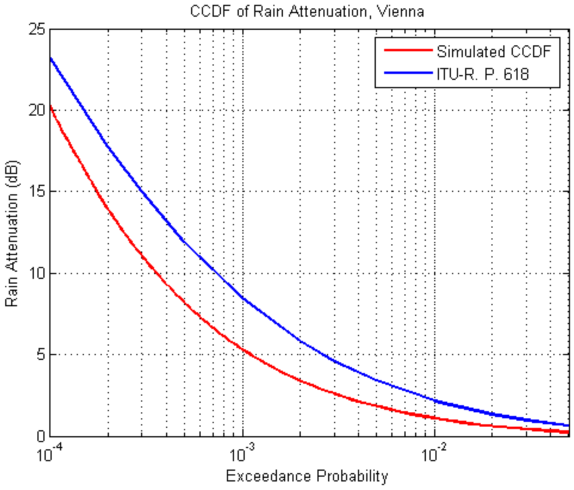

Figure 5.21. CCDF of rain attenuation for Vienna, Europe derived from simulations (red line) and ITU-R. P. 618 (blue line)

5.4.3 *Numerical Results*

In this Section, firstly, the model is validated with data derived from DBSG3 and compared to the prediction made by ITU-R. P. 618-10. In Figure 5.22, the CCDF of rain attenuation is shown for three cases: a) from the presented model, b) the ITU-R. P. 618-10 and c) the experimental data. The Earth station is located at Wallops Island in USA, the operating frequency of the link is 28.6 GHz and the elevation angle 41.6°. From this figure it can be observed that the prediction made by the proposed model for this case is very good and better than this of ITU.

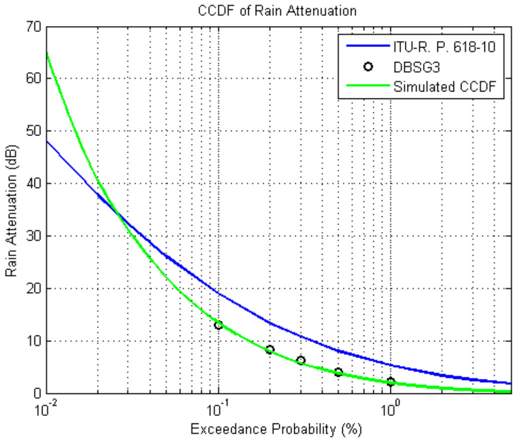

Figure 5.22 CCDF of Rain Attenuation at Wallops Island

In Figure 5.23, the same figure is shown but for another Earth-space link. For the latter case, the Earth-space link is located at Wakkanai of Japan with an operating frequency of 12.1 GHz and elevation angle 29.1°. From the resulted CCDF it can be referred that the model has almost similar performance with the ITU prediction. However, in high probabilities, the model seems to underestimate rain attenuation.

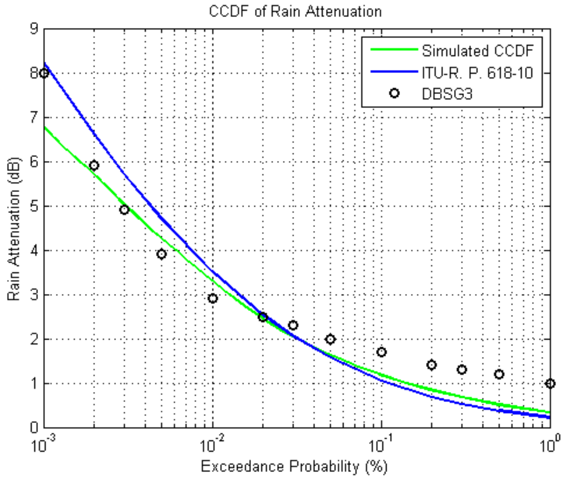

Figure 5.23 CCDF of Rain Attenuation at Wakkanai, Japan

Apart from single-link statistics, joint long-term first order statistics can be calculated with the proposed model. In Figure 5.24, the joint CCDF of rain attenuation is shown for a dual site diversity system with two Earth stations located at Athens with a separation distance of 9 km. The frequency of the link is 30 GHz and the elevation angle 25^o. In the same figure the single-site statistics are also shown.

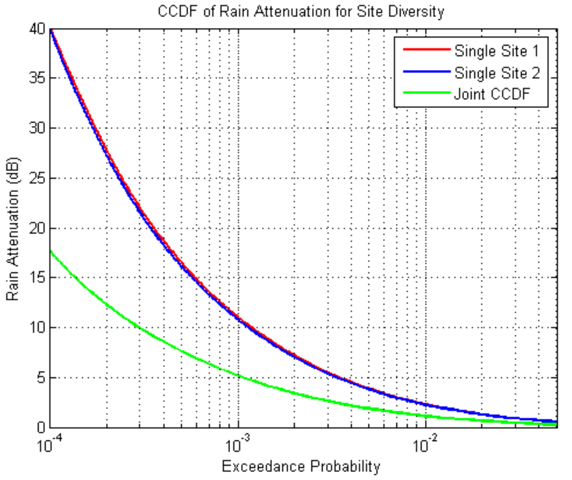

Figure 5.24 Single site and joint for site diversity systems CCDFs of rain attenuation

Finally, in Figure 5.25, the joint rain attenuation CCDF is shown for an orbital diversity satellite system. The Earth station is located at Athens of Greece and the angle separation between the two links is 180^o. The operating frequency is 30 GHz and the elevation angle 25^o.

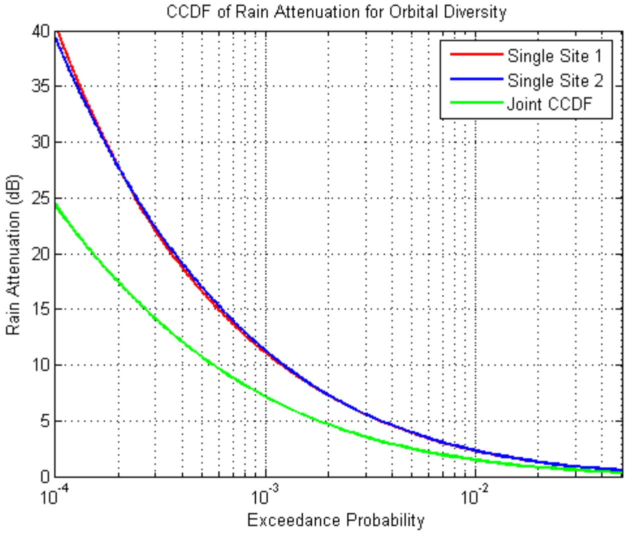

Figure 5.25 Single site and joint for orbital diversity systems CCDFs of rain attenuation

5.5 A Tropospheric Scintillation Time Series Synthesizer Based on Stochastic Differential Equations

In this Section, a time series synthesizer of scintillation is presented based on the Stochastic Differential Equations driven by fractional Brownian motion (fBM) [Mishura08]. It is shown that the synthesizer reproduces the first order long-term statistics of the log-amplitude as well as the power spectrum

5.5.1 *First Order Statistics of Scintillation*

In [Mousley82] and [Vasseur99], it is shown that in short-term the log-amplitude (χ) of the normalized received signal can be modeled as a zero-mean Gaussian process with a given variance σ_χ^2. Therefore, for a given variance, the Probability Density Function (PDF) of the log-amplitude is given:

$$p_{st}\left(\chi / \sigma_\chi^2\right) = \frac{1}{\sqrt{2\pi\sigma_\chi^2}} \exp\left(-\frac{\chi^2}{2\sigma_\chi^2}\right) \tag{5.35}$$

The long-term PDF of χ is:

$$p_{lt} = \int_0^{+\infty} p_{st}\left(\chi / \sigma_\chi^2\right) p\left(\sigma_\chi^2\right) d\sigma_\chi^2 \tag{5.36}$$

where $p\left(\sigma_\chi^2\right)$ is the PDF of the scintillation variance. Following the models in [Mousley82] and [Vasseur99], the PDF of σ_χ^2 is considered to follow the lognormal distribution with $\ln(m)$ and s the mean value and standard deviation of $\ln\left(\sigma_\chi^2\right)$, i.e.:

$$p\left(\sigma_\chi^2\right)=\frac{1}{\sqrt{2\pi}\sigma_\chi^2 s}\exp\left(-\frac{\left[\ln\left(\sigma_\chi^2/m\right)\right]^2}{2s^2}\right) \tag{5.37}$$

In [Vasseur99], the values of m and s are derived from radiosonde data for two links at Louvain-la-Neuve, Belgium, with operating frequencies 12.5 GHz and 30 GHz while in [Mousley82] the statistics of the scintillation variance are derived from satellite downlink measurements at Portsmouth, UK.

5.5.2 Scintillation Time Series Synthesizer

In this Section, a time series synthesizer of the log-amplitude χ is proposed based on SDEs driven by fBm. The time series of log-amplitude will be described by:

$$d\chi_t = f\left(t,\chi_t\right)dt + g\left(t,\chi_t\right)dB_H \tag{5.38}$$

where dB_H is the increments of the fBm with Hurst index H. Since for a given variance, χ_t can be considered as a Gaussian process with zero mean, we use the Langevin equation with fBm (fractional Langevin equation) to model the time series of log-amplitude, giving that the variance is equal to 1 ($\chi_{t,1}$) [Shao95]:

$$d\chi_{t,1} = -\lambda\chi_{t,1}dt + \sigma dB_H \tag{5.39}$$

The parameters λ and σ depend on the dynamic parameters of the stochastic process and its long-term statistics. The solution of the above equation is [Shao95], [Cheridito03]:

$$\chi_{t,1} = e^{-\lambda t}\left(\chi_0 + \sigma\int_0^t e^{\lambda u}dB_u^H\right) \tag{5.40}$$

where χ_0 is the initial value of the log-amplitude. Here we consider it as equal to 0 dB. Therefore, (5.40) becomes:

$$\chi_{t,1} = e^{-\lambda t}\sigma\int_0^t e^{\lambda u}dB_u^H \tag{5.41}$$

The above process is also called fractional Ornstein-Uhlenbeck process and it is a Gaussian process with zero mean and the variance of χ_t and χ_{t+s} is [Cheridito03]:

$$Cov\left(\chi_{t,1},\chi_{t+s,1}\right)=\sigma^2\frac{\Gamma\left(2H+1\right)\sin\left(\pi H\right)}{2\pi}\int_{-\infty}^{+\infty}e^{isy}\frac{|y|^{1-2H}}{\lambda^2+y^2}dy \tag{5.42}$$

Therefore, the variance of the Ornstein-Uhlenbeck process is (s=0):

$$\sigma_{\chi_{t,1}}^2=\sigma^2\frac{\Gamma\left(2H+1\right)\sin\left(\pi H\right)}{2\pi}\int_{-\infty}^{+\infty}\frac{|y|^{1-2H}}{\lambda^2+y^2}dy \tag{5.43}$$

Since, firstly we want to have a unitary variance process we set:

$$\sigma=\frac{1}{\sqrt{\frac{\Gamma\left(2H+1\right)\sin\left(\pi H\right)}{2\pi}\int_{-\infty}^{+\infty}\frac{|y|^{1-2H}}{\lambda^2+y^2}dy}} \tag{5.44}$$

For the energy spectrum $F_{\chi t,1}(f)$ of fractional Ornstein-Uhlenbeck process holds that [Shao95]:

$$F_{\chi t,1}(f) = \sigma^2 \frac{F_{\omega_b}(f)}{\lambda^2 + (2\pi f)^2} \tag{5.45}$$

where $F_{\omega_b}(f)$ is the energy spectrum of fractional Gaussian noise and it holds that:

$$F_{\omega_b}(f) \sim f^{-(2H-1)} \tag{5.46}$$

From (5.45) and (5.46), it holds for high frequencies that:

$$F_{\chi t,1}(f) \sim f^{-(2H+1)} \tag{5.47}$$

with corner frequency close to $\omega_c = \lambda^{\frac{1}{\mathrm{H}+1/2}}$

Finally, in order to obtain the scintillation time series we multiply the time series of $\chi_{t,1}$ derived from (5.41) with the scintillation standard deviation σ_χ .Consequently, the time series of log-amplitude are generated from:

$$\chi_t = \sigma_\chi \chi_{t,1} \tag{5.48}$$

From (5.48), considering that σ_χ is constant with time the scintillation log-amplitude is a Gaussian random variable with zero mean, standard deviation σ_χ and a spectrum slope of –(2*H*+1). However, scintillation variance follows a lognormal distribution and the question that can arise is for the time series of the scintillation variance. It has been shown that the instantaneous value of scintillation standard deviation is proportional to instantaneous value of rain attenuation (*A*) with a power law of 5/12 under the presence of rain [Matricciani95], [Matricciani08]:

$$\sigma_\chi = CA^{5/12} \tag{5.49}$$

From (5.49), and given that we take the unconditional distribution of rain attenuation and the Maseng-Bakken model [Maseng81] for the generation of time series of rain attenuation we can further assume that the scintillation standard deviation follows the Maseng-Bakken model as well, with the same dynamic parameter with the rain attenuation process equal to 0.0002 sec^{-1} [ITU-R. P.1853].

5.5.3 Numerical Results and Discussion

In this Section, numerical results are presented and the synthesizer is validated with first and second order statistics of scintillation log-amplitude. For the modelling of the lognormal distribution of the scintillation variance, we use the parameters *m* and *s* of scintillation variance as these were computed in [Vasseur99] for the OLYMPUS experiment at Louvain-la-Neuve for two frequencies 12.5 GHz and 30 GHz, and hereby will be labelled as experiments number 1 and 2, respectively. The parameters are shown in Table II.

TABLE II. Parameters of the scintillation variance

Experiment	Parameter *m*	Parameter *s*
No 1, 12.5GHz	$1.49\text{x}10^{-3}$	1.21
No 2, 30GHz	$4.13\text{x}10^{-3}$	1.21

The scintillation variance time series are extracted from the equivalent Maseng-Bakken model (with the appropriate parameters of the long-term first order statistics) using dynamic parameter of 0.0002 sec^{-1}. To generate time series of the scintillation process we set the Hurst index equal to 0.8333 in order to have the appropriate spectrum for high frequencies according to (5.47). The parameter λ was set equal to 0.5382 in order that according to theory the corner frequency is at 0.1 Hz. The sampling frequency of the time series is 10 Hz. In Figure 5.26 and Figure 5.27, scintillation time series snapshots are shown for the two experimental setups with frequency 12.5 and 30 GHz, respectively.

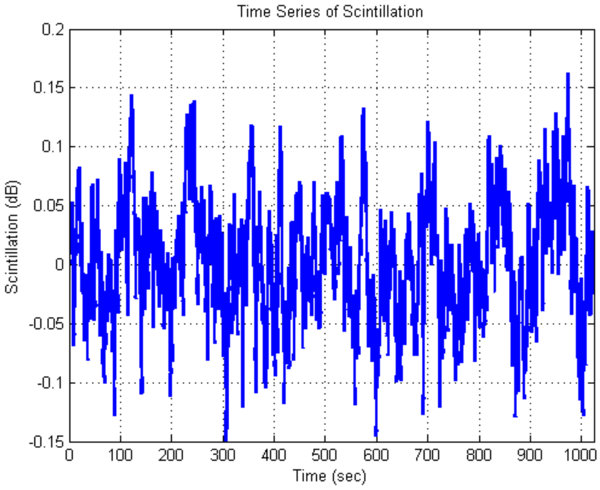

Figure 5.26 Simulated scintillation time series snapshots using the parameters for experiment no.1

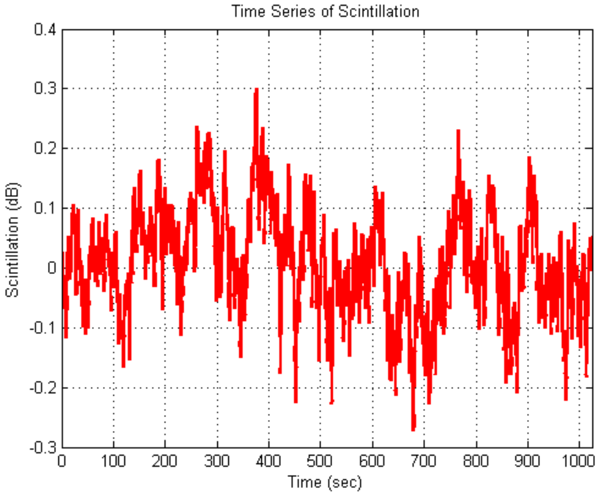

Figure 5.27 Simulated scintillation time series snapshots using the parameters for experiment no.2

Firstly, we verify the long-term exceedance probability of the absolute value of log-amplitude. In Figure 5.28, the Complementary Cumulative Distribution Function (CCDF) of log-amplitude derived from simulations and the theoretical distribution, whose PDF is given in (5.36) is shown for both experiments. It can be observed that the time series generator reproduces the theoretical first order statistics of scintillation.

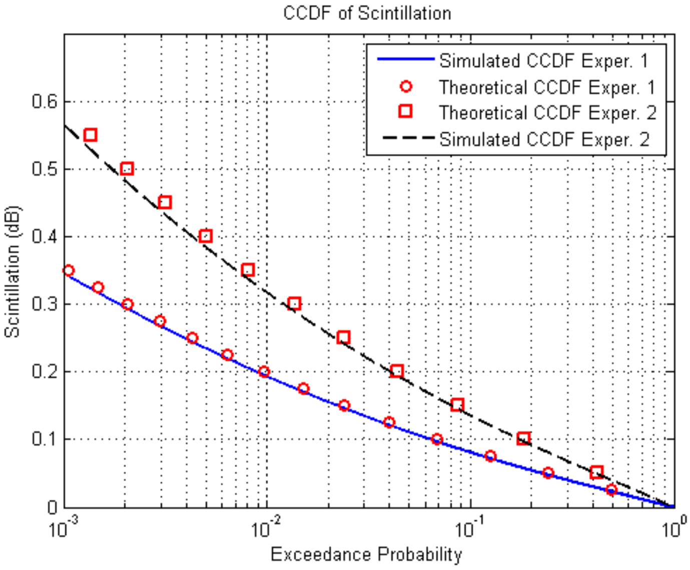

Figure 5.28 Simulated and theoretical CCDF of the absolute value of scintillation

Then, we calculated the power spectrum of scintillation derived from simulations. The results are shown in Figure 5.29 and Figure 5.30 for both experiments. It can be observed that for frequency higher than 0.1 Hz, the power spectrum is decreasing with frequency with a slope of -8/3, as this was found in experiments. Therefore, the synthesizer reproduces the considered spectrum of the scintillation log-amplitude.

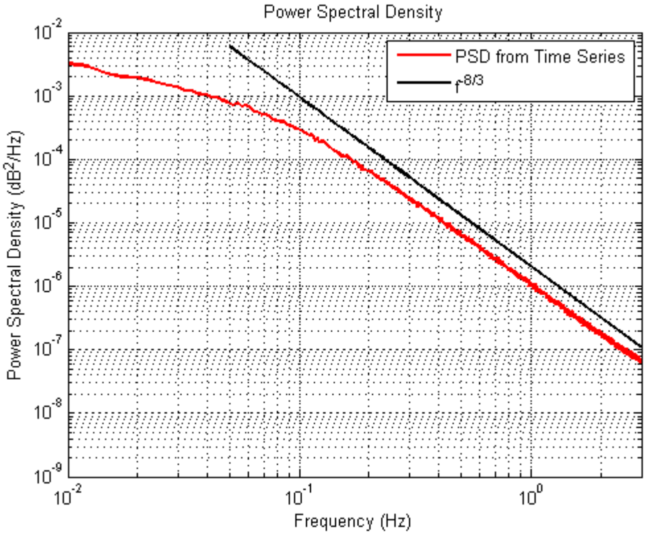

Figure 5.29 PSD derived from the time series generator for experiment no. 1

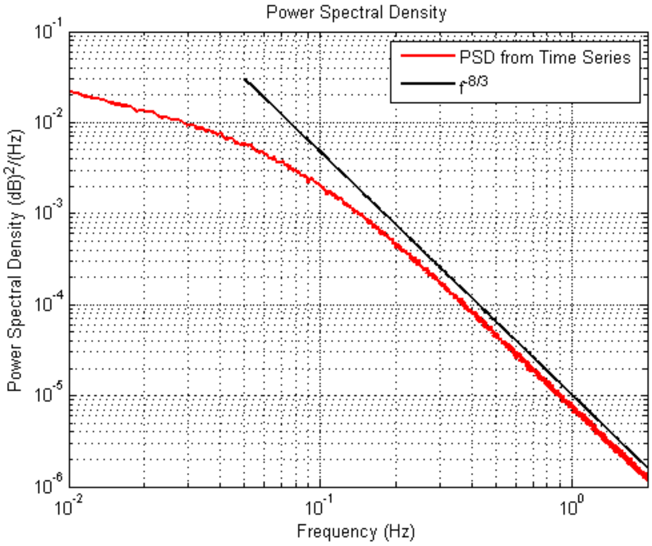

Figure 5.30 PSD derived from the time series generator for experiment no. 2

Appendix A. Fractional Brownian Motion

Fractional Brownian motion (fBm), $B^H = \{B_t^H, t \in \mathbb{R}\}$ is characterized by the Hurst index (H, with $H \in (0,1)$) and it is a Gaussian process with the following properties [Mishura08]:

$$B_0^H = 0$$

$$E\left[B_t^H\right]=0, t\in\mathbb{R}$$

$$E\left[B_t^H B_s^H\right]=\frac{1}{2}\left(|t|^{2H}+|s|^{2H}-|t-s|^{2H}\right), s,t\in\mathbb{R}$$

From the properties given above, it can be remarked that: $E\left[\left(B_t^H-B_s^H\right)^2\right]=|t-s|^{2H}, s,t\in\mathbb{R}$. The well-known standard Brownian motion has a Hurst index $H=1/2$. For $H<1/2$, the fBm is negatively correlated, while for $H>1/2$ is considered as positively correlated.

Considering the spectrum properties of the fBm, the following expression holds for the energy spectrum of fBm [Shao95]:

$$F_{B^H}(f)\sim f^{-(2H+1)} \tag{A.1}$$

There are various methods for simulating time series of fBm [Davies87], [Dieker03], [Yin96]. Here,the exact simulation (Davies and Harte approach [Davies87]) of fBm has been used. In Figure 5.31, Figure 5.32 and Figure 5.33 time series of fBm are shown for different values of Hurst index.

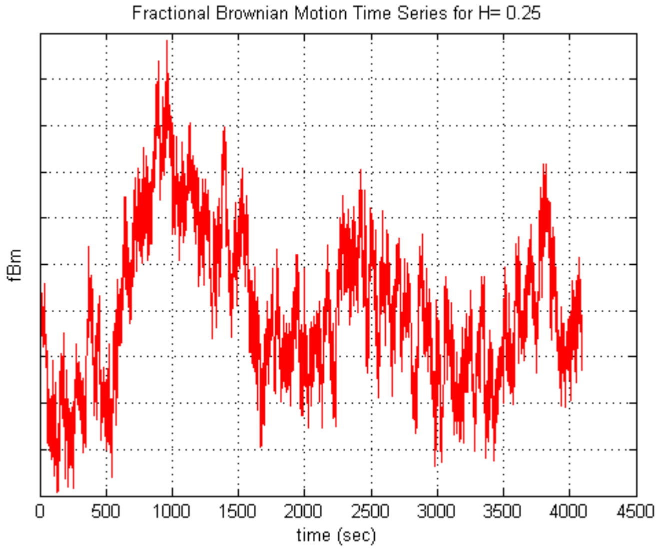

Figure 5.31 Time series of fractional Brownian motion with Hurst index 0.25

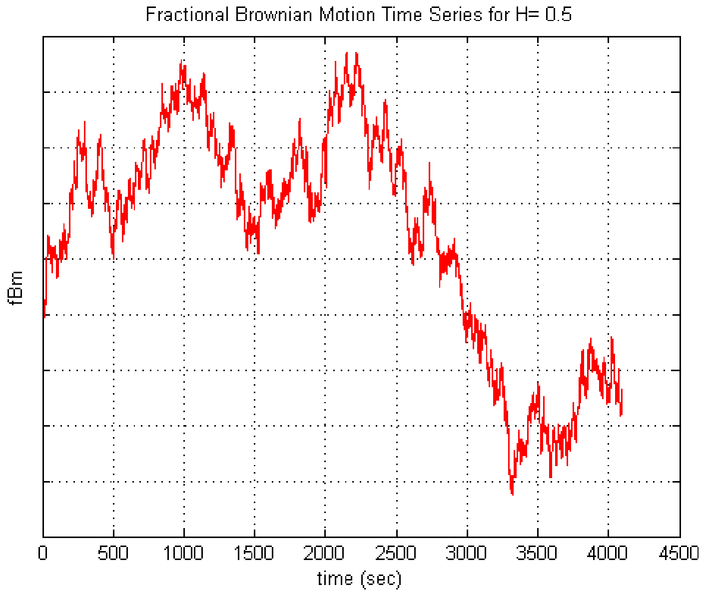

Figure 5.32 Time series of fractional Brownian motion with Hurst index 0.5

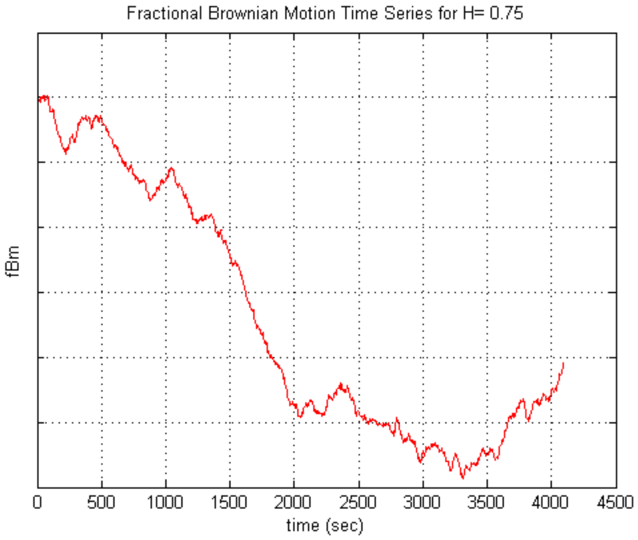

Figure 5.33 Time series of fractional Brownian motion with Hurst index 0.75

6 Performance Assessment of Cognitive and Earth Observation Satellite Communication Systems Operating above 10 GHz

The first part of this Chapter is devoted to the performance of cognitive communication systems which operate above 10 GHz through interference analysis. The idea of cognitive satellite starts gaining more and more attention due to the increasing demand of the use of Ka-band for terrestrial and satellite services. This first part is divided into three Sections. Firstly, a dual satellite cognitive system is analyzed for the noise dominant case, i.e. given that the links are available, through the statistical modeling of Signal-to-interference ratio (SIR). The Section has been published at [C1]. Then, the interference at the downlink (adjacent satellite interference) and uplink for Earth Stations on Mobile Platforms (ESOMPs) is modeled and theoretical expressions for the outage probability, i.e the probability that the Signal-to noise plus interference ratio (SNIR) is less than a threshold, for one interfering satellite at downlink and one interfering Earth station at the uplink are derived. Moreover, the outage probability for multiple interfering satellites and ESOMPs is calculated. The Section has been published in [J1]. The third Section on cognitive systems is devoted to the interference caused by a fixed satellite service user to a fixed terrestrial user [C2], considering SIR and SNIR analysis. In the second part of this Chapter, the performance of LEO to ground links is assessed using ACM for Ka and Q bands, using the model presented in Section 4.2, considering adaptive and static channel estimation techniques [J2]. The later work has been resuubmitted to a journal since it is accepted with minor revision and it was undertaken under the framework of SatNEx III.

[J1] C. Kourogiorgas, P.-D. Arapoglou, A. D. Panagopoulos, "Statistical Characterization of Adjacent Satellite Interference for Earth Stations on Mobile Platforms Operating at Ku and Ka Band", IEEE Wireless Communication Letters, vol. 4, issue 1, 2015.

[J2] Z. Katona, C. Kourogiorgas, A. D. Panagopoulos, N. Jeannin, "Capacity Analysis of High-Throughput Satellite Links for Earth Observation Missions", accepted at International Journal of Satellite Communications and Networking.

[C1] C. Kourogiorgas, A. D. Panagopoulos, "Interference Statistical Distribution for Cognitive Satellite Communication Systems Operating above 10 GHz", 7th Advanced Satellite Multimedia Systems Conference and the 13th Signal Processing for Space Communications Workshop, pp. 256-261, 8-10 September 2014, Livorno, Italy

[C2] C. Kourogiorgas, A. D. Panagopoulos, K. P. Liolis, "Cognitive Uplink FSS and FS Links Coexistence in Ka-band: Propagation based Interference Analysis", ICC 2015, London, UK, June 2015.

6.1 Interference Statistical Distribution for Cognitive Satellite Communication Systems Operating above 10GHz

6.1.1 System Model

The system which will be considered in this section, is a cognitive satellite system in which the incumbent and cognitive users are fixed satellite terminals and they both communicate with satellites at Ku-band and above. It is the scenario of dual cognitive SatComs. It is further considered that the incumbent and cognitive links operate simultaneously at downlink and the same frequency.

In Figure 6.1 the geometry of the system under evaluation, as well as the four satellite links (two interfering and the corresponding incumbent and cognitive links) are shown. It is considered that the ground stations are coordinated (cognition of the spectrum sharing) and the configuration is similar with the one described of a dual satellite system in [Sharma13]. We consider the dual single polarization scenario. The incumbent link is the S_1-GS_1, and the cognitive one is the S_2-GS_2. There are two interfering links: a) S_1-GS_2, which interferes the communications of the cognitive user and b) S_2-GS_1 which interferes the incumbent link. In the same figure, the variables of rain attenuation induced on the four links are shown: a) A_p is the rain attenuation induced on the desired link of incumbent user (S_1-GS_1), b) A_s is the rain attenuation induced on the desired link of the cognitive user (S_2-GS_2), c) A_{sp} is the rain attenuation induced on the interfering link of incumbent user (S_2-GS_1) and d) A_{ps} is the rain attenuation induced on the interfering link of the cognitive user (S_1-GS_2). All the rain attenuation variables are in dB.

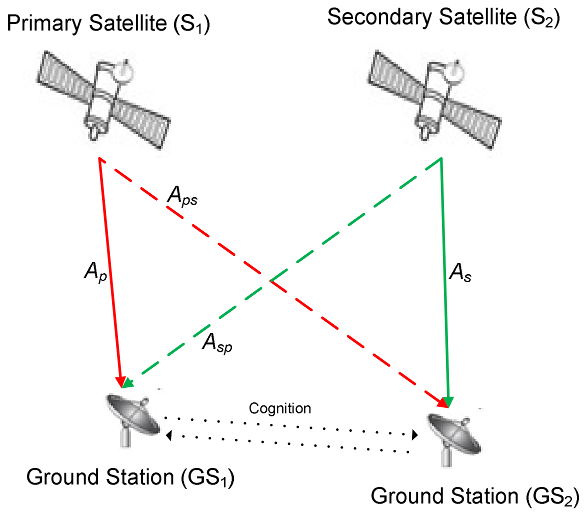

Figure 6.1 Geometry of a dual Cognitive SatCom system

In order to assess the performance of the incumbent link for the downlink case, the Signal-to-Interference Ratio (*SIR*) statistics are needed, in order to estimate the effect of the power level of interference to the signal power. The *SIR* ratio in linear terms is defined as the following ratio:

$$SIR = \frac{S}{I} \tag{6.1}$$

where S is the received signal power from the regular link and I is the power received in GS_1 terminal from the interfering link S_2-GS_1, both in linear terms.

Ignoring the atmospheric effects, the *SIR* under clear sky conditions can be computed through the following formula:

$$SIR_{CS} = \frac{EIRP_D G_{GS}(0^o) FSL_D}{EIRP_I G_{GS}(\theta^o) FSL_1} \tag{6.2}$$

where $EIRP_D$ and $EIRP_I$ are the effective isotropic power from the wanted satellite and the interfering satellite, respectively. $G_{GS}(0^o)$ and $G_{GS}(\theta^o)$ are the ground station's maximum antenna gain and the antenna gain observed at the angle of the interfering link. The latter can be calculated from the Recommendation of International Telecommunication Union ITU-R. S. 465-6 [ITU-R. S.465]. Finally, FSL_D and FSL_I are the free space losses of the direct and the interfering links, respectively.

The *SIR* in dB scale for the incumbent users considering also rain attenuation is:

$$SIR_p\big|_{dB} = SIR_{CS,dB} - A_p + A_{sp} \tag{6.3}$$

where SIR_{CS} is the signal to Interference Ratio under clear sky conditions at dB values and A_p and A_{sp} are the rain attenuation random variables in dB that correspond to rain attenuation values induced in the links as this was explained before. Similarly for the cognitive user, the *SIR* in dB values is:

$$SIR_s\big|_{dB} = SIR_{CS,dB} - A_s + A_{ps} \tag{6.4}$$

Equations (6.3), (6.4), show the dependence of *SIR* under rainfall conditions, on the differential rain attenuation.

6.1.2 Satellite Channel Model

As it can be observed by (6.3) and (6.4), the *SIR* depends on the rain attenuation induced on each link, as well as their correlated values. For the modeling of rain attenuation at Ka-band, the lognormal approximation is considered. The exceedance probability of rain attenuation for a single link is therefore given by:

$$P[A \geq A_{th}] = 0.5erfc\left(\frac{\ln\left(A_{th}/A_m\right)}{\sqrt{2}S_A}\right) \tag{6.5}$$

where S_A is the standard deviation of natural logarithm of rain attenuation and A_m is the median value of rain attenuation. The aforementioned statistical parameters of rain attenuation can be computed through the statistical-physical method proposed in [Panagopoulos03], or through regression to the prediction made by the recommendation of International Telecommunication Union ITU-R. P. 618-10 [ITU-R. P.618]. In this Section, it is assumed that rain attenuation induced on a single link follows the lognormal distribution, while for the dual link case the bivariate lognormal distribution is assumed for the joint PDF of rain attenuation.

Considering the dynamics of rain attenuation (A_t) induced in a single link, the first order Stochastic Differential Equation (SDE) proposed by Maseng and Bakken [Maseng81] is used:

$$dA_t = A_t\,\beta\left[S_A^2 - \ln\left(\frac{A_t}{A_m}\right)\right]dt + A_t\,\sqrt{2\beta}S_A dW_t \tag{6.6}$$

with β the dynamic parameter of rain attenuation and dW_t the standard Brownian motion increments [Karlin75]. For spatially separated links, rain attenuation time series correlated in spatial domain can be generated through the solution of the multi-dimensional SDE proposed in [Karagiannis12]. In the latter reference rain attenuation on multiple n links $\mathbf{A}_t = \left[A_t^1,...,A_t^n\right]^T$ can be described through the use of multi-dimensional SDEs as follows:

$$d\mathbf{A}_t = \mathbf{F}\left(\mathbf{A}_t\right)dt + \mathbf{Z}\left(\mathbf{A}_t\right)d\mathbf{W}_t \tag{6.7}$$

where

$$\begin{aligned}
&\mathbf{F}(\mathbf{A}_t) = \left[F_1\left(A_t^1,...,A_t^n\right),...,F_n\left(A_t^1,...,A_t^n\right)\right]^T \\
&\mathbf{Z}(\mathbf{A}_t) = \left[z_{ij}\left(A_t^1,...,A_t^n\right)\right]_{1\leq i,j\leq n} \\
&\mathbf{W}_t = \left[W_t^1,...,W_t^n\right]^T
\end{aligned} \tag{6.8}$$

with $W_t^1,...,W_t^n$ independent Brownian Motions [Karlin75], **F** the drift vector and **Z** the diffusion matrix [Karatzas05].

In Figure 6.2, time series of rain attenuation induced for two convergent links are shown. The separation angle of the links is considered to be 17°. The frequency of the links is 20GHz and the Ground station is located at Athens, Greece.

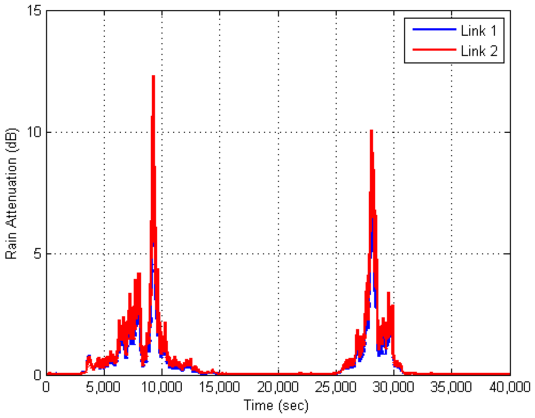

Figure 6.2 Spatially correlated time series of rain attenuation for two convergent links

6.1.3 Interference Statistical Distribution

In this Section, two methods for the evaluation of the performance of the links for the coexistence of two satellite links are presented. Firstly, we give a theoretical methodology, with analytical expressions and then a numerical approach for the calculation of *SIR* time series and then the appropriate statistics.

In a cognitive satellite scenario, i.e. a scenario of spectrum coexistence of two different services for a geographical area, the statistics that we are interested in is the probability of the *SIR* value of a user, either incumbent or cognitive, is below a certain threshold (SIR_{th}) given that the link of incumbent or cognitive user, respectively, is available. Therefore, the outage probabilities due to interference of the incumbent and cognitive users are, respectively [Panagopoulos03b]:

$$P_{out,p} = P\left[SIR_p \leq SIR_{th}, A_p \leq A_{th,p}\right] \tag{6.9}$$

$$P_{out,s} = P\left[SIR_s \leq SIR_{th}, A_s \leq A_{th,s}\right] \tag{6.10}$$

The probability of ($A_j \leq A_{th,j}$) refers to the case that the direct link of incumbent or cognitive user is available with $A_{th,j}$ the thresholds for the two links for the various services provided. In case that the rain attenuation exceeds this value, the link is in outage. Therefore, through (6.9) and (6.10), we examine the outage probability due to interference.

From (6.3) and (6.4), the outage probabilities of (6.9) and (6.10) we have:

$$\begin{aligned} &P\left[SIR_j \leq SIR_{th}, A_j \leq A_{th}\right] = \\ &= P\left[SIR_{CS,dB} - SIR_{th} \leq A_j \leq A_{th}, A_{ij} \leq A_j + SIR_{th} - SIR_{CS,dB}\right] \end{aligned} \tag{6.11}$$

with j={p or s} and {ij}={sp or ps}.

After straightforward probabilistic algebra the long term interference statistical distribution is given:

$$P_{out} = \frac{1}{2} erfc\left(\frac{u_r}{\sqrt{2}}\right) - \frac{1}{2} erfc\left(\frac{u_{th}}{\sqrt{2}}\right) - \int_{u_r}^{u_{th}} f_{U_1}(u_1) erfc\left(\frac{u_x - \rho_n u_1}{\sqrt{2(1-\rho_n^2)}}\right) du_1 \qquad (6.12)$$

where ρ_n is the correlation coefficient of the reduced zero mean standard deviation 1 Gaussian random variables of rain attenuation and

$$u_r = \frac{\ln\left(r \big/ A_{m,j} \right)}{S_{A,j}} \qquad (6.13)$$

$$u_{th} = \frac{\ln\left(A_{th} \big/ A_{m,j} \right)}{S_{A,j}} \qquad (6.14)$$

$$u_x = \frac{\ln\left(\left(A_{m,j} \exp\left(S_{A,j} u_1 \right) - r \right) \big/ A_{m,ij} \right)}{S_{A,ij}} \qquad (6.15)$$

$$f_{U_1}(u_1) = \frac{1}{\sqrt{2\pi}} \exp\left(-\frac{u_1^2}{2} \right) \qquad (6.16)$$

with $r = SIR_{CS,dB} - SIR_{th}$ and $A_{m,j}$, $S_{A,j}$, $A_{m,ij}$, $S_{A,ij}$ are the parameters of lognormal distribution for the rain attenuation induced in the satellite links respectively.

SIR time series for the incumbent or the cognitive user can be generated through the multi-dimensional rain attenuation time series generator given in the channel model Section. For the incumbent user spatially correlated time series of rain attenuation A_p and A_{sp} are generated and then through (6.3), *SIR* time series are obtained.

For the cognitive user, time series of rain attenuation values A_s and A_{ps} are generated and then through (6.4), the *SIR* time series are obtained. Finally, there is a second way to obtain simultaneously correlated *SIR* time series for the incumbent and cognitive users. Firstly, a four-dimensional SDE is used as this is given in (6.7) for the generation of correlated time series of A_p, A_{sp}, A_s and A_{ps}. Then, through (6.3) and (6.4), *SIR* statistics are obtained. In Figure 6.3, spatially correlated time series of rain attenuation are shown for the four links of Figure 6.3 generated using (6.7) and in Figure 6.4, the time series of *SIR* for the two users, using the parameters of Table I. The frequency of the link was considered equal to 20GHz. Here it must be noted that the *SIR* time series of the two users are correlated.

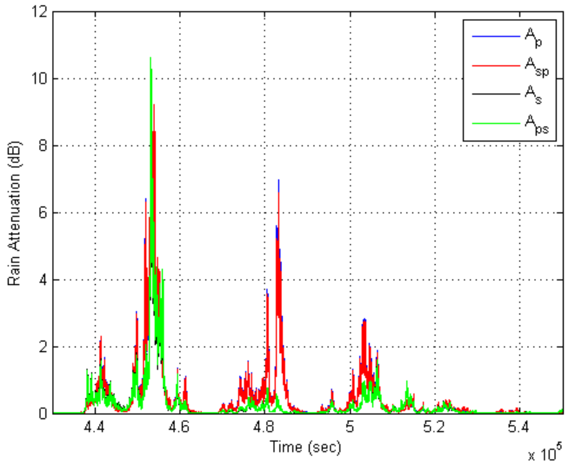

Figure 6.3. Spatially correlated time series of rain attenuation for the four links

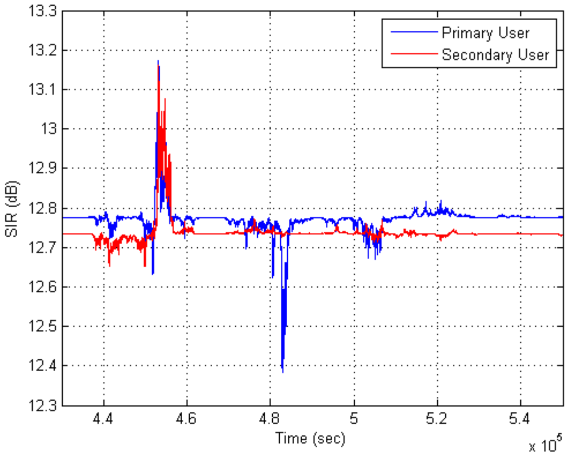

Figure 6.4 Correlated *SIR* time series for both users

6.1.4 Numerical Results and Discussion

In this Section, the numerical evaluation of the performance of the links for the coexistence of two satellite links is presented. The system's parameters are shown in Table I. Firstly, we consider the *SIR* statistics for the incumbent link. In Figure 6.5, the outage probability as this is given in (6.12) is presented for both frequencies and the parameters of Table I. The outage probability is computed with both methodologies of previous Section, while in Figure 6.6, the same curves are shown but for the cognitive user. It can be observed that the time series generator reproduces the first-order statistics.

TABLE I. System's Parameters

Parameters	Values
Frequency	20GHz, 14GHz
Incumbent Satellite (S_1)	22°E

Parameters	Values
Cognitive Satellite (S_2)	20°E
Satellite EIRP	54 dBW
G_{max}	32 dBi
Location of Ground Stations	Athens, Greece
Elevation angle S_1-GS_1	45.19°
Elevation angle S_2-GS_1	45.06°
Separation Angle for Incumbent Link	3.24°
Elevation angle S_1-GS_2	45.19°
Elevation angle S_2-GS_2	45.06°
Separation Angle for Cognitive Link	3.24°
Marginal Rain attenuation (Time Percentage Exceeded)	15.9 (0.01%)
Separation of Ground Stations	5 km

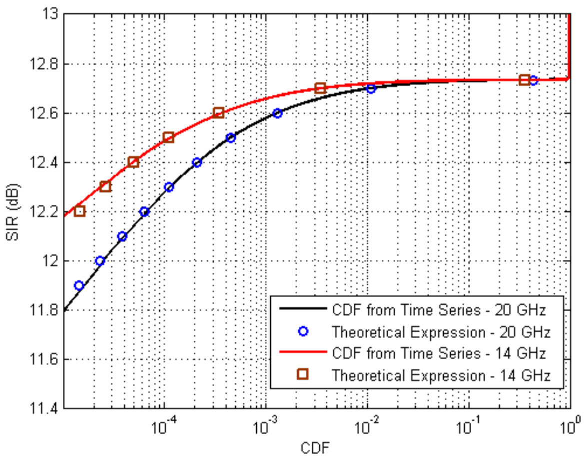

Figure 6.5 Outage probability due to interference for the incumbent user

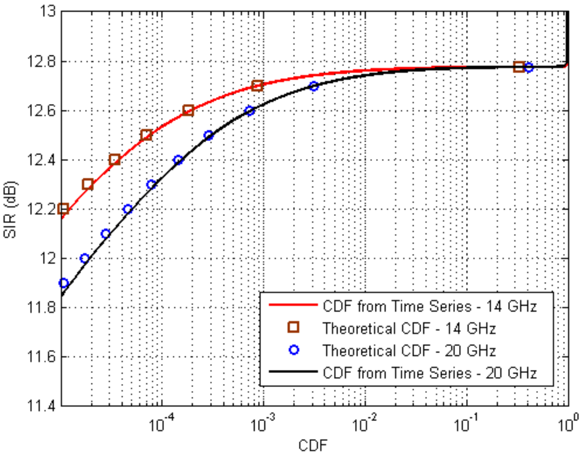

Figure 6.6. Outage probability due to interference for the cognitive user

Next we consider the parameters of Table I, except from the marginal rain attenuation. We consider the rain attenuation values of (31.88, 20.32, 15.9, 7.9, 5.6) which correspond to exceedance probabilities of (0.001%, 0.005%, 0.01%, 0.05%, 0.1%). The resulted CDF is shown in Figure 6.7.

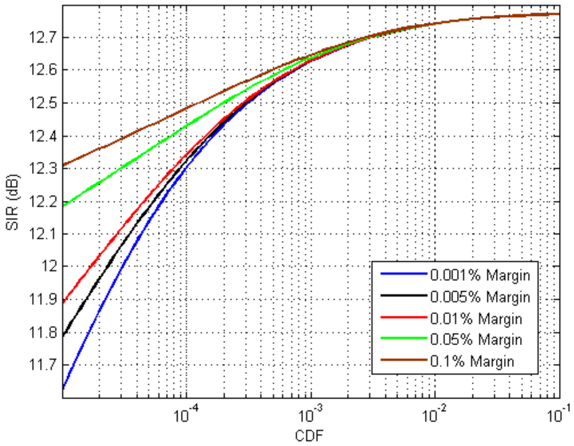

Figure 6.7 CDF of *SIR* given that rain attenuation does not exceed the marginal values corresponding to five different time percentages for the incumbent user

From Figure 6.7, it can be observed that the higher the marginal rain attenuation the higher the CDF of *SIR* at a given *SIR* threshold. This means that when the system can support lower rain attenuation values, the impact of the interference into the system is lower. Finally, we investigate the impact of the separation angle of the two convergent links on the *SIR* statistics. Again, we consider the value of Table I including the elevation angles. However, we do not consider these two satellites. For the given elevation angles of Table I, we consider four different separation angles: (30^o, 20^o, 10^o, 5^o). The results are shown in

Figure 6.8. As expected the higher the separation angle, the lower is the impact of interference in the system's performance.

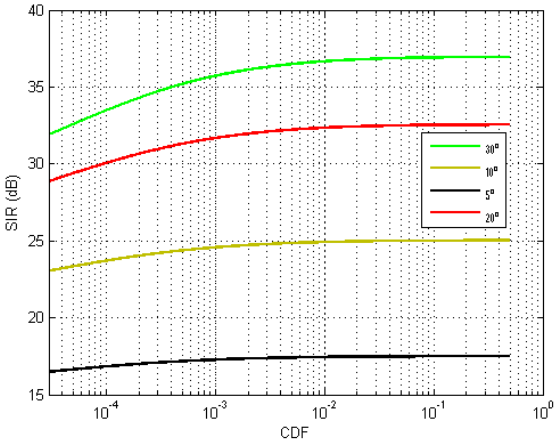

Figure 6.8. CDF of *SIR* given that rain attenuation does not exceed a marginal value for four different separation angles for the incumbent user.

6.2 Statistical Characterization of Adjacent Satellite Interference for Earth Stations on Mobile Platforms Operating at Ku and Ka Band

In this Section the downlink and uplink CNIR statistical distributions of a broadband ESOMP are tackled by analytical means. Aside from the statistical investigation of the problem, also an accurate CNIR time series synthesizer is developed based on Stochastic Differential Equations (SDE) capturing apart from the temporal also the spatial correlation between the wanted and interfering slant paths. This synthesizer enables then the link designer to perform dynamic simulation of the CNIR accounting for propagation impairments. In our view, the models proposed in this letter are very handy to the channel modeling group of the digital video broadcasting-satellite to extension (DVB-S2X) technical module [Ginesi14].

6.2.1 Channel Model

For a single mobile satellite link under line of sight (LOS) conditions and using directive antennas, the effects of shadowing and multipath are neglected. Similar to [Arapoglou12], we assume that the single path rain attenuation follows the long-term lognormal distribution. Its statistical parameters can be found by a regression fitting procedure on the long-term rain attenuation exceedance probabilitty of a mobile satellite link. The latter is calculated employing the transformation proposed in [Matrriciani95a] namely correcting the corresponding fixed link exceedance probability taking into account the average terminal speed and the prevailing weather front velocity. This yields the rain attenuation distribution over a single mobile link.

The fundamental assumption of our modeling -also consistent with experimental results-, is that the rain attenuation on two spatially separated links $A_i(t)$, $i=1,2$ follows the joint lognormal distribution (bivariate), namely that $\ln A_i$, $i=1,2$ follow the two-dimensional joint normal distribution [Panagopoulos04]. The long-term statistical parameters of the lognormal distribution for each of the two links are S_{ai}, $\ln A_{mi}$, $i=1,2$. The latter two parameters are the standard deviation of natural logarithm of rain attenuation and the median value of rain attenuation, respectively. The correlated rain attenuation stochastic processes are described through the following system of SDEs [Karagiannis12]:

$$dA_i(t) = A_i(t)\left[\frac{s_{ii}^2 + s_{ij}^2}{2} - \beta_i \ln\left(\frac{A_i(t)}{A_{mi}}\right)\right]dt + A_i(t)s_{ii}dW_t^i + A_i(t)s_{ij}dW_t^j, \quad (6.17)$$
$$\{i = 1,2,\ j = 2,1, \text{respectively}\}$$

where W_t^i, $i = 1,2$ are independent Wiener processes. Using the nonlinear transformations $X_t^i = \ln\left(A_i(t)\ /\ A_{mi}\right), i = 1,2$, (6.17) is transformed into the linear system of SDE of the Ornstein-Uhlenbeck type [Karatzas05]:

$$dX_t^i = -\beta_i X_t^i dt + s_{ii}dW_t^i + s_{ij}dW_t^j \quad (6.18)$$

In the above, β_i are the dynamic parameters of rain attenuation in the convergent slant paths evaluated using the methodology in [Karagiannis12]. The parameters s_{ij}, $1 \le i,j \le 2$ can be derived following a similar methodology as the one described in [Karagiannis12] by using the stationary covariances and cross-covariances of the solutions X_t^i. The solution $\mathbf{X}_t = [X_t^1, X_t^2]^T$ of the system in (6.18) is:

$$\mathbf{X}_t = e^{t\cdot\mathbf{B}}\cdot\mathbf{X}_0 + e^{t\cdot\mathbf{B}}\cdot\int_0^t e^{-s\cdot\mathbf{B}}\cdot\mathbf{S}\cdot d\mathbf{W}_s \quad (6.19)$$

where $e^{t\cdot\mathbf{B}} = \sum_{n=0}^{\infty}(t^n / n!)\mathbf{B}^n$ and $d\mathbf{W}_S$ is a two dimensional Wiener process. Here we have also used the matrix $\mathbf{B} = \operatorname{diag}\left[-\beta_1, -\beta_2\right]$ and the matrix $\mathbf{S} = \left[s_{ij}\right]_{1\le i,j\le 2}$.

6.2.2 *Statistical Interference Analysis*

In the next two subSections the CNIR is treated as a random variable and its outage probability is analytically calculated in the downlink and the uplink. In Figure 6.9, the geometry of the considered system is shown. We consider two mobile terminals ESOMP$_i$, i=1,2 in Figure 6.9.

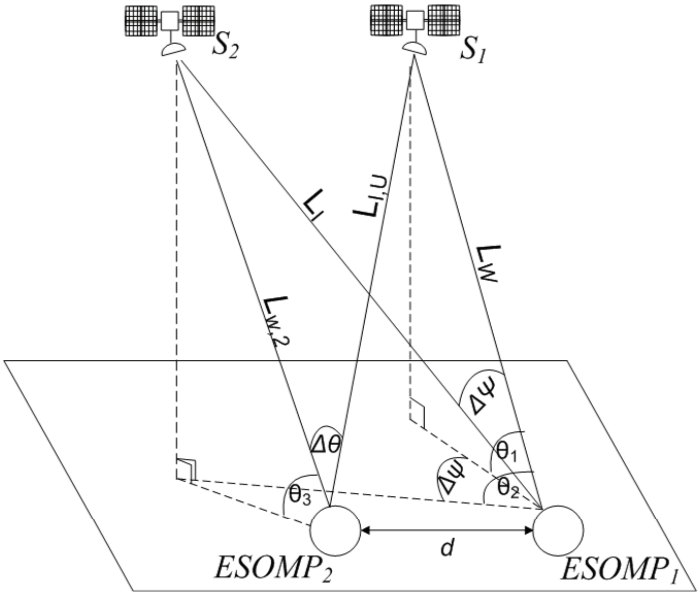

Figure 6.9 Configuration of the interference Scenarios.

6.2.2.1 Downlink Case

We consider ESOMP$_1$ receiving from satellite S1 (wanted link) and being interfered by the adjacent satellite S2 (interfering link). The *CNIR* under differential rain attenuation between the wanted and the interfering link is given by in linear terms as:

$$CNIR = \frac{\left(CNR\right)_{\mathrm{cs}}^{\mathrm{DL}}\left(T_{\mathrm{cs}}\ / T\left(A_{\mathrm{w}}\right)\right)10^{-\frac{A_{\mathrm{w}}}{10}}}{1+\left(INR\right)_{\mathrm{cs}}^{\mathrm{DL}}\left(T_{\mathrm{cs}}\ / T\left(A_{\mathrm{w}}\right)\right)10^{-\frac{A_{\mathrm{I}}}{10}}}\$ \qquad (6.20)$$

where CNR_{cs} is the carrier-to-noise ratio and INR_{cs} is the interference-to-noise ratio under clear sky conditions and A_{w} and A_{I} (dB) are the values of rain attenuation over the wanted and interfering link, respectively. Their values can be calculated by employing basic transmission theory:

$$\begin{aligned}\left(CNR\right)_{\mathrm{cs}}^{\mathrm{DL}} &= \left(EIRP_{\mathrm{S1}}G_{\mathrm{ESOMP}}(0^{o})FSL(L_{\mathrm{w}})\,/\,(kT_{\mathrm{cs}}B)\right)\\ \left(INR\right)_{\mathrm{cs}}^{\mathrm{DL}} &= \left(EIRP_{\mathrm{S2}}G_{\mathrm{ESOMP}}(\Delta\Psi)FSL(L_{\mathrm{I}})\,/\,(kT_{\mathrm{cs}}B)\right)\end{aligned} \qquad (6.21)$$

with $EIRP_{\mathrm{S1}}$ and $EIRP_{\mathrm{S2}}$ are the radiated powers from the satellites S1 and S2 towards the direction of the receiver. T_{cs} is the clear sky noise temperature. G_{ESOMP} (ΔΨ) is the antenna gain at angle ΔΨ from the maximum antenna gain. $FSL(L)$ is the free space loss of slant path L. The antenna sidelobe gain at an angle ΔΨ from the maximum can be computed from ITU-R Recommendation S.465 [ITU-R. S.465]. We also consider the following sky noise temperature under rain conditions [Toptsidis12]:

$$T(A_{\mathrm{w}}) = T_{\mathrm{cosmic}}\cdot 10^{-\frac{A_{\mathrm{w}}}{10}} + T_{\mathrm{eq}}\cdot(1-10^{-\frac{A_{\mathrm{w}}}{10}}) \qquad (6.22)$$

with T_{cosmic} the cosmic noise temperature equal to 3^{o} K and T_{eq} is the equivalent temperature of the receiver under clear sky conditions. It is taken that $T_{\text{cs}}=T_{\text{cosmic}}+T_{\text{eq}}$.

For the downlink, the outage probability (P_{out}) of the ESOMP suffering from ASI is expressed as $P_{\text{out}} = P(CNIR\leq CNIR_{\text{thr}})$. Following the general considerations of Section with channel model and after straightforward probabilistic algebra:

$$P_{out\_\text{DL}} = \int_{A_{0,\text{DL}}}^{A_{\infty,\text{DL}}} \int_{0}^{g_{\text{DL}}(A_{\text{w}})} f(A_{\text{w}}, A_{\text{I}}) dA_{\text{I}} dA_{\text{w}} + \int_{A_{\infty,\text{DL}}}^{\infty} f(A_{\text{w}}) dA_{\text{w}} \tag{6.23}$$

with $f(A_{\text{w}})$ and $f(A_{\text{w}}, A_{\text{I}})$ are the single and joint PDF of rain attenuation, single and bivariate lognormal distribution in our approach. After some algebra, the above limits are:

$$A_{0,\text{DL}} = -10\log\left(\frac{CNIR_{\text{thr}}\cdot T_{\text{eq}} + CNIR_{\text{thr}}\cdot\left(INR\right)_{\text{cs}}^{\text{DL}} T_{\text{cs}}}{\left(CNR\right)_{\text{cs}}^{\text{DL}} T_{\text{cs}} + CNIR_{\text{thr}}\cdot T_{\text{eq}} - CNIR_{\text{thr}}\cdot T_{\text{cosmic}}}\right) \tag{6.24}$$

$$A_{\infty,\text{DL}} = -10\log\left(\frac{CNIR_{\text{thr}}\cdot T_{\text{eq}}}{\left(CNR\right)_{cs}^{\text{DL}} T_{\text{cs}} + CNIR_{\text{thr}}\cdot T_{\text{eq}} - CNIR_{\text{thr}}\cdot T_{\text{cosmic}}}\right) \tag{6.25}$$

$$g_{\text{DL}}(A_{\text{w}}) = -10\log\left(\frac{\left(CNR\right)_{\text{cs}}^{\text{DL}} T_{\text{cs}}\cdot 10^{-\frac{A_{\text{w}}}{10}} - CNIR_{\text{thr}}\cdot T(A_{\text{w}})}{CNIR_{\text{thr}}\left(INR\right)_{\text{cs}}^{\text{DL}} T_{\text{cs}}}\right) \tag{6.26}$$

Introducing the following transformations which can be considered as the reduced Gaussian variables of rain attenuation:

$$\begin{aligned} U_{\text{W}}(x) &= \left(\ln x - \ln A_{m\text{W}}^{m}\right)/S_{a\text{W}}^{m} \\ U_{\text{I}}(y) &= \left(\ln y - \ln A_{m\text{I}}^{m}\right)/\, S_{a\text{I}}^{m} \end{aligned} \tag{6.27}$$

where the parameters $A_{m\text{k}}^{m}, S_{a\text{k}}^{m}, \text{k} = \text{W}$ or I refer to the parameters of the rain attenuation induced on the wanted and interfering link, respectively. Using the above Gaussian variables and after algebra (6.23) becomes:

$$P_{\text{out\_DL}} = \int_{U_{\text{w}}(A_{0,\text{DL}})}^{U_{\text{w}}(A_{\infty,\text{DL}})} f_{U_{\text{w}}}\left(U_{\text{w}}\right)\left[1-\frac{1}{2}erfc\left(\frac{U_{\text{I}}\left(g_{\text{DL}}\left(A_{m\text{w}}^{m}\exp\left(U_{\text{w}}S_{a\text{w}}^{m}\right)\right)\right)-\rho_{nD}U_{\text{w}}}{\sqrt{2\left(1-\rho_{nD}^{2}\right)}}\right)\right]dU_{\text{w}} + \frac{1}{2}erfc\left(\frac{U_{\text{w}}(A_{\infty,\text{DL}})}{\sqrt{2}}\right) \tag{6.28}$$

where $f_{U_{\text{w}}}(U_{\text{w}})$ is the single PDF of zero mean and unity variance normal random variable. The limits of the above integral are given applying the trasformations in (6.27) on equations (6.24)-(6.26). Finally, ρ_{nD} is the logarithmic correlation coefficient of the mobile slant paths that is calculated through the methodology in [Kanellopoulos00] assuming constant projected angular separation of the wanted and the interfering slant paths ΔΨ.

Uplink Case

In the uplink case, the desired link is from ESOMP$_1$ to satellite S1 and the interfering link is from a different ESOMP$_2$ due the side lobes of the ESOMP$_2$ antenna. The two interfering links are considered parallel due to their small separation compared to the slant path lengths. Following similar analysis as for the downlink, the CNIR outage probability is the same as (6.28), but with different parameters:

$$P_{\text{out\_UL}} = \int_{U_{\text{w}}(A_{0,\text{UL}})}^{U_{\text{w}}(A_{\infty,\text{UL}})} f_{U_{\text{w}}}\left(U_{\text{w}}\right)\left[1-\frac{1}{2}erfc\left(\frac{U_{\text{I}}\left(g_{\text{UL}}\left(A_{m\text{w}}^{m}\exp\left(U_{\text{w}}S_{a\text{w}}^{m}\right)\right)\right)-\rho_{nU}U_{\text{w}}}{\sqrt{2\left(1-\rho_{nU}^{2}\right)}}\right)\right]dU_{\text{w}}$$

$$+\frac{1}{2}erfc\left(\frac{U_{\text{w}}(A_{\infty,\text{UL}})}{\sqrt{2}}\right)$$

(6.29)

where ρ_{nU} is the correlation factor and depends on the distance between the ESOMPs. Its value can be computed from [Kanellopoulos00]. In (6.29) the integral limits can be found by applying the transformation of the random variables in (6.27) on the following parameters that have been obtained from algebra:

$$A_{0,\text{UL}} = -10\log\left(\frac{CNIR_{\text{thr}} + CNIR_{\text{thr}}\left(INR\right)_{\text{cs}}^{\text{UL}}}{\left(CNR\right)_{\text{cs}}^{\text{UL}}}\right) \quad (6.30)$$

$$A_{\infty,\text{UL}} = -10\log\left(\frac{CNIR_{\text{thr}}}{\left(CNR\right)_{\text{cs}}^{\text{UL}}}\right) \quad (6.31)$$

$$g_{\text{UL}}(A_{\text{w}}) = -10\log\left(\frac{\left(CNR\right)_{\text{cs}}^{\text{UL}}10^{-\frac{A_C}{10}} - CNIR_{\text{thr}}}{CNIR_{\text{thr}}\cdot\left(INR\right)_{\text{cs}}^{\text{UL}}}\right) \quad (6.32)$$

and

$$\begin{aligned}\left(CNR\right)_{\text{cs}}^{\text{UL}} &= \left(EIRP_1(0^{o})G_{S_1}FSL(L_{\text{w}})/(kT_{\text{cs,UL}}B)\right)\\ \left(INR\right)_{\text{cs}}^{UL} &= \left(EIRP_2(\Delta\theta)G_{S_2}FSL(L_{\text{I,UL}})/kT_{\text{cs,UL}}B\right)\end{aligned} \quad (6.33)$$

where *EIRP*$_1$ is the maximum EIRP of the wanted ESOMP and the *EIRP*$_2$ is the EIRP($\Delta\theta$) of the interfering ESOMP towards S1 at an angle $\Delta\theta$ from its maximum, given by ITU-R S.524 [ITU-R. S.524].

6.2.3 Numerical Results

Firstly, the downlink CNIR outage probability is examined for various ESOMP antenna diameters. The input parameters for the numerical results are mostly taken from [Ginesi14] and [Hibberd12].

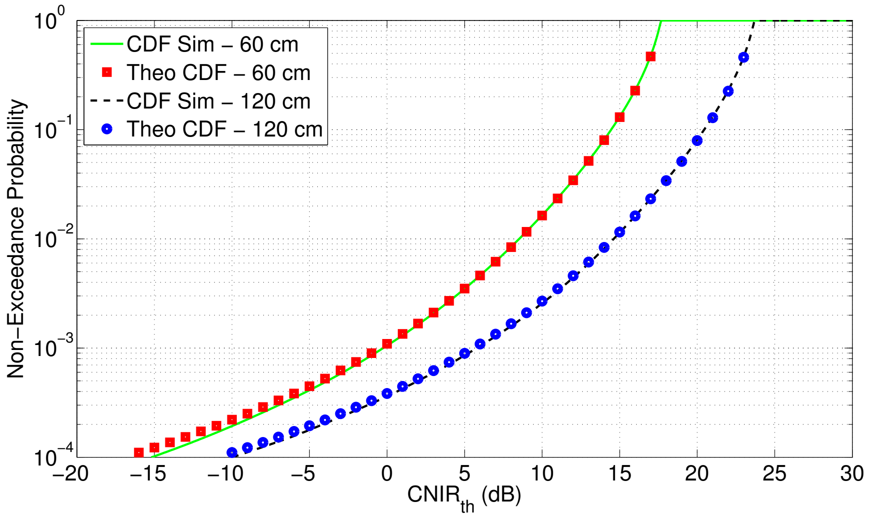

Figure 6.10 CDF of downlink CNIR at Ka Band

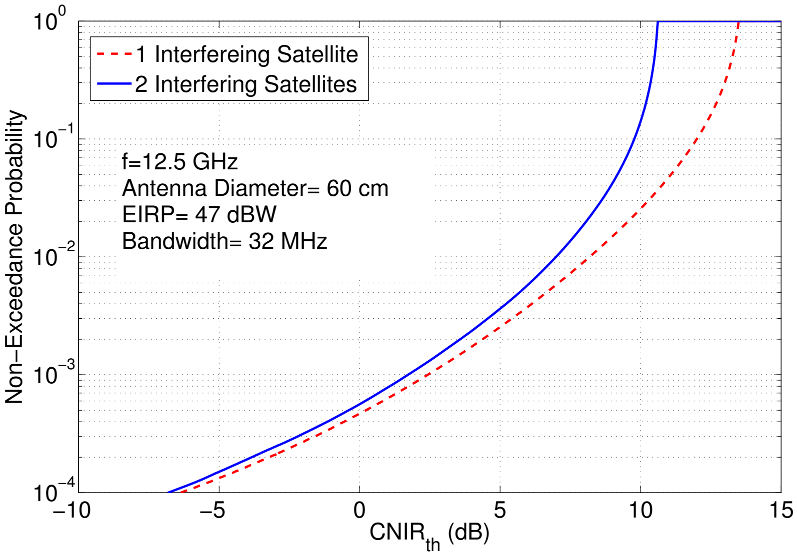

Figure 6.11 CDF of downlink CNIR for multiple inteferring satellites at Ku band

In Figure 6.10, the ESOMP (vessel in this case) is assumed to be located in the North Sea and employs two antenna diameters: 60 cm and 1.2 m. The wanted GEO satellite is at 3^{o}E, while the interfering one is at 5^{o}E. The downlink frequency is 20 GHz, the signal bandwidth 32MHz and the satellite EIRP 52 dBW for both satellites. The wind speed is 50 km/h, the ESOMP speed is 25 km/h (typical for vessels) and the realtive angle between wind and ESOMP velocity is 45^o. The correlation coefficient ρ_{nD}=0.9 since the separation angle between the two satellites is small. In the same figure, we compare the theoretical model against the simulation results from the proposed SDE based mobile rain attenuation synthesizer of mobile satellite channel Section. The results almost coincide. Moreover, for a typical outage of 99.7%, the CNIR for 60 cm and 1.2 m are approximately 5dB and 11dB, respectively. Please note that the new DVB-S2X standards foresees modulation and coding schemes down to about CNIR -10 dB.

In Figure 6.11, the impact of two adjacent interfering satellites at 1^{o}E and 5^{o}E operating in Ku band (carrier frequency 12.5 GHz) is investigated. It is observed that there are small differences between having one and two interfering satellites for small outage probabilities. However, at higher CNIR values, the impact of a second interfering satellite is more pronounced.

For the uplink case, we consider a Ka band (30 GHz) scenario, the signal bandwidth is 5 MHz and the EIRP of the ESOMPs are 55 dBW for 60 cm antenna diameter. The satellite $(G/T)_s$ is 10 dB/K. In order to consider the worst case, the rain attenuation correlation coefficient is considered equal to zero (uncorrelated). The uplink CNIR outage probability results are depicted in Figure 6.12 for two ESOMP speeds: 25 km/h and 50 km/h. The relative angle between the storm front and the ESOMP movement is 150^o. Both the analytical model of (6.29) and simulations are presented. It is worth noting that the decrease of the outage probability with the increase of the ESOMP speed occurs due to the choice of relative angle [Matricciani95a].

Finally, since analytically this problem becomes very much involved, in Figure 6.13 the proposed simulator is employed to assess the impact of more than one interfering ESOMPs. We assume Ku band (14 GHz) with 60cm antenna diameters (EIRP 53 dBW) and the cases of 1, 2 and 3 interfering ESOMPs. (The satellite $(G/T)_s$ is 3 dB/K.) From Figure 6.13, it can be deduced that increasing the number of ESOMPs, increases the outage probability for a certain CNIR threshold.

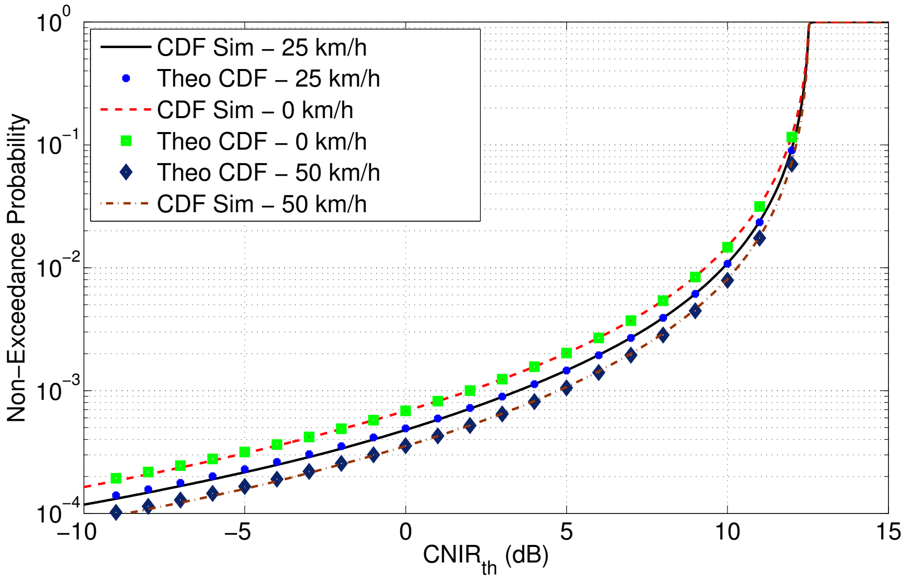

Figure 6.12 CDF of uplink CNIR for ESOMPS at Ka Band

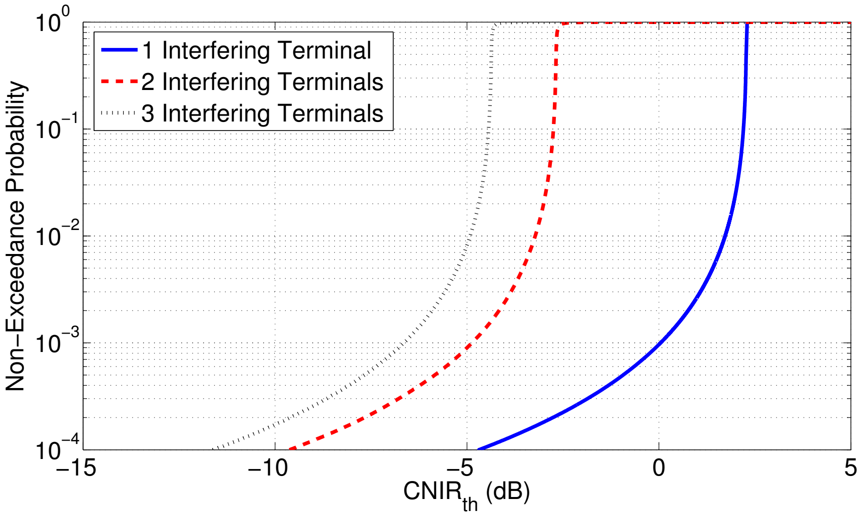

Figure 6.13 CDF of uplink CNIR at uplink for multiple interfering ESOMPS at Ku Band.

6.3 Cognitive Satellite Uplink and Terrestrial Fixed-Service Coexistence in Ka-band

This Section investigates the impact of the propagation phenomena in a co-existence scenario of satellite uplink Fixed Satellite Service (FSS) and terrestrial Fixed Service (FS) systems operating in Ka-band. Specifically, we analytically derive the Signal-to-Interference Ratio (*SIR*) and the Signal-to-Noise plus Interference Ratio (*SNIR*) statistical distributions considering an accurate space-time dependent propagation channel model, which is appropriate for these frequencies and is also used for validation.

6.3.1 Statistical Interference Analysis

6.3.1.1 SIR Analysis

A metric of interest in case of interference analysis is the *SIR* considering that the link is available in terms of SNR. In the case of Ka-band, the availability of the link is considered through a given percentage of rain attenuation compensation.

The goal is to examine the following CDF of *SIR*:

$$P_{out} = P\left[SIR \le SIR_{th}, A_{in} \le A_{th,in}\right] \tag{6.34}$$

In the above expression, the CDF of *SIR* is calculated for the case that the link is available, i.e. rain attenuation induced on the incumbent link A_{in} (in dB) is less than a given threshold $A_{th,in}$. The expression of (6.34) has been analytically calculated in Section 5.1 and the expressions are repeated here:

$$P_{out} = \frac{1}{2}erfc\left(\frac{u_r}{\sqrt{2}}\right) - \frac{1}{2}erfc\left(\frac{u_{th}}{\sqrt{2}}\right) - \int_{u_r}^{u_{th}} f_{U_1}(u_1) erfc\left(\frac{u_x - \rho_n u_1}{\sqrt{2(1-\rho_n^2)}}\right) du_1 \tag{6.35}$$

where ρ_n is the correlation coefficient of the reduced zero mean and unity standard deviation Gaussian random variables of rain attenuation and

$$u_r = \frac{\ln\left(r \middle/ A_{m,in} \right)}{S_{A,in}} \tag{6.36}$$

$$u_r = \frac{\ln\left(r \middle/ A_{m,in} \right)}{S_{A,in}} \tag{6.37}$$

$$u_{th} = \frac{\ln\left(A_{th} \middle/ A_{m,in} \right)}{S_{A,in}} \tag{6.38}$$

$$u_x = \frac{\ln\left(\left(A_{m,j} \exp\left(S_{A,in} u_1 \right) - r \right) \middle/ A_{m,I} \right)}{S_{A,I}} \tag{6.39}$$

$$f_{U_1}(u_1) = \frac{1}{\sqrt{2\pi}} \exp\left(-\frac{u_1^2}{2} \right) \tag{6.40}$$

In (6.36)-(6.40)(10)-(13), $r = SIR_{CS,dB} - SIR_{th}$ and $A_{m,in}$, $S_{A,in}$, $A_{m,I}$, $S_{A,I}$ are the statistical parameters of rain attenuation induced in the incumbent link and interfering link, respectively.

6.3.1.2 SNIR Analysis

The general case is the calculation of the *SNIR* cumulative distribution of the incumbent link. The methodology is the same with Section 5.2. However, the clear sky values change and the formulations since both links are terrestrial in the case of this Section. Given the system under consideration, the *SNIR* for one interfering link is:

$$SNIR = \frac{(SNR)_{\mathrm{CS}} \left(T_{\mathrm{C}} \;/ T(A_{\mathrm{in}}) \right) 10^{-\frac{A_{\mathrm{in}}}{10}}}{1 + (INR)_{\mathrm{CS}} \left(T_{\mathrm{C}} / T(A_{\mathrm{in}}) \right) 10^{-\frac{A_{\mathrm{I}}}{10}}} \tag{6.41}$$

where

$$\begin{aligned} (SNR)_{\mathrm{CS}} &= \left(EIRP_{in} G_{FS}(0^o) FSL(L_{in}) / (kT_{\mathrm{C}}B) \right) \\ (INR)_{\mathrm{CS}} &= \left(EIRP(\Delta\theta) G_{\mathrm{FS}}(\Delta\Psi) FSL(L_{\mathrm{I}}) / (kT_{\mathrm{C}}B) \right) \end{aligned} \tag{6.42}$$

$$T(A_{\mathrm{in}}) = T_{\mathrm{cosmic}} \cdot 10^{-\frac{A_{\mathrm{in}}}{10}} + T_{\mathrm{eq}} \cdot (1 - 10^{-\frac{A_{\mathrm{in}}}{10}}) \tag{6.43}$$

$$T_{\mathrm{C}} = T_{\mathrm{cosmic}} + T_{\mathrm{eq}} \tag{6.44}$$

In (6.42)-(6.44), $FSL(\ )$ is the corresponding free space loss, $\Delta\theta$ the angle with respect to satellite antenna bore-sight, $\Delta\psi$ the angular separate with respect to the antenna maximum gain of the incumbent link, k $1.38 \cdot 10^{-23}$J/K, T_C 278°K, B28 MHz, T_{cosmic} 3°K and T_{eq} 275°K. Following similar statistical analysis with the one presented in previous Section, the analytical expression for the calculation of outage probability, i.e. $P_{\mathrm{out}} = P\left(SNIR \le SNIR_{\mathrm{thr}} \right)$ is given by:

$$P_{\text{out}} = \int_{U_{\text{w}}(A_0)}^{U_{\text{w}}(A_\infty)} f_{U_{\text{w}}}(U_{\text{w}}) \left[1-\frac{1}{2} erfc\left(\frac{U_{\text{I}}\left(g\left(A_{m,\text{in}} \exp\left(U_{\text{w}} S_{a,\text{in}}\right)\right)\right) - \rho_{nD} U_{\text{w}}}{\sqrt{2\left(1-\rho_{nD}^2\right)}}\right)\right] dU_{\text{w}} + \frac{1}{2} erfc\left(\frac{U_{\text{w}}(A_\infty)}{\sqrt{2}}\right) \tag{6.45}$$

where

$$A_0 = -10\log\left(\frac{SNIR_{\text{thr}} \cdot T_{\text{eq}} + SNIR_{\text{thr}} \cdot (INR)_{\text{CS}} T_{\text{C}}}{(SNR)_{\text{CS}} T_{\text{C}} + SNIR_{\text{thr}} \cdot T_{\text{eq}} - SNIR_{\text{thr}} \cdot T_{\text{cosmic}}}\right) \tag{6.46}$$

$$A_\infty = -10\log\left(\frac{SNIR_{\text{thr}} \cdot T_{\text{eq}}}{(SNR)_{CS} T_{\text{C}} + SNIR_{\text{thr}} \cdot T_{\text{eq}} - SNIR_{\text{thr}} \cdot T_{\text{cosmic}}}\right) \tag{6.47}$$

$$g(A_{\text{w}}) = -10\log\left(\frac{(SNR)_{\text{CS}} T_{\text{C}} \cdot 10^{-\frac{A_{\text{w}}}{10}} - SNIR_{\text{thr}} \cdot T(A_{\text{in}})}{SNIR_{\text{thr}} (INR)_{CS} T_{\text{C}}}\right) \tag{6.48}$$

$$U_{\text{W}}(x) = \left(\ln x - \ln A_{m,\text{in}}\right) / S_{a,\text{in}} \tag{6.49}$$

$$U_{\text{I}}(y) = \left(\ln y - \ln A_{m\text{I}}\right) / S_{a\text{I}} \tag{6.50}$$

In (6.45), $f_{U_{\text{w}}}(U_{\text{w}})$ is the single probability density function (pdf) of a zero mean and unity variance normal random variable. The corresponding antenna diagrams for the calculation of the Effective Isotropic Radiated Power (EIRP) of the interfering link and the gain of antenna receiver of the wanted incumbent links are employed from the ITU-R Recommendation S.524 [ITU-R. S.524] and ITU-R Recommendation S.465 [ITU-R. S.465], respectively. Finally, the *SNIR* distribution considering multiple interfering links can be derived using the channel model presented in Section II.

6.3.2 Numerical Results and Discussion

In this Section, we investigate the effect of the propagation phenomena, mainly rain attenuation, on the *SNIR* and *SIR* statistics. The baseline scenario considered in this Section assumes that the FSS and FS ground terminals are located in the City of Luxembourg. The relevant system parameters are given in Table II.

TABLE II.

System Parameters

Parameter	Value
Operating frequency	29 GHz
Incumbent Link Path Length, L_{in}	3 km
Interfering Link Path Length, L_I	5 km

Parameter	Value
Bandwidth of Incumbent Link, B	28 MHz
FS Tx Antenna Gain, G_T	19 dBi
FS Rx Antenna Gain, $G_R(0^o)$	19 dBi
FS Tx Transmit Power, P_T	-6 dBW
$EIRP_{\mathrm{FSS}}$	See ITU-R. S. 524
FS Rx Antenna Gain, $G_R(\Delta\psi)$	See ITU-R. S. 465

In Table II, the EIRP of the FSS ground terminals is calculated through the ITU-R Recommendation S. 524, which gives the maximum EIRP of ground station for different angle from the directivity axis. Also, the antenna gain at the receiver of incumbent link from the interferers, $G_R(\Delta\psi)$, is calculated through ITU-R Recommendation S. 465. Hereinafter, numerical results are provided for two distinct cases: the single interferer case and the multiple interferers case.

6.3.2.1 Single Interferer Case

Firstly, the *SNIR* outage probability is calculated for a single FSS interferer with a separation angle of 30^o from the directivity axis. The CDF of *SNIR* was calculated analytically using (6.45) and from the time series generator. The results are shown in Figure 6.14. It can be observed that the CDF from the simulator coincides with that of the analytical expression.

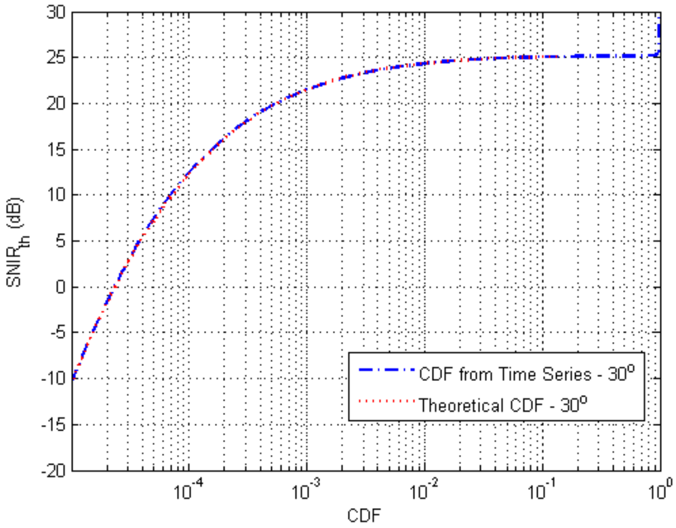

Figure 6.14 *SNIR* statistics for a separation angle of 30° and one FSS interfering link: Theoretical vs. Simulation results

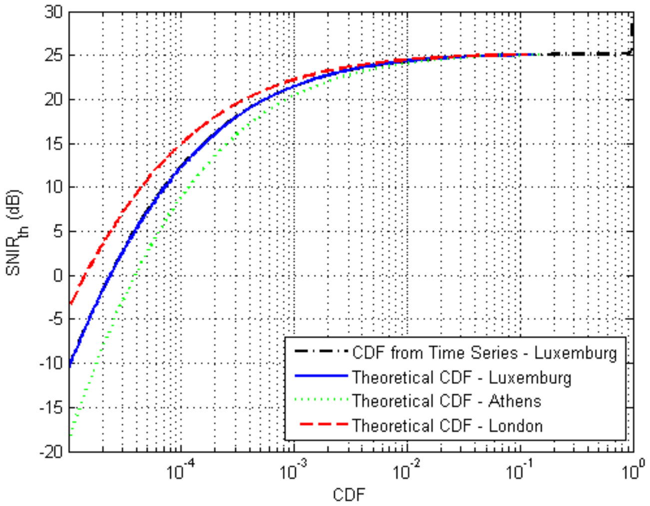

Figure 6.15 *SNIR* statistics for a separation angle of 30° and for different cities: Impact of climatic conditions

In Figure 6.15, the CDF of *SNIR* is shown for different locations of the FS and FSS terminals. In particular, apart the City of Luxembourg, Athens and London are assumed. It can be observed that the *SNIR* for a given probability level is higher at London, then at Luxembourg and finally at Athens. This is due to the fact that in Athens, rain attenuation exceeds higher values than the other sites, due to the higher rain rate (mm/hr) observed at Athens. The *SNIR* aggravation due to rain fading will be greater in heavier climatic regions (e.g., Brazil, Singapore, etc).

In Figure 6.16, the CDF of *SIR* is shown for two cases, an FSS interferer at 10° from directivity axis and at 60° from directivity axis. Again, as in Figure 6.14, the CDF is calculated analytically using (9) and from time series generator, showing for both cases that the generator reproduces the CDF of *SIR*. Moreover, from Figure 6.16, it can be observed that the *SIR* is lower for 10^o separation angle than for 60^o. The interference level in the former case is higher than in the later case since the antenna gain of the receiver of the incumbent link is also higher (due to the smaller separation angle).

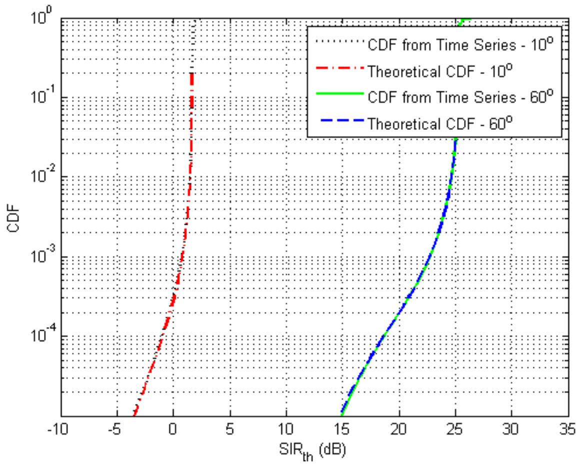

Figure 6.16 *SIR* statistics considering one FSS interfering link: Theoretical vs. simulation results and impact of separation angle.

6.3.2.2 *Multiple Interferers Case*

In this Section, the multiple interferers' case is examined. The statistics of *SNIR* and *SIR* for multiple FSS interferers are generated from the multi-dimensional synthesizer presented in [Karagiannis12]. For the *SNIR*, the cases of 1, 2 and 3 FSS interferers are examined and the results are presented in Figure 6.17. For the case of 1 interferer, the separation angle is 30^o. For the 2 interferers' case, the angle between the first interferer and the directivity axis is 30^o from one side and the second interferer has a separation angle of 60^o on the other side of the directivity axis. So, the two interferers have a 90^o separation angle between them. The spatial correlation of rain attenuation induced on the links from the two interferers is needed as input to the multi-dimensional synthesizer and is calculated through the modeling in [Karagianni12], [Kanellopoulos00]. For the case of the 3 interferers, the first one is located on the different side of directivity axis of the FS receiver than the other two. The first interferer has a separation angle of 30^o, while the second and the third one refer to 60^o and 80^o separation angles, respectively. Therefore, the separation angle between the first and second interferer is $\theta_{12}=90^o$, while $\theta_{13}=110^o$ and $\theta_{23}=20^o$.

From Figure 6.17, it can be observed that increasing the number of FSS interferers, the outage probability for a given *SNIR* threshold increases, since the interference level increases as well. In Figure 6.18, the CDF of *SIR* is shown for a single interferer and for two interferers. The separation angle of the first interferer to the directivity axis of the FS receiver is 10^o on the one side and 10^o of the second interferer but on the other side of the axis. Therefore, the separation angle between the links from the 2 FSS stations is 20^o.

Again as in Figure 6.17, it can be seen that the *SIR* is decreasing with the increase of interferers.

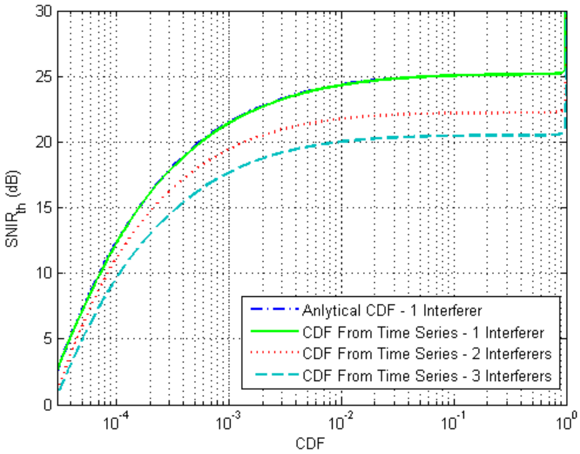

Figure 6.17. *SNIR* statistics considering the co-existence of 1, 2 and 3 FSS interfering links

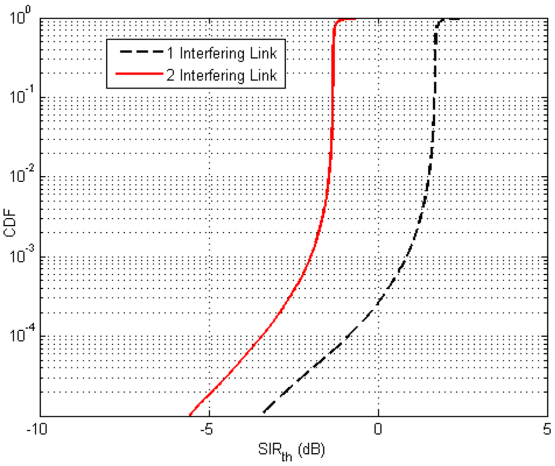

Figure 6.18. SIR statistics for 1 and 2 FSS interfering links.

6.4 Earth Observation High Date Rate Downlink Performance

The synthesizer proposed in Section 4.2 has been used for the assessment of Earth Observation links operating at Ka- and Q-band and using Adaptive Coding and Modulation system. This work has been undertaken under the SatNEx III project.. More particularly, the link budget used is given in Table VI for Ka-band and at Table VII at Q-band. In Table VIII, the modcod thresholds are given.

Table III. Link Budget Parameters for EO systems assessment at Ka-band

Parameter	Unit	Value

Channel bandwidth	MHz	500
Roll-Off factor		0.25
Carrier frequency	GHz	26.5
TWTA saturation power	W	70
OMUX and W/G losses	dB	2.4
OBO	dB	5
Antenna size	cm	30
Antenna efficiency	%	65
Boresight gain	dBi	36.54
Depointing Loss	dB	3
Total EIRP per channel	dBW	44.59
Slant range	km	1233.09
FSPL	dB	182.73
Additional losses	dB	2
GW Antenna diameter	m	7
GW Antenna efficiency	%	65
Pointing inaccuracy	°	0.03
Boresight gain	dBi	63.9
Depointing loss	dB	0.86
Clear Sky Noise Temperature	K	30
Birghtness Temperature of the Ground	K	10
Antenna Noise Temperature	K	40
Noise Figure of the LNA	dB	1
Receiver Noise Temperature	K	75.09
System Noise Temperature	K	115.09
G/T	dB/K	42.43
C/N_0	dBHz	130.9

Es/N0	dB	44.87
ModCod Threshold Es/N0	dB	29.5
Additional Degradation	dB	2.6
Link Margin	dB	12.77
Data Rate	Gbps	3.4
Additional Loss (radome)	dB	3
C/N_0	dBHz	127.9
Es/N0	dB	41.87
ModCod Threshold Es/N0	dB	29.5
Additional Degradation	dB	2.6
Link Margin	dB	9.77
Data Rate	Gbps	3.4

Table IV. Link Budget Parameters for EO systems assessment at Q-band

Parameter	Unit	Value
Channel bandwidth	GHz	1
Roll-Off factor		0.25
Carrier frequency	GHz	40
TWTA saturation power	W	100
OMUX and W/G losses	dB	4
OBO	dB	5
Antenna size	cm	30
Antenna efficiency	%	65
Boresight gain	dBi	40.12
Depointing Loss	dB	4
Total EIRP per channel	dBW	47.12
Slant range	km	1233.09

FSPL	dB	186.3
Additional losses	dB	2
GW Antenna diameter	m	7
GW Antenna efficiency	%	65
Pointing inaccuracy	°	0.03
Boresight gain	dBi	67.48
Depointing loss	dB	1.96
Clear Sky Noise Temperature	K	45
Birghtness Temperature of the Ground	K	10
Antenna Noise Temperature	K	55
Noise Figure of the LNA	dB	1
Receiver Noise Temperature	K	75.09
System Noise Temperature	K	130.09
G/T	dB/K	44.38
C/N_0	dBHz	131.8
Es/N0	dB	42.77
ModCod Threshold Es/N0	dB	29.5
Additional Degradation	dB	2.6
Link Margin	dB	10.67
Data Rate	Gbps	6.8
Additional Loss (radome)	dB	3
C/N_0	dBHz	128.8
Es/N0	dB	39.77
ModCod Threshold Es/N0	dB	29.5
Additional Degradation	dB	2.6
Link Margin	dB	7.67
Data Rate	Gbps	6.8

Table V. Assumed ModCods

Index	Modulation	Code rate	E_s/N_0 [dB]	Additional Degradation	Eta [bit/s/Hz]	OBO [dB]
1	2	0,36	-0,5	0,5	0,72	0,3
2	2	0,43	0,34	0,5	0,86	0,3
3	2	0,51	1,5	0,6	1,02	0,3
4	2	0,6	2,7	0,6	1,2	0,3
5	3	0,47	3,9	0,5	1,41	0,3
6	3	0,54	5,1	0,6	1,62	0,3
9	3	0,62	6,2	0,7	1,86	0,3
10	3	0,7	7,6	0,8	2,1	0,3
11	3	0,79	9	0,9	2,37	0,3
12	4	0,66	9,1	1,2	2,64	1
15	4	0,73	10,2	1,3	2,92	1
16	4	0,8	11,5	1,4	3,2	1,1
17	4	0,88	13	1,4	3,52	1,3
20	5	0,76	14	1,1	3,8	2,1
21	6	0,69	14,8	1,6	4,14	2,1
22	6	0,74	15,7	1,7	4,44	2,4
25	7	0,69	16,5	1,6	4,83	2,8
26	7	0,74	17,6	1,7	5,18	3,2
27	8	0,69	19	1,7	5,52	3
28	8	0,74	20,5	1,8	5,92	3,5
29	8	0,79	22	1,9	6,32	4,1
30	10	0,69	23,5	2,2	6,9	3,5
31	10	0,74	25,3	2,3	7,4	4
32	10	0,79	27	2,4	7,9	4,6

33	10	0,85	29,5	2,6	8,5	5

Using the proposed ModCods, the outage capacity of an ACM-based link, given that the link is available, employing the rain attenuation synthesizer is calculated for the three considered Earth Observation receiving stations.

Firstly, in order to take into account the total attenuation into the capacity statistics, the following formula is used:

$$A_T = A_{WV} + A_{OX} + A_R + A_C + A_S \tag{5.51}$$

where A_{WV}, A_{OX}, A_R, A_C are the attenuation due to water vapour, oxygen, rain and clouds, respectively and A_s is the scintillation depth. Rain attenuation is derived from the elevation angle time-dependent time series synthesizer presented in Section 4.2, with lognormal parameters derived from non-linear regression of theoretical lognormal distribution to the exceedance probability predicted by ITU-R. P. 618-10 [ITU-R. P.618]. Scintillation is taken into account through ITU-R. P. 618-10 [ITU-R. P.618] and computed for a given exceedance probability and then it is considered as constant in time. For the presented results the exceedance probability is considered 10%. Attenuation due to water vapour, clouds ad oxygen attenuation are taken into account through the recommendation ITU-R. P.1853-1 [ITU-R. P.1853]. For the derivation of all the attenuation statistics, the temporal change of elevation angles was taken into account. The formula presented in (5.51) was used as this is recommended in [ITU-R. P.1853] and the correlation of water vapour, clouds and rain attenuation was considered through the correlated noises of the synthesizers [ITU-R. P.1853]

Moreover, the following formula taken from the [Toptsidis12] has been used for the calculation of the sky noise temperature:

$$T_{sky} = T_{\cos mic} 10^{-A_R/10} + T_{equiv}\left(1-10^{-A_R/10}\right), \tag{5.52}$$

where T_{cosmic} is equal 3^{o}K and is for the cosmic noise and T_{equiv} is the equivalent noise temperature of the receiver under clear sky conditions and it was computed with

$$T_{equiv} = 275\left(1-10^{-(A_{WV}+A_{OX})/10}\right), \tag{5.53}$$

Furthermore, the channel error estimation in terms of rain attenuation is calculated with two different methods. In the first one, a constant error is considered equal to 0.5dB and for the second one the rain attenuation channel is estimated through the following formula provided by [Karagiannis13]:

$$E[A^t \mid A^0] = A_m^t \exp\left[\frac{S_A^t}{S_A^0}\ln\left[\frac{A^0}{A_m^0}\right]e^{-\beta_A t} + \frac{1}{2}\left(S_A^t\right)^2\left(1-e^{-2\beta_A t}\right)\right], \tag{5.54}$$

where t is the time lag delay A_m^t, A_m^0 are the median value of rain attenuation for the link after t seconds and the initial link, respectively, S_A^t, S_A^0 the standard deviation of natural logarithm of rain attenuation for the ink after *t* seconds and initial link, respectively, β_A the dynamic parameter of rain attenuation.

The time lag delay for the calculation of the receiving SNR is simply calculated as:

$$t = \frac{2*693\cdot 10^3}{\sin(\theta)\cdot 3\cdot 10^8}\text{(sec)}, \tag{5.55}$$

where θ is the time dependent elevation angle. In our analysis we consider that for the long-term characteristics of the two links rain attenuation are the same assuming that there is no significant change for rain attenuation due to the small time lag delay, during which the elevation is approximated as constant. For the latter, the time lag delay at 90^o is 4.62msec and for 5^o is 53msec.

Equation (5.54) actually calculates the expected value of rain attenuation after time *t*, given that the initial value is A_o. The estimation for the dynamic case was taken into account by subtracting the following term (Δch) by the received SNR:

$$\Delta ch = A^t - A^0 \tag{5.56}$$

Firstly, the outage capacity, given that the link is available, was computed for the three stations and the two different channel estimation methods at Ka band. In Figure 6.19, Figure 6.20, Figure 6.21 the outage capacity is shown for Matera, Svalbard and Wilheim, respectively, for the Ka band case. The figures are shown in the whole range of time percentages in which capacity is greater than 0 Gbps and for probability larger than 10^{-4}. Firstly, it can be observed that Svalbard has the best performance as it is expected. Matera and Weilheim provide approximately the same capacity. Considering the channel estimation error, for Ka band, the adaptive estimated error seems to give a slightly better performance for high probabilities. This may come due to the fact that at high probabilities rain attenuation is low and therefore considering a constant error of 0.5 dB is high for these probability levels.

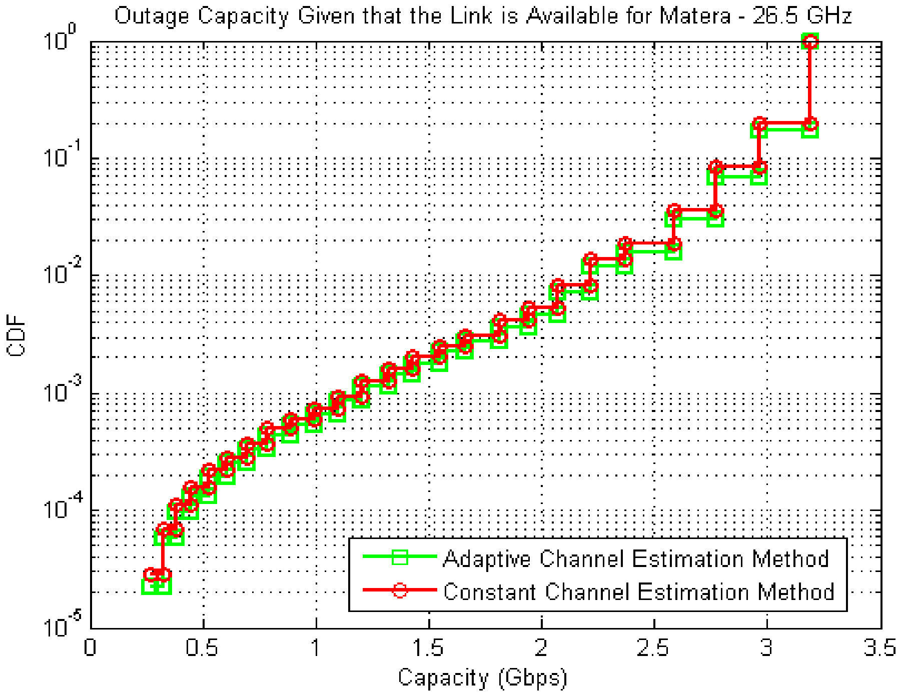

(a)

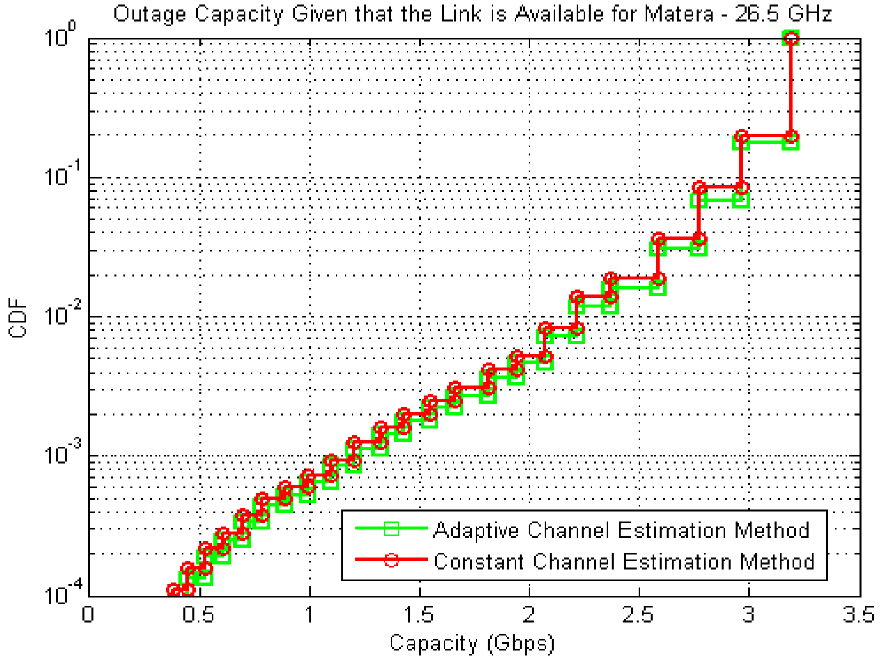

(b)

Figure 6.19: Outage capacity given that the link is available for Matera at Ka band: a) All time percentages b) Larger than 10^{-4}

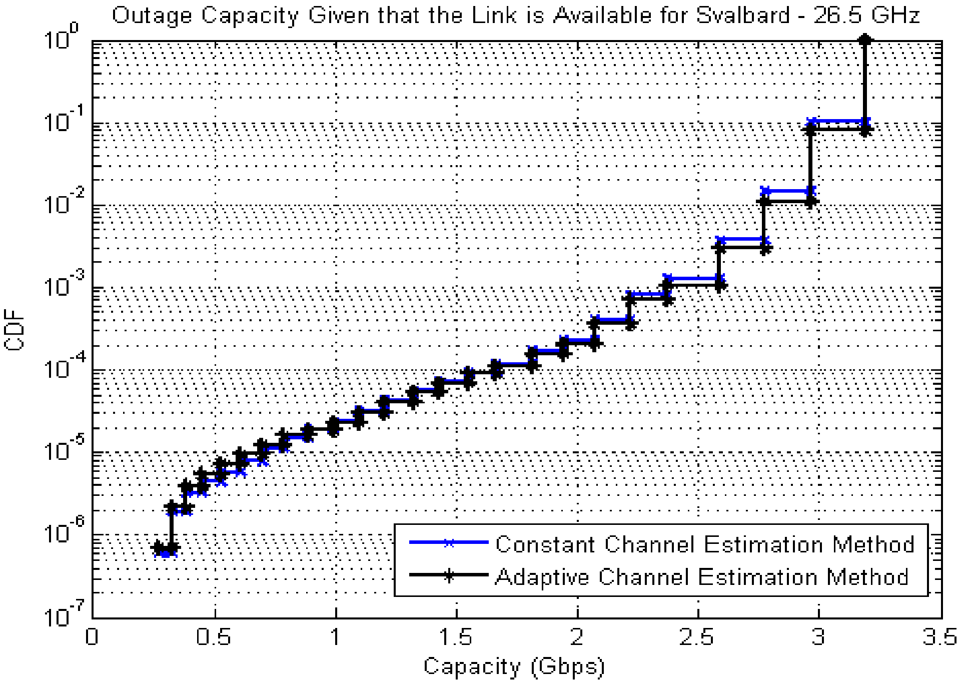

(a)

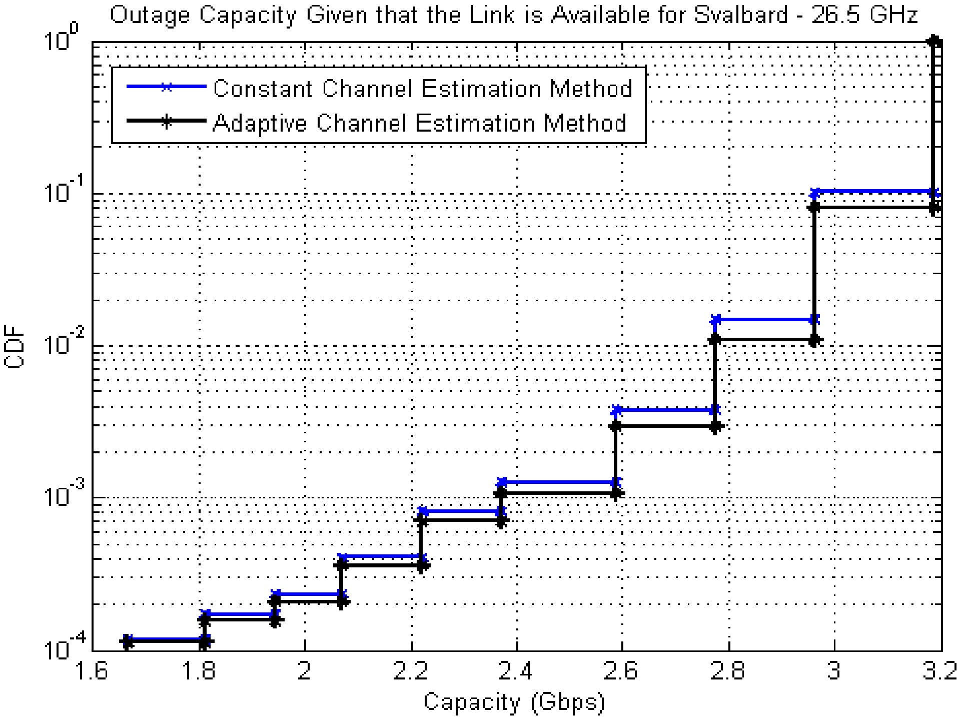

(b)

Figure 6.20: Outage capacity given that the link is available for Svalbard at Ka band: a) All time percentages b) Larger than 10^{-4}

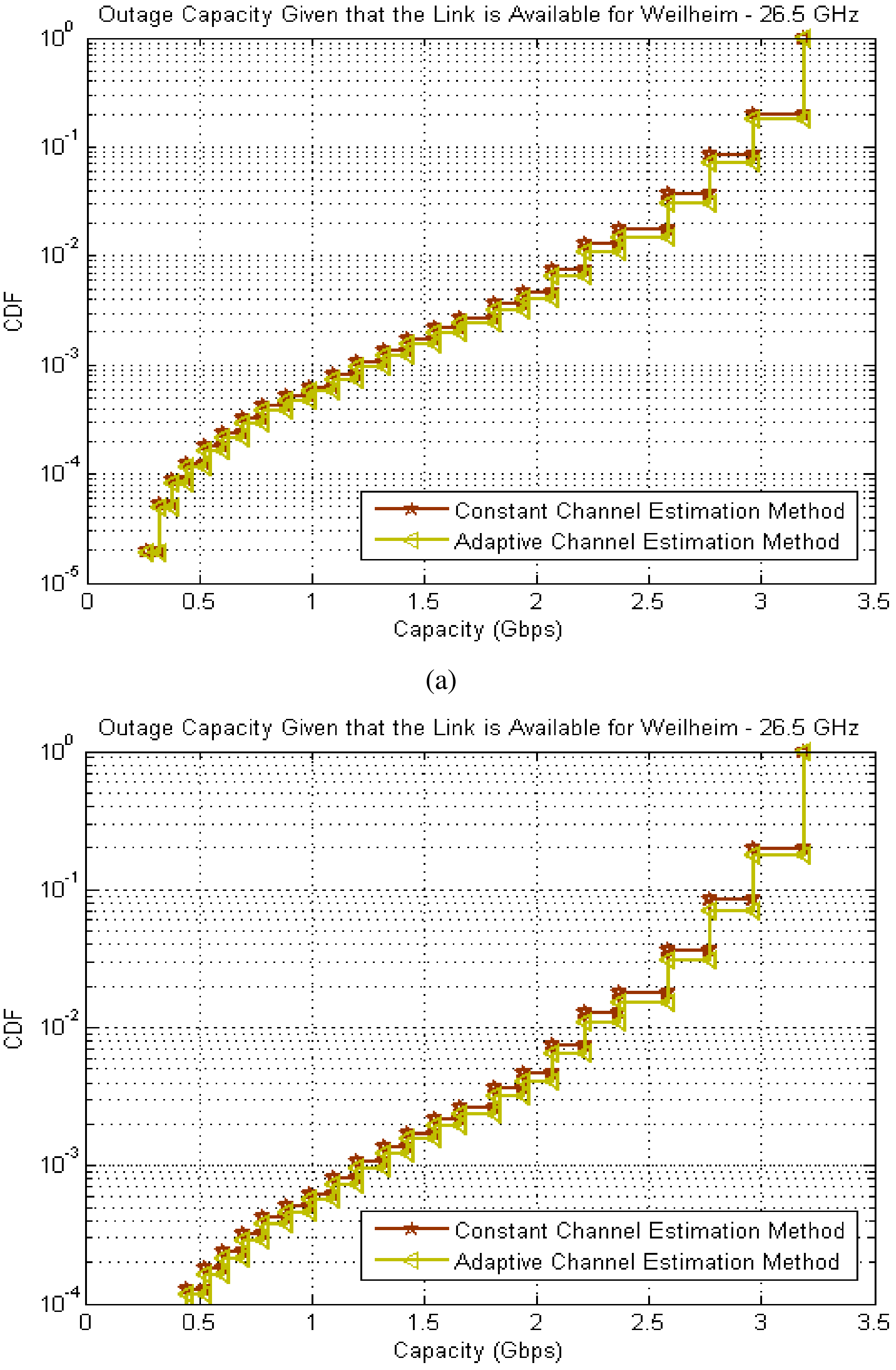

Figure 6.21: Outage capacity given that the link is available for Weilheim at Ka band: a) All time percentages b) Larger than 10^{-4}

Considering the case of Q-band, i.e. frequency of 40 GHz, in Figure 6.22, Figure 6.23, Figure 6.24, the outage capacity given that the link is available for Matera, Svalbard and Weilheim are shown, respectively. The same conclusions for Ka band capacity statistics apply also for the Q band statistics. Comparing the two methods, the adaptive channel estimation modeling gives a slight better performance than considering a constant channel estimation error of 0.5 dB.

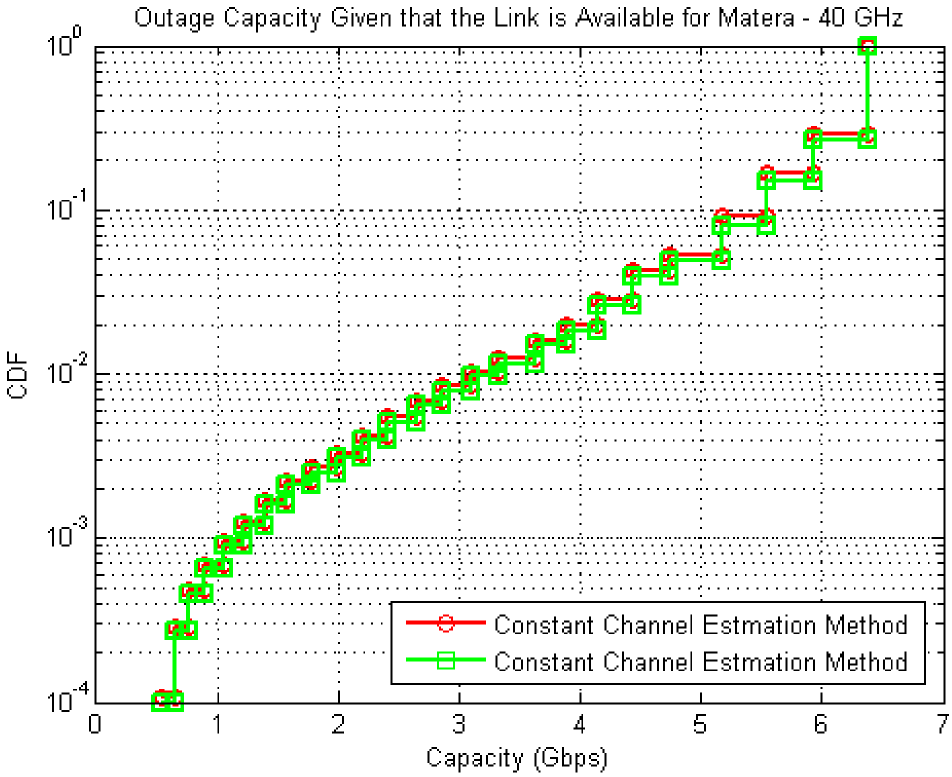

Figure 6.22 Outage capacity, given that the link is available, for Matera at Q band

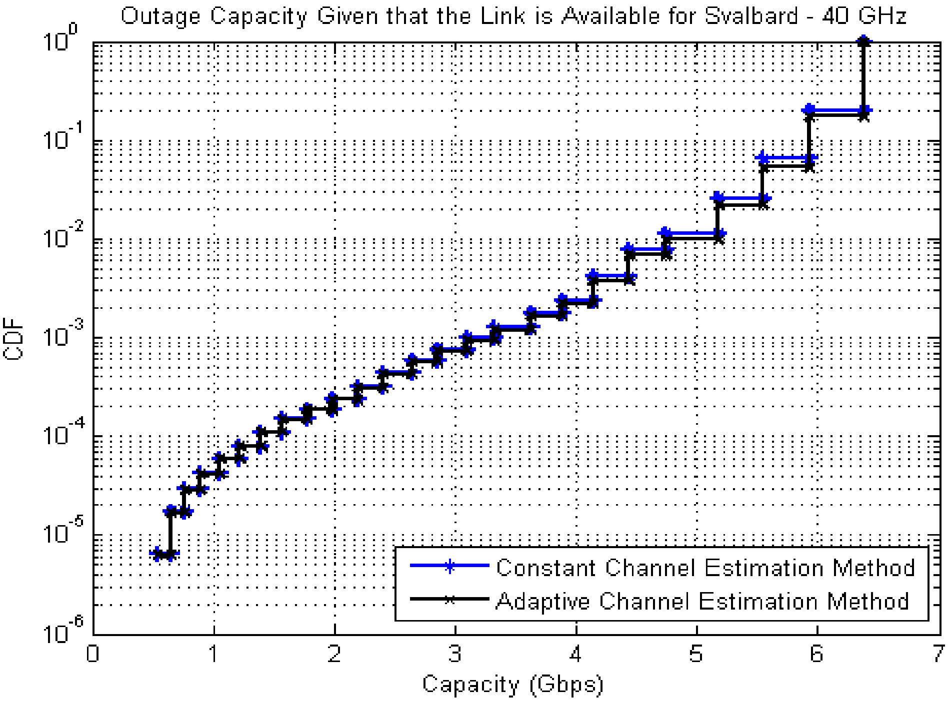

(a)

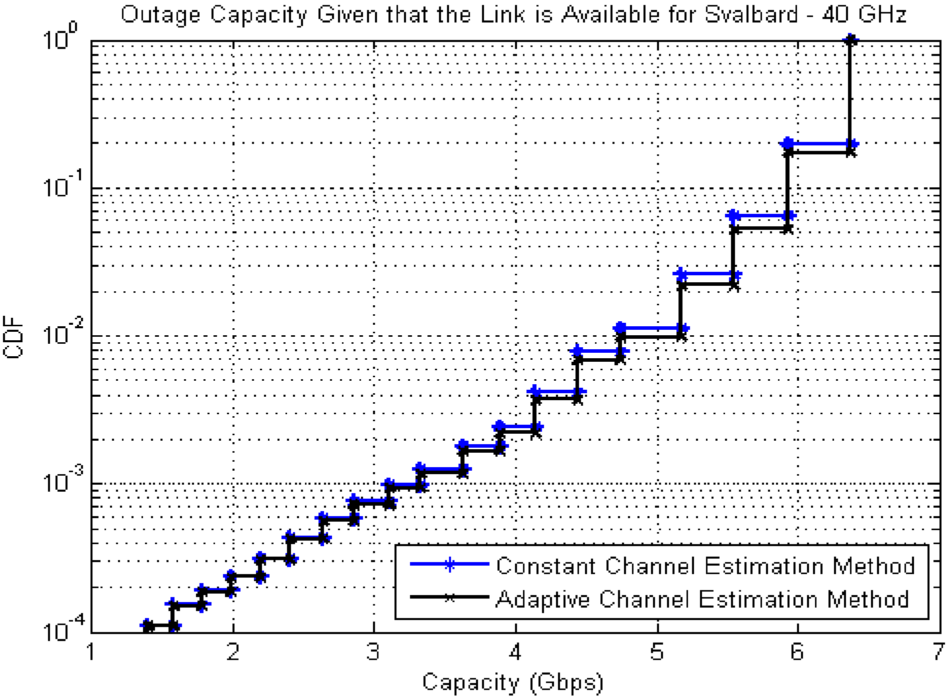

(b)

Figure 6.23 Outage Capacity, given that the link is available, for Svalbard at Q band: a) All time percentages, b) Larger than 10^{-4}

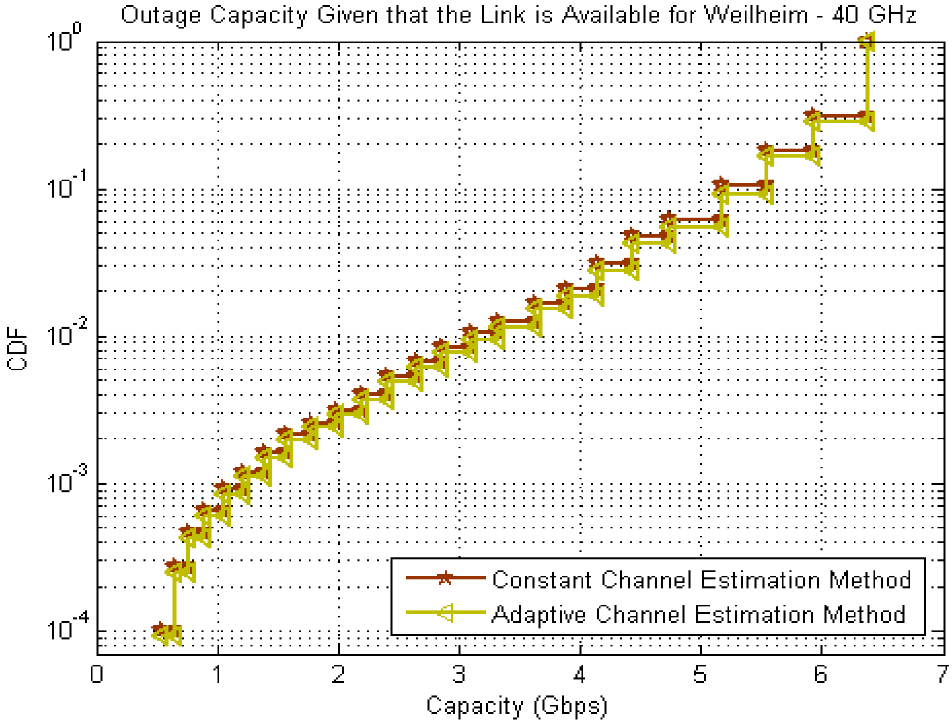

Figure 6.24: Outage capacity, given that the link is available, for Weilheim at Q band

7 Conclusions and Future Work

In this Chapter, the work carried out and presented in the PhD thesis is concluded and few directions for future work are given. This Chapter consists of two parts. The first one gives the conclusions of the Chapters 3-5 of the PhD thesis, while in the second part future work and future directions are given.

7.1 General Conclusions

7.1.1 Long Term Outage Prediction Modeling of Wireless Systems Operating above 10 GHz

In Chapter 3 of the PhD thesis, various models are defined and developed for capturing the first order statistics of rain attenuation for single links, spatially separated links and time diversity systems. The main conclusions from Chapter 3 are:

- A new distribution, i.e. IG, is identified for modeling the first order statistics of rain rate and rain attenuation induced on slant paths and terrestrial links.
- Two new models for predicting rain attenuation for terrestrial wireless systems and satellite systems operating above 10 GHz are developed. The models are based on the unconditional IG modeling of rain rate and rain attenuation. The models' inputs are given in terms of the statistical parameters of rain rate and the geometrical and electrical characteristics of the links.
- Motivated by the good behavior of the modeling of rain attenuation with IG distribution, a new model for predicting joint statistics of rain attenuation on spatially separate Earth-space paths is proposed. Using this methodology, the joint exceedance probability of rain attenuation is calculated for various distances between Earth stations. The model gives a better error performance than the methodology of ITU-R. P. 618-11.
- A new methodology for evaluating the performance of next generation fixed wireless terrestrial systems adopting diversity combining techniques (SC and MRC) exploiting the spatial inhomogeneity of the rainfall medium. The basic assumption is based on the assumption of the bivariate IG distribution for capturing the joint first-order statistics of rain attenuation on two links.

- Copulas are introduced for modeling joint statistics of rain attenuation in spatially separated links (site diversity systems) and time diversity systems. The Archimedean copulas are tested for capturing the joint exceedance probability of rain rate and rain attenuation in the two cases that the links are spatially separated or the time diversity technique is adopted.
- A model based on the solution of Fokker-Planck equation is developed for modeling the joint statistics of rain attenuation in temporal domain. Employing the assumptions of the Maseng-Bakken model and the TPDF resulted from the F-P equation, a new theoretical expression for calculating joint exceedance probability of rain attenuation for the evaluation of time diversity systems is derived. The methodology is tested against measurements showing good accuracy.

All the above long term models are flexible and show very good behavior globally and in most cases have better error performance comparing to the existing models in the literature. Most of them will be proposed to Study Group 3 Radio wave Propagation in order to be tested and extend the ITU-R Recommendations P.618-11 and P.530-14.

7.1.2 Rain Attenuations and Scintillation Dynamics Modeling

The topic of the fourth Chapter of this thesis is mainly focused on the dynamics and second-order statistics of rain attenuation. More particularly, a general and simple formula for the calculation of the dynamic parameter that is required for the stochastic modeling of rain attenuation is given. Moreover, the M-B model is extended in order to incorporate time-dependent parameters of the geometrical characteristics of the link and so a novel time series synthesizer of rain attenuation for LEO/MEO links is introduced. Moreover, in this Chapter the use of copulas functions are introduced for generating rain attenuation time series at Earth-GEO links and using the multi-dimensional stochastic differential equations, time series of two dimensional rain rate fields are generated for the calculation of rain attenuation. Finally, based on the SDEs driven by fBm, a scintillation time series synthesizer is proposed. . The main conclusions derived from the 4th Chapter are:

- A model for calculating the dynamic parameter of rain attenuation is introduced. Using as input the dynamic parameter of rain rate, the geometrical and electrical characteristics of the link, the dynamic parameter is calculated. A dependence from frequency, elevation angle, polarization and the climatic characteristics on the values of dynamic parameter is observed.

- A new SDE with time-dependent parameters is developed in order to generate rain attenuation time series for Earth-LEO or Earth-MEO links. The difference between these two links and an Earth-GEO link is that the elevation angle is time-dependent and therefore the rain attenuation parameters become time dependent. The SDE is based on the assumptions of the MB model and reproduces the first order statistics of rain attenuation for a time dependent link.
- A model for predicting the first order statistics of fade slope due to rain attenuation for a time dependent slant path is developed and tested with the results of the developed SDE for Earth-Leo links.
- Copulas functions are introduced for the modeling of rain attenuation dynamics. More particularly, the Gaussian copula is used for capturing the joint first order statistics of rain attenuation on temporal domain and tested with experimental results. Moreover, the copula parameter is modeled as a function of time delay. The proposed algorithm generates rain attenuation time series and reproduces the first order statistics, joint first order statistics and second order statistics (Kendall's tau correlation).
- Time series of two-dimensional rain fields are generated through the use of multi-dimensional stochastic differential equations. The main assumptions used are the lognormal distribution of rain rate, the MB assumptions for the point rainfall rate and that rain rate at two different points follow the bivariate lognormal distribution. Synthesizing rain rate fields, numerical methods can be used for deriving rain attenuation time series. The model is tested with a limited amount of data. However, the results can be considered as promising
- SDEs driven by fBm are introduced for generating the log-amplitude of the signal due to tropospheric turbulence. fBm driven SDEs are used in order to generate zero mean and desired variance (depending on the link characteristics and the presence of rain) Gaussian distributions which have a low-pass spectrum shape with a desired roll-off factor ($f^{-8/3}$ decrease at high frequency components). The synthesizer gives the appropriate spectrum shape and reproduces first order statistics.

7.1.3 Cognitive and Earth Observation Satellite Communication Systems

In the 5th Chapter of the thesis two main subjects of the next generation satellite communication systems are studied. Firstly, the assessment of the coexistence of two or more services in the same spectrum for high operating frequencies, i.e. Ka-band and above, and then using the time series proposed for LEO links in Chapter 4, the ACM technique is evaluated for an EO scenario. The main conclusions can be summarized to:

- A dual satellite cognitive system is evaluated considering that the incumbent and cognitive users have available links. Therefore, a SIR analysis has been carried out. Firstly, an analytical expression has been used for the calculation of the cumulative distribution of SIR. Also, multi-dimensional SDEs are used for generating rain attenuation on multiple links giving a second method for the SIR statistics calculation.
- Two models for the calculation of CDF of SNIR for ESOMPS at downlink and uplink have been developed. The motivation has been the joint share of spectrum at Ka-band for mobile satellite services and fixed satellite services. Analytical expressions were derived for the case of a single interferer, adjacent satellite interference for the downlink case and a interfering ESOMP at the uplink case. Moreover, multi-dimensional stochastic differential equations have been developed for modeling rain attenuation induced in links between a GEO satellite and mobile terminals operating at Ka-band. The latter model is used for evaluating interference from multiple terminals (uplink case) and multiple satellites (downlink case)
- The spectrum share between a fixed wireless terrestrial service and a fixed satellite service is gaining attention in order to increase the number of services which can be provided at a specific spectrum. More particularly, the case studied in this thesis is the coexistence of a point-to-point wireless terrestrial system (serving as incumbent user) and a fixed satellite system (cognitive services) both operating at the same bandwidth at Ka-band. For the system evaluation, analytical expression for the cumulative distribution of SIR and SNIR have been derived, as well as using multi-dimensional SDEs for rain

attenuation, multiple interferers cases were simulated for the derivation of statistics.

- Finally, using the methodology of Chapter 4 for generating rain attenuation time series at Earth-LEO links and the ITU-R. P. 1853 for the total atmospheric attenuation, the performance of Earth-LEO links is evaluated and in particular the performance of the use of ACM technique in Earth observation systems.

7.2 Future Work

Based on the results and the limitations of the models developed under the framework of this thesis a number of actions can be identified.

7.2.1 Long Term Outage Prediction Modeling of Wireless Systems Operating above 10 GHz

Starting from the third Chapter, useful future actions can be:

- Considering the use of IG distribution for the modeling of first order statistics of rain rate and rain attenuation, it must be noted that other distributions have been also identified for the same goal. Therefore, an analysis on the identification of cases, categorized by the best fit of a distribution is needed as a further insight on the modeling of a system's outage.
- On the models for the prediction of rain attenuation using the IG distribution, refinement on the spatial distribution of specific rain attenuation is needed. Although, the results are satisfying comparing to ITU method, since the spatial correlation of specific rain attenuation is used, its dependence on the geometrical and electrical characteristics of the links shall be fully investigated using either measured beacon signals or radar data from several regions.
- Moreover, on the copulas analysis for joint statistics of rain attenuation on temporal and spatial domain, only Archimedean copulas have been tested. This is a limitation, since more copulas exist which may give a better results. Furthermore, copulas theory gives the ability to construct new copulas which

in our case can be considered for the modeling of rain attenuation and tropospheric attenuation in general.

7.2.2 *Rain Attenuations and Scintillation Dynamics Modeling*

Considering the analysis on second order statistics:

- Of great importance is the validation of the expression of the dynamic parameter with experimental data. The proposed expression for the calculation of the dynamic parameter at the first section of fourth Chapter has been derived following a number of theoretical assumptions. Although, the results give an outcome, as theoretically expected, extra measurements are necessary to validate the results.
- The measurement validation is also required for the rain attenuation time series synthesizer at Earth-LEO/MEO links. In this case, both first order and second order statistics are needed to be evaluated with measured rain attenuation. Moreover, since MEO constellations have been already deployed for delivering high data rates at Earth stations, the proposed synthesizer must be extended to multi-dimensional synthesizer for capturing the spatial correlation between the links, employing either orbital or site diversity schemes.
- An interesting issue to be tackled is the modeling of rain attenuation induced on Earth-MEO links for mobile terminals. The first issues considering available spectrum at Ka band for the realization of communications between ESOMPs and MEO or LEO satellites have been studied. Therefore, for the evaluation of the system's performance using the proposed rain attenuation time series synthesizers are required. Maritime and aeronautical communication scenarios can also be investigated.
- Considering the copulas based rain attenuation synthesizer, the copula parameter needs to be remodeled using more measured joint temporal statistics of rain attenuation with different electrical, geometrical characteristics of the links and different climatic regions. Also, the

introduction of the probability that rain attenuation is induced on the link would capture the intermittency of rain.

- The validation of the methodology for the rain attenuation calculation with measured CCDFs from DBSG3 considering the first order statistics and measured rain attenuation autocorrelation from rain attenuation time series. Moreover, an analysis on the introduction of wind speed and wind direction directly into the model, would result to the examination of the necessity of their incorporation into the synthesized rain rate fields. The extension of the methodology for incorporating clouds and water vapor attenuation into a general model. Such models can be used for the channel model at Q/V bands and optical frequencies. Also, their initialization and condition with real-meteorological data would make the channel more realistic.
- Considering the scintillation time series generator, it is of primary importance the use of measurements for its further validation

7.2.3 Cognitive and Earth Observation Satellite Communication Systems

Considering the cognitive systems, what is mainly needed as future action is:

- The calculation of SNIR statistics for services provided by MEO constellations. The introduction of the MEO constellations in the data delivery services is congesting more the spectrum at Ka-band. Since, the great advantage of Ka-band is the higher bandwidth, spectrum share between the various services is a main issue. Therefore, SNIR statistics for dual satellite cognitive system (either both MEO or MEO and GEO) or a coexistence of fixed terrestrial service and MEO services are needed.
- Moreover, the derivation of SNIR statistics for MEO constellations using ESOMPs as Earth stations is really significant for the introduction of mobile satellite services with MEO satellites and the increase of the spectrum which can be used.
- The examination of site diversity for EO downlinks is a task to be made in order to increase the availability of the systems and decrease the memory size since the technique of time diversity due to rain will be less used. Moreover,

the case of frequency re-use for EO systems could be helpful, in case that more and more EO satellites are used in the future.

In the last few years, new frequency bands are examined for their use in applications in which high data rates are required. More particularly, due to congestion of Ka band, Q/V bands are examined as well as W band not only for satellite communication systems but also for terrestrial communications. As mentioned in the first Chapter, ESA has launched the ALPHASAT propagation experiment in which many countries along the European continent are participating for measurements at Ka and Q bands. Up to now, only one experiment has taken place at Q band using the ITALSAT. Therefore, with the new campaign more data at high frequencies will be obtained and will be used for the extension of the models.

Moreover, due to the advantages of the lack of liscence necessities and interference issues and the very high bandwidth that can be used, optical frequencies are examined for Deep space communications, EO applications and feeder links. Although, clouds cause the outage of the link, site diversity schemes can be used for obtaining the required availability. However, in optical frequencies a number of aerosols affect the signal leading to transmitting windows on the wavelength and also scintillation is mainly caused by the variations on the temperature along the troposphere. Therefore, new channel models are required.

Finally, in the 5G networks mmWave spectrum will be probably used. However, in the classical mobile communication systems of 2G, 3G and 4G the systems were operating mainly at L- and S-bands. Therefore, new models are needed not only for the local environment effects but also for the combination of them with atmospheric effects. Such studies are very limited in the literature.

References

[AGI] AGI's STK, https://www.agi.com/products/by-product-type/applications/stk/

[Al-Hussaini81] E. K. Al-Hussaini, N. S. Abd-El-Hakim, "Bivariate Inverse Gaussian Distribution", Annals of the Institute of Statistical Mathematics, vol. 33, no. 1, pp. 57-66, 1981.

[Allnutt82] J. E. Allnutt, D. V. Rogers, "Novel Method for Predicting Site Diversity Gain on Satellite-to-Ground Radio Paths", Electronic Letters, vol. 18 ,no. 5, pp. 233-235, 1982.

[ALPHASAT15] http://www.esa.int/Our_Activities/Telecommunications_Integrated_Applications/Alphasat, accessed in April 2015.

[Arapoglou08] P.-D. M. Arapoglou, A. D. Panagopoulos, P. G. Cottis, "An Analytical Prediction Model of Time Diversity Performance for Earth-Space Fade Mitigation", International Journal of Antennas and Propagation, vol. 2008, 5 pages

[Arapoglou11] P.-D. Arapoglou, K. Liolis, M. Bertinelli, A. Panagopoulos, P. Cottis, R. De Gaudenzi, "MIMO over Satellite: A Review", IEEE Communications Surveys and Tutorials, vol. 13, no. 1, pp. 27-51, 1st Quarter 2011.

[Arapoglou11b] P. D. M. Arapoglou, P. Burzigotti, M. Bertinelli, A. B. Alamanac, R. De Gaudenzi, "To MIMO or Not To MIMO in Mobile Satellite Broadcasting Systems", IEEE Transactions on Wireless Communications, vol. 10, no. 9, pp. 2807-2811, Sept. 2011

[Arapoglou12] P.-D. Arapoglou, K.P. Liolis, A.D. Panagopoulos, ``Railway satellite channel at Ku band and above: Composite dynamic modeling for the design of fade mitigation techniques," \emph{Int. J. Satell. Commun. Network}, vol. 30, pp. 1-17, 2012.

[BADC] British Atmospheric Data Center, http://www.badc.nerc.ac.uk

[Bell87] T. L. Bell, "A Space-Time Stochastic-Dynamic Model of Rainfall for Satellite Remote Sensing Studies", Journal of Geophysical Research, vol. 92, no. D8, pp. 9631-9643, 1987.

[Bertorelli05] S. Bertorelli, A. Paraboni: "Simulation of short-term frequency scaling using ITALSAT data", European Conference on Propagation and systems, Brest, March 2005.

[Bertorelli05a] S. Bertorelli, A. Paraboni, "Simulation of Joint Statistics of Rain Attenuation in Multiple Site Across Wide Areas Using ITALSAT Data", IEEE Transactions on Antennas and Propagation, vol. 53, no. 8, pp. 2611-2621, 2005.

[Bertorelli08] Bertorelli, S.; Riva, C.; Valbonesi, L., "Generation of Attenuation Time Series for Simulation Purposes Starting From ITALSAT Measurements," *Antennas and Propagation, IEEE Transactions on* , vol.56, no.4, pp.1094,1102, April 2008

[Bolea-Alamañac04] Bolea-Alamañac, A., "Fade Mitigation techniques to optimize the radio resource in a fixed satellite communication link", PhD of SUPAERO, Toulouse, France.

[Bosisio98] A. V. Bosisio, C. Riva, “A novel method for the statistical prediction of rain attenuation in site diversity systems: theory and comparative testing against experimental data”, International Journal of Satellite Communications, vol. 16, pp. 47-52, 1998.

[**Boulanger11]** X. Boulanger, G. Carrie, L. Castanet, L. Feral, “Overview of a more simplified new channel model to synthesize total attenuation time series for satellite communication systems at Ka and Q/V band”, ESA Workshop on Radiowave Propagation, 2011.

[Boulanger13] Boulanger, X.; Feral, L.; Castanet, L.; Jeannin, N.; Carrie, G.; Lacoste, F., "A Rain Attenuation Time-Series Synthesizer Based on a Dirac and Lognormal Distribution," *Antennas and Propagation, IEEE Transactions on* , vol.61, no.3, pp.1396,1406, March 2013

[Burgueno90] A. Burgueno, E. Vilar, M. Puigcerevr, “Spectral analysis of 49 years of rainfall rate and relation to fade dynamics”, IEEE Trans. Commun., vol. 38, no. 9, September 1990.

[Capsoni87a] C. Capsoni, F. Fedi, C. Magistroni, A. Paraboni, A. Pawlina, “Data and Theory for a new Model of the Horizontal Structure of Rain Cells for Propagation Applications”, *Radio Science*, vol. 22, no. 3, pp. 395-404, 1987.

[Capsoni87b] Capsoni, F. Fedi, A. Paraboni, “A Comprehensive Meteorologically Oriented Methodology for the Prediction of Wave Propagation Parameters in Telecommunication Applications beyond 10 GHz”, *Radio Science,* vol. 22, no. 3, pp. 387-393, 1987.

[Capsoni06] C. Capsoni, L. Luini, C. Riva, “Stratiform and Convective Rain Discrimination Starting from the Site P(R)”, IEEE Transaction on Antennas and Propagation, vol. 54, no. 11, pp. 3566-3569, 2006.

[Capsoni09] C. Capsoni, L. Luini, A. Paraboni, C. Riva, A. Martellucci, “A New Prediction Model of Rain Attenuation that Separately Accounts for Stratiform and Convective Rain”, IEEE Transactions on Antennas and Propagation, vol. 57, no.1, 2009.

[Carrie11] Carrie, G., Lacoste, F. and Castanet, L. (2011), A new ‘event-on-demand’ synthesizer of rain attenuation time series at Ku-, Ka- and Q/V-bands. Int. J. Satell. Commun. Network., 29: 47–60

[Castanet03] L. Castanet, T. Deloues, J. Lemorton, “Channel Modeling based on N-state Markov Chains for SatCom System Simulation”, ICAP 2003, Exeter UK, April 2003.

[Castanet06] Castanet L., Bourgoin J., Pradie M., Bertorelli S., Paraboni A., Martellucci A. : "Characterisation and modelling of instantaneous frequency scaling in 20-50 GHz band", 3rd CNES workshop on Earth-space propagation, Toulouse, France, September 2006.

[Castanet08] L. Castanet, “Influence of the Variability of the Propagation Channel on Mobile, Fixed Multimedia and Optical Satellite Communications”, Shaker Verlag, 2008

[Celadroni99] N. Celadroni, F. Potorti, “Modeling Ka-Band Scintillation as a Fractal Process”, IEEE Journal on Selected Areas in Communications, vol. 17, no. 2, pp. 164-172, 1999.

[Chatzidiamantis11a] N. D. Chatzidiamantis, H. G. Sandalidis, G. K. Karagiannidis, S. A. Kotsopoulos, “On the Inverse Gaussian shadowing”, 2011 International conference on communications and information technology, 2011.

[Chatzidiamantis11b] N. D. Chatzidiamantis, H. G. Sandalidis, G. K. Karagiannidis, M. Matthaiou, "Inverse Gaussian modeling of turbulence-induced fading in free-space optical systems", Journal of Lightwave technology, vol.29, no.10, pp.1590-1596, 2011.

[Cheffena08] M. Cheffena, C. Amaya, "Prediction Model of Fade Duration Statistics for Satellite Links Between 10-50 GHz", IEEE Antennas and Wireless Propagation Letters, vol. 7, pp. 260-263, 2008.

[Cheffena09] M. Cheffena, L. E. Braten, T. Ekman, "On the Space-Time Variations of Rain Attenuation", IEEE Transactions on Antennas and Propagation, vol. 57, no. 6, pp. 1771-1782, 2009.

[Cheridito03] P. Cheridito, H. Kawaguchi, M. Maejima, "fractional Ornstein-Uhlenbeck Processes", Electronic journal of Probability, 8, 2003

[Chikkara89] R. S. Chikkara, J. L. Folks, "The Inverse Gaussian Distribution: Theory, Methodology and Applications", New York: M. Dekker, 1989.

[Coleman94] T. F. Coleman, Y. Li, "On the convergence of interior-reflective Newton methods for nonlinear minimization subject to bounds", Mathematical programming, vol. 67, no. 2, pp.189-224, 1994.

[Coleman96] T. F. Coleman, Y. Li, "An interior, trust region approach for nonlinear minimization subject to bounds", SIAM journal on optimization, vol. 6, pp. 418-445, 1996.

[CORASAT13] CoRaSat Deliverable D2.3, "Scenarios Definition and Selection", Deliverable of CoRaSat Project, Nov. 2013.

[COST205] COST205: "Influence of the atmosphere on radiopropagation on satellite earth paths at frequencies above 10GHz", COST Project 205, Report EUR 9923 EN, ISBN 92-825-5412-0, Sections 5.3 and 5.6, 1985.

[COST255] COST Action 255, "Radiowave Propagation Modeling for SatCom Services at Ku-Band and Above", Final Report, 2002

[**Crane80]** R. K. Crane, "Prediction of Attenuation by Rain", IEEE Transactions on Communications, vol. 28, no. 9, pp. 1717-1733, 1980.

[Crane96] R. K. Crane, "Electromagnetic Wave Propagation through Rain", Wiley, 1996.

[Crane03] R. K. Crane, "Propagation Handbook for Wireless Communication Systems Design", CRC press LLC, 2003.

[Davies87] R. B. davies, D. S. Harte, "Tests for Hurst Effect", Biometrica, 1987

[DBSG3] (2010) ITU-R. Databank DBSG3, http://www.itu.int/publ/R-SOFT-SG3/en

[Dieker03] A. B. Dieker, M. Mandjes, "On Spectral Simulation of Fractional Brownian Motion", Probability in the Engineering and Informational Sciences, 17(2003), page, 417

[DigAgenda10] A Digital Agenda for Europe, European Commission COM (2010) 245, Brussels, 26/8/2010.

[Dintelmann93] Dintelman F., Ortgies G, Jakoby R : "Results from 12- to 30-GHz German propagation experiments carried out with radiometers and the Olympus satellite", Proceedings of the IEEE, vol. 81, no6, 1993, pp. 876-883.

[Dissanayake00] A. Dissanayake, K. T. Lin, "Ka-Band Site Diversity Measurements and Modeling", 6th Ka-Band Utilization Conference, Cleveland , Ohio, 2000.

[Drougas08] A. E. Drougas, A. D. Panagopoulos, P. G. Cottis, "Stochastic Verification of the First-Order Markovian assumption of Rain Attenuation for Satellite Channel Dynamic Modeling", IEEE Communication Letters, vol.12, Issue 9, pp. 663-665, Sep. 2008.

[Drufuca74] Drufuca, G.: "Rain attenuation statistics for frequencies above 10 GHz from rain-gauge observations", Journal de Recherches Atmosperiques, pp. 399-411, 1974.

[EDRS] "The European Data Relay System", European Space Agency - http://www.esa.int/esaTE/SEM5GGKTYRF_index_0.html

[ESTECRep] ESTEC Contr. 17760/03/NL/JA, "Characterization and Modeling of Propagation Effects in the 20-50 GHz Band", Final Report

[ESTEC04] ESTEC Contr. 16865/03/NL/EC: "Development of propagation models for telecommunication satellite systems", Final Report, 31/7/2004

[Euclid14] EUCLID Scientific Mission, http://sci.esa.int/euclid/46661-mission-operations/, accessed May 2014

[Fabbro09] V. Fabbro, L. Castanet, S. Croce, C. Riva, "Characterization and Modelling of Time Diversity Statistics for Satellite Communications from 12 to 50 GHz", International Journal of Satellite Communications, vol. 27, pp. 87-101, 2009

[Feral03a] L. Feral, H. Sauvageot, L. Castanet, J. Lemorton, "HYCELL-A New Hybrid Model of the Rain Horizontal Distribution for Propagation Studies: 1. Modeling of the Rain Cell", *Radio Science*, 2003.

[Feral03b] L. Feral, H. Sauvageot, L. Castanet, J. Lemorton, "HYCELL-A New Hybrid Model of the Rain Horizontal Distribution for Propagation Studies: 2. Statistical Modeling of the Rain Rate Field", Radio Science, 2003.

[Feral06] L. Feral, H. Sauvageot, L. Castanet, J. Lemorton, F. Cornet, K. Leconte, "Large-Scale Modeling of Rain Fields from a Rain Cell Deterministic Model", Radio Science, 2006.

[Fiebig02] U.C. Fiebig, "A time-series generator modelling rain fading" Open Symposium on propagation and remote sensing", URSI Commission F, Garmisch-Partenkirchen, Germany, 2002.

[Gaurard09] Jean-Didier Gaurard, "Terabit Satellite: Myth or Reality?", SPACOMM 2009, The First International Conference on Advances in Satellite and Space Communications, 20-25 July, Colmar, France, 2009.

[Ginesi14] A. Ginesi, S. Cioni, M. Angelone, ``DVB-S2X Channel Models: Rationale and Justifications," in 7th ASMS/13th SPSC, Livorno, Sept. 2014.

[Goldhirsh82] J. Goldhirsh, "Space Diversity Performance Prediction for Earth-Satellite Paths using Radar Modellign techniques", Radio Science, vol. 17, no.6, pp. 1400-1410, 1982.

[Goldhirsh95] J. Goldhirsh, "Rain-Rate Duration Statistics over a Five-Year Period: A Tool for Assessing Slant Path Fade Durations", IEEE Transactions on Antennas and Propagation, vol. 43, no. 5, pp. 435-439, 1995.

[Goldhirsh00] J. Goldhirsh, "Two-Dimension Visualization of Rain Cell Structures", Radio Science, vol. 35, 2000

[Gosh14] A. Ghosh, et al, " Millimeter wave enhanced local area systems: A high data-rate approach for future wirelss networks", IEEE Journ. On Selected Areas in Communications, vol.32, no.6, June 2014.

[Gradshteyn07] I. S. Gradshteyn, I. M. Ryzhik, "Table of Integrals, Series and Products", Elsevier Academic Press, 2007.

[Gremont98] Gremont B.C., Filip M.: "Modeling and applications of the instantaneous frequency scaling factor (IFSF) of rain attenuation", COST 255 First International Workshop on Radiowave Propagation Modelling for SatCom Services at Ku-band and Above, Noordwijk, the Netherlands, WPP-146, ISSN 1022-6656, pp. 269-276, 1998

[Gremont99] B. Gremont, M. Filip, P. Gallois, S. Bate, "Comparative Analysis and Performance of Two Predictive Fade Detection Schemes for Ka-Band Fade Countermeasures", IEEE Journal on Selected Areas in Communications, vol. 17, no. 2, pp. 180-192,1999.

[Gremont00] B. Gremont, D. L. Ndzi, "First-Order and Conditional Statistics of Rain Attenuation Fade Slope", Electronic Letter, vol. 36, no. 20, pp. 1733-1734, 2000.

[Gremont04] B. C. Gremont, M. Filip, "Spatio-Temporal Rain Attenuation Model for Application to Fade Mitigation Techniques", IEEE Transactions on Antennas and Propagation, vol. 52, no. 5, pp. 1245-1255, 2004.

[Hibberd12] C. Hibberd, ``Inmarsat Global Xpress Network – meeting the challenges of providing a seamless global Ka-band service to mobile terminals," 30th AIAA (ICSSC), 2012.

[Hodge82] D. B. Hodge, "An improved model for diversity gain on earth-space propagation paths", Radio Science, vol. 17, no. 6, pp. 1393-1399, 1982.

[IEEE802.16] IEEE 802.16: "IEEE Standard for Local and Metropolitan Area Networks - Part 16: Air Interface for Fixed Broadband Wireless Access Systems," Oct. 2009.

[ISI10] ISI Strategic Research and Innovation Agenda, November 2010, http://www.isi-initiative.org/

[Ismail00] A.F. Ismail, P.A Watson, "Characteristics of Fading and Fade Countermeasures on a Satellite-Earth Link Operating in an Equatorial Climate, with Reference to Broadcast Applications," IEE Proc. Microw. Antennas Propag., vol. 147, no. 5, pp. 369-373, 2000

[Ismail11] A. Ismail, S. Sezginer, J. Fiorina, H. Sari, "A Simple and Robust Equal-Power Transmit Diversity Scheme", IEEE Communications Letters, vol. 15, no. 1, 2011.

[ITU-E. M.1643] ITU-R. Recommendation M.1643, ``Technical and operational requirements for aircraft earth stations of aeronautical mobile-satellite service including those using fixed-satellite service network transponders in the band 14-14.5 GHz (Earth-to-space)," 2003.

[ITU-R. P.311] ITU-R. P. 311-13, "Acquisition, presentation and analysis of data in studies of tropospheric propagation", Geneva, 2009.

[ITU-R. P.530] ITU-R P.530-14, "Propagation data and prediction methods required for the design of terrestrial line-of-sight systems", Geneva, 2012.

[ITU-R. P.618] ITU-R P.618-10: "Propagation data and prediction methods required for the design of Earth-space communication systems", Geneva, 2009.

[ITU-R. P.676] ITU-R. P. 676-9, "Attenuation by Atmospheric Gases", International Telecommunication Union, Geneva, 2012

[ITU-R. P.835] ITU-R. P. 835-5, "Reference Standard Atmospheres", International Telecommunication Union, Geneva, 2012.

[ITU-R. P.836] ITU-R. P. 836-4, "Water Vapour: Surface Density and Total Columnar Content", International Telecommunication Union, 2009

[ITU-R.P.837] ITU-R. P. 837-6, "Characteristics of Precipitation for Propagation Modeling", International Telecommunication Union, Geneva, 2012.

[ITU-R.P.838] ITU-R. P. 838-3, "Specific Attenuation Model for Use in Prediction Models", International Telecommunication Union, Geneva, 2005.

[ITU-R.P.839] ITU-R. P. 839-3, "Rain Height for Prediction Methods", International Telecommunication Union, Geneva, 2001.

[ITU-R. P.840] ITU-R. P. 840-5, "Attenuation due to Clouds and Fog", International Telecommunication Union, Geneva, 2012.

[ITU-R. P.1410] ITU-R. P. 1410-5: "Propagation Data and Prediction Methods Required for the Design of Terrestrial Broadband Radio Access Systems Operating in Frequency Range from 3 to 60 GHz", ITU, Geneva, 2012.

[ITU-R.P.1511] ITU-R. P. 1511, "Topography for Earth-Space Modeling", International Telecommunication Union, Geneva, 2001.

[ITU-R. P. 1623] ITU-R. P. 1623, "Prediction Method of Fade Dynamics on Earth-Space Paths", International Telecommunication Union, Geneva, 2005.

[ITU-R. P.1853] ITU-R. P. 1853-1, “Tropospheric Attenuation Time Series Synthesis”, International Telecommunication Union, Geneva, 2012.

[ITU-R. S. 2223] ITU-R Report S.2223, ``Technical and operational requirements for GSO FSS earth stations on mobile platforms in bands from 17.3 to 30.0 GHz,'' 2011.

[ITU-R. S.465] ITU-R. S. 465-6, “Reference Radiation Pattern for Earth Station Antennas in the Fixed Satellite Service for Use in Coordination and Interference Assessment in the Frequency Range from 2 to 31 GHz”, International Telecommunication Union, Geneva, 2010.

[ITU-R. S.524] ITU-R Recommendation S.524-9, ``Maximum permissible levels of off-axis e.i.r.p. density from earth stations in geostationary-satellite orbit networks operating in the fixed-satellite service transmitting in the 6 GHz, 13 GHz, 14 GHz and 30 GHz frequency bands,'' 2006.

[ITUTelW11]Mapping is Vital to Future Broadband Investment, Point Logic, ITU Telecom World 2011

[Jeannin08] N. Jeannin, L. Feral, H. Sauvageot, L. Castanet, “Statistical Distribution of Integrated Liquid Water and Water Vapor Content From Meteorological Reanalysis," *Antennas and Propagation, IEEE Transactions on* , vol.56, no.10, pp.3350,3355, Oct. 2008

[Jeannin11] N. Jeannin, L. Castanet, J. Radzik, M. Bousquet, “Assessment of the Availability of Different Macro-Diversity Schemes for Q/V Band Feeder Links of SatCom Systems Targeting TB/s”, in 17th Band Broadband Communications, Navigation and Earth Observation Conference, Palermo, Italy, October, 2011.

[Jeannin11b] N. Jeannin, G. Carrie, L. Castanet, F. Lacoste, “A Space Time Channel Model for the Simulation of Total Attenuation Fields”, ESA Workshop on Radiowave Propagation, Noordwijk, Netherlands

[Jeannin12] N. Jeannin, L. Feral, H. Sauvageot, L. Castanet, F. Lacoste, “A Large-Scale Space-Time Stochastic Simulation Tool of Rain Attenuation for the Design and Optimization of Adaptive Satellite Communication Systems Operating between 10 and 50 GHz”, International Journal of Antennas and Propagation, vol. 2012, 2012.

[Kamp02] M. Van de Kamp, L. Castanet, “Fade Dynamics Review”, First COST 280 Workshop, Malvern, Uk, 1-3 July 2002.

[Kamp03] M. van de Kamp, “Rain Attenuation as a Mrakov Process: How to Make an Event”, COST280 Second International Workshop, Noordwijk, Netherlands, May 2003.

[Kamp03a] M. Van de Kamp, “Statistical Analysis of Rain Fade Slope”, IEEE Transactions on Antennas and Propagation, vol. 51, no. 8, pp. 1750-1759, 2003.

[Kanellopoulos87] J. D. Kanellopoulos, S. G. Koukoulas, “Analysis of the Rain Outage Performance of Route Diversity System”, Radio Science, vol. 22, no. 4, pp. 549-565, 1987

[Kanellopoulos00] J.D. Kanellopoulos, A.D. Panagopoulos, S.N. Livieratos, ``A Comparison of co-polar and co-channel satellite interference prediction models with experimental results at 11.6 GHz and 20 GHz,'' Int. J. Satell. Commun., vol. 18, no. 2, pp. 107-120, 2000.

[Kanellopoulos07] S. A. Kanellopoulos, A. D. Panagopoulos, J. D. Kanellopoulos, "Calculation of the Dynamic Input Parameter for a Stoch stic Model Simulating Rain Attenuation: A Novel Mathematical Approach", IEEE Transactions on Antennas and Propagation, vol. 55, no. 11, pp. 3257-3264, 2007.

[Kanellopoulos13a] S. A. Kanellopoulos, A. D. Panagopoulos, C. Kourogiorgas, J. D. Kanellopoulos, "Slant Path and Terrestrial Links Rain Attenuation Time Series Generator for Heavy Rain Climatic Regions", IEEE Transactions on Antennas and Propagation, vol. 61, no. 6, pp. 3396-3399, April 2013.

[Kanellopoulos13b] S. A. Kanellopoulos, C. Kourogiorgas, A. D. Panagopoulos, S. N. Livieratos, G. E. Chatzarakis, "Channel Model for Satellite Communication Links above 10 GHz based on Weibull Distribution", accepted to IEEE Communication Letter, September 2013.

[Karagiannis12] G. Karagiannis, A. D. Panagopoulos, J. D. Kanellopoulos, "Multi-Dimensional Rain Attenuation Stochastic Modelling: Application to Earth-Space Diversity Systems', IEEE Transactions on Antennas and Propagation, October 2012.

[Karagiannis13] G. Karagiannis, A. D. Panagopoulos, J. D. Kanellopoulos, "Short-Term Rain Attenuation Frequency Scaling for Satellite Up-Link Power Control Applications", IEEE Transactions on Antennas and Propagation, vol. 61, no. 5, pp. 2829-2837, May 2013.

[Karasawa91] Y. Karrasawa, T. Matsudo, "Characteristics of fading on low-elevation angle Earth-Space Paths with Concurrent rain Fade and Scintillation", IEEE Transactions on Antennas and Propagation, vol. 39, 1991.

[Karatzas05] I. Karatzas, S. E. Shreve, "Brownian motion and stochastic calculus", Springer-Verlag, 2005

[Karlin75] S. Karlin, H. M. Taylor, "A first course in stochastic processes", Academic Press, 1975.

[Karlin81] S. Karlin and H. Taylor, "A second course in stochastic processes", New York: Academic, 1981

[Kassianides03] C. N. Kassianides and I. E. Otung, "Dynamic Model of Tropospheric Scintillation on Earth-Space Paths", IEE Proceedings, vol. 150, no. 2, 2003.

[Kastamonitis02] K. Kastamonitis, B. Gremont, M. Filip, "A Study of Rain Fade Slope, 4th COST280 MC Meeting, Prague, Czech Republic, November 2002.

[Kedem90] B. Kedem, L. Chiu, Z. Karni, "An analysis of the threshold method for measuring area-average rainfall", Journal of Applied Meteorology, vol. 29, 1990

[**King06]** P. R. King, S. Stavrou, "Capacity Improvement for a Land Mobile Single Satellite MIMO System", *IEEE Antennas and Wireless Propagation Letters*, vol. 5, pp. 98-100, 2006

[Knopp10] Andreas Knopp, Robert T. Schwarz, Berthold Lankl, "On the Capacity Degradation in Broadband MIMO Satellite Downlinks with Atmospheric Impairments", ICC 2010, 1-6, 2010.

[Kourogiorgas10] C. Kourogiorgas, L. Feral, V. Fabbro, N. Jeannin, J. Lemorton, "Use of HYCELL Model for Predicting Rain Attenuation on UAS Low Elevation Datalinks", 4th EuCAP, Barcelona, Spain, 2010.

[Kourogiorgas12] Kourogiorgas, C. I., Panagopoulos, A. D., Moraitis, N., Kanellopoulos, J. D., Livieratos, S. N., and Chatzarakis, G. E.: "Analysis of 15-months rain rate measurements at NTUA campus", IEEE Proceedings of 6th European Conference on Antennas and Propagation (EuCAP), 26-30 March 2012, Prague, Czech Republic.

[Kourogiorgas12a] C. I. Kourogiorgas, S. A. Kanellopoulos, A. D. Panagopoulos, S. N. Livieratos, G. E. Chatzarakis, J. D. Kanellopoulos, "Rain Attenuation Hitting Time Statistical Distribution: Application to Fade Mitigation Techniques of Future Satellite Communication Systems", Accepted in 1st IEEE ESTEl, Rome, Italy, October, 2012.

[Kourogiorgas13] Kourogiorgas, C.I., Panagopoulos, A.D., Kanellopoulos, J.D., Livieratos, S.N. and Chatzarakis, G.E.: 'Investigation of rain fade dynamic properties using simulated rain attenuation data with synthetic storm technique,' Antennas and Propagation (EuCAP), 2013 7th European Conference on , vol., no., pp.2277,2281, 8-12 April 2013

[Kourogiorgas13b] C. Kourogiorgas, A. D. Panagopoulos, "A Rain Attenuation Stochastic Dynamic Model for LEO Satellite Systems Operating at Frequencies above 10 GHz", IEEE Transactions on Vehicular Technology, early access.

[Kourogiorgas14a] C. Kourogiorgas, S. N. Livieratos, A. D. Panagopoulos, G. E. Chatzarakis, "Modeling of Joint Rainfall Rate and Rain Attenuation Statistics Using Archimedean Copula Functions", EuCAP 2014, 6-11 April 2014, The Hague, The Netherlands.

[Kourogiorgas14b] Kourogiorgas, C.I.; Panagopoulos, A.D.; Livieratos, S.N.; Chatzarakis, G.E., "Time diversity prediction modeling using Copula functions for satellite communication systems operating above 10GHz," General Assembly and Scientific Symposium (URSI GASS), 2014 XXXIth URSI , vol., no., pp.1,4, 16-23 Aug. 2014

[Kourogiorgas14c] C. I. Kourogiorgas, A. D. Panagopoulos, P.-D. M. Arapoglou, "Rain Attenuation Time Series Generator for Medium Earth Orbit Links Operating at Ka Band and above", EuCAP 2014, the Hague, Netherlands, 6-11 April 2014.

[Kuhar14] U. Kuhar, A. Hrovat, G. Kandus, A. Vilhar, "Statistical analysis of 19.7 GHz satellite beacon measurements in Ljubljana, Slovenia," Antennas and Propagation (EuCAP), 2014 8th European Conference on , pp.681,685, 6-11 April 2014.

[Lacoste05] F. Lacoste, M. Bousquet, L. Castanet, F. Cornet, J. Lemorton, "Improvement of the ONERA-CNES rain attenuation time series synthesiser and validation of the dynamic characteristics of the generated fade events", Space Communications 2005; 20:45–59.

[Laneman04] J.N. Laneman, D.N.C. Tse, G.W. Wornell, "Cooperative diversity in wireless networks: Efficient protocols and outage behavior," IEEE Transactions on Information Theory, vol.50, no.12, pp. 3062-3080, Dec. 2004.

[Laster95] Laster J.D., Stutzman W.L. : "Frequency scaling of rain attenuation for satellite communication links", IEEE Trans. on Antennas and Propagation, Vol. AP 43, n°11, 1995, pp. 1207-121

[Lekkla98] R. Lekkla, K. S. McCormick, D. V. Rogers, "12-GHz Fade Duration Statistics on Earth-Space Paths in South-East Asia" Proceedings of URSI Commission F Open Symposium on Climatic Parameters in Radiowave Prediction, Ottawa, Canada, pp. 167-170, 1998.

[Liebe89] H. Liebe, "MPM-An Atmospheric Millimiter-Wave Propagation Model", International Journal of Infrared and Millimeter Waves, vol. 10, no. 6, 1989

[Lin75] S. H. Lin,: "A method for calculating rain attenuation distributions on microwave paths", Bell system technical journal, vol. 54, no. 6, pp. 1051-1083, 1975.

[Liolis07] K. P. Liolis, A. D. Panagopoulos, and P. G. Cottis, "Multi-Satellite MIMO Communications at Ku Band and above: Investigations on Spatial Multiplexing for Capacity Improvement and Selection Diversity for Interference Mitigation", *EURASIP Journal on Wireless Communications and Networking*, vol. 2007, issue 2, January 2007.

[Liolis10] K. P. Liolis, J. Gomez-Vilarbedo, E. Casini, A. I. Perez-Neira, "Statistical modeling of dual-polarized MIMO land mobile satellite channels*", IEEE Transactions on Communications*, vol. 58, no. 11, pp. 3077-3083, Nov. 2010.

[Liolis13] K. Liolis et al., "Cognitive Radio Scenarios for Satellite Communications: The CoRaSat Approach", Future Network and Mobile Summit 2013.

[Liu12] W. Liu, D. G. Michelson, "Effect of turbulence layer height and satellite altitude on tropospheric scintillation on Ka-Band Earth-LEO satellite links", *IEEE Trans. Veh. Technol.*, vol. 59, no. 7, pp. 3181-3192, 2012.

[Livieratos14] S. N. Livieratos, C. Kourogiorgas, A. D. Panagopoulos, G. E. Chatzarakis, "On the Prediction of Joint Rain Attenuation Statistics in Earth-Space Diversity Systems using Copulas", IEEE Transactions on Antennas and Propagation, vol. 62, no. 4, pp. 2250-2257, April 2014.

[Lo99] T. K. Y. Lo, "Maximum Ratio Transmission", IEEE Transactions on Communications, vol. 47, no. 10, 1999.

[Lobao13] X. Lobao and A. Ginesi, Colloquium: Satellite Services for Global Mobility in the frame of 31st AIAA Int. Commun. Satell. Syst. Conf. (ICSSC 2013), Florence, Italy, 14 Oct. 2013.

[Luini11] L. Luini, C. Capsoni, "MultiEXCELL: A New Rain Field Model for Propagation Applications", IEEE Transactions on Antennas and Propagation, vol. 59, no. 11, 2011.

[Luini12] L. Luini, C. Capsoni, "A Methodology to Generate Cloud Attenuation Fields from NWP Products", 6th EuCAP 2012, 26-30 March 2012, Prague, Czech Republic.

[Luini13] L. Luini, C. Capsoni, "On the Relationship between the Spatial Correlation of Point Rain Rate and of Rain Attenuation on Earth-Space Links", IEEE Transactions on Antennas and Propagation, vol. 61, no. 10, pp. 5255-5263, Oct. 2013.

[MacCartney13] G. R. MacCartney Jr., J. Zhang, S.Nie and T. S. Rappaport, " Path Loss Models for Propagation Channel in Urban Microcells", IEEE Global Communications Conference (GLOBECOM), Dec.9-13, 2013.

[Manning90] R. M. Manning, "A unified statistical rain-attenuation model for communication link fade predictions and optimal stochastic fade control design using a location-dependent rain-statistics database", Intern. Jour. of Sat. Commun., vol. 8, pp. 11-30, 1990.

[Maseng81] T. Maseng, P. Bakken, "A stochastic dynamic model of rain attenuation", *IEEE Trans. Commun.*, vol. COM-29, no.5, pp. 660-669, 1981.

[Mass87] J. Mass, "A Simulation Study of Rain Attenuation and Diversity Effects on Satellite Links", Comsat Technical Review, vol. 17, nno. 1,, pp. 15-186, 1987.

[MATLAB] MATLAB http://www.mathworks.com/products/ matlab/index.html

[Matricciani81] E. Matricciani, "Rate of Change of Signal Attenuation from SIRIO at 11.6 GHz", Electronic Letter, vol. 17, no. 3, pp. 139-141, 1981.

[Matricciani91] Matricciani, E., Rain attenuation predicted with two-layer rain model, Eur. Trans. Telecomm., 2 (6), 715–727, 1991.

[Matricciani94] E. Matricciani, "Prediction of Site Diversity Performance in Satellite Communication Systems Affected by Rain Attenuation: Extension of the Two Layer Model", European Transactions on telecommunications, vol. 5, no. 3, pp. 27-36, 1994.

[Matricciani95] E. Matricciani, E. Mauri, C. Riva, "Scintillation and Simultaneous Rain Attenuation at 49.5 GHz", International Conference on Antennas and Propagation, 1995.

[Matricciani95a] E. Matricciani, ``Transformation of rain attenuation statistics from fixed to mobile satellite communication systems," IEEE Trans. Veh. Technol., vol. 44, no. 2, pp. 565-569, 1995.

[Matricciani96] Matricciani, E.:"Physical-mathematical model of the dynamics of rain attenuation based on rain intensity time series and two layer vertical structure of precipitation", Radio Science, vol. 31, pp. 281-295, 1996.

[Matricciani03] E. Matricciani, "Micro scale site diversity in satellite and tropospheric communications systems affected by rain attenuation", Space Communications, vol. 19, no. 2, pp. 83-90, 2003.

[Matricciani05] Matricciani, E., and Riva, C.: "The search for the most reliable long-term rain attenuation CDF of a slant path and the impact on propagation models", IEEE Transactions on Antennas and Propagation, vol. 53, no. 9, pp. 3075-3079, 2005.

[Matricciani08] E. Matricciani, C. Riva, "18.7 GHz Tropospheric Scintillation and Simultaneous Rain Attenuation Measured at Spino d'Adda and Darmstadt with Italsat", Radio Science, vol. 43, 2008

[Mishura08] Y. Mishura, "Stochastic Calculus for Fractional Brownian Motion and Related Processes", Springer, 2008

[Morita76] K. Morita and I. Higuti, "Prediction methods for rain attenuation distributions of micro and millimeter waves,", Rev. Elec. Commun . Labs, vol. 24, no. 5-6, 1976.

[Mousley82] T. Mousley, E. Vilar, "Experimental and Theoretical Statistics of Microwave Amplitude Scintillation on Satellite Down-Links", IEEE Transactions on Antennas and Propagation, col. AP-30, no. 6, pp. 1099-1106, 1982

[Nelsen06] R. Nelsen, "An Introduction to Copulas", Springer, 2006.

[Nelson96] B. Nelson, W. L. Stutzman, "Fade Slope on 10 to 30 GHz Earth-Space Communication Links – Measurements and Modeling" IEE Proceedings on Microwave, Antennas and Propagation, vol. 143, no. 4, pp. 353-357, 1996.

[O3b] http://www.o3bnetworks.com/o3b-advantage/our-technology, accessed September 2013

[Oestges08] C. Oestges, B. Clerckx, M. Guillaud, M. Debbah, "Dual Polarized Wireless Communications: From Propagation Models to System Performance Evaluation", *IEEE Transactions on Wireless Communications*, vol. 7, no. 10, pp. 4019-, Oct. 2008.

[Olsen78] R. Olsen, D. Rodgers, D. Hodge, "The aR^b Relation in the Calculation of Rain Attenuation", IEEE Transactions on Antennas and Propagation, vol. 26, no. 2, pp. 318-329, 1978.

[OPEX94] OPEX: "Reference Book on Attenuation", 2nd Workshop of the Olympus propagation experimenters (OPEX), Doc. ESA-ESTEC-WPP-083 volume 2, Noordwijk, The Netherlands, 1994.

[Paillassa11] B. Paillassa, B. Escrig, R. Dhaou, M.-L. Boucheret and C. Bes, "Improving satellite services with cooperative communications", Int. J. Satell. Commun. Network., DOI: 10.1002/sat.989, 2011.

[Panagopoulos01] A. D. Panagopoulos, J. D. Kanellopoulos, "Spatio-Temporal Analysis of Rainfall Rate for the Prediction of Slant Path Fade Duration Statistics", IEEE Antennas and Propagation Society International Symposium, vol. 3, pp. 100-103, 8-13 July 2001, Boston, USA

[Panagopoulos02] A. D. Panagopoulos and J. D. Kanellopoulos "Cell-Site Diversity Performance of Millimeter-Wave Fixed Cellular Systems Operating at Frequencies above 20 GHz", IEEE Antennas and Wireless Propagation Letters, Volume: 1, Issue 10, pp.183-185, 2002.

[Panagopoulos02a] A. D. Panagopoulos and J. D. Kanellopoulos "Adjacent Satellite Interference Effects as applied to the Outage Performance of an Earth-Space System located in a Heavy Rain Climatic Region", Annals of Telecommunications, No 9-10, pp.925-942, 2002.

[Panagopoulos03] A. D. Panagopoulos, J. D. Kanellopoulos, "On the rain attenuation dynamics: Spatial-temporal analysis of rainfall rate and fade duration statistics", Intern. Jour. of Sat. Commun. and Netw., vol. 21, pp. 595-611, 2003.

[Panagopoulos03b] A. D. Panagopoulos, J. D. Kanellopoulos, "Statistics of Differential Rain Attenuation on Converging Terrestrial Propagation Paths", IEEE Transaction on Antennas and Propagation, vol. 51, no. 9, pp. 2514-2517, Sept 2003

[Panagopoulos04] A. D. Panagopoulos, P.-D. M. Arapoglou, G. E. Chatzarakis, J. D. Kanellopoulos, P. G. Cottis, "A new formula for the prediction of the site diversity improvement factor", International Journal of Infrared and Millimeter Waves, vol. 25, no. 12, pp. 1781-1789, 2004.

[Panagopoulos04a] A. D. Panagopoulos, P.-D. M. Arapoglou, P. G. Cottis, "Satellite communications at Ku, Ka and V bands: propagation impairments and mitigation techniques", IEEE Communication Surveys and Tutorials, 2004.

[Panagopoulos05] A. D. Panagopoulos, P.-D. M. Arapoglou, G. E. Chatzarakis, J. D. Kanellopoulos, P. G. Cottis, "Long-term rain attenuation probability and site diversity gain prediction formulas", IEEE Trans on Antennas and Propagation, vol 53, no. 7, pp. 2307-2313, 2005.

[Papoulis02] A. Papoulis, S. U. Pillai, "Probability, random variables and stochastic processes", McGraw-Hill, 2002.

[Paraboni94] A. Paraboni, C. Riva, "A New Method for the Prediction of Fade Duration Statistics in Satellite Links Above 10 GHz", Internation Journal on Satellite Communications, vol. 12, pp. 387-394, 1994.

[Paraboni02] A. Paraboni, F. Barbaliscia, "Multiple Site Attenuation Prediction Models Based on Rainfall Structures (Mes- or Synoptic Scales) for Advanced TLC or Broadcasting Systems", XXVII URSI General Assembly, Maastricht, 2002.

[Paraboni09] Paraboni, M. Buti, C. Capsoni, D. Ferraro, C. Riva, A. Martellucci, P. Gabellini, "Meteorology-Driven Optimum Control of a Multibeam Antenna in Satellite Telecommunications", *IEEE Transactions on Antennas and Propagation,* vol. 57, no. 2, 2009.

[Paulraj03] A. Paulraj, R. Nabar, D. Gore, "Introduction to Space-Time Wireless Communications", Cambridge University Press, 2003.

[Rappaport13] T.S. Rappaport et al, "Broadband millimeter wave propagation measurements and models using adaptive-beam antennas for outdoor urban cellulat communications", IEEE Trans. On Antennas and Propagation vol. 61, no.4, pp. 1850-1859, Apr. 2013

[Ritchie11] S. Ritchie, B. Evans, "Smart Gateways for a Terabit/s Satellite System", in 17th Ka Band Broadband Communication, Navigationa dn Earth Observation Conference, Palermo, Italy, October, 2011.

[Rosello12] J. Rosello, A. Martellucci, R. Acosta, J. Nessel, L. E. Braten, C. Riva "26-GHz Data Downlink for LEO Satellites", 6th European Conference on Antennas and Propagation (EUCAP), Prague, Czech, March 2012.

[Sakarellos14] V. K. Sakarellos, C. Kourogiorgas, A. D. Panagopoulos, "Cooperative Hybrid Land Mobile Satellite – Terrestrial Broadcasting Systems: Outage Probability Evaluation and Accurate Simulation", Wireless Personal Communications, vol. 79, pp. 1471-1481, 2014.

[Salonen03] E. Salonen, P. Heikkinen, "Fade Slope Analysis for Low Elevation Angle Satellite Links" COST280/COST272 Joint Workshop, Noordwijk, Netherlands, 2003.

[Seshardi93] B. Seshardi, "The Inverse Gaussian Distribution", Clarendon Press, Oxford, 1993.

[Shao95] Y. Shao, "The Fractional Ornstein-Uhlenbeck Process as a Representation of Homogeneous Eulerian Velocity Turbulence", Physica D, 83, pp. 461-477, 1995

[Sharma13] S. K. Sharma, S. Chatzinotas, B. Ottersten, “Cognitive Radio Techniques for Satellite Communication Systems”, 78th VTC Fall, 2-5 Sept. 2013.

[Sharma13b] S. K. Sharma, S. Chatzinotas, B. Ottersten, “Satellite Cognitive Communications: Interference Modeling and Techniques Selections”, 6th ASMS and 12th SPSC, 5-7 Sept. 2013.

[Skraparlis] D. Skraparlis, V. K. Sakarellos, A. D. Panagopoulos, J. D. Kanellopoulos, “Performance of N-Branch Receive Diversity Combining in Correlated Lognormal Channels”, IEEE Communication Letters, vol. 13, no. 7, pp. 489-491.

[Stafford01] J. Stafford, N. Terril, “Extension fo Existing Models for Evaluating Site Diversity Performance for Rain Fade Mitigation”, 7th Ka-Band Utilization Conference, Santa Margherita Ligure, Genoa, Italy, 2001.

[Stuber01] G. L. Stuber. “Principles of Mobile Communications”, Kluwer, Academic Publishers, 2001.

[Sweeney92] D. G. Sweeney, C. W. Bostian, “The Dynamics of Rain-Induced Fade”, IEEE Transactions on Antennas and Propagation, vol. 40, no. 3, pp. 275-278, 1992.

[Thompson11] Paul Thompson, Barry Evans, Michel Bousquet, Laurent Castanet, Takis Mathiopoulos, “Concepts and Technologies for a Terabit/s Satellite: Supporting Future Broadband Services via Satellite”, SPACOMM 2011, The Third International Conference on Advances in Satellite and Space Communications, 17-22 April, Budapest, Hungary, 2011

[Timothy98] Timothy et al., 1998] k. I. Timothy, N. C. Mondal, S. K. Sarkar, “Dynamical Properties of Rainfall for Performance Assessment of Earth/Space Communication Links at Ku and Ka Bands” International Journal on Satellite Communications, vol. 16, pp. 53-57, 1998.

[Timothy00] K. I. Timothy, J. T. Ong, E. B. L. Choo, “Descriptive Fade Slope Statistics on INTELSAT Ku-Band Communication Link”, Electronic Letters, vol. 36, no. 16, 2000.

[Toptsidis12] N. Toptsidis, P.-D. Arapoglou, M. Bertinelli, "Link adaptation for Ka band low Earth orbit Earth Observation systems: A realistic performance assessment," Int. J. Satell. Commun. Network., vol. 30, no. 3, pp. 131-146, 2012.

[Vasseur98] H. Vasseur and D. Vanhoenacker, “Characterisation of tropospheric turbulent layers from radiosonde data,” *Electron. Lett.*, vol. 34, no. 4, pp. 318–319, Feb. 19, 1998.

[Vasseur99] H. Vassuer, “Prediction of Tropospheric Scintillation on Satellite Links from Radiosonde Data”, IEEE Transactions on Antennas and Propagation, vol. 47, no. 2, pp. 293-301, 1999

[Warnock85] J. M. Warnock, T. E. VanZandt, “A Statistical Model to Estimate Refractivity Turbulence Structure Constant C_n^2 in the Free Atmosphere”, NOOA Tech. MEMO ERL, AL-10, NOOA, Aeronom. Lab., boulder Co, 1985.

[Yin96] Z.-M. Yin, “New Methods for Simulation of Fractional Brownian Motion”, Journal of Computational Physics, pp. 66-72, vol. 127, 1996

CURRICULUM VITAE

NAME: Charilaos Kourogiorgas

DATE OF BIRTH: 6 July 1985

E-MAIL: hkourog@gmail.com, harkour@mail.ntua.gr

ACADEMIC BACKGROUND

December 2011-May 2015: Pursuing PhD at National Technical University of Athens, School of Electrical and Computer Engineering
Topic: *Channel Modeling and Performance Evaluation of High Data Rate Next Generation Wireless Terrestrial and Satellite Communication Systems*
Supervisor: Prof. A. D. Panagopoulos

2003-2009: National Technical University of Athens, School of Electrical and Computer Engineering
Average Grade: 8,06/10 (June 2009)
Major: Telecommunication Systems
Minor: Electromagnetics

2000-2003: Leonteio Senior High School of Patission
Average Grade: 18,6 / 20

WORKING EXPERIENCE

October 2009- June 2011: Researcher at Office National d'Études et de Recherches Aérospatiales (ONERA)
During my work at ONERA, I studied channel modelling of high frequency telecommunication systems for low elevation angles, with application to UAVs. Particularly, the HYCELL modelling of rain fields was used in order to compute the exceedance probability of rain attenuation and to evaluate its performance for low elevation links.

JOURNAL PUBLICATIONS

1. **C. Kourogiorgas**, A. D. Panagopoulos, J. D. Kanellopoulos, "*On the Earth-space Site Diversity Modeling: A novel physical mathematical model*", IEEE Transactions on Antennas and Propagation, vol. 60, no. 9, pp. 4391-4397, November 2011

2. V. K. Sakarellos, **C. Kourogiorgas**, D. Skraparlis, A. D. Panagopoulos, J. D. Kanellopoulos, "*End-to-End Performance Analysis of Millimeter Wave Triple-Hop Backhaul Transmission Systems*", Wireless Personal Communications, vol. 71, no. 4, pp. 2725-2744, August 2013.

3. S. A. Kanellopoulos, A. D. Panagopoulos, **C. Kourogiorgas**, J. D. Kanellopoulos, "*Slant Path and Terrestrial Links Rain Attenuation Time Series Generator for Heavy Rain Climatic Regions*", IEEE Transactions on Antennas and Propagation, vol. 61, no. 6, pp. 3396-3399, April 2013.

4. **C. Kourogiorgas**, A. D. Panagopoulos, J. D. Kanellopoulos, "*An Engineering Method for the Prediction of Outage Probability of LOS Terrestrial Links Operating above 10 GHz*", IEEE Antennas and Wireless Propagation Letters, vol. 12, pp. 516-519, 2013.

5. **C. Kourogiorgas**, A. D Panagopoulos,, "*A Physical-Mathematical Model for Predicting Slant Path Rain Attenuation Statistics*", IET Microwave, Antennas and Propagation, vol. 7, no. 12, pp. 970-975, 2013.

6. **C. Kourogiorgas**, A. D. Panagopoulos, S. N. Livieratos, G. E. Chatzarakis, "*On the Outage Probability Prediction of Time Diversity Scheme in Broadband Satellite Communication Systems*", Progress In Electromagnetics Research C, vol. 44, pp. 175-184, 2013

7. S. A. Kanellopoulos, **C. Kourogiorgas**, A. D. Panagopoulos, S. N. Livieratos, G. E. Chatzarakis, "*Channel Model for Satellite Communication Links above 10 GHz based on Weibull Distribution*", IEEE Communication Letter, vol. 18, no. 4, pp. 568-571, pril 2014.

8. S. N. Livieratos, **C. Kourogiorgas**, A. D. Panagopoulos, G. E. Chatzarakis, "*On the Prediction of Joint Rain Attenuation Statistics in Earth-Space Diversity Systems using Copulas*", IEEE Transactions on Antennas and Propagation, vol. 62, no. 4, pp. 2250-2257, April 2014.

9. **C. I. Kourogiorgas**, A. D. Panagopoulos, "*Outage Performance of Dual Branch Diversity Techniques in Broadband Fixed Wireless Access Networks*", IET Communications, vol. 8, no. 9, pp. 1648-1653, June 2014.

10. **C. I. Kourogiorgas**, A. D. Panagopoulos, "*A Rain Attenuation Stochastic Dynamic Model for LEO Satellite Systems Operating at Frequencies above 10 GHz*", IEEE Transactions on Vehicular Technology, vol. 64, no. 2, pp. 829-834, 2015.

11. **C. Kourogiorgas**, M. Kvicera, D. Skraparlis, T. Korinek, V. Sakarellos, A. D. Panagopoulos, P. Pechac, "*Modeling of First-Order Statistics of MIMO Dual Polarized Channel at 2 GHz for Land Mobile Satellite Systems Under Tree Shadowing*", IEEE Transactions on Antennas and Propagation, vol. 62, no. 10, pp. 5410-5415, Oct. 2014.

12. **C. Kourogiorgas**, P.-D. Arapoglou, A. D. Panagopoulos, "*Statistical Characterization of Adjacent Satellite Interference for Earth Stations on Mobile Platforms Operating at Ku and Ka Band*", IEEE Wireless Communication Letters, vol. 4, no. 1, pp. 82-85, 2015.

13. V. K. Sakarellos, **C. Kourogiorgas**, A. D. Panagopoulos, "*Cooperative Hybrid Land Mobile Satellite – Terrestrial Broadcasting Systems: Outage Probability Evaluation and Accurate Simulation*", Wireless Personal Communications, vol. 79, pp. 1471-1481, 2014.

14. **C. Kourogiorgas**, A. D. Panagopoulos, S. N. Livieratos, G. E. Chatzarakis, "*Dynamic Properties of Rain Attenuation in Athens, Greece: Slant Path Rain Attenuation Synthesizer and Dynamic Diversity Gain*", accepted at Progress In Electromagnetics Research

15. Z. Katona, C. Kourogiorgas, A. D. Panagopoulos, N. Jeannin, "*Capacity Analysis of High-Throughput Satellite Links for Earth Observation Missions*", accepted at International Journal of Satellite Communications and Networking

CONFERENCE PUBLICATIONS

1. **C. Kourogiorgas**, L. Feral, V. Fabbro, N. Jeannin, J. Lemorton, "*Use of the HYCELL model for predicting rain attenuation on UAS low elevation datalinks*", EuCAP 2010 , pp. 1-5, 12-16 April 2010, Barcelona, Spain.

2. J. Lemorton, V. Fabbro, **C. Kourogiorgas**, C. Amaya, P. Bouchard, D. Rogers, L. Luini, C. Riva, D. Vanhoenacker-Janvier, F. Lacoste, L. Braten, L. Castanet, "*Prediction models for the radio propagation*

channel at low elevation angles for high frequency aerospace applications", 1st COST IC0802 International Workshop, 8-9 November 2010, Erice, Italy.

3. J. Lemorton, V. Fabbro, **C. Kourogiorgas**, C. Amaya, L. Luini, C. Riva, D. Vanhoenacker-Janvier, "*Review of Prediction Methods for Low-Elevation Aerospace Systems and New Achievements*", EuCAP 2011, pp. 1-5, 11-15 April 2011, Rome, Italy.

4. **C. Kourogiorgas**, A. D. Panagopoulos, G. K. Karagiannidis, J. D. Kanellopoulos, "*On the modeling of rain rate and of slant path and terrestrial links rain attenuation with Inverse Gaussian distribution*", MCM6 COST Action IC0802, 28-30 September 2011, Prague, Czech Republic.

5. **C. Kourogiorgas**, A. D. Panagopoulos, J. D. Kanellopoulos, "*Site Diversity Performance Using Two-Dimensional Inverse Gaussian Distribution*", ESA Workshop on Radiowave Propagation 2011, 30 November–2 December, Noordwijk, Netherlands.

6. **C. Kourogiorgas**, A. D. Panagopoulos, G. K. Karagiannidis, J. D. Kanellopoulos, "*On the Inverse Gaussian Modeling of Rain Rate and Slant Path and Terrestrial Links Rain Attenuations*", EuCAP 2012, 26–30 March, Prague, Czech Republic.

7. **C. Kourogiorgas**, A. D. Panagopoulos, N. Moraitis, J. D. Kanellopoulos, "*Analysis of 15-Months Rain Rate Measurements at NTUA Campus*", EuCAP 2012, 26–30 March, Prague, Czech Republic.

8. **C. Kourogiorgas**, A. D. Panagopoulos, J. D. Kanellopoulos, "*Synthesizing Rain Attenuation Time Series for an Earth-LEO Satllite Link*", MCM7 COST Action IC0802, 16-18 April 2012, Portsmouth, Great Britain.

9. G. Karagiannis, A. D. Panagopoulos, **C. Kourogiorgas**, J. D. Kanellopoulos, "*Multi-Dimensional First Order Stochastic Differential Equation for Simulating Correlated Space-Time Rain Attenuation Time Series*", MCM7 COST Action IC0802, 16-18 April 2012, Portsmouth, Great Britain.

10. **C. Kourogiorgas**, A. D. Panagopoulos, J. D. Kanellopoulos, P.-D. M. Arapoglou, "*Rain Attenuation Time Series Synthesizer for LEO Satellite Systems Operating at Ka Band*", ASMS/SPSC 2012, 5-7 September 2012, Baiona, Spain.

11. **C. Kourogiorgas**, S. A. Kanellopoulos, A. D. Panagopoulos, S. N. Livieratos, G. E. Chatzarakis, J. D. Kanellopoulos, "*Rain Attenuation Hitting Time Statistical Distribution: Application to Fade Mitigation Techniques of Future Satellite Communication Systems*", ESTEL Conference 2012, 2-5 October 2012, Rome, Italy.

12. V. Sakarellos, **C. Kourogiorgas**, A. D. Panagopoulos, "*Hybrid Satellite-Terrestrial Broadband Backhaul Links: Capacity Enhancement through Spatial Multiplexing*" ESTEL Conference, 2-5 October 2012, Rome, Italy.

13. **C. Kourogiorgas**, S. A. Kanellopoulos, A. D. Panagopoulos, S. N. Livieratos, G. E. Chatzarakis, "*Hitting Time Distribution of Weibull-Based Rain Attenuation Synthesizer: Application to Satellite Communications FMTs*", First CNES-ONERA Workshop on Earth-Space Propagation, 21-23 March 2013, Toulouse France.

14. **C. Kourogiogras**, G. A. Karagiannis, A. D. Panagopoulos, "*Smart Gateway Diversity Outage Performance using Multi-Dimensional Rain Attenuation Synthesizer*", First CNES-ONERA Workshop on Earth-Space Propagation, 21-23 January 2013, Toulouse France.

15. **C. Kourogiorgas**, A. D. Panagopoulos, "*On the Route Diversity Improvement Modeling for Broadband Radio Access Networks*", EuCAP 2013, 8-12 April 2013, Gothenburg, Sweden.

16. **C. Kourogiorgas**, G. A. Karagiannis, A. D. Panagopoulos, "*Space-Time Rain Rate Field Generator for Multi-Antenna Satellite Communication Applications*", EuCAP 2013, 8-12 April 2013, Gothenburg, Sweden.

17. **C. Kourogiorgas**, A. D. Panagopoulos, S. N. Livieratos, G. E. Chatzarakis, "*Investigation of Rain Fade Dynamic Properties using Simulated Rain Attenuation Data with Synthetic Storm Technique*", EuCAP 2013, 8-12 April 2013, Gothenburg, Sweden.

18. D. Vanhoenacker-Janvier, P. Bouchard, L. E. Braten, V. Fabbro, **C. Kourogiorgas**, D. V. Rogers, "*Channel Models for Aeronautical and Low Elevation Radio Links*", EuCAP 2013, 8-12 April 2013, Gothenburg, Sweden.

19. **C. Kourogiorgas**, A. D. Panagopoulos, "*A Tropospheric Scintillation Time Series Synthesizer based on Stochastic Differential Equations*", 2013 Joint Conference: 19th Ka and Broadband Communications, Navigation and Earth Observation Conference and 31st AIAA ICSSC, 14-17 October 2013, Florence, Italy.

20. **C. Kourogiorgas**, A. D. Panagopoulos, "*Modelling of Joint Rain Attenuation for Time Diversity Satellite Communication Systems*", 2013 Joint Conference: 19th Ka and Broadband Communications, Navigation and Earth Observation Conference and 31st AIAA ICSSC, 14-17 October 2013, Florence, Italy.

21. **C. Kourogiorgas**, M. Kvicera, D. Skraparlis, T. Korinek, V. Sakarellos, A. D. Panagopoulos, P. Pechac, "*Modeling of First-Order Statistics of LMS Channel under Tree Shadowing for Various Elevation Angles at L-Band*", EuCAP 2014, 6-11 April 2014, The Hague, The Netherlands.

22. **C. Kourogiorgas**, A. D. Panagopoulos, "*Multi Satellite MIMO Systems at Ka Band and Above: Outage Capacity Analysis Using Bivariate IG Distribution*", EuCAP 2014, 6-11 April 2014, The Hague, The Netherlands.

23. **C. Kourogiorgas**, S. N. Livieratos, A. D. Panagopoulos, G. E. Chatzarakis, "*Modeling of Joint Rainfall Rate and Rain Attenuation Statistics Using Archimedean Copula Functions*", EuCAP 2014, 6-11 April 2014, The Hague, The Netherlands.

24. **C. Kourogiorgas**, A. D. Panagopoulos, P.-D. M. Arapoglou,"*Rain Attenuation Time Series Generator for Medium Earth Orbit Links Operating at Ka Band and above*", EuCAP 2014, 6-11 April 2014, The Hague, The Netherlands.

25. G. Pitsiladis, **C. Kourogiorgas**, A. D. Panagopoulos, "*Connectivity Gain Evaluation Using Diversity in Wireless Sensor Networks Under Correlated Shadowing*", EuCAP 2014, 6-11 April 2014, The Hague, The Netherlands.

26. G. Pitsiladis, **C. Kourogiorgas**, A. D. Panagopoulos, "*Connectivity Evaluation in Random Wireless Multi-hop Networks Under Inverse Gaussian Shadowing Channels*", European Wireless 2014, 12-15 May 2014, Barcelona, Spain.

27. S. Vassaki, G. Pitsiladis, **C. Kourogiorgas**, M. Poulakis, A. D. Panagopoulos, G. Gardikis, S. Costicoglou, "*Satellite-based Sensor Networks: M2M Sensor Communications and Connectivity Analysis*", International Conference on Telecommunications and Multimedia (TEMU), 2014, pp. 132-137, Heraklion, 28-30 July 2014

28. **C. Kourogiorgas**, A. D. Panagopoulos, S. N. Livieratos, G. E. Chatzarakis, "*Time Diversity Prediction Modeling Using Copula Functions for Satellite Communication Systems Operating Above 10 GHz*", 2014 XXXIth URSI General Assembly and Scientific Symposium, 16-23 August 2014, Beijing, China

29. **C. Kourogiorgas**, A. D. Panagopoulos, "*Application of Stochastic Differential Equations for the Performance Evaluation of Broadband Satellite Communication Systems*", 2014 XXXIth URSI General Assembly and Scientific Symposium, 16-23 August 2014, Beijing, China

30. **C. Kourogiorgas**, A. D. Panagopoulos, "*Interference Statistical Distribution for Cognitive Satellite Communication Systems Operating above 10 GHz*", 7th Advanced Satellite Multimedia Systems Conference

and the 13th Signal Processign for Space Communications Workshop, pp. 256-261, 8-10 September 2014, Livorno, Italy

31. **C. Kourogiorgas**, A. D. Panagopoulos, S. N. Livieratos, G. E. Chatzarakis, "*Pico-Scale Dynamic Diversity Gain Evaluation in Broadband satellite Communication Systems*", 20th Ka and Broadband Communications, Navigation and Earth Observation Conference, 1-3 October 2014, Vietri sul Mare/Salerno, Italy

32. M. Poulakis, S. Vassaki, **C. Kourogiorgas**, G. Pitsiladis, A. D. Panagopoulos, "*Use of Satellite Communication Systems and Services for Monitoring of Critical Infrastructures and Safety Applications*", 20th Ka and Broadband Communications, Navigation and Earth Observation Conference, 1-3 October 2014, Vietri sul Mare/Salerno, Italy

33. **C. Kourogiorgas**, S. Sagriotis, A. D. Panagopoulos, "*Coverage and Outage Capacity Evaluation in 5G Millimeter Wave Cellular Systems: Impact of Rain Attenuation*", EuCAP 2015, 12-17 April 2015, Lisbon Portugal.

34. **C. Kourogiorgas**, A. D. Panagopoulos, P.-D. Arapoglou, S. Stavrou, "*MIMO Dual Polarized Fixed Satellite Systemsabove 10 GHz: Channel Modeling and Outage Capacity Evaluation*", EuCAP 2015, 12-17 April 2015, Lisbon Portugal.

35. **C. Kourgiorgas**, A. Kelmendi, A. D. Panagopoulos, S. N. Livieratos, A. Vilhar, G. E. Chatzarakis, "*Rain Attenuation Time Series Synthesizer based on Copula Functions*", EuCAP 2015, 12-17 April 2015, Lisbon Portugal.

36. **C. Kourogiorgas**, A. D. Panagopoulos, K. P. Liolis, "*Cognitive Uplink FSS and FS Links Coexistence in Ka-band: Propagation based Interference Analysis*", paper accepted at ICC 2015.

37. A. Z. Papafragkakis, N. K. Lyras, **C. Kourogiorgas**, A. D. Panagopoulos, "*Propagation Measurements Campaign in Athens with ALPHASAT at Ka-Band using Software Defined Radio Technologies*", paper accepted at AWPC/ICEAA

38. N. K. Lyras, **C. Kourogiorgas**, A. D. Panagopoulos, "*Cloud Attenuation Time Series Synthesizer for Earth-Space Links Operating at Optical Frequencies*", paper accepted at AWPC/ICEAA

BOOK CHAPTERS

1. **C. Kourogiorgas**, V. Sakarellos, S. A. Kanellopoulos, A. D. Panagopoulos, "*Enhancing Resiliency of Broadband Satellite Communication Emergency Networks through Propagation Impairment Mitigation Techniques*", Book Title: *Recent Advances in Satellite Research and Development*", NOVA Publishers, 2012.

2. A. D. Panagopoulos**, C. Kourogiorgas**, "*Application of Channel Models to System Cases*", COST ACTION IC0802.

3. **C. Kourogiorgas**, A. D. Panagopoulos, "*Tropospheric Attenuation Synthesizers*", Book entitled: Radio Wave Propagation and Channel Modeling for Earth-Space Systems at CRC Press.

4. **C. Kourogiorgas**, N. Moraitis, A. D. Panagopoulos, "*Radio Channel Modeling and Propagation Prediction for 5G Mobile Communication Systems*", IGI Global Handbook of Research on Next Generation Mobile Communication Systems 2015.

5. M. I. Poulakis, S. Vassaki, G. T. Pitsiladis, **C. Kourogiorgas**, A. D. Panagopoulos, G. Gardikis, S. Costicoglou, "*Wireless Sensor Networks Management using Satellite Communication Technologies*", Book chapter in the Book entitled: Emerging Communication Technologies Based on Wireless Sensor Networks: Current Research and Future Applications at CRC Press

TRAINING SCHOOLS ATTENDED

- 1st Course on Radiowave Propagation for Space Systems, 28–29 November 2011, ESA/ESTEC, Noordwijk, Netherlands.

GRANTS AND AWARDS

- Chairman in the session of "Tropospheric Propagation" at EUCAP 2015
- Grant for participation at EuCAP 2013 from EuCAP Committee
- URSI Young Scientist Award 2014
- Grant from EurAAP for Short-Term Scientific Mission at Jozef Stefan Institute, Ljubljana, Slovenia

INTERNSHIPS

While I was working at ONERA, I had an internship of one month, October 2011, with Univeristé Catholique de Louvain-la-neuve at Belgium. During this internship, a model for computing the parameters of spatial variations of the refractive index at the troposphere and models for predicting the exceedance probability of the scintillation of tropospheric turbulence were studied.

A two-week duration STSM funded by EurAAP took place for two weeks at the middle of December 2014 at Jozef Stefan Institute, Ljubljana, Slovenia. During my work at JSI, the obtained measurements of rain attenuation at 20 GHz from three ground stations were statistically analyzed. More particularly, propagation models were compared to experimental data for 3 dual site diversity systems and one triple site diversity system. Moreover, statistics of rain attenuation on temporal domain were studied as well as the scintillation dynamics.

RESEARCH PROJECTS

- COST Action IC0802: Propagation tools and data for integrated Telecommunication, Navigation and Earth Observation systems
- COST Action IC1004: Cooperative Radio Communications for Green Smart Environments
- SatNEx III, Call of Order 3 (Project funded by European Space Agency)
- THALES-NTUA MIMO Techniques in Satellite Communication Systems (MIMOSA) (Project funded by EU and National Funds)
- FLAME- Flexible Radio Communication Optimization Framework (Project funded by EU and National Funds)
- Greece-Czech Republic Cooperation (Project funded by EU and National Funds)
- Archimedes III – RAINFADYN (Project funded by EU and National Funds)
- SatNEx IV – Next Generation Satellite Trunking Systems, Working Item 1 (Project funded by European Space Agency)

SIMULATION SOFTWARE: Simulink, ADS, Spice, Network Simulator 2, MiniNEC, AGI's STK

PROGRAMMING LANGUAGES: Matlab, Python, C++, R, Fortran90, Mathematica, Java, Prolog, Assembly (MIPS)

FOREIGN LANGUAGES: English, French